Advanced Control, Identification and Optimisation of Energy Systems

Obadah S. Zaher

A thesis submitted for the degree of Doctor of Philosophy

Department of Mechanical and Aerospace Engineering
University of Strathclyde

2013

COPYRIGHT DECLARATION

Signed:_____

Date:_____

Table of Contents

Index of Figures

Index of Tables

Abstract

An increased emphasis is being put on energy efficiency and reduction of carbon emissions. The importance of comfort and energy savings to building designers and occupants has driven the development of more efficient building technologies. This has led to building control engineers and researchers developing more advanced and efficient control strategies in attempts to maximize the potential of these technologies and improve the efficiency of existing technologies. The buildings industry has been slow to adopt these advanced control strategies however, due to complexity issues or increases in cost and commissioning time. In order to bridge the gap between advanced controller design and the buildings industry, it is necessary that the controller designs that are being developed remain low cost and simple to implement. Ultimately, the objective for the design of a controller for use in industry is a robust high performance controller that is easy to implement, requires minimal user input and has low implementation and installation costs i.e. does not require extra/excessive costly hardware. The research presented in this thesis is focused on this problem and delivers solutions that satisfy these criteria.

This thesis considers the development of a robust high performance heating, ventilation and air-conditioning (HVAC) control strategy that is capable of dealing with the complexities associated with modern building control whilst being a low cost solution which is easy to implement. When designing a HVAC control system, a number of difficulties are encountered which the control system must be able to deal with in order to ensure accurate set-point tracking (thermal comfort) and efficient energy usage. These include dealing with time delay, parameter uncertainty, nonlinearity, interacting multi-input multi-output (MIMO) systems, unknown system parameters (identification) and tuning/re-tuning. Throughout this thesis a number of novel contributions to knowledge and controller design methodologies have been developed in order to deliver solutions which overcome these problems whilst remaining practical enough for use in industrial applications. The methods developed are based on a practical approach to inverse dynamics controller design and come together as two distinct main controller design methodologies. Firstly, a novel Genetic Algorithm (GA) based auto-tuning algorithm for the Robust Inverse

Dynamics Estimation (RIDE) controller design which accounts for modelling parameter uncertainty. Secondly, a novel robust system identification based inverse dynamics controller design which incorporates a novel dead-time compensation methodology within the inverse dynamics controller structure. This controller design is termed System Identification based Rate Compensated Inverse Dynamics (SI-RCID). The SI-RCID controller algorithm is an advanced controller design which is relatively easy to implement, requiring a similar level of user input as the initial design procedure for the popular self-tuning proportional integral derivative (ST-PID) controller designs. When applied to a nonlinear MIMO HVAC system, the SI-RCID controller shows a significant performance improvement when compared to traditional ST-PID control and a more advanced controller design recently developed in the literature.

Acknowledgements

Firstly, I would like to extend my gratitude to my first Supervisor Professor John Counsell for his continual support, guidance and invaluable advice throughout the duration of this PhD project. I would also like to thank my second Supervisor Dr. Yonghao Zhang for his support.

Many individuals have unknowingly helped me in my research throughout my PhD and therefore I would like to thank all of my fellow researchers and academics at the BRE Centre of Excellence in Energy Utilisation at the University of Strathclyde for their insight and experience. Without the fantastic research environment created by these individuals, the completion of this project would not have been possible.

I would also like to acknowledge the support and encouragement of my friends for their valuable contributions.

Most importantly, a special thanks to my mum, dad and all my family for their unconditional love, patience and moral support throughout this period of my life. I love you too unconditionally.

Obadah S. Zaher Glasgow June 2013.

Nomenclature

A_s	=	Area (structure) (m^2)
A_{ft}	=	Area (internal mass) (m^2)
A_F	=	Area (floor) (m^2)
A_R	=	Area (roof) (m^2)
A_W	=	Area (windows) (m^2)
C_a	=	Specific Heat Capacity (air) (J/KgK)
C_s	=	Specific Heat Capacity (external wall structure) (J/KgK)
C_{ft}	=	Specific Heat Capacity (internal mass i.e. building elements other than external wall structure) (J/KgK)
C_h	=	Overall thermal capacitance of the humidifier (J/K)
C_{ah}	=	Overall thermal capacitance of the air-handling unit (AHU) (J/K)
C_{duct}	=	Specific Heat Capacity (duct material) (J/KgK)
$h(t)$	=	Humidification rate of humidifier (kg/s)
h_{in}	=	Heat transfer coefficient inside AHU duct (W/m^2K)
h_{out}	=	Heat transfer coefficient in the ambient (outside AHU duct) (W/m^2K)
h_i	=	Heat transfer coefficient of internal wall structure (W/m^2K)
h_e	=	Heat transfer coefficient of external wall structure (W/m^2K)
K_{si}	=	Thermal Conductivity (internal structure) (W/mK)
LL_{Qh}	=	Minimum heater power output (Case 1 actuator) (W)
LL_{mv}	=	Minimum ventilation rate (kg/s)
LL_{coil}	=	Minimum heating coil power (W)
LL_{hum}	=	Minimum humidification rate (W)
M_a	=	Mass (air) (Kg)
M_{duct}	=	Mass (duct) (Kg)
M_{si}	=	Mass (internal structure) (Kg)
M_{se}	=	Mass (external structure) (Kg)
M_{ft}	=	Mass (internal mass) (Kg)
$\dot{m}_c$	=	Mass flow rate (mechanical ventilation) (Kg/s)
$\dot{m}_{nv}$	=	Mass flow rate (natural ventilation) (Kg/s)

n_{occ} = Number of occupants

ρ_a = Density (air) (Kg/m^3)

P_{occ} = Evaporation rate of occupants (Kg/h)

$\dot{Q}_R$ = Heat Transfer through Roof (W)

$\dot{Q}_W$ = Heat Transfer through Windows (W)

$\dot{Q}_F$ = Heat Transfer through Floor (W)

$\dot{Q}_{free}$ = Heat Transfer from Free Heats (W)

$\dot{Q}_{si}$ = Heat Transfer through internal structure (W)

$\dot{Q}_{se}$ = Heat Transfer through external structure (W)

$\dot{Q}_{ft}$ = Heat Transfer from internal mass (W)

$\dot{Q}_h$ = Heat added to zone from heater (W)

$\dot{Q}_{coil}$ = Heat added to AHU supply air from heating coil (W)

$\dot{Q}_{mv}$ = Heat transferred through mechanical ventilation (W)

$\dot{Q}_{nv}$ = Heat transferred through natural ventilation (W)

T_a = Zone Air Temperature (K)

T_{duct} = Air temperature inside AHU duct (K)

T_h = Air temperature inside AHU at humidifier (K)

Th_{wall} = Wall thickness (m)

T_o = Outside Air Temperature (K)

T_m = Air temperature inside mixing box (K)

T_{coil} = Air temperature inside AHU at heating coil (K)

τ_{coil} = Heating coil time constant (s)

τ_h = Heating system time constant (Case 1 actuator) (s)

τ_{hum} = Humidifier time constant (s)

τ_v = Ventilation system time constant (Case 1 actuator) (s)

τ_{mv} = Ventilation system time constant (Case 2 actuator) (s)

U_F = Heat Transfer Coefficient of Floor (W/m^{2}K)

U_{ft} = Heat Transfer Coefficient of Internal Mass (W/m^{2}K)

U_R = Heat Transfer Coefficient of Roof (W/m^{2}K)

U_W = Heat Transfer Coefficient of Windows (W/m^{2}K)

$uc_{hum}(t)$ = Humidifier demand (kg/s)

$uc_{Qh}(t)$ = Heating demand (W)

$uc_v(t)$ = Ventilation demand (kg/s)

UA_{ah} = Overall thermal capacitance area factor of the AHU (J/sK)

UL_{Qh} = Maximum heater power output (Case 1 actuator) (W)

UL_{mv} = Maximum ventilation rate (kg/s)

UL_{coil} = Maximum heating coil power (W)

UL_{hum} = Maximum humidification rate (W)

V_h = Volume of humidifier (m^3)

V_{ah} = Volume of AHU (m^3)

W_a = Zone humidity (kg/kg)

W_h = Humidity inside AHU at humidifier (kg/kg)

W_{coil} = Humidity inside AHU at heating coil (kg/kg)

W_m = Humidity inside AHU mixing box (kg/kg)

W_o = Outside humidity (kg/kg)

$\propto_h$ = Overall transmittance area factor of the humidifier (J/sK)

γ = Ratio of outside air to internal zone air entering AHU

Algorithm definitions

max_stall = Maximum no. of stall generations allowed

tol_fun = Tolerance for variations of mean fitness between generations

gen_max = Maximum number of generations allowed

popsize = Population size

elite_count = Number of elite children selected from population

nvars = Number of variables requiring tuning

crossover_fract = Fraction of population to be selected for crossover children

mut_prob = Probability of mutation occurring

UB = Upper constraint for optimisation

LB = Lower constraint for optimisation

stall_num = Number of stall generations that have occurred

mean_fit = Mean fitness value for the population

1. Introduction

Energy and climate change have become highly publicised and political issues around the world today. It has become common knowledge that the world's traditional energy resources, i.e. fossil fuels, are diminishing rapidly whilst carbon emissions are growing due to the high rate of global energy consumption. Consequently, fuel prices are on the rise causing further financial stress in an already poor economic climate. It is thought that energy consumption will continue to increase with the growth in population size and developing countries such as China and India experiencing dramatic economic growth (Perez-Lombard, Ortiz et al. 2008). Broadly speaking, there are two sides to the energy predicament; supply and demand. In order to tackle the energy supply side of the problem, there has been, and continues to be, significant efforts directed towards the development of alternative energy sources, particularly clean renewable sources such as wind, solar and tidal. These efforts are aimed at decreasing the world's dependence on fossil fuels and eventually replacing them. Replacing the world's energy supply however, is a long term goal and renewable energy sources currently do not have the capacity or are stable enough to meet global energy demands. On the other side of the problem, researchers and technology manufacturers are working to improve the efficiency of current technologies and develop more energy efficient solutions in order to reduce global energy demand. One of the main contributors to global energy demand is buildings. Studies have shown that the consumption of energy from buildings, both residential and commercial, constitutes between 20% and 40% of global energy consumption in developed countries, and has exceeded the other major sectors: industrial and transportation (Perez-Lombard, Ortiz et al. 2008). In the United Kingdom, the built environment is thought to account for as much as 50% of its total energy requirement (Clarke, Johnstone et al. 2008). Buildings also contribute significantly to carbon emissions with the domestic sector alone in the United Kingdom being responsible for 27% of all UK carbon emissions (Yao and Steemers 2005). This high consumption from buildings can be expected since people spend most of their time indoors be it at work, at home or shopping etc. The internal comfort conditions (indoor air quality, air temperature, lighting etc.) of these indoor

spaces therefore have to be controlled in order to ensure occupants comfort and health. People's demands for indoor thermal comfort, considered a luxury not long ago, have risen over the past few decades and a comfortable indoor environment has become a basic expectation, regardless of the outside environmental conditions (ASHRAE 2009). Indoor comfort conditions are largely dependent on these key factors; thermal conditions, indoor air quality, acoustic conditions and lighting conditions (Khalid 2011). In recent times, there has been increased interest in the development of more energy efficient and sophisticated technologies for climate adaptive buildings in order to achieve improved control of comfort and energy savings (Wang 2010). Some of the developed technologies are listed below (Khalid 2011):

- Passive stack ventilation
- Chilled beams and Under-floor heating
- Sun-shading /louvers
- Waste heat and ground pump heat exchangers
- Heat stores such as roof ponds and Michel-Trombe walls
- Natural light shelves and automatic lighting
- Phase change material walls

With the advent of these new technologies, climate adaptive buildings have the ability to actively adapt to changes in the environmental conditions by changing their characteristics and properties accordingly, in order to maintain the desired comfort levels (Wigginton and Harris 2002). Despite this increased flexibility, many climate adaptive buildings fail to exploit the potential of their advanced systems, often underperforming with regard to improved comfort and energy savings. This underperformance can often be attributed to poor control of equipment and the development of faults (Salsbury 2005).

Studies indicate that controlling indoor thermal comfort conditions proves to be the costliest and most energy consuming aspect of regulating indoor comfort levels, as heating, ventilation and air conditioning (HVAC) systems are the largest energy end use both in the residential and non-residential sectors (Perez-Lombard, Ortiz et

al. 2008). Energy consumption figures for different energy end uses in buildings are shown in the tables below:

End uses in the residential sector (%)	Spain	EU	USA	UK
Space conditioning	42	68	53	62
Domestic hot water (DHW)	26	14	17	22
Lighting and appliances	32	18	30	16

Table 1-1: Energy consumption by end uses in the residential sector

Year 2003. Source EIA, IDEA and BRE - cited by (Perez-Lombard, Ortiz et al. 2008)

Energy end uses	USA (%)	UK (%)	Spain (%)
HVAC	48	55	52
Lighting	22	17	33
Equipment (appliances)	13	5	10
DHW	4	10	-
Food preparation	1	5	-
Refrigeration	3	5	-
Others	10	4	5

Table 1-2: Energy consumption in offices by end use

Sources: EIA, IDEA and BRE - cited by (Perez-Lombard, Ortiz et al. 2008)

The consumption figures clearly indicate that HVAC systems are the largest consumers of energy in buildings; both domestic and non-domestic. In light of this, improving the efficiency of HVAC systems can be considered a logical step towards reducing overall energy demand.

1.1 The HVAC Control Problem

Designing an effective Building Energy Management System (BEMS) to achieve accurate and efficient control of the indoor conditions of a building is a complex task, particularly with the increasingly sophisticated designs, materials as well as advanced HVAC systems found in modern climate adaptive buildings. These

buildings are complex dynamic systems that are subjected to many disturbances and are uncertain in nature. Adding to this complexity is the many systems within the buildings with differing time constants whose dynamics are strongly coupled. This means that changing one parameter can have unforeseen consequences on other parameters (Clarke 2001). This coupling effect makes it difficult to control the buildings indoor environment. The control problem is exacerbated by the improved air tightness and insulation of modern buildings which make the indoor comfort conditions even more dynamic and sensitive [(CIBSE 1998), (BRE-SAP 2005) Table S7, (EST 2004) cited by (Khalid 2011)]. Therefore, the indoor environment of these buildings must be controlled effectively, as poor control can lead to conditions that are unpleasant for occupants and which, in extreme cases, can be detrimental to their health [(McMullan 2007), (Hanie and Aryan 2010)].

The amount of energy used in the process of controlling internal thermal conditions is dependent on two factors: the efficiency of the HVAC delivery systems e.g. heater efficiency, under floor heating etc. and the efficiency/efficacy of the HVAC automation system i.e. control systems. The simple control systems which are still widely used in the buildings industry are often unable to cope with the aforementioned complex dynamics of buildings. A substantial amount of energy is wasted as a result of these poor control systems which cause unnecessary heating, fabric and ventilation losses**.** Furthermore, in addition to the obvious negative financial implication of the wasted energy caused by poor control, an uncomfortable or unpleasant indoor environment in the work place (attributed to poor control) has also been associated with reduced productivity of employees (Lomonaco and Miller 1997). This means that poor control of the indoor environment can have a dual financial impact on a company. The control methods currently in use in the buildings industry are typically restricted in their design to Proportional-Integral-Derivative (PID) control, as in many other industrial applications. This strategy is commonly used in industry on account of its simplicity, ease of commissioning and relatively low capital cost. PID control produces satisfactory results in many cases where system complexity is limited and performance requirements are not too demanding (Åström and Hägglund 2001). However, due to the aforementioned complexity of HVAC systems, it is often difficult for traditional PID controllers to compensate

fully for load disturbances and to achieve accurate set point tracking in HVAC systems. Furthermore, finding the optimal gains for traditional PID designs can be difficult, time consuming and consequently be an expensive process particularly if re-tuning is required, as is often the case in large HVAC systems (Bi, Cai et al. 2000). Even if the PID controller has been well tuned at its commissioning, the changes in operating conditions and structural degradation that occurs over time in buildings may cause the controller performance to deteriorate (Bai and Zhang 2007). Therefore, despite the relatively low initial investment required, the subsequent running costs which are incurred in the long term can be far greater than those associated with improved control strategies.

In contrast to conventional energy reduction techniques e.g. the installation of new HVAC systems and insulation which can require a large investment, significant energy savings can be made with minimal additional cost by improving a building's control systems (Siroky, Oldewurtel et al. 2011). Consequently, there have been significant efforts in recent years to develop HVAC control strategies which improve energy efficiency and thermal comfort. A number of advanced controllers have been developed based on fuzzy logic [(Pal and Mudi 2008); (Soyguder and Alli 2009)], neural networks [(Guo, Song et al. 2007); (Soyguder and Alli 2009; Moon and Kim 2010)], and model predictive control [(Huang, Wang et al. 2009); (Huang and Wang 2008); (Hazyuk, Ghiaus et al. 2012)]. Despite these efforts however, the buildings industry has been slow to adopt advanced control strategies as replacements for PID (Salsbury 2005). There are a number of contributing factors to this; firstly, there is no explicit stability assessment criterion established for adaptive fuzzy logic methods; robustness can be difficult to guarantee, especially for the non-linear methods, when subjected to the parameter uncertainty and disturbances that can occur in building systems (Khalid 2011); methods that require the specification of additional parameters resulting in an increase in set-up time are considered impractical in industry; some of the advanced methods that have been developed can be too computationally intensive for the type of low-cost hardware used in buildings; finally, the buildings industry is generally reluctant to adopt methods that may have to be treated as 'black box' as they are difficult to guarantee stability with and don't

always behave well when faced with actuator saturation (Khalid 2011). Therefore, PID controllers are still widely used in the buildings industry.

1.2 Problem Summary

The increased emphasis that is being put on energy efficiency and reduction of carbon emissions and increased importance of comfort and energy savings to building designers and occupants has driven the development of more efficient building technologies. This has led to building control engineers and researchers developing more advanced and efficient control strategies in attempts to maximize the potential of these technologies and improve the efficiency of existing technologies. The buildings industry has been slow to adopt these advanced control strategies however, due to complexity issues or increases in cost and commissioning time. In light of the discussion in the previous section, it is clear that in order to bridge the gap between advanced controller design and the buildings industry, the controller designs should remain low cost and simple to implement. It can be said then that, ultimately, the objective for the design of a HVAC controller is a robust high performance controller that is easy to implement, requires minimal user input and has low implementation and installation costs i.e. does not require extra/excessive costly hardware. The research presented in this thesis is focused on this problem and delivers solutions that satisfy these criteria.

1.3 Research Objectives

The objective of the research undertaken during this PhD project, as mentioned in the previous section, was to design a robust high performance HVAC control strategy that is capable of dealing with the complexities associated with modern building control whilst being a low cost solution which is easy to implement. This is a very broad aim which can be broken down into a number of more specific objectives. When designing a HVAC control system, a number of difficulties are encountered which the control system must be able to deal with in order to ensure accurate set-point tracking (thermal comfort) and efficient energy usage. These issues are:

- **Parameter uncertainty** – It is often difficult to determine certain building parameters exactly e.g. heat transfer coefficients, air mass and surface areas etc. These parameters may also change over time due to factors such as building fabric degradation and changes in room layout and uses. Therefore, control systems must be designed to be robust against these uncertainties.
- **Nonlinearity** – If a plant is nonlinear i.e. the response characteristics change with operating conditions, the control system must be able to account for these changes and maintain accurate and stable tracking.
- **Tuning/Re-tuning** – Finding the optimal gains for a control system can be a difficult and tedious process in practice and it has been the subject of a great deal of research in HVAC systems. Some control systems may also have to be re-tuned in certain circumstances, such as seasonal climate changes. This can prove costly as re-tuning fees accrue over time.
- **Disturbance rejection** – Buildings are subjected to many disturbances such as heat gains from occupants and IT equipment, or opening and closing of doors etc. Control systems must be able to reject these disturbances effectively in order to maintain adequate thermal comfort for occupants
- **Actuator power limitations** – When an actuator reaches its maximum or minimum power limit, poorly designed control systems can damage the actuation system either by driving the actuator further such that it is locked on its limit for prolonged periods of time or entering into a state known as a limit cycle. This is when the control system causes the actuator to repeatedly oscillate between its upper and lower limits.
- **Decoupling of MIMO system**s – As mentioned earlier, buildings are complex systems with multiple inputs and outputs with strongly coupled dynamics. This coupling can cause severe degradation in controller performance if not dealt with correctly. Many single-input-single-output (SISO) controller designs currently employed in industry fail to account for coupled dynamics and can result in poor thermal comfort and inefficient energy usage.
- **Time delay** – Buildings often have large transport lag as a result of the time taken for energy to be transferred and its effects to be recognized by the

measurement sensors. Time delays in systems can cause severe degradation in controller performance if not dealt with properly and are often one of the reasons for poor controller performance in many practical systems.

From a practical standpoint, the control system must be able to deal with the abovementioned issues while at the same time remaining simple to use and implement i.e. no additional user input and extra commissioning time required. Furthermore, the control algorithm should not be computationally intensive so as to allow for implementation on the low cost hardware that is currently being used in industry.

1.4 Thesis Outline and Methodology

A detailed review of the literature pertaining to the research in this thesis is given in chapter 2 of this thesis. The literature review sets the applicability and context of this research by assessing the relevant control techniques developed in the literature and highlighting their advantages and disadvantages.

Details of the mathematical model of the zone and air-handling unit that were developed and used for the testing of all of the control strategies developed in this thesis are given in chapter 3.

A description of the fundamentals of the robust high performance control theory, Robust Inverse Dynamics Estimation (RIDE), which provides the basis of many of the algorithms developed in this thesis, is given in Chapter 4. The fundamentals of this algorithm are used extensively in this research and therefore it is imperative that the reader is familiarized with its key properties in order to clarify the developments and contributions of this thesis.

Chapter 5 then goes on to explain the development of a high performance MIMO HVAC controller for temperature and humidity regulation, which is robust against parameter uncertainty, using a novel auto-tuning algorithm for the RIDE controller. This method is applied to a zone model with a fast acting direct heater and mechanical ventilation.

A novel Nonlinear Inverse Dynamics (NID) controller design for temperature and humidity regulation of a zone with an air-handling unit (AHU) actuation system is demonstrated in Chapter 6. This includes the development of a novel system identification method for the NID controller and its application to the zone and AHU, a novel dead-time compensation method for the NID controller and a novel commutation law for governing the behaviour of the system at actuator power limits.

Finally, chapter 7 details the conclusions drawn from the presented research and suggestions for future research directions are made.

1.5 Main Novelties/Contributions

The main contributions of the research presented in this thesis can be summarized as follows:

- Development of a mathematical model of a building with a full AHU actuation system using models developed in (Murphy 2012) and (Tashtoush, Molhim et al. 2005).

- Development of a novel auto-tuning algorithm for the RIDE controller with robustness for parameter uncertainty using Genetic Algorithm optimization.

- Novel use of the RIDE algorithm in a two loop control structure for building zone control with AHU inner control loop.

- Novel system identification based NID controller strategy using system identification from step response for inverse dynamics estimation and transport lag compensation.

- Development of a novel improved commutation law for governing the behaviour of equivalent control based controllers SI-RCID and RIDE.

- Contribution of knowledge providing valuable insight and explanation of the effects of large time delays on equivalent control based controller designs.

- Design of a novel transport lag/dead time compensation method for an equivalent control based NID controller using modified smith's predictor principle.

- Presentation of a full methodology for designing a low cost controller which is simple to implement and is capable of dealing with time delay, parameter uncertainty, nonlinearity, interacting MIMO systems, unknown system parameters (identification) and tuning/re-tuning.

- Novel application of inverse dynamics to HVAC systems using a practical approach for designing full HVAC system and zone control.

1.6 Dissemination of Research Contributions

Throughout this research an effort has been made by the author in order to help convey the ideas and methodologies proposed in this thesis to a variety of different audiences through both peer reviewed publications and presentations. The publications made throughout the duration of the author's research are listed below:

1.6.1 Publications

Counsell J., Zaher O., Brindley J., and Murphy G. (2013), Robust Nonlinear HVAC Systems Control With Evolutionary Optimisation, Special Issue - Computational Methods in Engineering Design and Optimisation, J. of Engineering Computations

Brindley, J., Counsell, J., Zaher, O., and Pearce, J. G. (2012), Design and simulation of a non-linear, discontinuous, flight control system using rate actuated inverse dynamics, Proceedings of the Institution of Mechanical Engineers, Part G: Journal of Aerospace Engineering. ISSN 0954-4100 (In Press)

Zaher O., Counsell J., and Brindley J. (2011), Robust Control of Room Temperature and Relative Humidity using Advanced Nonlinear Inverse Dynamics and Evolutionary Optimisation, in Nineth International Eurogen Conference September 2011, Capua, Italy.

Counsell J. M., Zaher O., and Brindley J. (2010), Auto-Tuning for High Performance Autopilot Design Using Robust Inverse Dynamics Estimation, International Multi-conference on Computing in the Global Information Technology, 10-17.

Brindley, Joseph and Counsell, John and Zaher, Obadah Samir (2010), Design of a non-linear missile autopilot design using Rate Actuated Inverse Dynamics (RAID). In: AIAA Guidance, Navigation and Control Conference, 2010-08-02 - 2010-08-05, Toronto, Canada.

1.7 Chapter References

ASHRAE (2009). ASHRAE Handbook: Fundamentals, ASHRAE Inc.

Åström, K. J. and T. Hägglund (2001). "The future of PID control." Control Engineering Practice **9**(11): 1163-1175.

Bai, J. B. and X. S. Zhang (2007). "A new adaptive PI controller and its application in HVAC systems." Energy Conversion and Management **48**(4): 1043-1054.

Bi, Q., W. J. Cai, et al. (2000). "Advanced controller auto-tuning and its application in HVAC systems." Control Engineering Practice **8**(6): 633-644.

BRE-SAP (2005). Standard Assessment Procedure for Energy Rating of Dwellings. Compliance Method, Building Research Establishment.

CIBSE (1998). Building Energy and Environmental Modelling. Applications Manual 11. London, CIBSE.

Clarke, J. A. (2001). Energy Simulation in Building Design. Oxford, Butterworth - Heinemann.

Clarke, J. A., C. M. Johnstone, et al. (2008). "The role of built environment energy efficiency in a sustainable UK energy economy." Energy Policy **36**(12): 4605-4609.

EST, E. S. T. (2004). CE84 Energy efficiency best practice in housing Scotland: Asessing U values of existing housing, BRE/ EST.

Guo, C. Y., Q. Song, et al. (2007). "A neural network assisted cascade control system for air handling unit." Ieee Transactions on Industrial Electronics **54**(1): 620-628.

Hanie, O. and A. Aryan (2010). "Understanding the Importance of Sustainable Buildings in Occupants Environmental Health and Comfort." Journal of Sustainable Development **3**(2): 194-200.

Hazyuk, I., C. Ghiaus, et al. (2012). "Optimal temperature control of intermittently heated buildings using Model Predictive Control: Part II - Control algorithm." Building and Environment **51**: 388-394.

Huang, G. S. and S. W. Wang (2008). "Two-loop robust model predictive control for the temperature control of air-handling units." Hvac&R Research **14**(4): 565-580.

Huang, G. S., S. W. Wang, et al. (2009). "A robust model predictive control strategy for improving the control performance of air-conditioning systems." Energy Conversion and Management **50**(10): 2650-2658.

Khalid, Y. A. (2011). Controllability of Building Systems. PhD, University of Strathclyde.

Lomonaco, C. and D. Miller (1997). "Environmental Satisfaction, Personal Control and the Positive Correlation to Increased Productivity." Johnson Controls, Inc.

McMullan, R. (2007). Environmental Science in Building, Palgrave Macmillan.

Moon, J. W. and J. J. Kim (2010). "ANN-based thermal control models for residential buildings." Building and Environment **45**(7): 1612-1625.

Murphy, G. B. (2012). Inverse Dynamics based Energy Assessment and Simulation. PhD, University of Stratchlyde.

Pal, A. and R. Mudi (2008). "Self-tuning fuzzy PI controller and its application to HVAC systems." International Journal of Computational Cognition **6**(1): 25-30.

Perez-Lombard, L., J. Ortiz, et al. (2008). "A review on buildings energy consumption information." Energy and Buildings **40**(3): 394-398.

Salsbury, T. I. (2005). A survey of control technologies in the building automation industry. International Federation of Automatic Control World Congress, Prague.

Siroky, J., F. Oldewurtel, et al. (2011). "Experimental analysis of model predictive control for an energy efficient building heating system." Applied Energy **88**(9): 3079-3087.

Soyguder, S. and H. Alli (2009). "An expert system for the humidity and temperature control in HVAC systems using ANFIS and optimization with Fuzzy Modeling Approach." Energy and Buildings **41**(8): 814-822.

Tashtoush, B., M. Molhim, et al. (2005). "Dynamic model of an HVAC system for control analysis." Energy **30**(10): 1729-1745.

Wang, S. (2010). Intelligent Buildings and Building Automation, Spon Press: ISBN 0203890817.

Wigginton, M. and J. Harris (2002). Intelligent Skins. Oxford, Architectural Press.

Yao, R. and K. Steemers (2005). "A method of formulating energy load profile for domestic buildings in the UK." Energy and Buildings **37**(6): 663-671.

2. Review of Works in the HVAC Controls Literature

When regulating internal building thermal conditions, there are typically three parameters which are controlled: air temperature, relative humidity and CO_2 concentration. The development of automated control solutions for regulating these comfort parameters has been an on-going problem for a few decades now. Building control systems are often designed to regulate two of these parameters, most commonly zone air temperature and zone relative humidity. The regulation of these parameters can be considered as two processes: regulation of the HVAC systems and regulation of the zone thermal comfort, as shown in Figure 2.1. Ultimately, the aim is to regulate the zone thermal comfort and the regulation of the HVAC systems within is a means to achieving this. Firstly, let us consider the regulation of the zone thermal comfort. If the inputs and outputs of this process are considered, then the inputs to the process are the output conditions of the HVAC system supply air i.e. the heat and humidity transferred to the zone from the HVAC system. The outputs of the process are the zone air temperature and the relative humidity of the zone air. In order to achieve the desired zone thermal comfort, the outputs of the HVAC system i.e. the inputs to the zone control process must be controlled. The inputs to the HVAC system control process are typically the heating, fan or humidifier power etc. required to control the properties of the supply air.

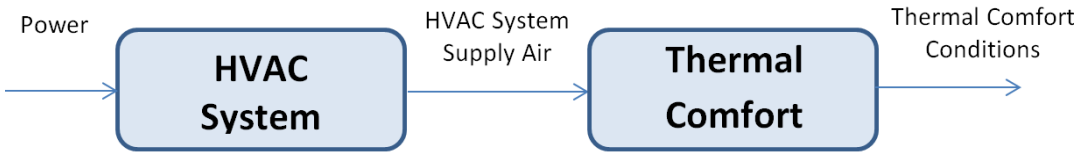

Figure 2.1: Thermal Comfort Regulation Process

As mentioned in the previous chapter, both of these processes are typically complex nonlinear and multivariable processes with strongly coupled dynamics. The development of control solutions for the regulation of both of these processes has been the subject of significant research efforts for many years. Most methods found in the literature focus on tackling the control problem for one of these processes i.e. either HVAC control systems or zone control systems. The research presented in this

thesis addresses the control challenge presented by both the regulation of HVAC systems output and zone thermal comfort.

2.1 Building Control Systems Overview

The concept of automated building control systems was introduced with the aim of reducing energy consumption (Dounis and Caraiscos 2009). Initially, thermostats with only two states, on or off, were used to control air temperature in buildings. This type of control system is commonly referred to as bang-bang control. These thermostats however, gave rise to frequent alterations between the two states, consequently leading to the development of bang-bang thermostats with a dead zone in order to overcome this issue (Dounis and Caraiscos 2009). The bang-bang control scheme was observed to be inefficient however, with large overshoots occurring and poor set point tracking in general causing excessive energy consumption. Therefore, control systems designers began using PID controllers in an attempt to alleviate the issues encountered with bang-bang control [(Levermore 1992); (Dounis, Bruant et al. 1996)]. Despite the improved performance that could be achieved with these controllers, the performance of fixed gain PID control systems was found to be very sensitive to the selection of the gain values. Poorly tuned PID controllers, could result in poor performance and potentially make the whole system unstable (Dounis and Caraiscos 2009).

With the emphasis on energy efficiency increasing over time and occupants demands for thermal comfort rising, substantial research efforts have been directed towards the development of improved building automation strategies. Control engineers have made significant advancements with optimal, predictive, adaptive and intelligent control techniques. Generally speaking, the advancements in HVAC control strategies utilise four main techniques: Adaptive/Self-Tuning control, Fuzzy Logic Control (FLC), Artificial Neural Networks (ANNs) and Model Predictive Control (MPC). These techniques are often used to augment PID controllers. Some control strategies also utilise a combination of the techniques e.g. Neuro-Fuzzy controllers and adaptive Fuzzy controllers.

As mentioned previously, the control methods developed in this thesis focus on a method that is highly effective whilst being simple to use and implement and which would be low cost both financially and computationally. The subsequent sections in this chapter will provide an overview of the various methods that have been developed for designing building control systems. This review is by no means exhaustive however it provides a good indication of the research that has taken place in the literature, with an emphasis on the research that is most relevant to the methods presented in this thesis.

2.2 Conventional Control Systems in Buildings

PID controllers are used extensively in the buildings industry, as in many industrial applications, and can be considered to be the most common control method. The simple design and low cost associated with PID controllers as well as the numerous PID tuning methods available make them desirable in industry. At a given operating point, a PID controller can be tuned manually to achieve the desired closed loop response using prior knowledge of an AHU's characteristics. The Zeigler-Nichols tuning method is a well-known approach that was commonly used to tune the parameters of PID controllers. In reality, the operating conditions of most systems will vary with time due to changes in the environment. Manually tuned PID controllers with fixed gains are unable to deal with the complexities and variations in the dynamics of buildings and their HVAC systems, often leading to inadequate performance. Furthermore, the manual tuning process for PID controllers can be difficult and tedious for complex systems. This led to the developments of new tuning strategies and advancements for PID controllers in attempts to improve system performance.

Geng and Geary (1993) investigated the effects of disturbances and process time delays on controller performance. Load disturbances were approximated by first order models with transport delays and the effects of these disturbances on the overshoot and settling time of the closed loop responses of the system were assessed. Through analysing the relationships between tuning rules based on open loop

parameters and those based on ultimate parameters, they found that the Zeigler-Nichols rules based on ultimate parameters were more conservative than the latter. Based on the modified relationships between the normalised time delay and the ultimate parameters, the authors then generated an improved Zeigler-Nichols set of rules for the design of a PID controller for a HVAC system. The authors state that the refined Zeigler-Nichols tuning rules based on open loop parameters were valid for a small time delay.

Nesler (1986) developed an adaptive PI control scheme. The self-tuning controller consists of five distinct blocks: an auto-tuning routine; an online parameter estimation step using a recursive least squares (RLS) estimator; a controller design block for calculating control parameters; a PI controller; and a performance monitor. The auto-tuning routine provides parameter estimates for a first order plus dead-time (FOPDT) model of the system based on open loop step response data using a batch least-squares algorithm. The RLS estimator provides estimates of the gain, time constant and dead-time of the process model. In order to avoid unnecessary computations and possible miss tuning of the controller due to continuous estimation of parameters, the RLS estimation is halted and reinitiated based on rule-based logic in the performance monitor. In this sense, the controller presented would be considered as a self-tuning controller as opposed to a fully adaptive controller. The results show that satisfactory control is achieved using the self-tuning controller however, when the system is subjected to an un-modelled disturbance, the RLS estimation algorithm diverges and can cause the controller to become unstable. An interesting point to note from this work is that it was observed by the author that HVAC process parameters generally change on a seasonal basis. Therefore, continuous estimation of the HVAC process parameters was considered unnecessary.

Self-tuning and adaptive controllers for HVAC systems with various methodologies for tuning and adaption were researched and developed from a relatively early stage in the HVAC controls literature [(Dexter and Haves 1989); (Dexter, Geng et al. 1990); (Özsoy 1993); (Zhou and Liu 1998)]. The methodology of developing self-tuning and adaptive PID controllers using tuning rules based on

estimated parameters of a FOPDT model also became recognised as an effective and practical method with recent advancements being made with this method in the literature.

Bi, Cai et al. (2000) developed an advanced PID auto-tuning algorithm using the tuning laws developed by (Wang, Hang et al. 1997) and (Wang, Hang et al. 2000) with process identification from step or relay plus step tests for SISO and MIMO processes. The identification method presented in (Bi, Cai et al. 1999) was used. The controller was applied for the control of a HVAC system in industry. The auto-tuner has three different settings; manual control; step or relay plus step test identification and gain calculation; and PID control. The gains are calculated based on the tuning law developed by (Wang, Hang et al. 2000) being applied to the identified process model. For MIMO processes, the identification methods are performed sequentially for each channel. The authors' present improved results using this auto-tuning PID controller compared to a modified Zeigler-Nichols tuning method. Implementation of the auto-tuner is simple and low cost which makes it useful in practice. A limitation of the traditional PID control method used however is that it does not have robustness measures for un-modelled dynamics and changes in plant operating condition over time. Furthermore, the traditional PID controller structure generally requires high gain values in order to reject disturbances effectively. The paper does not present any results showing the disturbance rejection capability of the controller.

Bai and Zhang (2007) use a recursive least squares method with exponential forgetting combined with model matching of a zero frequency method to estimate the parameters of a first order plus dead time (FOPDT) model of the HVAC process. A simple tuning algorithm adjusts the controller gains for a PI controller based on the identified model parameters which are continuously updated using online estimation. The tuning rule however, guarantees stability based on the exact cancellation of the PI controllers zero and the HVAC systems pole using the identified model parameters. The method does not account for inaccuracies in the identification procedure however, which could lead to inexact cancellation. The paper also does not consider the effects that actuator saturation could have on the online

identification procedure which could cause further problems with the pole-zero cancellation. Results are presented comparing the adaptive PI controller developed in this work with a H_∞ adaptive PI controller and a Z-N adaptive PI controller. The presented adaptive PI controller shows an improved response time and less overshoot and oscillations compared with the other methods. The controller shows a similar response to the H_∞ adaptive PI controller when subjected to load disturbances.

Bai, Wang et al. (2008) developed an adaptive Smith predictor-based self-tuning PI controller for an air-conditioning system in a test room. In this method, the parameters of the air conditioning process, including the time delay, are estimated online in the closed loop through the use of a recursive least squares algorithm combined with a z-domain fitting method. The estimated values are then used in two parts of the control system: an adaptive Smith predictor and a self-tuning PI controller. The Smith predictor, which uses a reference model, is constructed based on the estimated time delay in order to diminish the adverse effects of the time delay in the air-conditioning system. Providing the Smith predictor works correctly, such that it removes the effects of the time delay in the system, the self-tuning PI controller is then applied to the time delay free system. The self-tuning PI controller utilises the estimated process values and the predicted error from the Smith predictor in order to determine the control signal of the control loop using integral of time absolute error (ITAE) tuning rules. The authors applied their proposed controller design to a simulation model of an experimental HVAC system and compared its performance with the adaptive PI control strategy presented in (Wang, Lee et al. 1999). The proposed controller produces smaller overshoots than the adaptive PI controller and has a shorter settling time when subjected to a step change and disturbances. The online identification algorithm used was able to identify the process parameters effectively however when the system was subjected to load disturbances, a mismatch between the identified reference model and the real HVAC process would arise.

Qu and Zaheeruddin (2004) developed an adaptive PI control strategy using a recursive least squares method to update the parameters of a FOPDT model

describing the HVAC process. The H_∞ PID tuning rules developed by (Tan, Liu et al. 1998) are then used to update the parameters of the PI controller using the updated model parameters while the system is in closed loop. The authors transform the H_∞ PID tuning rules for continuous-time systems to PI tuning rules for discrete-time systems using the equivalent transform method. The controller was applied to a discharge air temperature (DAT) control system. In the identification results, it is shown that the consideration of the input delay improves the identified model response however it is unclear how the input delay is identified as the authors' state that the delay is assumed to be fixed. A comparison of controller performance is made with an LQR optimal adaptive PI controller. The H_∞ adaptive PI controller produces an improved response to set point changes, displaying slightly less oscillation and overshoot. Results are then shown with the system being subjected to noise and disturbances. The controller is able to reject the disturbances and maintains stable tracking. A limitation of the online identification method used is that it does not consider the effects that actuator saturation could have on the controller performance. The authors also do not show any stability assessment of the system in their methods. The same authors published a more recent article (Qu and Zaheeruddin 2010) showing an experimental study of the application of this method in a variable air volume (VAV) HVAC test facility. Results for several individual tests conducted using set point step changes while the system was subjected to different sets of disturbances are presented. The disturbances included changes in airflow rates, zone cooling loads and temperature of chilled water. The performance of the authors' proposed controller design was compared with a constant gain PI controller. The results show an improved response over the constant gain PI controller as the H_∞ adaptive PI controller was able to stabilize an oscillatory output from the DAT system and steer it towards steady state. However, the results show that in order for the H_∞ adaptive PI controller to achieve a good response, an accurate estimate of the dead time of the DAT system (within 10%) is required otherwise the response is highly oscillatory.

The benefit of the adaptive/self-tuning methods mentioned above is that they are generally practical in their implementation and straightforward to use. The RLS

optimisation scheme commonly used for online parameter estimation however, suffers from the drawback that the estimator diverges when the control loop is subjected to un-modelled load disturbances. Furthermore, self-tuning control systems do not perform adequately when faced with actuator nonlinearities (Dounis and Caraiscos 2009). It is clear that these methods have the desirable characteristics of simplicity and practicality however they have flaws with regards to robustness and actuator nonlinearities. A method which could retain the simplicity and practicality offered by these methods whilst overcoming their drawbacks would be highly desirable.

Robust control theory addresses the effects that discrepancies between the model and the physical system (model uncertainty) may have on the design and performance of (linear) feedback systems. Robust control provides a unified design approach under which the concepts of gain margin, phase margin, tracking, disturbance rejection and noise rejection are generalized into a single framework. In this method, nonlinearities are considered as uncertainties such that a linear uncertain model can be utilised instead of a nonlinear model. Typically, the uncertainties considered in robust control theory are bounded using norms. Many robust H_∞ control methods have been developed for temperature control of air-handling units to deal with dynamic uncertainties.

Al-Assadi, Patel et al. (2004) present a study on the use of H_∞ performance measures for the design of robust decentralised output feedback control of a HVAC system. The robust decentralised controller is based on the work of Zaheeruddin (Zaheeruddin, Patel et al. 1993). The authors developed a seventh-order bilinear model of a HVAC system and linearized it about an operating point. The model was then expressed in state space format and the transmission zeros of the model determined in order to ensure the stability of the closed loop system. Performance specifications and robust stability for a robust decentralised servomechanism were incorporated within an H_∞ optimisation criterion. The proposed controller design differs from conventional H_∞ design in that it employs a servo-compensator and a constant gain feedback controller as opposed to the higher order controllers

associated with conventional H_∞ designs. The MATLAB Optimisation Toolbox was used to solve the H_∞ optimisation problem. Results show a comparison of the decentralised HVAC control system obtained by minimising a quadratic performance cost function and minimising the H_∞ - norm of the sensitivity function. The H_∞ solution generates a faster response in most cases and reduces the input energy used. The H_∞ solution also achieves improved disturbance attenuation and robustness against model uncertainties.

Anderson, Buehner et al. (2008) investigated the improvements in HVAC system performance that could be achieved using MIMO robust controllers. The authors present three different MIMO controller designs; a "minimal" MIMO robust controller; a "constrained" MIMO robust controller; and a "full" MIMO robust controller. These control systems were designed and tested on a simulation model of a HVAC system and then applied in practice to an experimental HVAC system. The HVAC system had five variables which could be regulated: water supply temperature, mass flow rate of water through the coil, air temperature entering the coil, air flow rate and temperature of the supply air. The "minimal" MIMO setup consisted of; a MIMO controller tracking two reference signals; a SISO PI controller; two free control variables. The "constrained" and "full" MIMO setups consist of a MIMO controller tracking four reference signals and one free control variable. The "full" MIMO controller differs from the others in that it requires a separate water supply for each discharge air system (DAS) as opposed to a shared supply. These three controllers are compared to a traditional SISO PI controller setup consisting of three SISO PI control loops tracking three reference signals. All three MIMO controllers were designed using a H_∞ robust controller philosophy which required the experimental system model to be represented in canonical form. The results show that the "full" MIMO controller achieves the best controller performance however it would not economically feasible to have an independent water supply for each DAS. The "minimal" and "constrained" controllers achieve a significantly improved performance in settling times and disturbance rejection over the PI controller setup. In this work, the authors stress the importance of robust controller design for dealing with discrepancies between the model and the physical system due to approximation,

neglected or un-modelled dynamics, unknown parameters or even sensor and actuator imperfections.

The main challenge with H_∞ robust control design is the selection of the control parameters, including model uncertainty weights and optimization criteria weights, which constitute the main part of the controller design. Although robust H_∞ control deals with uncertainties directly, the associated constraints in the HVAC processes are not taken into account and could potentially lead to negative effects on the robustness and stability of the controlled system (Huang and Wang 2008).

2.3 Model Predictive Control

Important research has been conducted on model predictive controller (MPC) methods for HVAC control systems. MPC methods use a model of the process which includes a model for future disturbances in order to anticipate the behaviour of the building during a finite horizon and calculate the necessary control action accordingly. The control input is computed through the minimization of a cost function which is based on the model of the system. Typically, the cost function consists of two terms; one that includes the prediction error and another that includes the control effort. The anticipative effect of MPC methods is helpful in improving thermal comfort by reducing overheating and under-heating, particularly in the transitional periods between inoccupation and occupation (Morosan, Bourdais et al. 2010). If the heating of a building at the beginning of the day is considered as an example, the dynamics of the heating system can be accounted for using the MPC method and the zone can be heated up to the desired temperature by the time the zone occupation begins as opposed to heating the zone after the zone occupation has already begun. This is illustrated in Figure 2.2. Many MPC methods have been applied to HVAC systems with various cost function designs modifications (Naidu and Rieger 2011).

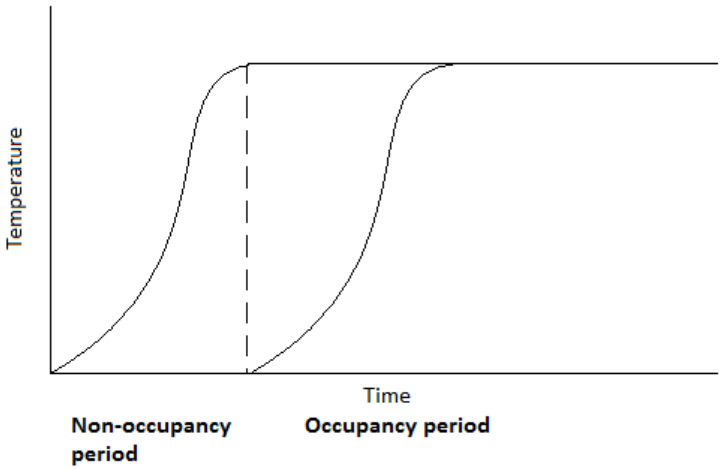

Figure 2.2: Anticipative effect of MPC approach

Huang, Wang et al. (2009) present a robust model predictive control (MPC) strategy for supply air temperature control of an air-handling unit. A FOPDT model with uncertain time delay and system gain is used to describe the process of the air-handling unit. The uncertainties in the time delay and system gain are formulated using an uncertainty polytope and an offline LMI (linear matrix inequalities) based robust model predictive control algorithm is used to design a robust controller for the air-handling unit. The performance of the controller is evaluated on a simulated HVAC system in hot summer and cool winter conditions and its performance compared with a conventional PID control algorithm. In the hot summer conditions, the proposed controller shows less overshoot in its step response, however the response time is slower than that of the PID controller. In the winter conditions the proposed controller displays a faster response than the PID controller. In both cases, the PID controller and the proposed controller achieve accurate set point tracking. The proposed controller also demonstrates improved disturbance rejection over the PID controller.

Morosan, Bourdais et al. (2010) proposed a model predictive control structure for temperature regulation in buildings. The authors show that a drawback of common MPC strategies is that, due to the requirement of a set point during periods of inoccupation, the comfort level may be decreased during the beginning and end of the occupation period. A new cost function for the model predictive controller which

incorporates the future occupation profile of the zone as the error weighting term is proposed in order to allow for the removal of the set point during inoccupation periods. The cost function also minimises the energy consumption. The MPC strategy was applied to a single-zone and multi-zone building model. Comparisons were made with a decentralized PI controller and a centralized MPC method. The results show a reduction in overshoot in comparison with the decentralised PI controller. The centralised MPC method produces a very similar response to the proposed distributed MPC method however the proposed method is less computationally demanding. The distributed MPC strategy also reduces the energy consumption over the simulation period in comparison to the other methods tested. A drawback of this method however, is that an accurate model of the system is required in order for the control law to be determined effectively. The control law is also reliant on knowledge of the future occupation profile.

Siroky, Oldewurtel et al. (2011) developed a model predictive controller which uses weather predictions for a building heating system. The framework of the MPC controller consists of a finite horizon optimisation problem. The cost function accounts for stability and the performance targets, which are to minimise the energy cost while respecting comfort constraints. The comfort requirements are specified as a minimum desired temperature of 22°C during the day and 19°C at night and during the weekends. The authors deal with the minimum temperature requirement by penalising the displacement below the reference trajectory in the optimisation criterion. A linear model of the building is used to represent the building dynamics in the MPC controller. The proposed controller was tested for two months in a real building in Prague, Czech Republic. A cross comparison study is performed using the proposed controller and a heating curve controller on two similar building blocks for one week. The controllers are then switched round for another week. Another comparison was based on the use of heating degree days (HDD) for the normalisation of the building energy consumption. HDD is a quantitative index designed to reflect the demand for energy needed to heat a building. The MPC strategy achieved a significant reduction in energy requirement peaks over the compared control method. The energy savings achieved using the MPC strategy was

in the range of 15-28% depending on various factors, mainly insulation level and outside temperature. It is interesting to note that the authors recognise that the implementation of the MPC strategy would be difficult in practice. However they believe that, due to the potential energy savings, the method could be adopted in the future.

Hazyuk, Ghiaus et al. (2012) propose a MPC controller for temperature regulation of intermittently heated buildings. The controller is based on a new cost function which minimises the energy consumption whilst maintaining the thermal comfort in the building. In order to allow for the cost function to be solved by the linear programming method, the cost function is linear and subjected to linear constraints. These constraints bound the command input in the feasible range of the heating system. The authors state that, in their proposed controller, it is assumed that the maximal value of the command input is large enough to ensure the minimal comfort temperature. In reality, this is not always the case. A linear dynamic model of the nonlinear water-based heating system was obtained by considering the heat flux of the radiator as the controlled input and then, using a linearization method suggested by the authors, a linear model which is valid for the entire operating range is derived. This is achieved by representing the system as a linear dynamic model and a separate static nonlinearity. By passing the command calculated by the controller through the inverse function of the system nonlinearity, the nonlinearity of the model is compensated for and the controller performs as if the system were linear. Simulation results showing a comparison of the proposed MPC method against an MPC controller obtained using a conventional locally linearized building model are presented. On certain days, the proposed controller is able to achieve an improved performance due to the locally linearized method being outside of the validity range of the linearized model.

The main drawback of MPC methods is the potential model mismatch which can cause the predictive controller to produce an incorrect control signal. Many MPC methods also rely on accurate predictions of weather and disturbances which in reality may not be available. Robust MPC strategies aim to eliminate this drawback,

however, in order to ensure robust stability, extra constraints may be required (Mayne, Rawlings et al. 2000). These are not easy to determine and therefore may cause robust MPC strategies to be considered impractical in industry (Huang and Wang 2008).

2.4 Artificial Intelligence Control Techniques in HVAC Systems

Artificial intelligence (AI) techniques such as artificial neural networks (ANNs) and fuzzy logic control (FLC) possess attractive properties which have gained them significant interest as alternative methods for building control systems. ANNs have a strong ability to capture nonlinear models which can then be used as part of the controller design process. This makes them desirable for use with nonlinear HVAC control systems. FLC has become particularly popular in the HVAC research field due to its ability to deal with uncertainties in a straightforward manner. A number of control methods for buildings which utilise these AI techniques for building control systems can be found in the literature (Dounis and Caraiscos 2009). Some methods also use an overlap of these techniques in order to incorporate the benefits of the different techniques. This section provides an overview of some of the AI control methods which have been developed for HVAC systems in the literature.

2.4.1 Fuzzy Logic Control

Fuzzy logic (FL) is based on human approximate classification and reasoning. It operates using a rule-based system that can rely on the practical experience of an operator. There are three main processes that comprise FL as illustrated in Figure 2.3 (Moon, Jung et al. 2011):

1) Fuzzification (input stage) where a crisp set of input data are gathered and converted to a fuzzy set using fuzzy linguistic variables, fuzzy linguistic terms and membership functions

2) Inference (processing stage) for generating inferred results based on previously fuzzified values and linguistic IF/THEN statements
3) Defuzzification (output stage) for totalling the result using linguistic rules, then converting it to crisp output values.

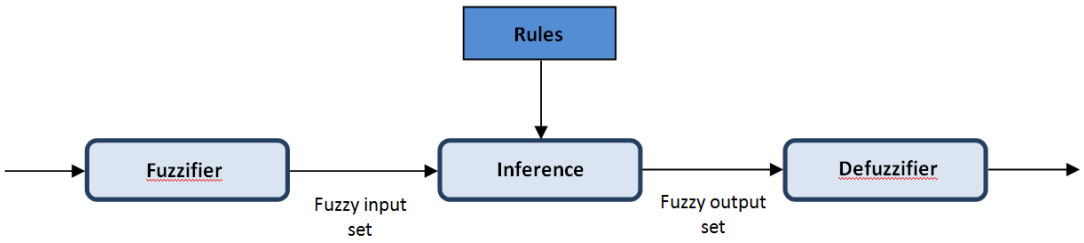

Figure 2.3: **Fuzzy Logic Process**

FL systems are well suited to nonlinear and MIMO systems as well as systems that cannot be modelled easily by conventional means. Therefore, they have gained interest as an attractive alternative to conventional HVAC control systems and have been applied in various HVAC control problems. Many advanced control methods have been developed using fuzzy adaptive control and the combination of fuzzy logic with varying PID control structures. In the latter case, conventional PID controllers are used in conjunction with a set of fuzzy rules and a fuzzy reasoning mechanism to tune the PID gains online (Dounis and Caraiscos 2009). Typically, the fuzzy PI controller is an incremental controller which can be described by the following equation:

$$u(k+1) = u(k) + du(k) \qquad (2.2)$$

Where k is he sampling instance and du(k) is the incremental change in controller output determined by fuzzy rules. A diagram of the structure of a fuzzy PI controller is shown in Figure 2.4.

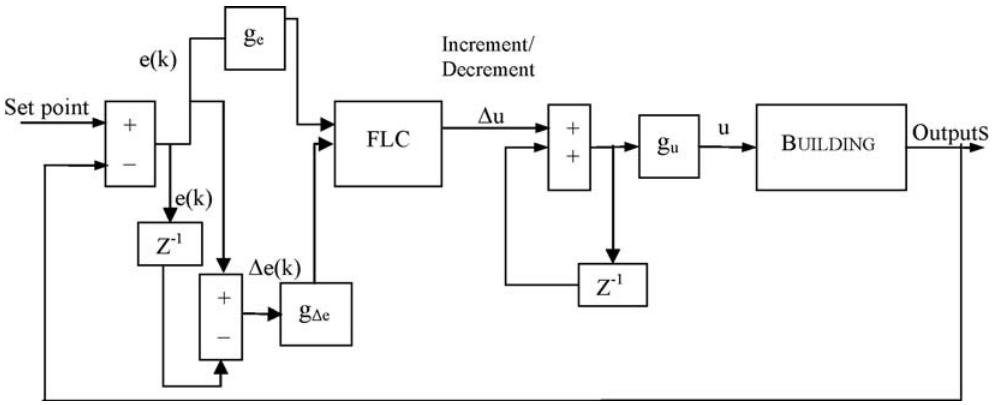

Figure 2.4: **Fuzzy PI Controller Structure (Dounis and Caraiscos 2009)**

Fuzzy PD controllers also exist however they are only applicable to a limited class of systems (Qiao and Mizumoto 1996). They are typically not applicable when sudden load disturbances and measurement noise exist (Dounis and Caraiscos 2009). Fuzzy PID controllers are uncommon due to the associated difficulties in creating an efficient rule base and the large number of parameters that require tuning (Dounis and Caraiscos 2009). Therefore, fuzzy PI controllers are more commonly used. Guzelkaya, Eksin et al. (2003) proposed a new approach for tuning the coefficients of PID-type fuzzy logic controllers (FLCs). A self-organizing fuzzy controller which extends the rule based fuzzy controller with an additional learning capability has also been developed (Kazemian 2001). Woo, Chung et al. (2000) proposed a PID type fuzzy controller with self-tuning scaling factors.

Hongli, Peiyong et al. (2008) proposed a fuzzy logic control strategy for a HVAC system which is designed based on PID gains. A nominal fuzzy controller is designed and the input and output variables of the fuzzy controller are normalized. The output of the fuzzy controller, i.e. the resulting control law, is then rearranged into a conventional PID format and the corresponding coefficients of the error, integral of error and error difference are considered as the proportional, integral and derivative gains respectively. From this relationship the normalized factors of the fuzzy controller can be determined from the PID gains. It is unclear however, which method the authors use for selecting the PID gains. Simulation results show that the authors' method is able to achieve an improved response over a wider operating range in comparison to a conventional fixed gain PID controller. The fuzzy controller

method was also applied to an experimental HVAC system. An improved response time and tracking performance is achieved with the fuzzy controller. A limitation of the method is that there appears to be no explicit stability assessment method for the controller. Furthermore, the fuzzy control law does not account for actuator saturation in that the control action might demand more power from the actuator when it has reached its power limit.

Baek, Kim et al. (2008) developed an adaptive fuzzy output feedback control method for temperature and relative humidity regulation in a nonlinear HVAC system. The controller uses an observer to estimate the systems unknown state variables via which the fuzzy control scheme is formulated. An improved tracking performance is achieved with the proposed method when compared to a controller designed using a classical feedback linearization approach.

Pal and Mudi (2008) developed a self-tuning Fuzzy PI (STFPI) controller for the supply air pressure loop of a HVAC system. The authors use a conventional PI type fuzzy controller in conjunction with a self-tuning mechanism which updates the output scaling factor online using a fuzzy rule base. The rule-base for tuning the output-scaling factor is based on the error and change of error in the controlled variable. The fuzzy controller uses a 7x7 if-then rule matrix for determining the control signal (u) as well as the updating factor for the output scaling factor (β). Triangular fuzzy membership functions were used in the controller. The rule matrices used for the determination of u and β are shown in Table 2-1 and Table 2-2 respectively. The authors chose to apply the self–tuning mechanism to the tuning of the output scaling factor due to its strong influence on the performance and stability of the system.

Δe \ e	NB	NM	NS	ZE	PS	PM	PB
NB	NB	NB	NB	NM	NS	NS	ZE
NM	NB	NM	NM	NM	NS	ZE	PS
NS	NB	NM	NS	NS	ZE	PS	PM
ZE	NB	NM	NS	ZE	PS	PM	PB
PS	NM	NS	ZE	PS	PS	PM	PB
PM	NS	ZE	PS	PM	PM	PM	PB
PB	ZE	PS	PS	PM	PB	PB	PB

Table 2-1: **Fuzzy rules for computation of *u* in (Pal and Mudi 2008)**

Δe \ e	NB	NM	NS	ZE	PS	PM	PB
NB	VB	VB	VB	VB	B	MB	SB
NM	VB	VB	VB	B	MB	SB	S
NS	VB	VB	B	MB	SB	S	VS
ZE	VB	B	MB	SB	S	VS	ZE
PS	B	MB	SB	S	VS	ZE	ZE
PM	MB	SB	S	VS	ZE	ZE	ZE
PB	SB	S	VS	ZE	ZE	ZE	ZE

Table 2-2: **Fuzzy rules for computation of *β* in (Pal and Mudi 2008)**

Where the contents of the tables are linguistic expressions of magnitude: NB (negative big), NM (negative medium), NS (negative small), ZE (zero), PS (positive small), PM (positive medium), PB (positive big). In Table 2-2 the expressions of magnitude are all positive where: VS (very small), S (small), SB (small big), MB (medium big), B (big), VB (very big). The HVAC system was modelled as a second order plus dead time (SOPDT) transfer function and simulation results showing the performance of the STFPI controller under process parameter variations were presented. Under normal operating conditions, the controller displays accurate set point tracking with no overshoot occurring. When the process parameters are varied however, changes in the response characteristics can be observed e.g. overshoots and

slower response times are produced. The process scaling factors used for the STFPI controller are changed for the different process parameter variations. These are determined based on prior knowledge of the process or trial and error. The proposed controller was compared to a PID controller and an adaptive Neuro-Fuzzy (ANF) controller. The STFPI controller shows an improvement over the other controllers tested with respect to peak overshoot and settling time. It would have been interesting however if the authors had presented results showing the controller applied to a nonlinear HVAC plant with actuation power limits.

A self-tuning PID-type fuzzy adaptive controller for an expert HVAC system was presented by Soyguder, Karakose et al. (2009). The auto-adaptive controller is designed using an incremental fuzzy logic controller to tune the parameters of a PID controller. The controller uses the error and error change as inputs for three separate fuzzy rule bases which determine the proportional, integral and derivative gains for a PID controller. Each fuzzy rule base consists of 25 IF-THEN rules and gauss membership functions are used for all variables. The physical domain of the inputs and outputs are selected based on trial and error. The authors use a HVAC system model with two zones to evaluate the performance of their proposed controller design. A comparison is made with a conventional PID controller and a fuzzy-PD controller which uses FL directly to determine the required mass flow rate of cooled air entering the zone. Triangular membership functions are used for the fuzzy-PD controller. The simulation results indicate that the proposed self-tuning PID-type fuzzy adaptive controller outperforms the PID and fuzzy-PD controllers with regards to settling time and steady state error.

Therese and Nair (2012) developed a simplified decoupled self-tuning fuzzy-PI controller in order to eliminate the interaction which occurs between the controlled parameters in MIMO HVAC systems. A decoupling matrix is multiplied by the system matrix in order to create a decoupled process matrix as shown in equation 2.2.

$$\begin{bmatrix} h_{11}(s) & h_{12}(s) \\ h_{21}(s) & h_{22}(s) \end{bmatrix} \begin{bmatrix} 1 & d_{12}(s) \\ d_{21}(s) & 1 \end{bmatrix} = \begin{bmatrix} {h_{11}}^*(s) & 0 \\ 0 & {h_{22}}^*(s) \end{bmatrix} \qquad (2.2)$$

The elements of the decoupling and decoupled process matrices are determined by performing the matrix multiplication, then rearranging and solving the resulting equations symbolically. The simplified decoupling process makes the system internally stable during process interactions by making the individual elements of the decoupling matrix stable. The controller is used to regulate the temperature of a room with two temperature sensors at either side of the room. The temperature of the room is controlled through manipulation of the positions of two dampers on the room ceiling which in turn adjust the rate of cold air entering the room. The system is coupled since altering the position of one damper will have an effect on both temperature sensors. The authors use the self-tuning fuzzy-PI (STFPI) controller proposed by (Pal and Mudi 2008) to control the decoupled HVAC process. A comparison is made between the STFPI controllers with and without decoupling. The presented results show that a significantly less coupled response is obtained with the decoupling controller when subjected to a step change in set point for one temperature sensor and observing the effect on the other temperature sensor. A drawback of this decoupling method however is that accurate knowledge of the process model is assumed as there appears to be no robustness measures in place for dealing with inaccuracies in the process model. Furthermore, one of the main arguments for the use of FL is the non-requirement of a process model, however the method presented here necessitates the use of a process model.

It is clear that the linguistic nature and robustness properties of Fuzzy control make it an attractive method for use with HVAC control systems which can replace conventional PID controllers. However, despite the fact that Fuzzy controllers are typically more robust than conventional PID controllers, the lack of existence of a systematic way of generating control rules for FLCs is a drawback (Huang and Wang 2008). Furthermore, they do not explicitly contain any objective knowledge about the system unless that knowledge can be expressed and/or incorporated into the fuzzy set framework (Yager and Filev 1994).

2.4.2 Artificial Neural Network Control

The artificial neural network (ANN) is a biologically inspired technique which is based on the parallel architecture of the human brain. Analogous to the human brain, an ANN is comprised of a number of interconnected neurons, often referred to as perceptrons. Each neuron in the ANN is a mathematical relationship which aims to replicate the functionality of a biological neuron. The composition of an artificial neuron is illustrated in Figure 2.5.

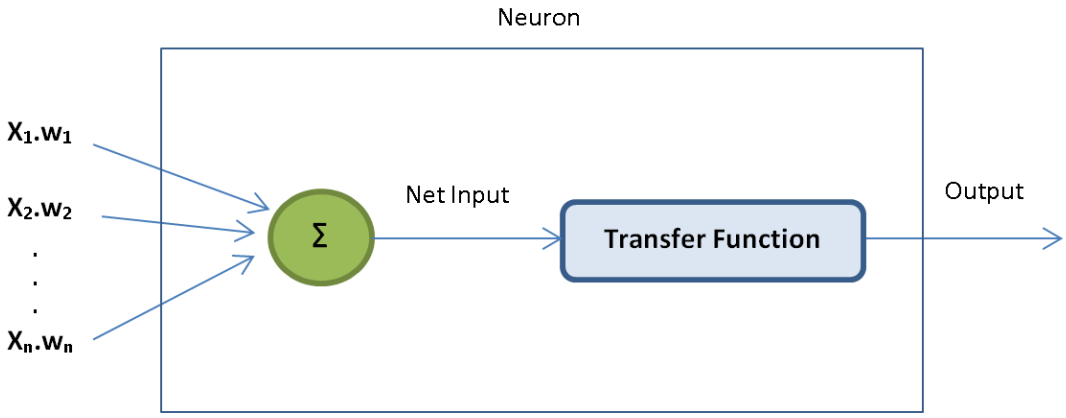

Figure 2.5: **Artificial neuron composition**

In Figure 2.5, $X_1 \ldots X_n$ are the inputs to the neuron and $w_1 \ldots w_n$ are the corresponding weights. Each input to the neuron is multiplied by its corresponding weight, which signifies the strength of the connection. The summation of the inputs modified by the weights is related to the neuron output by a transfer function, typically a sigmoid, tan sigmoid or pure linear relationship. The interconnection of all of the neurons in an ANN provides a powerful non-linear data-processing structure. With this structure, ANNs have the ability to somewhat replicate some functions of a biological neural network such as pattern matching and learning. These abilities prove to be very useful for modelling in applications where obtaining an algorithmic or mathematical model of the system is difficult, however there is access to large amounts of input output data which is representative of the system over a wide operating range. The neurons in an ANN are typically arranged into a number of layers consisting of an

input layer, output layer and any number of hidden layers in between, providing the link between the input and output layers. A typical structure for an ANN is illustrated in Figure 2.6.

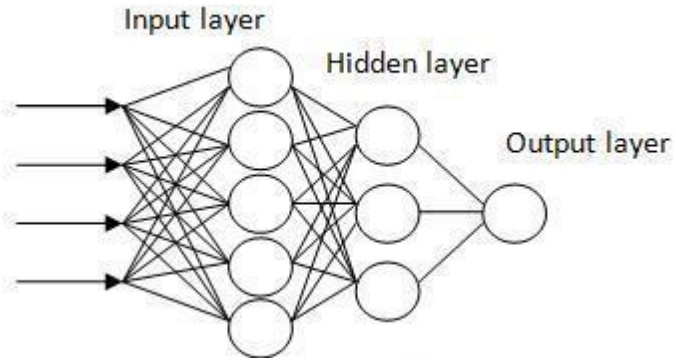

Figure 2.6: **Typical ANN Structure**

The advanced nonlinear modelling capability of ANNs has been recognised as a useful tool for control systems design, particularly for highly nonlinear systems. In ANN based control systems, an ANN is used to capture the nonlinear dynamics of the system and then a control system based on the nonlinear model is created. These control systems are designed to use ANNs in various different setups and structures e.g. direct and indirect, adaptive, combined with PID etc. This section provides an overview of some of the works found in the literature which utilise ANN based control in buildings.

Zaheeruddin and Tudoroiu (2004) explore the use of neural network (NN) based tuning and tracking functions for improving the performance of a PID controller applied to a discharge air temperature system. In this control strategy a three layer feed forward NN is trained on an input-output data set using the error back propagation algorithm. Once the NN is trained, the PID controller gains are output from the hidden layer. The training process can be initiated by arbitrarily assigning values for the PID gain parameters or by computing the gain values using another method such as the Zeigler-Nichols method. The authors state that the convergence of the algorithm is greatly improved if the Z-N method is used. It is also stated that, in order to improve the efficiency of the NN, one of the gain parameters are fixed

and when operating with a full PID controller, a target gain must be specified. A tracking control technique presented by (Anderson and Moore 1990) is adopted in order to eliminate large overshoots with the neuro-PID method. The results using this method show less overshoot, however, the response time is significantly slower with the controller taking more than double the time to reach the set point. This suggests that the gains have been reduced significantly. The extra parameters which must be specified in this method mean that it could be considered impractical for implementation in the buildings industry.

Wang, Zhang et al. (2007) designed a hybrid neural network PID controller and conventional PID controller for the control of a variable frequency air-conditioning system. The NN-PID controller is trained using the back propagation algorithm on the predicted system output and is used for adapting the gains for the PID controller. A conventional PID controller is used to eliminate steady state error which occurs. This hybrid control strategy produces improved results over conventional PID controller alone with regard to changing model parameters due to its ability to adapt the PID gains.

Guo, Song et al. (2007) developed a neural network assisted cascade control system for an air handling unit. The outer loop consists of a NN controller regulating the supply air temperature from the AHU. The inner loop regulates the flow rate of chilled water using a proportional controller. The NN is trained online using a simultaneous perturbation stochastic approximation (SPSA) based algorithm. The authors state that the SPSA based training algorithm guarantees the weight convergence of the NN and stability of the control system. The cascade control scheme was tested on an experimental HVAC system. A comparison of the authors' method was made with a traditional single loop PID controller and a cascade controller with a PI inner loop and PID outer loop controller. The tests show improved results with the NN cascade controller over a traditional single loop PID controller for temperature set point tracking and disturbance rejection for the chilled water flow rate.

Guo and Song (2009) present a neural network assisted PI (NNAPI) control strategy aimed at improving the performance of the air pressure control in a variable air volume (VAV) system. The neural network is trained online using an adaptive dead zone training algorithm which eliminates the requirement of a bounded regression signal to the system and aims to alleviate the problems normally associated with disturbances in the neural network training process. The conic sector theory is used to guarantee stability of the neural network control scheme. The authors apply the proposed method to an experimental VAV air-conditioning system in order to evaluate its performance and compare it to a conventional PI controller. A series of experiments were run with various disturbances and set point changes. The NNAPI controller displays improved disturbance rejection over the PI controller as well as better set point tracking.

An advanced ANN based thermal control method for indoor thermal comfort regulation in residential buildings was proposed by Moon and Kim (2010). The authors developed a control logic framework consisting of four component control logics suing MATLAB and its NN toolbox. This included two predictive and adaptive logics using ANN models to predict future thermal conditions of air temperature, humidity, and predicted mean vote (PMV). The structure of the ANNs used is shown in Figure 2.7.

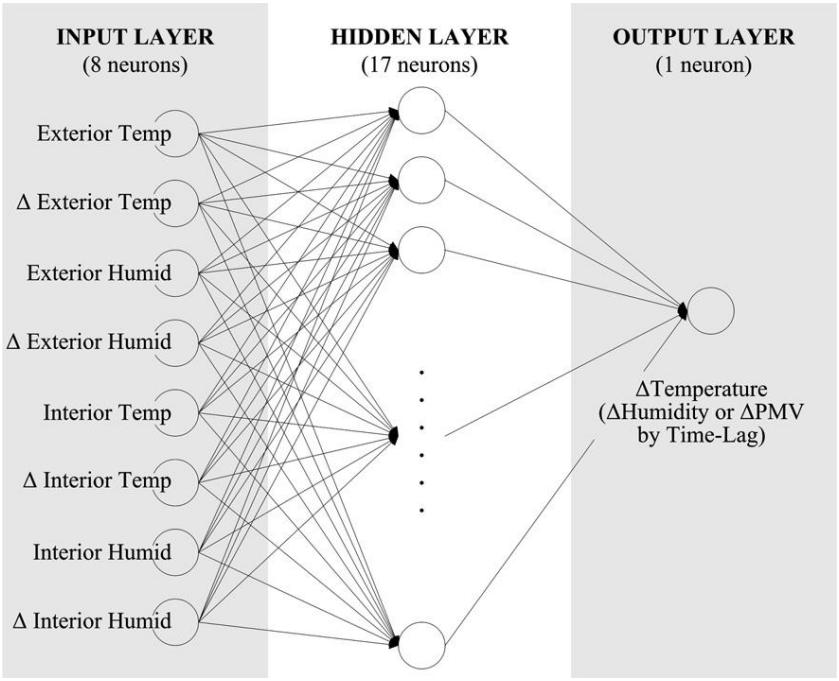

Figure 2.7: **Structure of ANN models used in (Moon and Kim 2010)**

The models were designed to reduce overshoot and undershoot of the controlled variable using the ANN-based predictive and adaptive control as well as achieve indoor thermal comfort by taking into account air temperature, humidity and PMV. The training data sets for the ANNs were obtained in a test chamber and a sliding window method was used for the training algorithm such that the new training data set would be added to the other training data sets and the oldest data set would be removed. The authors modelled a two story single family home in the U.S. by incorporating International Building Physics Toolbox (IBPT) and MATLAB in order to test the performance of their proposed thermal control method. Four different control logics were tested: temperature and humidity control without ANNs; temperature and humidity control with ANNs; PMV control without ANNs; and PMV control with ANNs. The ANN-based predictive and adaptive control logics were able to create more comfortable thermal conditions than the control logics without the ANNs, displaying reduced overshoot and undershoot and increased comfort periods of air temperature, humidity and PMV.

The efficacy of ANNs at modelling nonlinear systems makes them a valuable tool for nonlinear control systems design. The main drawback of neural network

control however, is that gaining information over the full operating range of an AHU necessitates the collection of a large amount of training data, which cannot always be easily obtained in practice. Furthermore, the learning algorithms which must be employed are often complex making the on-line identification process time consuming. Consequently, ANN based controllers can often be considered impractical in industry (Naidu and Rieger 2011).

2.4.3 Neuro-Fuzzy Control

Recently, control methods that incorporate FL with ANNs have been introduced in order to overcome the difficulties associated with developing optimal fuzzy rules whilst maintaining the desirable robustness of FL controllers. The Adaptive Neuro-Fuzzy Inference System (ANFIS) is one of the Neuro-Fuzzy approaches. In order to enable the Fuzzy inference system to track given input/output data, the membership function parameters are tuned using neuro-adaptive learning techniques. The tuning process of membership function parameters is similar to the process of training ANNs i.e. the utilisation of training data sets, which are comprised of input/output data, and a training algorithm such as back propagation. Through this tuning process, the ANFIS aims to obtain the best parameters to produce an optimal response to the given environment. In addition, through the iterative retuning process for adaptation, a global solution is obtainable [(Dounis and Caraiscos 2009); (Krarti 2003)]. A number of Neuro-Fuzzy controllers have been developed for HVAC systems control in the literature. Wu and Cai (2000) designed an Adaptive Neuro-Fuzzy (ANF) controller for the supply air pressure control loop in an HVAC system. A Neuro-Fuzzy Controller (NFC) was designed with the aim of using a smaller number of fuzzy rules leading to savings in computational time by Pal (2008).

Ertunc and Hosoz (2008) performed a comparative study between ANN and ANFIS techniques for the prediction of the performance of an evaporative condenser. An experimental evaporative condenser setup consisting of a copper tube condensing coil with air and water circuit elements was equipped with temperature, pressure and flow rate measurement instrumentation. Experimental data was gathered and used for training the ANN and ANFIS models. The models were then used to predict the

condenser heat rejection rate, refrigerant temperature leaving the condenser as well as the dry and wet bulb temperatures of the leaving air stream. The prediction performances of both modelling techniques were measured in terms of correlation coefficient, mean relative error, root mean square error and absolute fraction of variance. The prediction accuracy of the ANFIS models were observed to be marginally better than those of ANN ones, however the predictions of ANN models also yielded a good statistical performance. The improvement in performance achieved using the ANFIS model can be attributed to the fact that ANFIS combines the learning capabilities of a neural network and reasoning capabilities of fuzzy logic thus improving its prediction capability compared to ANN and FL techniques.

Soyguder and Alli (2009) present an expert system for temperature and humidity control in a HVAC system using Adaptive Neural Fuzzy Interface System (ANFIS) and optimization with a fuzzy modelling approach. A dynamic fuzzy logic control method is used to determine and adapt the gain values for a classical PID controller. The control method was tested on an experimental HVAC system. Input-output data sets for the system were then stored and used to obtain the intelligent model based on the ANFIS approach. This model is used to predict the systems damper gap rates. The ANFIS method uses a multi-layer feed forward network where each node performs a particular function on incoming signals. The adaptive learning parameters of the network are updated using gradient learning rules. The control system is able to track the temperature and relative humidity set points accurately although no comparison is made with an alternative method. Results showing the prediction of the ANFIS model indicate that the authors' approach is able to model the experimental HVAC system well and produce an accurate prediction.

A comparative study between fuzzy, ANFIS and ANN based building thermal control methods was presented by Moon, Jung et al. (2011). The ANFIS and ANN based controllers developed were adaptive methods utilising an iterative self-tuning process during system operation, however the fuzzy–based controller was non-adaptive. A Fuzzy model with two input variables (error and error change) and one output variable (control signal) was developed using the MATLAB Fuzzy Logic

toolbox. Membership functions of variables were organized based on the heuristic tuning process. Trapezoidal and triangular membership functions were used for the fuzzy logic controller. The MATLAB FL toolbox was also used to develop the Sugeno-type ANFIS model. The ANFIS-based logic generates variable output for the control system, similar to the fuzzy logic controller. The input variable types used for the ANFIS model were the same as used with the Fuzzy-based logic however different output membership functions and rules were used. Through the iterative training process during the system operation, the model continuously adjusted parameters of the output membership functions in order to produce the optimal output in the given environment. The ANN model was developed using the NN toolbox in MATLAB and is used to calculate a variable ratio of system operation. A three layer ANN structure was used with the input, hidden and output layers consisting of two, five and one neurons respectively. The performance of each method was tested on a simulation model of a two story residential building which was developed using the International Building Physics Toolbox (IBPT) and MATLAB. The two adaptive control methods (the ANFIS and ANN methods) were able to achieve more stable and accurate control of the thermal conditions compared to the Fuzzy-based non-adaptive method. All three control methods utilised a similar amount of energy.

Neuro-Fuzzy control techniques have proven to be effective for HVAC control in many cases. However, due to both ANN-based control and fuzzy control requiring a large amount of system operation data, which covers the whole process operating range, for model training, there still remains a drawback with this AI technique. Moreover, they often cannot take account of constraints directly in the control design. Therefore, the application of such intelligent methods might be limited in practice (Salsbury 2005).

2.5 Other Relevant Works

There are other techniques in the literature which have been used to develop control systems for buildings which do not fall directly into the subcategories

mentioned above. Some of these methods use adaptive and nonlinear controller design techniques. The use of nonlinear controller design methods for HVAC control systems surprisingly, has been rare despite it being a valuable approach to dealing with nonlinear and time-varying systems. Adaptive control on the other hand has been used extensively in this area. In this section, some of the relevant works using these alternative methods are reviewed.

Wang, Zhang et al. (2008) present a self-adaptive human-imitating intelligent PID controller design for HVAC control. The authors state that simulating human intelligent control consists of four steps; simulating human divisional control; online parameter tuning; feed-forward control; and lag compensation. Human divisional control is simulated using a set of rules based on the error and error gradient. The proportional, integral and derivative gains, which have been pre-selected, are modified according to different values of error and error gradient. The gains are also tuned online based on a cumulative error signal over a period of 300 seconds. Based on this error, new values for the gains are calculated. A feed-forward controller is also employed in order to adjust the flow of fresh air into the room based on changes in amplitude of the outside temperature or flow rate. In order to compensate for the lag characteristic in the temperature control process, alterations are made to the input control signal based on the values of the error and error gradient. The results presented show an improvement with regard to overshoot over a traditional PID controller although it is not clear how the traditional PID controller was tuned. The intelligent PID controller however produces a more oscillatory response. The results also do not show the disturbance rejection capability of the controller. A limitation of the method is that it does not consider the problems which could arise from actuator saturation and the tracking set point is out with the reach of the control system (unreachable).

Moradi, Saffar-Avval et al. (2011) present a comparison of two nonlinear multivariable controller designs for indoor temperature and humidity control. The method is applied to a nonlinear MIMO air handling unit model. The authors use an observer to estimate state variables and design a hybrid control system. A regulation

system designed using state feedback control laws is used for disturbance rejection. The control laws are constructed based on the assumption that full state feedback is available however the observer is in fact used to estimate the process states. Two nonlinear control methods are designed and compared for tracking objectives; gain scheduling and feedback linearization. The performance of the control methods are evaluated based on the tracking responses to a sequence of step/ramp-step commands. The results show that the controller based on the feedback linearization approach achieves a quicker response time than the gain scheduled controller however it produces higher overshoots. The authors state that the gain scheduled controller consumes less energy due to less variation of air and cold water flow rates being required for the tracking objectives to be attained. Results demonstrating the ability of both controllers to deal with model uncertainty are also shown. The feedback linearization controller produces a superior performance over the gain scheduled controller. The authors state that this is due to inaccurate parameter adjustments in the gain scheduled controller.

Chaudhry and Das (2012) developed an adaptive one step ahead (OSA) and an adaptive weighted one step ahead (WOSA) controller for regulation of indoor temperature of a building. A simulation study was performed with the controller methods applied to a building modelled as a bilinear system. The authors use a recursive least squares estimation algorithm to estimate unknown model parameters and the control signal is computed based on these parameters. The global stability of the system is proven using a theorem provided by the authors. The performance of the control system is tested in a scenario where the controller is required to raise the temperature of the room to a desired set point by following a user-specified trajectory. A comparison of the controller performance is made with a PID-fuzzy controller. The PID-fuzzy controller shows an oscillatory response with a large overshoot before settling down to the desired set point. The adaptive OSA controller displays a much smaller overshoot and accurate set point tracking. A similar response is produced with the adaptive WOSA controller however a steady state error is observed. By tuning the weight parameter in the controller however, accurate tracking of the set point is achieved.

Rehrl and Horn (2009) present a supply air temperature controller for an industrial HVAC pilot plant based on a Smith predictor and Inward approach. The authors utilise a controller with two degrees of freedom in order to overcome the structural constraints of conventional PI controllers. A standard Smith predictor is used in order to compensate for the dead time in the HVAC plant. The controller is then designed based on the dead time free plant. An overall transfer function is derived based on user defined specifications for overshoot and rise-time. Through the application of the linear algebraic method in (Chen 1993), the controller transfer functions are determined. The control system design was performed using MATLAB/Simulink and implemented on an electronic control unit using automatic code generation. Experimental results were obtained on an industrial HVAC pilot plant with a comparison being made between the proposed controller design applied and a conventional PI controller tuned using the T-sum rule. Two configurations of the PI controller were tested: "standard" and "fast". The results show that the "fast" PI controller has slightly more accurate set point tracking and a faster response than the "standard" PI controller. The proposed controller shows a similar response time to the "fast" PI controller however a larger steady state error exists over the PI controller. The response is also more oscillatory than the PI controller.

Inverse dynamics based controller methods is another technique which has received little or no attention in the HVAC controls field. Nonlinear inverse dynamics controllers are typically utilised in high performance control applications such as aerospace or robotics (Counsell, Khalid et al. 2011). The methods developed in this thesis utilise an inverse dynamics based controller methodology, which was originally used in the aerospace field, namely Robust Inverse Dynamics Estimation (RIDE) (Bradshaw and Counsell 1992). More recent uses and developments of this method in the aerospace and other fields can be found in the literature [(Ding, Bradshaw et al. 2004); (Counsell, Brindley et al. 2009); (Counsell, Zaher et al. 2010); (Brindley, Counsell et al. 2012)]. To the knowledge of the author, there is no published literature on the use of the RIDE controller algorithm for HVAC control systems design other than the works of the author of this thesis (Zaher, Counsell et

al. 2011). Recently, however, it has been utilised for assessing the controllability of buildings (Counsell, Khalid et al. 2011) as well as developing a simplified dynamic method for energy estimation of dwellings (Murphy, Khalid et al. 2011). A review of these works has been included in this section for completeness.

Murphy, Khalid et al. (2011) developed a simplified dynamic method of assessing the controllability and energy estimation of a dwelling and its servicing systems. The method, Inverse Dynamics based Energy Analysis and Simulation (IDEAS), aims to supplement the Standard Assessment Procedure (SAP) used in the buildings industry for calculating a rating for the energy efficiency and environmental impact of a specific dwelling. With IDEAS, the authors take into account statistical parts of the model such as impact of casual heat gains and solar gains by inheriting this from the current SAP model. Therefore, a model which is more advanced but is also backwards compatible with the current SAP model was developed. The underlying theory is that the use of more detailed data in the model will produce more detailed results. Using this model, the authors use inverse dynamics to evaluate the perfect control input at each model time step and to enable the implementation of the dynamic model in Microsoft Excel. The inverse dynamics method used to determine the perfect control is the RIDE methodology. This method can be used to estimate the energy or power input required to maintain an ideal standard occupancy temperature and time profile.

Counsell, Khalid et al. (2011) presented a methodology to assess the controllability of a building and its servicing systems such as heating, lighting and ventilation. The Robust Inverse Dynamics Estimation (RIDE) algorithm, which is a nonlinear inverse dynamics method that has been successfully applied in the aerospace and robotics industries, was used to develop a controllability science for buildings similar to that which exists in the aerospace industry (Muir and Bradshaw 1996). The authors developed a simplified dynamic building model using differential equations that provides answers to fundamental questions of controllability and accurately captures the dynamic and cross-coupling behaviour of the building. The nonlinear dynamic equations that were constructed were then linearized in order to enable the

application of the aerospace controllability science. The engineering science presented in this paper is based on 'A Perfect Control Philosophy'. In this philosophy, the feasibility of perfect control whilst maintaining stability for the closed-loop control system is established for a given design. Through this feasibility assessment, a designer would be able to assess the ease in which perfect control could be achieved. The authors' reasoning behind this is that it can be assumed that the easier it is to achieve perfect control, the easier the real system will be to control in reality. In this work, the controllability of the building model is assessed by using Nonlinear Inverse Dynamics and the RIDE Methodology (Bradshaw and Counsell 1992), which in a modelling exercise provides a perfect control solution. Using these methods, the main aspects which should be considered when designing control systems are assessed such as stability, degree of coupling and reachability. The methods presented in this work provide a tool that can aid architects in their decisions on which building design and services to use. In addition to this, the method can also be used to assist the control systems designer in developing high performance control systems for buildings. Therefore, the principles behind the controllability science presented in this work proved to be valuable when designing the control systems presented in this PhD thesis.

2.6 Chapter Conclusions

The research community has been active in developing advanced control systems for buildings in order to improve their performance and efficiency for many years. In light of the review presented in this chapter, it is clear that researchers have utilised several different techniques for developing adaptive, learning and robust controllers that aim to achieve the desired improvement in thermal comfort control performance.

2.6.1 Summary of Reviewed Techniques

Adaptive and self-tuning PID control methods are practical and easy to implement. This is a highly important attribute as it has been identified that controllers that are complex or require extra commissioning time can often be disregarded in industry (Salsbury 2005). Another desirable feature which this type of controller possesses is

that they can be applied to different buildings without alteration due to their adaptive nature. Their performance however, can often be similar to fixed gain PID controllers due to the fact that they usually do not have robustness measures for dealing with inaccuracies in the identified models (Naidu and Rieger 2011). Furthermore, the performance of their online estimation algorithms deteriorates when faced with un-modelled disturbances and actuator nonlinearities. Geng and Geary (1993) however recognised that since buildings typically have slowly varying parameters, constant online adaption is unnecessary. Control systems developed based on robust (H_∞) control theory provide a framework for dealing with modelling inaccuracies. This principle is valuable as it could, conceptually, provide a solution for the inaccuracies in the identification procedure in self-tuning and adaptive controllers. Implementation of these methods in practice however can be complicated and impractical due to the difficulty associated with the selection of the control parameters. MPC methods provide an interesting approach to HVAC systems control in that they possess an anticipative property. These methods can reduce energy usage due to the minimisation of a cost function which incorporates the prediction error and the control effort. The main drawback of these methods however is their reliance on an accurate model of the system. AI techniques utilised in control systems design aim to tackle the problem from a human perspective i.e. through learning and reasoning etc. These methods possess many advantages due to their ability to learn complex nonlinear relationships and deal with uncertainties. ANN and FL based controllers however, typically require a large amount of system operation data which covers the whole process operating range for model training (Huang and Wang 2008). Therefore the application of AI techniques is still limited in the buildings industry.

2.6.2 Advantages of Proposed Control Methods

The methods developed in this thesis will be explained in detail in Chapters 5 and 6, however at this point it would be useful to highlight some of the beneficial and novel aspects of the methods developed by the author in this thesis. As mentioned previously, the controller structure used as the basis of the methods developed is that of a robust nonlinear inverse dynamics controller, namely the RIDE methodology.

NID controller designs cannot be found easily in the HVAC literature. Specifically, to the knowledge of the author, the RIDE methodology has not been applied in the control of HVAC systems, other than in the work of the author (Zaher, Counsell et al. 2011). The lack of use of NID techniques in HVAC control may be attributed to the requirement of an accurate model of the system in order for the NID control law to produce suitable results. The controller structure used in this thesis alleviates this problem associated with other NID methods however, as it does not require full knowledge of the system dynamics. This feature is useful, particularly in systems that have large differences in time constants like buildings, as it overcomes part of the problem associated with identifying system models. Furthermore, the structure of the control system is designed to be robust to modelling inaccuracies, which makes it ideal for dealing with inaccuracies in identified models. The inverse dynamics based control law also cancels the system dynamics and replaces them with the designed closed loop system dynamics. This improves the performance of the system since time constants for buildings are usually very large.

It is a known problem that the online estimation methods typically used in the adaptive HVAC control methods suffer from deteriorated estimation accuracy when subjected to changes in loads and disturbances. These methods however, require constant estimation of the plant process parameters due to the structure of the control system not being robust to modelling inaccuracies or disturbances. The robust control structure and inverse dynamics estimation algorithm used in this thesis negate the necessity for constant online adaption. Adaption can therefore be performed infrequently and in times when the system is not subjected to many disturbances. An additional benefit of this aspect is the reduced computational demand due to infrequent adaption.

The inverse dynamics control law used in the developed controller determines a property of the system known as the equivalent control. The equivalent control is based on high gain control principles and is the control action required to decouple and linearize a nonlinear MIMO system (Bradshaw and Counsell 1992). High gain control, theoretically, is the optimum type of control for rejecting disturbances and dealing with uncertainties etc. however it cannot be applied in practice due to high frequency oscillations and sensitivity to noise etc. The control algorithm used in this

thesis, despite being derived from high gain principle, is mathematically a low gain technique and therefore it can be applied in practice.

In spite of being a high performance control algorithm, the structure of the control system developed in this thesis is no more complicated than the adaptive PID control methods already in use in the buildings industry. The controller still consists of proportional and integral gains, albeit in the structure of a pseudo derivative feedback (PDF) controller (Phelan 1977). The inverse dynamics part of the control law is straightforward in its implementation and requires a simple identification procedure of a FOPDT model. The tuning of the control system is a more transparent procedure than that of a PID controller, due to the gains being tuned by the selecting the natural frequency and damping ratio of the closed loop system. There are two options for controller tuning presented in this thesis: a self-tuning controller and a controller tuned by a genetic algorithm (GA).

Finally, the majority of works in the literature focus on one control problem in buildings: either the control of the HVAC systems or the control of the zone thermal comfort. The research presented by the author in this thesis shows a full control system for regulating both the zone thermal comfort conditions as well as the HVAC systems inside it.

2.7 Chapter References

Al-Assadi, S. A. K., R. V. Patel, et al. (2004). "Robust decentralized control of HVAC systems usiing H-infinity-performance measures." Journal of the Franklin Institute-Engineering and Applied Mathematics **341**(7): 543-567.

Anderson, B. D. O. and J. B. Moore (1990). Optimal control : linear quadratic methods. Englewood Cliffs, N.J., Prentice Hall.

Anderson, M., M. Buehner, et al. (2008). "MIMO robust control for HVAC systems." Ieee Transactions on Control Systems Technology **16**(3): 475-483.

Baek, J., E. Kim, et al. (2008). "Adaptive Fuzzy Output Feedback Control for the Nonlinear Heating, Ventilating, and Air Conditioning System." ITC-CSCC: 2008, 1477~ 1480 쪽 (총 4 쪽).

Bai, J. B., S. W. Wang, et al. (2008). "Development of an adaptive Smith predictor-based self-tuning PI controller for an HVAC system in a test room." Energy and Buildings **40**(12): 2244-2252.

Bai, J. B. and X. S. Zhang (2007). "A new adaptive PI controller and its application in HVAC systems." Energy Conversion and Management **48**(4): 1043-1054.

Bi, Q., W. J. Cai, et al. (1999). "Robust identification of first-order plus dead-time model from step response." Control Engineering Practice **7**(1): 71-77.

Bi, Q., W. J. Cai, et al. (2000). "Advanced controller auto-tuning and its application in HVAC systems." Control Engineering Practice **8**(6): 633-644.

Bradshaw, A. and J. Counsell (1992). "Design of autopilots for high performance missiles." Proceedings of the Institution of Mechanical Engineers, Part I: Journal of Systems and Control Engineering **206**(2): 75-84.

Brindley, J., J. M. Counsell, et al. (2012). "Design and simulation of a non-linear, discontinuous, flight control system using rate actuated inverse dynamics." Proceedings of the Institution of Mechanical Engineers, Part G: Journal of Aerospace Engineering.

Chaudhry, S. I. and M. Das (2012). Adaptive control of indoor temperature in a building. Electro/Information Technology (EIT), 2012 IEEE International Conference on, IEEE.

Chen, C.-T. (1993). Analog and digital control system design : transfer-function, state-space, and algebraic methods. Fort Worth, Saunders College Pub.

Counsell, J. M., J. Brindley, et al. (2009). Non-linear autopilot design using the philosophy of variable transient response. AIAA Guidance, Navigation and Control Conference.

Counsell, J. M., Y. A. Khalid, et al. (2011). "Controllability of buildings: A multi-input multi-output stability assessment method for buildings with slow acting heating systems." Simulation Modelling Practice and Theory **19**(4): 1185-1200.

Counsell, J. M., O. S. Zaher, et al. (2010). Auto-Tuning for High Performance Autopilot Design Using Robust Inverse Dynamics Estimation. Computing in the Global Information Technology (ICCGI), 2010 Fifth International Multi-Conference on, IEEE.

Dexter, A., G. Geng, et al. (1990). The application of self-tuning PID control to HVAC systems. Control in Building Energy Management Systems, IEE Colloquium on, IET.

Dexter, A. and P. Haves (1989). "A robust self-tuning predictive controller for HVAC applications." ASHRAE Transactions (American Society of Heating, Refrigerating and Air-Conditioning Engineers);(USA) **95**(CONF-890609--).

Ding, L., A. Bradshaw, et al. (2004). Robustness Comparison of Control Systems for a Nuclear Power Plant. UKACC international conference on Control.

Dounis, A. I., M. Bruant, et al. (1996). "Comparison of conventional and fuzzy control of indoor air quality in buildings." Journal of Intelligent & Fuzzy Systems **4**(2): 131-140.

Dounis, A. I. and C. Caraiscos (2009). "Advanced control systems engineering for energy and comfort management in a building environment-A review." Renewable & Sustainable Energy Reviews **13**(6-7): 1246-1261.

Ertunc, H. M. and M. Hosoz (2008). "Comparative analysis of an evaporative condenser using artificial neural network and adaptive neuro-fuzzy inference system." International Journal of Refrigeration-Revue Internationale Du Froid **31**(8): 1426-1436.

Geng, G. and G. M. Geary (1993). "On Performance and Tuning of Pid Controllers in Hvac Systems." Second Ieee Conference on Control Applications, Vols 1 and 2: 819-824.

Guo, C. Y. and Q. Song (2009). "Real-Time Control of Variable Air Volume System Based on a Robust Neural Network Assisted PI Controller." Ieee Transactions on Control Systems Technology **17**(3): 600-607.

Guo, C. Y., Q. Song, et al. (2007). "A neural network assisted cascade control system for air handling unit." Ieee Transactions on Industrial Electronics **54**(1): 620-628.

Guzelkaya, M., I. Eksin, et al. (2003). "Self-tuning of PID-type fuzzy logic controller coefficients via relative rate observer." Engineering Applications of Artificial Intelligence **16**(3): 227-236.

Hazyuk, I., C. Ghiaus, et al. (2012). "Optimal temperature control of intermittently heated buildings using Model Predictive Control: Part II - Control algorithm." Building and Environment **51**: 388-394.

Hongli, L., D. Peiyong, et al. (2008). "A Novel Fuzzy Controller Design Based-on PID Gains for HVAC Systems." 2008 7th World Congress on Intelligent Control and Automation, Vols 1-23: 736-739.

Huang, G. S. and S. W. Wang (2008). "Two-loop robust model predictive control for the temperature control of air-handling units." Hvac&R Research **14**(4): 565-580.

Huang, G. S., S. W. Wang, et al. (2009). "A robust model predictive control strategy for improving the control performance of air-conditioning systems." Energy Conversion and Management **50**(10): 2650-2658.

Kazemian, H. B. (2001). "Comparative study of a learning fuzzy PID controller and a self-tuning controller." Isa Transactions **40**(3): 245-253.

Krarti, M. (2003). "An overview of artificial intelligence-based methods for building energy systems." Journal of Solar Energy Engineering-Transactions of the Asme **125**(3): 331-342.

Levermore, G. J. (1992). Building energy management systems : an application to heating and control. London ; New York, E. & FN Spon.

Mayne, D. Q., J. B. Rawlings, et al. (2000). "Constrained model predictive control: Stability and optimality." Automatica **36**(6): 789-814.

Moon, J. W., S. K. Jung, et al. (2011). "Comparative study of artificial intelligence-based building thermal control methods - Application of fuzzy, adaptive neuro-fuzzy inference system, and artificial neural network." Applied Thermal Engineering **31**(14-15): 2422-2429.

Moon, J. W. and J. J. Kim (2010). "ANN-based thermal control models for residential buildings." Building and Environment **45**(7): 1612-1625.

Moradi, H., M. Saffar-Avval, et al. (2011). "Nonlinear multivariable control and performance analysis of an air-handling unit." Energy and Buildings **43**(4): 805-813.

Morosan, P. D., R. Bourdais, et al. (2010). "Building temperature regulation using a distributed model predictive control." Energy and Buildings **42**(9): 1445-1452.

Muir, E. and A. Bradshaw (1996). "Control law design for a thrust vectoring fighter aircraft using robust inverse dynamics estimation (RIDE)." Proceedings of the Institution of Mechanical Engineers Part G-Journal of Aerospace Engineering **210**(G4): 333-343.

Murphy, G., Y. Khalid, et al. (2011). A Simplified Dynamic Systems Approach For The Energy Rating Of Dwellings. Accepted Paper. Twelfth International IBPSA Conference, Sydney, Australia.

Naidu, D. S. and C. G. Rieger (2011). "Advanced control strategies for heating, ventilation, air-conditioning, and refrigeration systems-An overview: Part I: Hard control." Hvac&R Research **17**(1): 2-21.

Nesler, C. (1986). "Adaptive control of thermal processes in buildings." Control Systems Magazine, IEEE **6**(4): 9-13.

Özsoy, C. (1993). "Self-tuning control of a heating, ventilating and air-conditioning system." Proceedings of the Institution of Mechanical Engineers, Part I: Journal of Systems and Control Engineering **207**(4): 243-251.

Pal, A. and R. Mudi (2008). "Self-tuning fuzzy PI controller and its application to HVAC systems." International Journal of Computational Cognition **6**(1): 25-30.

Pal, A. K. (2008). "Development of neuro-fuzzy controller for applications to HVAC system, inverted pendulum and other processes." INTERNATIONAL JOURNAL OF COMPUTATIONAL COGNITION (HTTP://WWW. IJCC. US) **6**(2): 1.

Phelan, R. M. (1977). Automatic control systems. Ithaca, N.Y., Cornell University Press.

Qiao, W. Z. and M. Mizumoto (1996). "PID type fuzzy controller and parameters adaptive method." Fuzzy Sets and Systems **78**(1): 23-35.

Qu, G. and M. Zaheeruddin (2004). "Real-time tuning of PI controllers in HVAC systems." International Journal of Energy Research **28**(15): 1313-1327.

Qu, G. and M. Zaheeruddin (2010). "Online H-infinity tuning of PI controllers for discharge air temperature system." Energy Conversion and Management **51**(6): 1179-1195.

Rehrl, J. and M. Horn (2009). Supply Air Temperature Control in an Industrial HVAC Pilot Plant Based on Smith Predictor and Inward Approach. Computational Intelligence, Modelling and Simulation, 2009. CSSim'09. International Conference on, IEEE.

Salsbury, T. (2005). A survey of control technologies in the building automation industry. 16th IFAC World Congress.

Siroky, J., F. Oldewurtel, et al. (2011). "Experimental analysis of model predictive control for an energy efficient building heating system." Applied Energy **88**(9): 3079-3087.

Soyguder, S. and H. Alli (2009). "An expert system for the humidity and temperature control in HVAC systems using ANFIS and optimization with Fuzzy Modeling Approach." Energy and Buildings **41**(8): 814-822.

Soyguder, S., M. Karakose, et al. (2009). "Design and simulation of self-tuning PID-type fuzzy adaptive control for an expert HVAC system." Expert Systems with Applications **36**(3): 4566-4573.

Tan, W., J. Liu, et al. (1998). "PID tuning based on loop-shaping H-infinity control." Iee Proceedings-Control Theory and Applications **145**(6): 485-490.

Therese, P. S. and N. K. Nair (2012). "Simplified Decoupled Self-Tuning Fuzzy-PI Controller for Eliminating Interaction in HVAC System." European Journal of Scientific Research **67**(2): 180-193.

Wang, J., C. Zhang, et al. (2008). Application of an intelligent PID control in heating ventilating and air-conditioning system. Intelligent Control and Automation, 2008. WCICA 2008. 7th World Congress on, IEEE.

Wang, J. J., C. F. Zhang, et al. (2007). "Study of neural network PID control in variable frequency air-conditioning system." 2007 Ieee International Conference on Control and Automation, Vols 1-7: 2809-2814.

Wang, Q. G., C. C. Hang, et al. (1997). "Process frequency response estimation from relay feedback." Control Engineering Practice **5**(9): 1293-1302.

Wang, Q. G., C. C. Hang, et al. (2000). "Multivariable process identification and control from decentralized relay feedback." International journal of modelling & simulation **20**(4): 341-348.

Wang, Q. G., T. H. Lee, et al. (1999). "PID tuning for improved performance." Ieee Transactions on Control Systems Technology **7**(4): 457-465.

Woo, Z. W., H. Y. Chung, et al. (2000). "A PID type fuzzy controller with self-tuning scaling factors." Fuzzy Sets and Systems **115**(2): 321-326.

Wu, J. and W. J. Cai (2000). "Development of an Adaptive Neuro-Fuzzy method for supply air pressure control in HVAC system." Smc 2000 Conference Proceedings: 2000 Ieee International Conference on Systems, Man & Cybernetics, Vol 1-5: 3806-3809.

Yager, R. R. and D. P. Filev (1994). "Essentials of fuzzy modeling and control." New York.

Zaheeruddin, M., R. V. Patel, et al. (1993). "Design of decentralized robust controllers for multizone space heating systems." Control Systems Technology, IEEE Transactions on **1**(4): 246-261.

Zaheeruddin, M. and N. Tudoroiu (2004). "Neuro-PID tracking control of a discharge air temperature system." Energy Conversion and Management **45**(15-16): 2405-2415.

Zaher, O. S., J. Counsell, et al. (2011). "Robust control of room temperature and relative humidity using advanced nonlinear inverse dynamics and evolutionary optimisation."

Zhou, Q. and M. Liu (1998). "An On-line Self-tuning Algorithm of PI Controller for the Heating and Cooling Coil in Buildings."

3. Modelling of Building Zone and HVAC Systems

This chapter aims to elucidate the development of the building model that was used to assess the performance of all of the control algorithms developed and tested throughout this thesis. The advanced controller design methods developed in this research require that the system to be controlled can be represented in a relatively low order state space form. The detailed, high order energy simulation models typically used for energy performance evaluation are not suitable for controller design due to the necessity to use the state space model in the control law design as well as to investigate system stability. This necessitates the development of a simplified, low order model that captures the essential dynamic properties of the building thermodynamics [(Tashtoush, Molhim et al. 2005); (Gouda, Underwood et al. 2003)].

The thermal dynamics of a building can be described by classical differential equations for heat transfer and thermodynamics. The thermal model of the building is typically developed using the principal of analogy such that the resulting equations are translated to an electrical circuit model relating the temperatures and voltages, the heat fluxes and the currents, the heat transmission resistances and the electrical resistances, the thermal capacities and the electrical capacities, etc. (De Keyser, Dumortier et al. 1984). This type of dynamic modelling approach is often referred to as lumped parameter modelling.

The thermal model developed in this research using the aforementioned approach, consists of equations representing the rates of change of temperature of indoor air, walls, roof, floor and internal thermal mass. This model is based on the dynamic models developed in [(Murphy 2012); (Khalid 2011)] but with additional components which are detailed in the following sections.

Section 3.1 describes the differential equations comprising the zone model. The state space representation of the model is detailed in Section 3.2. Section 3.3 provides a description of the actuation systems that have been modelled. These are two different types of actuation system; a fast acting direct heater with a separate mechanical ventilation system; a full air handling unit comprising a heater,

humidifier and ventilation system. Open loop simulation results demonstrating the dynamics of the system are given in Section 3.4.

3.1 Zone Model

The zone model developed in this research consists of four state variables for temperature and one state variable for humidity. These are: zone air temperature (T_a), internal wall structure temperature (T_{si}), external wall structure temperature (T_{se}), furniture and internal mass temperature (T_{ft}) and zone humidity (W_a). The zone air is assumed to be fully mixed meaning the temperature distribution across the zone is uniform. The air density is also assumed to be constant and unaffected by changes in temperature and humidity of the zone. A diagram illustrating the heat transfer dynamics of the zone is given in Figure 3.1. The nonlinear differential equations that govern the zone temperature and humidity are detailed in the following sections.

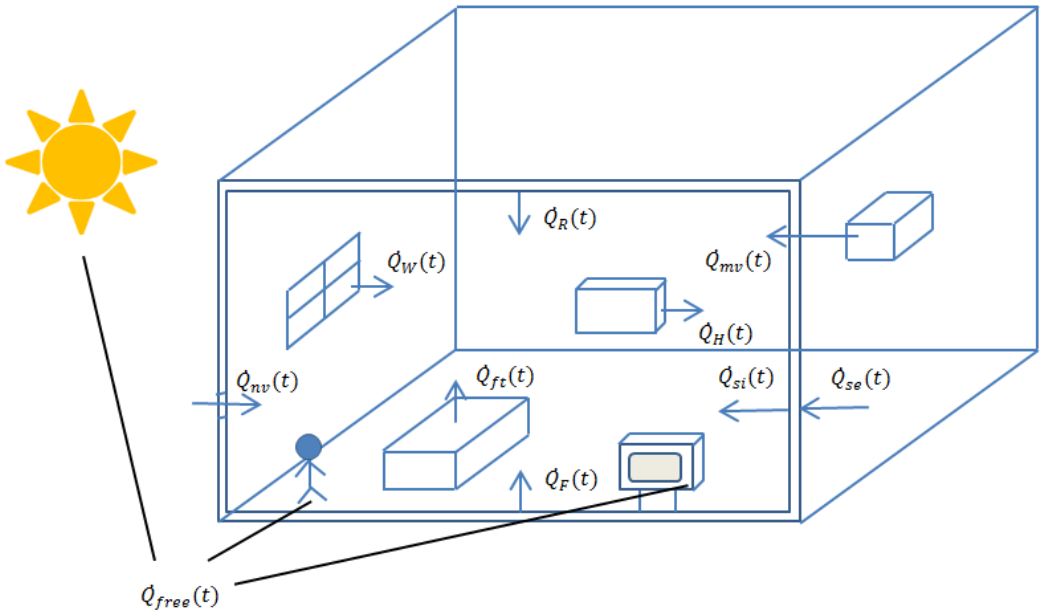

Figure 3.1: Zone thermal dynamics

3.1.1 Wall Structure Temperatures:

The walls of the zone are assumed to be composite and are comprised of an internal surface, the wall structure and an external surface. Therefore, the heat loss

through the wall is approximated by two energy stores, the thermal mass of the bricks and the overall U-Value for conductions through the wall (Murphy 2012). This effectively means that there are two temperature nodes for the wall; an inner temperature (T_{si}) and an external temperature (T_{se}). This is illustrated in Figure 3.2. Equation 3.1 shows that the internal wall temperature is related to the difference between the heat entering it from the zone and the heat lost to the external node of the wall structure. The temperature of the external node is related to the difference between the heat transfer from the inner node and the heat loss to the environment (T_o), as described by Equation 3.2.

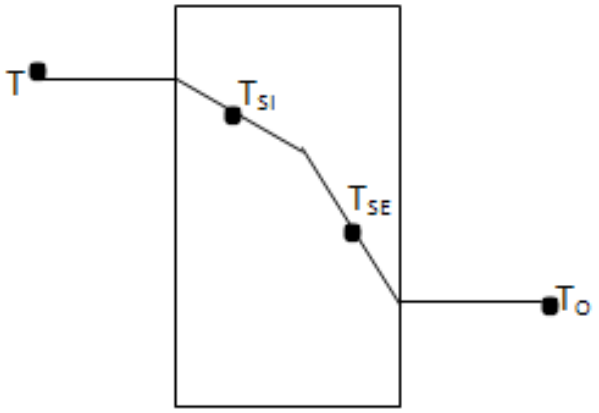

Figure 3.2: Temperature nodes across the wall

$$M_{si}C_s\frac{dT_{si}(t)}{dt} = \dot{Q}_{si} - \frac{K_{si}}{Th_{wall}}A_s(T_{si}(t) - T_{se}(t)) \qquad (3.1)$$

$$M_{se}C_s\frac{dT_{se}(t)}{dt} = \frac{K_{si}}{Th_{wall}}A_s(T_{si}(t) - T_{se}(t)) - \dot{Q}_{se}(t) \qquad (3.2)$$

The terms $\dot{Q}_{si}$ and $\dot{Q}_{se}$ in equations 3.1 and 3.2 represent the heat transfer between the internal zone and inner wall structure node and the outer wall structure node and the external environment respectively. They are expressed as follows:

$$\dot{Q}_{si} = h_i A_s(T_a - T_{si}) \qquad (3.3)$$

$$\dot{Q}_{se} = h_e A_s (T_{se} - T_o) \quad (3.4)$$

3.1.2 Internal thermal mass and furniture temp:

The temperature of the internal thermal mass is determined from the heat transfer between the internal zone and the thermal mass. The internal thermal mass here relates to the heat stored in the building elements other than the external wall structure. This includes the heat stored in the furniture, roof, floor and windows. Equation 3.5 shows the heat transfer between the internal zone and the thermal mass.

$$M_{ft} C_{ft} \frac{dT_{ft}(t)}{dt} = U_{ft} A_{ft} (T_a(t) - T_{ft}(t)) \quad (3.5)$$

3.1.3 Internal Air (Zone) Temperature:

The air in the zone is assumed to be fully mixed at constant pressure, so that the internal zone air temperature distribution is uniform and is modelled as a single node representing an average temperature of the zone. This assumption dictates that the air in the zone is fully stratified. This assumption is generally not valid for thermal buoyancy force-dominated flow and does not conform to reality. The resulting equations however, are far less complex whilst remaining detailed enough for the purposes of controller design (Khalid 2011). This assumption is adopted by most building models that are used for controller analysis in the literature [(Counsell, Khalid et al. 2011); (Gouda, Underwood et al. 2003)]. In reality, due to occupant behaviour etc the air temperature is never uniform in all parts of the zone and this has a significant impact on the controller performance and design. This effect however, is taken as a transport lag. It is extremely important to assess the effects of transport lag when designing a HVAC control system as it is a common cause of underperforming and unstable control systems in practice. The effects of transport lag and the countermeasures developed in this research are discussed in detail in Chapters 4 and 5. The rate of change of air temperature is described by equation 3.6.

$$M_a C_a \frac{dT_a(t)}{dt} = \dot{Q}_H(t) + \dot{Q}_{free}(t) - \dot{Q}_{si}(t) - \dot{Q}_F(t) - \dot{Q}_R(t) - \dot{Q}_W(t) - \dot{Q}_{FT}(t) - \dot{Q}_{mv}(t) - \dot{Q}_{nv}(t) \quad (3.6)$$

The structural mass of the zone i.e. the walls, is a source of heat storage (Balaras 1996). The heat stored in the wall is a result of the heat transfer between the structure and the internal and external environments. If the internal or external temperature is high relative to that of the structure, then heat is transferred to, and stored in, the structure. If the zone temperature drops then this stored heat is transferred to the zone. In this model, the energy stored in the building elements other than the external walls is captured in the internal thermal mass parameter (denoted by the subscript ft) as explained in section 3.1.2(Murphy 2012), such that:

Windows Heat Loss is:

$$\dot{Q}_w = U_w A_w (T_a(t) - T_o(t)) \quad (3.7)$$

Floor Heat Loss is:

$$\dot{Q}_F = U_F A_F (T_a(t) - T_o(t)) \quad (3.8)$$

Roof Heat Loss is:

$$\dot{Q}_R = U_R A_R (T_a(t) - T_o(t)) \quad (3.9)$$

Furniture and Internal Mass Heat Loss is:

$$\dot{Q}_{FT} = U_{FT} A_{FT} (T_a(t) - T_{FT}(t)) \quad (3.10)$$

Equations 3.7 to 3.10 are always in steady state implying that there is constant heat loss through windows, furniture and internal mass, roof and floor.

The term $\dot{Q}_H$ in equation 3.6 signifies the heat added to the zone from the controlled heater. Since actuator dynamics are not included in main plant model for the controller design method developed in this research, the equations describing the dynamics of the heating system are not included in this zone model. They are detailed in Section 3.3 on Actuation System Dynamics. Details on why actuator dynamics are not included in the main plant model and how actuator dynamics are dealt with are given in Chapter 4.

The heat lost through natural ventilation and the controlled mechanical ventilation system is denoted by $\dot{Q}_{nv}$ and $\dot{Q}_{mv}$ respectively, as shown in equation 3.6. The heat transfer equations for both types of ventilation are given below:

$$\dot{Q}_{nv} = \dot{m}_{nv}(t)C_a\big(T_a(t) - T_o(t)\big) \tag{3.11}$$

$$\dot{Q}_{mv} = \dot{m}_c(t)C_a\big(T_a(t) - T_o(t)\big) \tag{3.12}$$

Heat gains that arise in a building from uncontrolled sources such as heat emitted from occupants or solar gains are often referred to as casual heat gains. Casual heat gains can be useful as they can contribute to the heating of a building and consequently reduce the amount of power required from a controlled heating source. The impact of casual heat gains becomes more significant with improved insulation in buildings and can constitute a high proportion of the total heat needed in a building. Whilst this impact can be useful, it can also prove problematic for a control system. Consider the fact that, due to heating systems being used intermittently in buildings, they are sized for early morning pre-heating when casual heat gains are generally not available (Khalid 2011). This means that the heating systems are often significantly oversized for times when casual heat sources are present, typically being the majority of the day. This can often render accurate and efficient control difficult to attain. Hence, considering the impact of casual gains on the internal temperature is crucial for control system design. Furthermore, understanding the effect of casual gains is necessary if the heating and cooling plant systems are to be

sized accurately. The $\dot{Q}_{free}(t)$ term in equation 3.6 represents the heat transfer from casual heat gains, which are comprised of the following contributors:

- Solar Gain
- People
- Lighting
- Appliances

The equations describing these elements which were used in this thesis can be found in (Khalid 2011). The data used for external temperature and solar gains is for Glasgow, Scotland during the winter/spring months January to March.

3.1.4 Internal Zone Humidity

Indoor humidity levels within a building have a significant bearing on the health of occupants, energy consumption as well as construction durability (Zhang and Yoshino 2010). It is therefore essential that humidity levels in an indoor environment are regulated at suitable levels in order to ensure the health of occupants and sustainability of the building. Control of indoor humidity levels is not trivial however, on account of the many influencing factors such as moisture sources (human presence and activity, equipment, plants), mechanical ventilation and air infiltration in the building, air flow and temperature distributions in rooms, moisture adsorption and desorption from surrounding surfaces (interior walls, floor, carpet, furniture, futon and books, etc.), as well as the absolute humidity of the outdoor air (Khalid 2011). Thus, a control system must be designed to effectively regulate indoor temperature and humidity levels at the same time. In order to do this, it is essential that the effects of humidity are included in the zone model. The humidity model used in this research is based on the model presented by (Rentel-Gomez and Velez-Reyes 2001).

$$\frac{M_a}{\rho_a}\frac{dW_a}{dt} = \frac{\dot{m}_c(t)}{\rho_a}(W_s(t) - W_a(t)) + \frac{(n_{occ}P_{occ})}{\rho_a} - \frac{\dot{m}_{nv}}{\rho_a}(W_a(t) - W_o(t)) \quad (3.12)$$

Equation 3.12 demonstrates that the moisture content (absolute humidity) in the zone is determined by the vapour added to and removed from the zone through the mechanical ventilation system as well as natural ventilation in the zone (air infiltration). Moisture is also added to the zone air through occupancy, which is linear proportional to the number of occupants. A more practical measure for humidity with regards to occupant comfort is relative humidity. An empirical relation between the absolute and relative humidity is derived from data from the Psychrometric chart in (Rentel-Gomez and Velez-Reyes 2001). This relation is taken from an operating point of 23°C and an absolute humidity of 0.007 kg/kg. The resulting expression defining the relative humidity in the zone is given below:

$$W_{rel}(t) = 5000.0W_a(t) - 0.771T_a(\mathrm{t}) + 131.68 \quad (3.13)$$

3.2 State Space Representation

In order to apply the control system design methods developed in this research to the building model, the differential equations must be rewritten in state space format. The generalised state space format for differential equations is shown in equations 3.14 and 3.15.

$$\dot{\vec{x}}(t) = A\vec{x}(t) + B\vec{u}(t) + F\vec{d}(t) \quad (3.14)$$

$$\vec{y}(t) = C\vec{x}(t) \quad (3.15)$$

Where $\vec{x}(t)$ is the state vector, $\vec{u}(t)$ is the input vector, $\vec{d}(t)$ is the disturbance vector and $\vec{y}(t)$ is the output to be controlled. A, B, C and F are the state, input, output and disturbance matrices respectively. There are a number of ways to express a set of differential equations in state space format depending on the selection of the input,

output and disturbance vectors. This section demonstrates how the differential equations described in the previous section are expressed in state space format if the actuation system described in section 3.3.1 is used such that the inputs to the system are the heating power $\dot{Q}_h(t)$ and the mass flow rate provided by the mechanical ventilation system $\dot{m}_c(t)$. The system outputs i.e. the states that are being regulated, are the air temperature, $T_a(t)$ and relative humidity, $W_{rel}(t)$. The disturbances (uncontrolled inputs) to the system are the free heats, external temperature and humidity and the number of occupants in the zone. The state space vectors are therefore described as follows:

$$\vec{x}(t) = \begin{bmatrix} T_a(\mathrm{t}) \\ T_{si}(\mathrm{t}) \\ T_{se}(\mathrm{t}) \\ T_{ft}(\mathrm{t}) \\ W_a(\mathrm{t}) \end{bmatrix} \tag{3.16}$$

$$\vec{u}(t) = \begin{bmatrix} \dot{Q}_h(t) \\ \dot{m}_c(t) \end{bmatrix} \tag{3.17}$$

$$\vec{d}(t) = \begin{bmatrix} \dot{Q}_{free}(t) \\ T_o(t) \\ W_o(t) \\ n_{occ}(t) \end{bmatrix} \tag{3.18}$$

$$\vec{y}(t) = \begin{bmatrix} W_{rel}(t) \\ T_a(t) \end{bmatrix} \tag{3.19}$$

From the differential equations describing the model in the previous section, it can be observed that the *B* matrix is nonlinear and is a function of the state and disturbance vectors. A generalized nonlinear form of state space representation should therefore be used in order to enable a nonlinear controller design to be used. The resulting state space format used to express the model is as follows:

$$\dot{\vec{x}}(t) = A\vec{x}(t) + B(\vec{x}(t), d(t))\vec{u}(t) + F\vec{d}(t) \tag{3.20}$$

$$\vec{y}(t) = C\vec{x}(t) + G \tag{3.21}$$

The full nonlinear state space description of the model is shown in equations 3.22 and 3.23. The expansion of the coefficients of the state space matrices A, $B\left(\vec{x}(t), \vec{d}(t)\right)$ and F can be found in Appendix A.

$$\begin{bmatrix} \dot{T}_a(t) \\ \dot{T}_{si}(t) \\ \dot{T}_{se}(t) \\ \dot{T}_{ft}(t) \\ \dot{W}_a(t) \end{bmatrix} = \begin{bmatrix} a_{11} & a_{12} & 0 & a_{14} & 0 \\ a_{21} & a_{22} & a_{23} & 0 & 0 \\ 0 & a_{32} & a_{33} & 0 & 0 \\ a_{41} & 0 & 0 & a_{44} & 0 \\ 0 & 0 & 0 & 0 & a_{55} \end{bmatrix} \begin{bmatrix} T_a(t) \\ T_{si}(t) \\ T_{se}(t) \\ T_{ft}(t) \\ W_a(t) \end{bmatrix} + \begin{bmatrix} b_{11} & b_{12} \\ 0 & 0 \\ 0 & 0 \\ 0 & 0 \\ 0 & b_{52} \end{bmatrix} \begin{bmatrix} \dot{Q}_H(t) \\ \dot{m}_c(t) \end{bmatrix} + \begin{bmatrix} f_{11} & f_{12} & 0 & 0 \\ 0 & 0 & 0 & 0 \\ 0 & f_{32} & 0 & 0 \\ 0 & 0 & 0 & 0 \\ 0 & 0 & f_{53} & f_{54} \end{bmatrix} \begin{bmatrix} \dot{Q}_{free}(t) \\ T_o(t) \\ W_o(t) \\ n_{occ}(t) \end{bmatrix} \tag{3.22}$$

$$\begin{bmatrix} W_{rel}(t) \\ T_a(t) \end{bmatrix} = \begin{bmatrix} -0.771 & 0 & 0 & 0 & 5000 \\ 1.0 & 0 & 0 & 0 & 0 \end{bmatrix} \begin{bmatrix} T_a(t) \\ T_{si}(t) \\ T_{se}(t) \\ T_{ft}(t) \\ W_a(t) \end{bmatrix} + \begin{bmatrix} 131.68 \\ 0 \end{bmatrix} \tag{3.23}$$

3.3 Actuation System Dynamics

One of the fundamental assumptions the RIDE controller design method is based on is that the actuation system dynamics of the system to be controlled are fast relative to the plant and therefore are not required to be represented in the plant model for the controller design. By ensuring that the closed loop controller bandwidth is slower than the actuation system bandwidth by a factor of three or more, the actuator dynamics can be considered as 'parasitics' i.e. the transients die out very quickly and therefore do not need to be included in the controller design model [(Counsell, Khalid et al. 2011); (Counsell 1992)]. They are however, dealt with in the controller design as they have a significant bearing on controller performance. This will be explained in detail in Chapter 4. Modelling the actuator dynamics in order to understand their effects is very important as in reality these dynamics are sometimes the reason for uncontrollable effects which cause poor

thermal comfort and excessive energy usage in a building as well as damaging the actuators themselves. One of the key issues is that all actuator plants are nonlinear in reality due to limitations on their power output. Thus, despite the fact that the building physics might be relatively simple and could be approximated with linear functions, the plant dynamics are nonlinear.

3.3.1 Fast Direct Acting Heater and Mechanical Ventilation (Case1)

The actuation systems models used to control the temperature and humidity of the zone in this case are a direct acting heater and mechanical ventilation with first order dynamics. The time constants of the first order models of both actuation systems represent the inertia present in the actuation system between the commanded controller output and the actual output achieved by the actuator (Bi, Cai et al. 2000). The dynamics of the heater are characterised by a nonlinear first order transfer function with amplitude limits representing the actuation system's heating power limitations as shown in equations 3.24 and 3.25. The mass flow rate provided by the mechanical ventilation system is also characterised by a nonlinear first order transfer function with amplitude limits directly proportional to the maximum fan speed. The flow rate is also directly proportional to the fan speed and therefore the time constant represents the delay resulting from the power limitations of the fan motor and the fan inertia. The ventilation system supplies air to the zone at the outside air temperature and with a constant humidity value of 0.02 kg/kg to represent a constant humidification rate. The dynamics of the ventilation system are described by equations 3.26 and 3.27.

$$\ddot{Q}_h = \frac{1}{\tau_h}\left(uc_{Qh}(t) - \dot{Q}_h(t)\right) \tag{3.24}$$

$$LL_{Qh} \leq \dot{Q}_h(t) \leq UL_{Qh} \tag{3.25}$$

$$\ddot{m}_c = \frac{1}{\tau_v}\left(uc_v(t) - \dot{m}_c(t)\right) \tag{3.26}$$

$$LL_{mv} \leq \dot{m}_c(t) \leq UL_{mv} \tag{3.27}$$

3.3.2 Full Air Handling Unit (Case2)

The components comprising the full air handling unit (AHU) modelled in this thesis are a fan, mixing box, heating coil, ducting and humidifier. The layout of the AHU is shown in Figure 3.3.

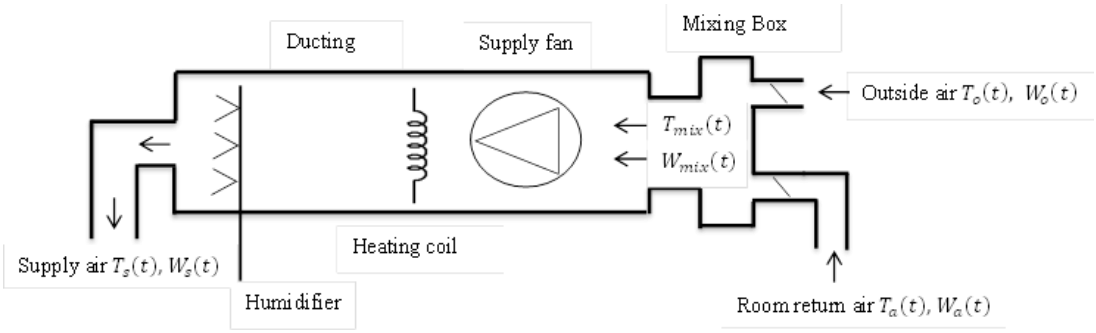

Figure 3.3: Layout of AHU

The AHU is operated by the control system which responds to the feedback signals from the temperature and humidity sensors. The thermostat senses the temperature in the zone and sends a signal to the controller which determines the heating power required from the heating coil based on the control law. Similarly, based on the signal from the humidity sensor, the control system determines the vapour rate required from the humidifier in order to regulate the humidity ratio in the air. The airflow rate in the system is varied using a variable flow fan and the ratio of return air to outside air is controlled using dampers. The outputs of the AHU are the temperature and humidity ratio of the supplied air. The three control inputs to the AHU are: the heating power supplied by the heating coil, the vapour produced by the humidifier and the mass flow rate provided by the variable flow fan. The different control strategies and AHU setups, e.g. Constant Volume – Variable Temperature, Variable Volume – Constant Temperature etc., that were tested in this research and the corresponding changes in the model representation are discussed in Chapter 6. Since the inputs to the zone from this actuation system (heat and humidity added from the supplied air) differ from inputs to the zone from the actuation system described in Section 3.3.1, the equation representing the rate of change of air temperature, namely equation 3.6, must be altered slightly. The term representing the heat transfer through mechanical ventilation ($\dot{Q}_{mv}(t)$) is taken out of equation 3.6

since there is no longer a separate mechanical ventilation system in this AHU. Therefore, equation 3.6 becomes equation 3.28.

$$M_a C_a \frac{dT_a(t)}{dt} = \dot{Q}_H(t) + \dot{Q}_{free}(t) - \dot{Q}_{si}(t) - \dot{Q}_F(t) - \dot{Q}_R(t) - \dot{Q}_W(t) - \dot{Q}_{FT}(t) - \dot{Q}_{nv} \quad (3.28)$$

3.3.2.1 Heating Coil Model

The heating coil heats the air in the AHU for ventilation which in turn is used to condition the air in the zone. The coil is modelled with a nonlinear first order differential equation with power limitations. This model is used as the majority of heating systems, whether they are wet or dry, have first order dynamics. The differences in response characteristics are typically down to differing time constants. Therefore the first order model used here for the heating coil can represent a wet or dry system. The nonlinearities arise due to the power limitations of the system e.g. the maximum and minimum heat outputs that can be delivered from the heating coil. The first order model of the heating coil is shown in equations 3.29 and 3.30.

$$\ddot{Q}_{coil}(t) = \frac{1}{\tau_{coil}}\left(uc_{coil}(t) - \dot{Q}_{coil}(t)\right) \quad (3.29)$$

$$LL_{coil} \leq \dot{Q}_{coil}(t) \leq UL_{coil} \quad (3.30)$$

The overall energy balance between the heating coil and the air flowing through the AHU is expressed as follows:

$$C_{ah} \frac{dT_{coil}(t)}{dt} = \dot{Q}_{coil}(t) + UA_{ah}\left(T_o(t) - T_{coil}(t)\right) + \dot{m}_c(t) C_a (T_m(t) - T_{coil}(t)) \quad (3.31)$$

The mass balance is:

$$V_{ah}\frac{dW_{coil}(t)}{dt} = \frac{\dot{m}_c(t)}{\rho_a}(W_m(t) - W_{coil}(t)) \quad (3.32)$$

The energy transferred to the air passing through the coil equates to the energy added from the heating coil and the energy transferred to the surroundings by the return air.

3.3.2.2 Humidifier Model

The humidification process increases the amount of water vapour in the atmospheric air. Humidification is necessary when there is low moisture content in the air which has undesirable health implications for the occupants. Therefore the regulation of indoor humidity levels in a building is an important task for HVAC systems. The humidifier model used in this thesis is that which was developed by (Kasahara, Yamazuki et al. 2001) cited by (Tashtoush, Molhim et al. 2005). The energy and mass balance equations for the humidifier model are expressed as

$$C_h\frac{dT_h(t)}{dt} = \frac{\dot{m}_c(t)C_a}{\rho_a}\left(T_{duct}(t) - T_h(t)\right) + \alpha_h(T_o(t) - T_h(t)) \quad (3.33)$$

$$V_h\frac{dW_h(t)}{dt} = \frac{\dot{m}_c(t)}{\rho_a}\left(W_{coil}(t) - W_h(t)\right) + \frac{h(t)}{\rho_a} \quad (3.34)$$

Where h(t) is the rate of humid air that the humidifier can produce. In this work the humidification rate is described with first order dynamics and amplitude limits representing the maximum humidification rate the humidifier can produce. This is expressed in equations 3.35 and 3.36.

$$\dot{h}(t) = \frac{1}{\tau_{hum}}(uc_{hum}(t) - h(t)) \quad (3.35)$$

$$LL_{hum} \leq h(t) \leq UL_{hum} \quad (3.36)$$

3.3.2.3 Duct Model

The transient model developed by (Clark, Hurley et al. 1985) cited by (Tashtoush, Molhim et al. 2005) for a duct unit is used. The inlet and exit air temperatures are $T_{coil}(t)$ and $T_{duct}(t)$ respectively. The rate change of air temperature through the duct is:

$$\frac{dT_{duct}(t)}{dt} = \frac{(h_{in} + h_{out})\dot{m}_c(t)C_a}{h_{in}M_{duct}C_{duct}}(T_{coil}(t) - T_{duct}(t)) \qquad (3.37)$$

3.3.2.4 Mixing Box

Return air from the zone is mixed with outside air in the mixing box before it is fed through the AHU. The ratio of outside air to return air can be adjusted with dampers which in turn has an effect on air quality and humidity within the zone. The mixing of air streams typically happens under steady and adiabatic conditions. For the work presented in this thesis, it is assumed that no frictional losses occur through the mixing box. The equations describing the energy and mass balance across the mixing box are given below:

$$T_m(t) = \frac{\gamma\dot{m}_c(t)T_a(t) + (1-\gamma)\dot{m}_c(t)T_o(t)}{\dot{m}_c(t)} \qquad (3.38)$$

$$W_m(t) = \frac{\gamma\dot{m}_c(t)W_a(t) + (1-\gamma)\dot{m}_c(t)W_o(t)}{\dot{m}_c(t)} \qquad (3.39)$$

Where γ is the ratio of return air to outside air adjusted by the dampers. It is clear that the mass flow rate of air, $\dot{m}_c(t)$, can be cancelled out in equations 3.38 and 3.39 such that the temperature and humidity of the air after the mixing box can be expressed as follows:

$$T_m(t) = \gamma T_a(t) + (1-\gamma)T_o(t) \qquad (3.40)$$

$$W_m(t) = \gamma W_a(t) + (1-\gamma)W_o(t) \tag{3.41}$$

3.3.2.5 Fan Model

The dynamics of the fan are described with a first order. For the purposes of this research it is assumed that the fan has negligible effects on the air temperature and consequently its effects on the physical properties of the air are also negligible. The fan also has no effect on the humidity ratio of the air as there is no mass transfer occurring over the fan. Power limitations for the fan are taken into account in the maximum flow rate of air that can be produced. This is shown in equations 3.42 and 3.43:

$$\dot{m}_c = \frac{1}{\tau_v}\left(uc_v(t) - \dot{m}_c(t)\right) \tag{3.42}$$

$$LL_{mv} \leq \dot{m}_c(t) \leq UL_{mv} \tag{3.43}$$

3.4 Simulation

The modelling and simulation package that was used for all simulations in this thesis is ESL (European Simulation Language, ISIM Limited). Despite being originally developed for the European Space Agency for satellite and spacecraft simulation, ESL is a general purpose Continuous System Simulation Language (CSSL) which can be used to model all types of dynamical systems. ESL possesses many desirable features e.g. discrete event capability, separate experiment and model specification sections, a submodel concept, clear model definition code and advanced discontinuity handling which is particularly important when modelling dynamic systems for controller design purposes. These features lend themselves well to solving the problem at hand and hence, this simulation package has been used in the work presented in this thesis.

The simulation model developed in this research is comprised of sub models files representing the zone, actuation system, controller and external environment and casual heat gains. A separate data package file contains all of the data for the buildings parameters such as heat transfer coefficients and room size etc. Each of the submodels was created using the ESL code implementation as opposed to the block diagram modelling approach.

This section presents the open loop responses of the system with both actuation systems in order to observe its characteristics and time response of its components. The simulations for Case 1 were run with 1 minute communication intervals and 10 integration steps per communications interval i.e., a time step of 6 seconds. Due to the faster dynamics associated with the components within the actuation system in Case 2, the simulations for Case 2 were run with 300 integration steps per 1 minute communication interval equating to a 0.2 second time step. Details of the building parameters are given in Table 3-1.

Parameter	Value (Units)	Parameter	Value (Units)
$\boldsymbol{C_a}$	1012 (J/kgK)	U_F	0.2 (W/m^{2}K)
$\boldsymbol{C_s}$	1000 (J/kgK)	U_{ft}	2.0 (W/m^{2}K)
$\boldsymbol{C_{ft}}$	900 (J/kgK)	M_a	691 (kg)
$\boldsymbol{A_s}$	192 (m^2)	M_{si}	7000 (kg)
$\boldsymbol{A_R}$	144 (m^2)	M_{se}	7000 (kg)
$\boldsymbol{A_w}$	17 (m^2)	M_{ft}	8000 (kg)
$\boldsymbol{A_F}$	144 (m^2)	K_{si}	0.1 (W/mK)
$\boldsymbol{A_{ft}}$	138 (m^2)	Th_{wall}	0.5 (m)
$\boldsymbol{U_R}$	0.13 (W/m^{2}K)	h_e	6.9277 (W/m^{2}K)
$\boldsymbol{U_W}$	1.5 (W/m^{2}K)	h_i	6.3557 (W/m^{2}K)

Table 3-1: Building Parameters

3.4.1 Open loop transient response - Case 1

The system was simulated running in open loop in order to demonstrate the effect of the actuation system on the zone air temperature and relative humidity. For the first test, the heater was turned on with a constant power of 4kW for a period of three hours, between 7 AM and 12 PM, and the mechanical ventilation switched off. The zone air temperature and relative humidity responses for this test are shown in Figure 3.4 and Figure 3.5 respectively. In order to show the effect of the mechanical ventilation system on the zone air temperature, the room must be heated so that the temperature of the air in the zone is higher than that of the outside air. Providing the outside air temperature is lower than the zone air temperature, the mechanical ventilation system has a cooling effect on the zone air by blowing the cold outside air into the zone. If the zone air temperature is already the same temperature as the outside air, then the effect of the mechanical ventilation system cannot be observed. Hence, for the second test, the heater was kept on at a constant power of 4kW with the ventilation being switched on for three hours at a mass flow rate of 0.25kg/s. The results of the second test are illustrated in Figure 3.6 and Figure 3.7. The values used for the parameters of the actuation system are given in Table 3-2.

Parameter	Value (Units)
LL_{Qh}	0 (W)
UL_{Qh}	10000 (W)
LL_{mv}	0 (kg/s)
UL_{mv}	0.35 (kg/s)
τ_h	120 (s)
τ_v	60 (s)

Table 3-2: **Actuation system parameters (Case 1)**

From Figure 3.4, it can be seen that when the zone air temperature reaches steady state, i.e. zero heat transfer to or from the air, the slope of the zone air temperature can be observed to follow the slope of the outside air temperature. This is to be expected since the only heat transfer process that is non-zero is the heat transferred

when the outside air temperature changes. When the heater is initially switched on, the air temperature rises before reaching steady state after approximately 15 minutes. The relative humidity of the zone can be seen to effectively mirror the response of the zone air temperature as expected from the relationship between relative humidity and air temperature expressed in equation 3.13.

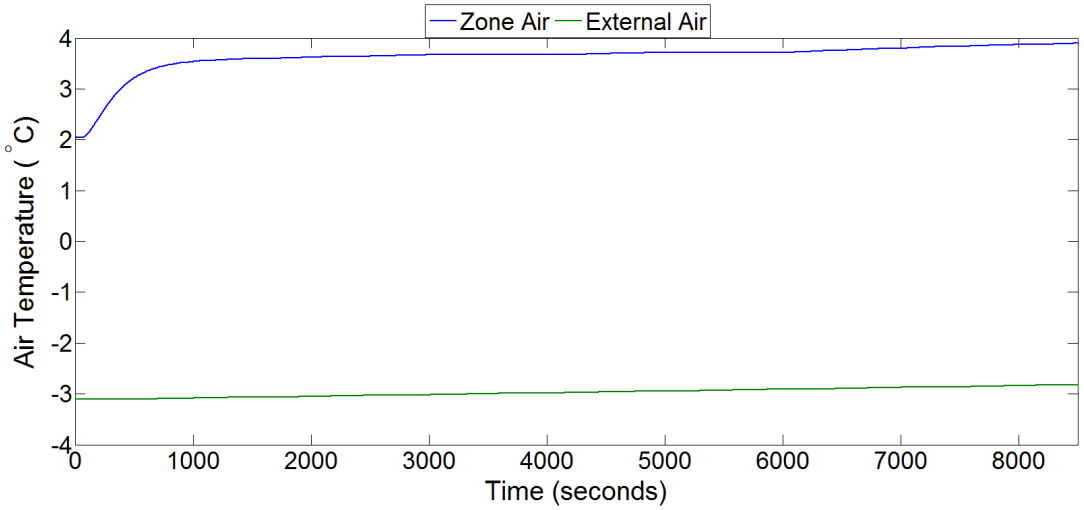

Figure 3.4: **Zone air temperature (Open Loop Heater Test - Case 1)**

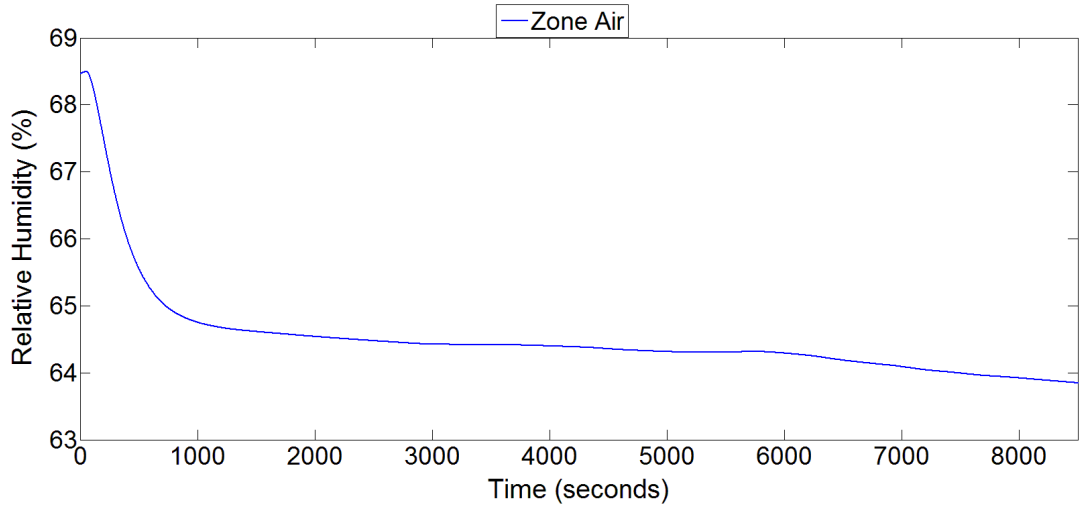

Figure 3.5: **Zone relative humidity (Open Loop Heater Test - Case 1)**

Figure 3.6 shows the response of the zone air temperature when the ventilation is switched on. The ventilation, delivering a flow rate of 0.25kg/s, causes the temperature to drop by approximately 0.7˚C. The relative humidity of the zone experiences a large increase from 68% to 90%. This large increase in relative humidity is due to the fact that the air supplied by the ventilation has a constant

humidity value of 0.02kg/kg which is significantly higher than the zone humidity. The slight decrease in the zone temperature also causes the zone relative humidity to increase. It is important to note that, from the results of both open loop tests, the response of the system can be seen to be predominantly first order.

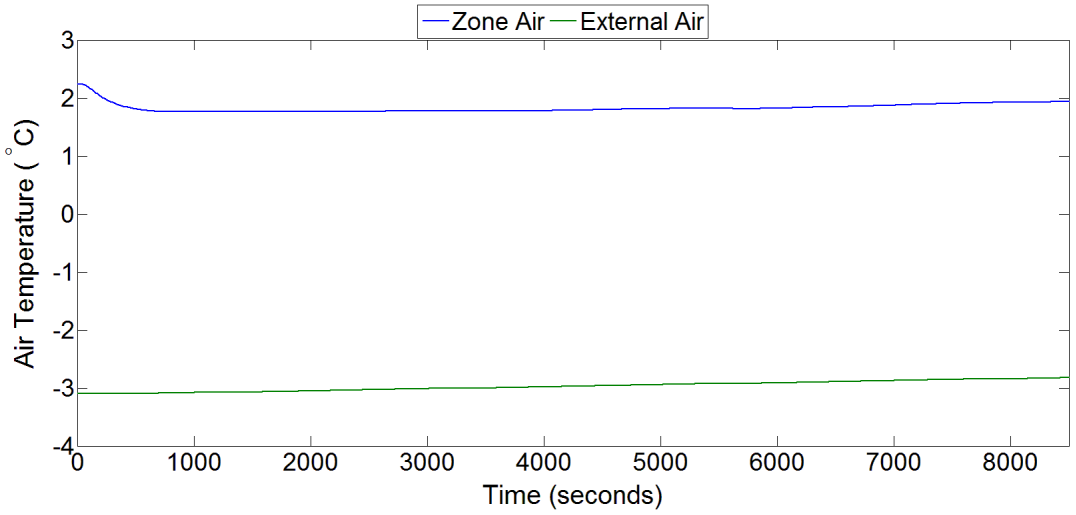

Figure 3.6: **Zone air temperature and heater power (Open Loop Ventilation Test - Case 1)**

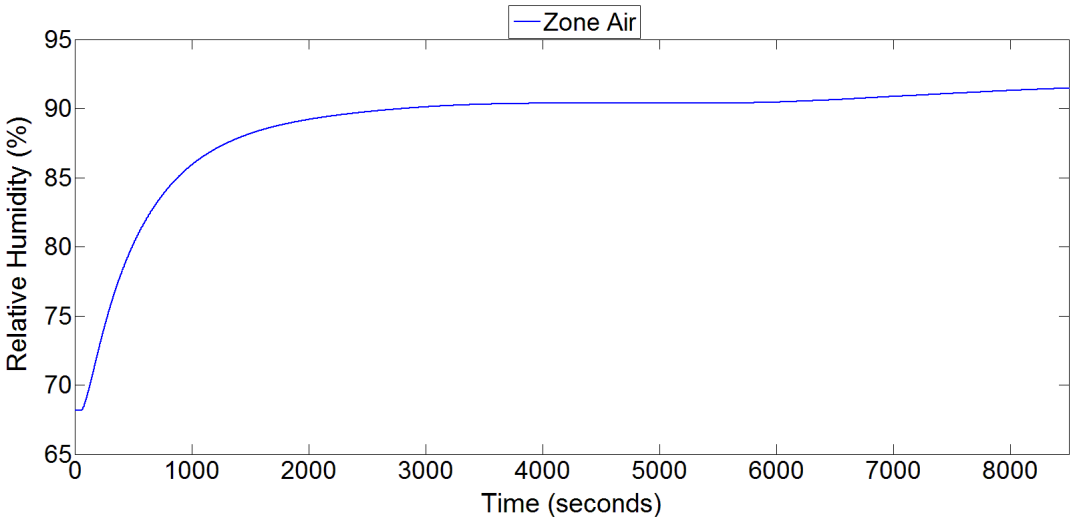

Figure 3.7: **Zone air temperature and ventilation mass flow rate (Open Loop Ventilation Test - Case 1)**

3.4.2 Open loop transient response - Case 2

The open loop tests for the AHU actuation system in Case 2 indicate how the system responds to heat input from the heating coil and humidification from the

humidifier. Similar to the open loop tests for the Case 1 actuation system, the heating coil is switched on for 3 hours at a power of 4kW for the first test. For the second test, the humidifier is switched on for a period of 3 hours with a humidification rate of 7.2kg/h. The parameter values for the AHU are given in Table 3-3.

Parameter	Value(Units)	Parameter	Value(Units)
$\boldsymbol{LL_{coil}}$	0 (W)	C_{ah}	4500 (J/K)
$\boldsymbol{UL_{coil}}$	20000 (W)	UA_{ah}	40 (J/sK)
$\boldsymbol{LL_{mv}}$	0 (kg/s)	h_{in}	8.33 (W/m^{2}K)
$\boldsymbol{UL_{mv}}$	0.5 (kg/s)	h_{out}	16.6 (W/m^{2}K)
$\boldsymbol{UL_{hum}}$	0 (kg/s)	M_{duct}	160.1 (kg)
$\boldsymbol{LL_{hum}}$	0.004 (kg/s)	V_h	1.44 (m^3)
$\boldsymbol{\tau_{coil}}$	15 (s)	V_{ah}	2.88 (m^3)
$\boldsymbol{\tau_{mv}}$	10 (s)	α_h	18.3 (J/sK)
$\boldsymbol{C_h}$	630 (J/K)	C_{duct}	418.7 (J/kgK)

Table 3-3: **Actuation system parameters (Case 2)**

The temperature of the supply air from the AHU rises by approximately 10˚C as a result of the heat input from the heating coil. This in turn causes a comparatively small increase in the zone air temperature of approximately 1.6˚C. The corresponding drop in the zone relative humidity is approximately 3.5% as shown in Figure 3.9.

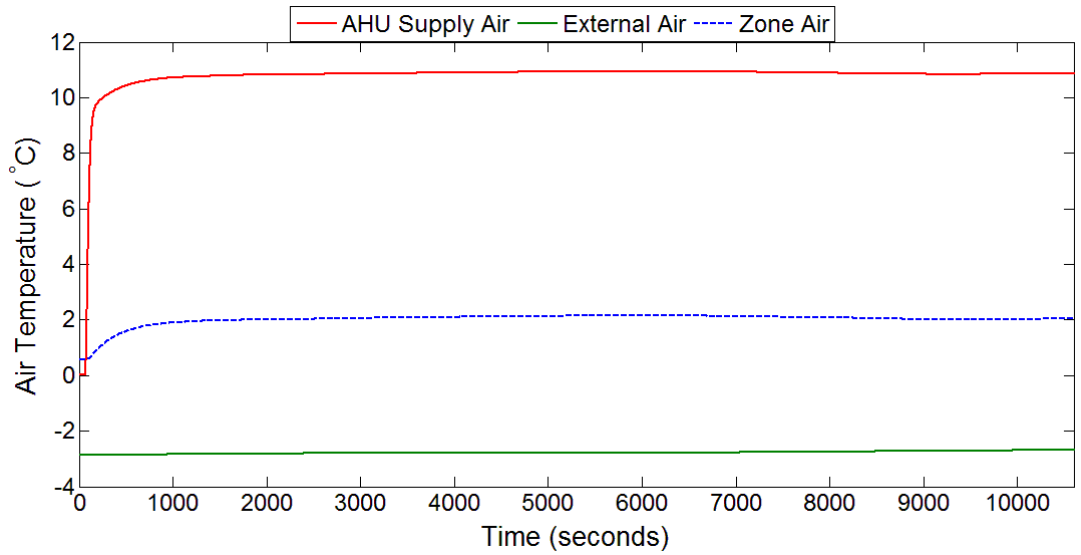

Figure 3.8: **Zone air temperature, AHU supply temperature and heater power (Open Loop Heater Test - Case 2)**

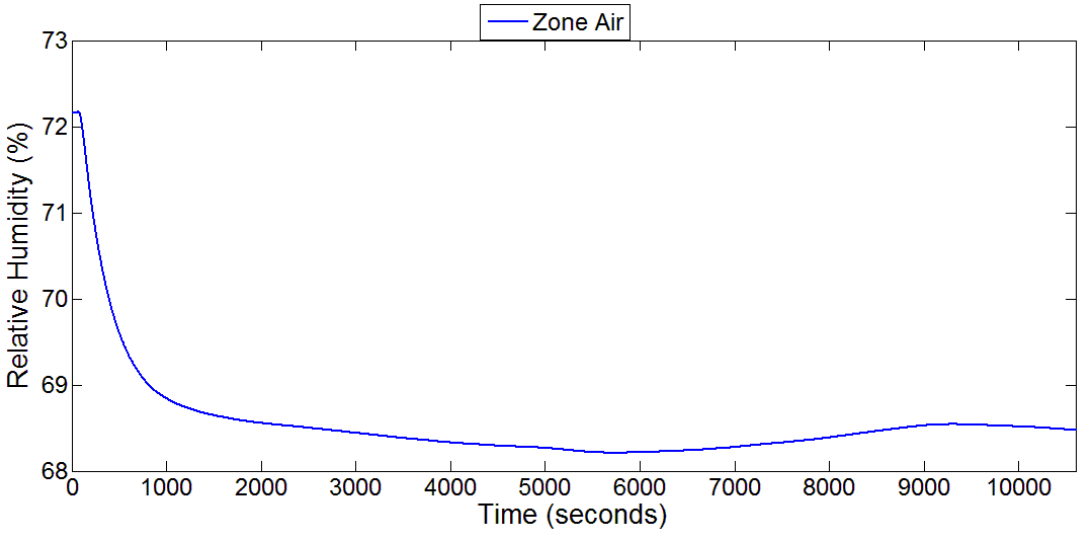

Figure 3.9: **Zone relative humidity (Open Loop Heater Test - Case 2)**

Figure 3.10 indicates that the humidifier does not affect the temperature of the zone air. This is to be expected as the humidification process only increases the moisture content in the air and there is no heat transfer taking place. The humidification causes the relative humidity of the zone to increase from approximately 78% to approximately 88%.

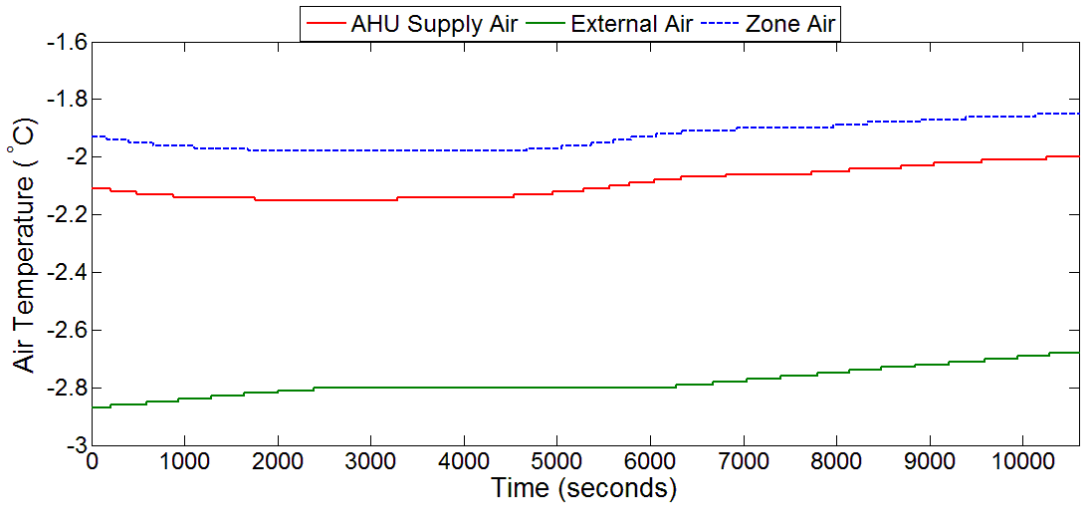

Figure 3.10: Zone air temperature, AHU supply temperature and heater power (Open Loop Humidifier Test - Case 2)

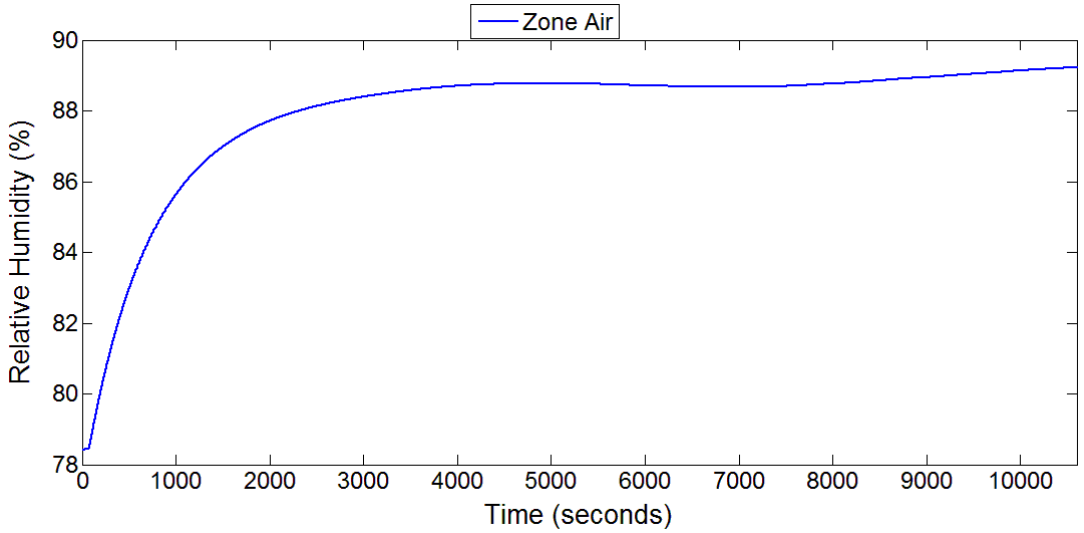

Figure 3.11: Zone relative humidity (Open Loop Humidifier Test - Case 2)

3.5 Chapter Conclusions

This chapter demonstrated the development a simplified low order building zone model which is suitable for controller design purposes. The building zone was represented as a fifth order model with four state variables for temperature and one for humidity. Two different actuation systems were developed for conditioning the zone thermal comfort. Firstly, a fast acting direct heater and mechanical ventilation

system, represented with first order models, were developed for controlling the zone air temperature and humidity respectively – case 1 in chapter 3. Secondly, the zone model was combined with a full air handling unit model which included a humidifier and a heating coil for conditioning the supply air – case 2 in chapter 3. The AHU was represented as a fifth order model with three states for temperature and two states for humidity. The overall system model was nonlinear with multiple inputs and outputs and dynamic casual gains and weather data. This provided a complex control task which included many of the complexities that would be encountered when designing a HVAC control system in practice. Open loop simulation tests showed that the model exhibits a predominantly first order response, despite being of higher order, as would be expected. It is important to note that this model is not intended as a model for accurately assessing the building zone energy performance behaviour. It is intended as a model which can produce representative dynamic behaviour of a building zone and actuation system and is suitable for controller design purposes. This model is used to assess the different aspects of the controller algorithms designed in this thesis and therefore the realism of the energy performance is not of particular importance. Furthermore, the purpose of the control algorithms developed in this thesis was to be able to control building HVAC systems with a wide range of dynamic characteristics, thus calibrating the model such that it performed with particular dynamic behaviour would have been redundant.

As shown in section 3.2, the model can be represented in state space format and can therefore be used in the controller algorithm design processes developed in this thesis. The following chapter explains the fundamentals of the high performance controller designs used in this thesis.

3.6 Chapter References

Balaras, C. (1996). "The role of thermal mass on the cooling load of buildings. An overview of computational methods." Energy and Buildings **24**(1): 1-10.

Bi, Q., W. J. Cai, et al. (2000). "Advanced controller auto-tuning and its application in HVAC systems." Control Engineering Practice **8**(6): 633-644.

Clark, D., C. Hurley, et al. (1985). "Dynamic models for HVAC system components." ASHRAE transactions **91**(1): 737-751.

Counsell, J. (1992). Optimum and Safe Control Algorithm for Modern Missile Autopilot Design. PhD, Lancaster University.

Counsell, J. M., Y. A. Khalid, et al. (2011). "Controllability of buildings: A multi-input multi-output stability assessment method for buildings with slow acting heating systems." Simulation Modelling Practice and Theory **19**(4): 1185-1200.

De Keyser, R., F. Dumortier, et al. (1984). Modelling, simulation and adaptive control of a domestic floor heating system. Proceedings of the International Symposium on the Performance of HVAC Systems and Controls in Buildings, Garston, United Kingdom.

Gouda, M., C. Underwood, et al. (2003). "Modelling the robustness properties of HVAC plant under feedback control." Building Services Engineering Research and Technology **24**(4): 271-280.

Kasahara, M., T. Yamazuki, et al. (2001). "Stability analysis and tuning of PID controller in VAV systems." TRANSACTIONS-AMERICAN SOCIETY OF HEATING REFRIGERATING AND AIR CONDITIONING ENGINEERS **107**(1): 285-296.

Khalid, Y. A. (2011). Controllability of Building Systems. PhD, University of Strathclyde.

Murphy, G. B. (2012). Inverse Dynamics based Energy Assessment and Simulation. PhD, University of Stratchlyde.

Rentel-Gomez, C. and M. Velez-Reyes (2001). Decoupled control of temperature and relative humidity using a variable-air-volume HVAC system and non-interacting control. Control Applications, 2001.(CCA'01). Proceedings of the 2001 IEEE International Conference on, IEEE.

Tashtoush, B., M. Molhim, et al. (2005). "Dynamic model of an HVAC system for control analysis." Energy **30**(10): 1729-1745.

Tashtoush, B., M. Molhim, et al. (2005). "Dynamic Model of an HVAC System for Control Analysis." **30**: 1729-1745.

Zhang, H. and H. Yoshino (2010). "Analysis of indoor humidity environment in Chinese residential buildings." Building and Environment **45**(10): 2132-2140.

4. Fundamentals of Robust High Performance Control Theory

The objective of the research in this PhD project, as mentioned in Chapter 1, was to design a robust high performance HVAC control strategy that is capable of dealing with the complexities associated with modern building control whilst being a low cost solution which is easy to implement. Robust high performance control means achieving the desired tracking objectives quickly and efficiently whilst dealing with the following issues:

- Uncertainties
- Nonlinearity
- Interacting MIMO systems
- Actuator power limitations
- Disturbances

Since buildings and their HVAC systems often possess all of the complexities mentioned above, advanced control strategies are required in order to ensure that comfort requirements are met efficiently. Therefore it is intuitive that the fundamental structure of the control systems developed must be robust and enable high performance. This chapter describes the fundamentals of the robust control methods used in this thesis including the RIDE control theory which is a robust nonlinear inverse dynamics (NID) controller design originally applied in the aerospace industry (Counsell 1992). To the extent of the author's knowledge, this algorithm has not been used for the design of HVAC control systems, other than in the author's own work (Zaher, Counsell et al. 2011). This algorithm provides an interesting approach to HVAC control systems design which is not typically used in the buildings industry. This theory was used as the structure for the various advancements developed in this thesis. Hence, it is imperative that the reader is familiarised with its concepts so as to clarify its robust structure and enabling

features which are essential to the control methods described in the subsequent chapters.

4.1 Inverse Dynamics

The fundamental concept of inverse dynamics is a straightforward and logical one. If the dynamics of the system are known such that, for a given input, the output of the system can be determined then the dynamics can be inverted in order to determine the required input for a desired output as illustrated below.

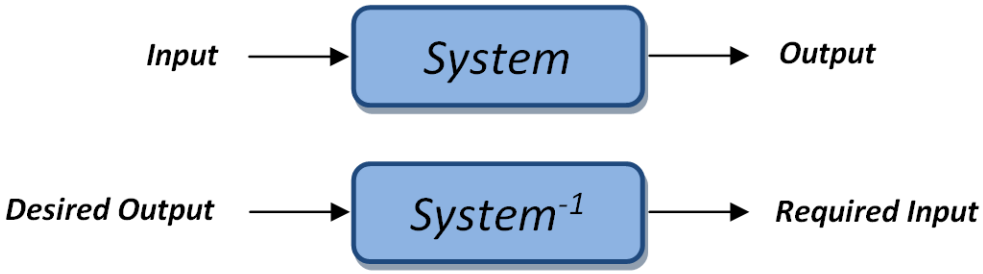

Figure 4.1: Inverse Dynamics Concept

For a given system, inverse dynamics can be utilised in the control system design in order to cancel the systems dynamics, enabling the control system designer to specify the desired closed loop dynamics. By using the dynamic inverse to cancel the systems dynamics, any cross coupling between control channels, disturbances and nonlinear behaviour which would otherwise cause control problems are removed (Lane and Stengel 1988).

In practice, the implementation of inverse dynamics can be difficult, or in some cases, impossible as full knowledge of the system dynamics, including any disturbances, is required. The RIDE control algorithm however, provides an effective and practical approach to implementing inverse dynamics. It possesses many desirable features which have proven invaluable in the design of the HVAC control strategies developed in this thesis. These advantageous enabling features work hand in hand with the methods developed in order to create robust high performance HVAC control strategies. In order for the reader to understand the novel controller methods described in the subsequent chapters, the fundamentals behind the RIDE methodology must be explained.

4.2 Equivalent Control – The Perfect Control Input

Equivalent control is the nonlinear dynamic inverse of a plant required to remove any interaction between controlled channels, nonlinear plant dynamics and disturbances. This type of control is derived from high gain and sliding mode control principles. Equivalent control is an integral part of the RIDE control theory and therefore it is imperative that the reader is familiarised with its properties and effects.

Equivalent control is based on the simple observation that controlling a first order system is straightforward in comparison to controlling higher order systems. The equivalent control method (Utkin 1971), in the output feedback mode, produces a reduced-order system which exhibits output feedback equivalent dynamics (Slotine and Li 1991). This methodology can be viewed as a form of realisable inverse dynamics due to the use of the equivalent control input which inverts the model with respect to the controlled outputs (Khalid 2011).

Consider a system whose measured output is denoted by *y(t)* and the desired output is denoted by *v(t)*. Steady state tracking of a constant reference input, *v(0)*, for a feedback control system (Bradshaw and Counsell 1992) can be expressed as:

$$\lim_{t\to\infty} e(t) = v(t) - y(t) \to 0 \tag{4.1}$$

If condition 3.14 is satisfied, then steady state tracking is attained even in the presence of a disturbance vector, *d(t)*. The tracking objective then, is to drive the system output to track the desired output such that *y(t)=v(t)* in steady state. When this criterion is satisfied, the tracking error, defined as *e(t)=v(t)-y(t)*, is zero and the system is in a condition referred to as sliding mode, where the sliding surface, denoted by *s(t)*, is the tracking error, *e(t)*. When in sliding mode, the rate of change of *e(t)* is zero as shown below (Khalid 2011):

$$\dot{s}\,(t) = \dot{v}(t) - \dot{y}(t) = 0 \tag{4.2}$$

$$when\ v(t)\ is\ constant\ \rightarrow \dot{v}(t) = \dot{y}(t) = 0 \tag{4.3}$$

The actuator inputs required to ensure the criterion in equation 4.3 is achieved are determined by the equivalent control using inverse dynamics. This is achieved by accounting for the disturbances and system dynamics that would otherwise prevent the system from operating like an ideal integrating system. Let us consider that the system is linear and is represented by the following state equation:

$$\dot{x}(t) = Ax(t) + Bu(t) + Fd(t) \tag{4.4}$$

The output or measured variable *y(t)* is related to the state *x(t)* by:

$$y(t) = Cx(t) \tag{4.5}$$

When the system is in sliding mode i.e. steady state, the rate of change of the system output is equal to zero as shown below.

$$\dot{y}(t) = C\dot{x}(t) = 0 \tag{4.6}$$

The state equation representing the system can then be substituted into equation 4.6 to give:

$$\dot{y}(t) = CAx(t) + CBu(t) + CFd(t) = 0 \tag{4.7}$$

From equation 4.3, it can be seen that, when *v(t)* is constant, the tracking objective entails driving the rate of change of the system output to zero i.e. steady state. The input signal which drives the system dynamics $\dot{s}_x(t)$ to zero is:

$$u(t) = -(CB)^{-1}CAx(t) - (CB)^{-1}CFd(t) \tag{4.8}$$

Substituting equation 4.8 back into equation 4.4 gives:

$$\dot{x}(t) = Ax(t) + B(-(CB)^{-1}CAx(t) - (CB)^{-1}CFd(t)) + Fd(t) \quad (4.9)$$

This results in $\dot{x}(t) = 0$. Therefore it can be seen that when the system is in sliding mode, it is unaffected by external disturbances and is able to reach steady state. This virtual control input U derived above is known as the equivalent control input, $u_{eq}(t)$.

4.2.1 Effects of Equivalent Control

In order to understand the benefits of using equivalent control, it is necessary that the effects of its use are explained. Consider the basic feedback control system illustrated in Figure 4.2 which combines the equivalent control input with a controller matrix *K*.

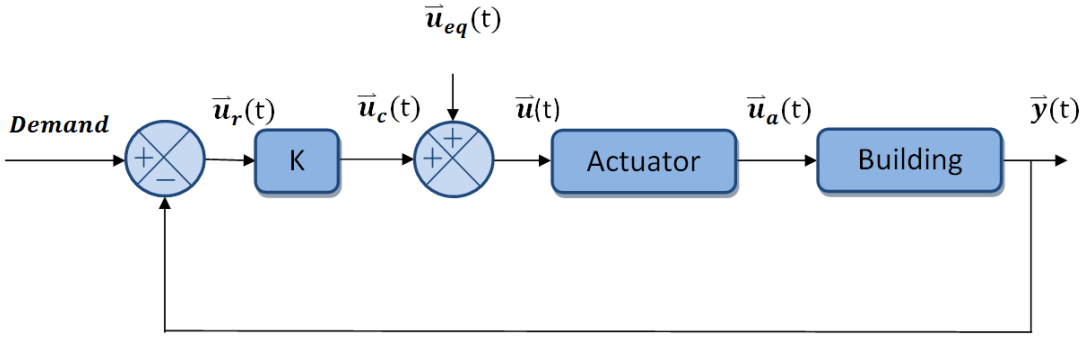

Figure 4.2: Control system with controller matrix K(t) and dynamic inverse input $U_{eq}(t)$

Where $u_r(t)$ is the reference input to the controller, $u_c(t)$ is the controller output, $u(t)$ is the control signal to the actuator, $u_a(t)$ is the actuator output and $y(t)$ is the actual system output. When designing a control system, it is of course necessary that the relevant actuator dynamics are represented in the state equations. However, high frequency dynamical modes should not be included as they would serve only to obscure the important features at the initial design stage (Khalid 2011). It has been shown that, if the control system bandwidth is designed such that it is three times slower than the actuator and sensor bandwidths, the actuator and sensor dynamics can be neglected as 'parasitics' (Khalid 2011). In order to demonstrate how the use of equivalent control reduces the order of the system, the actuator bandwidth is considered to be fast in comparison to the control system bandwidth and thus the actuator transfer function is equal to 1. Hence $u(t)$ becomes $u_a(t)$. If the control signal

from Figure 4.2, $u(t)=u_c(t) + u_{eq}(t)$, is substituted into the state equation 4.4, it becomes:

$$\dot{x}(t) = Ax(t) + B\left(u_c(t) + u_{eq}(t)\right) + Fd(t) \qquad (4.10)$$

Equation 4.5 can then be differentiated in order to obtain the rate of change of output and equation 4.10 substituted into it. A Laplace transform ('s') of the resulting equation can then be taken in order to give a transfer function from input to output and from disturbance to output:

$$sy(s) = CAx(s) + CB\left(u_c(s) + u_{eq}(s)\right) + CFd(s) \qquad (4.11)$$

Substituting the input from equation 4.8 into 4.11 yields:

$$sy(s) = CBu_c(s) \qquad (4.12)$$

$$\frac{y(s)}{u_c(s)} = s^{-1}ICB \qquad (4.13)$$

Thus it is shown that the equivalent control input can reduce a higher order system to a first order system represented by the transfer function, $s^{-1}ICB$. Any n^{th} order system with the equivalent control input and controller gain K will be reduced to the generic reduced order transfer function in equation 4.13. Therefore, u_{eq} can be considered to be the perfect control input which is able to control a complex higher order system such that it behaves like a first order system, even in the presence of disturbances.

4.3 Robust Inverse Dynamics Estimation (RIDE)

The structure of the RIDE controller is based on the remarkable pseudo-derivative-feedback (PDF) control structure developed by Richard Phelan (Phelan 1977). Phelan demonstrated that simple first order systems could be perfectly controlled using the mathematically simple PDF control strategy. As explained in the

preceding section, through the use of equivalent control, higher order systems can be reduced to behave like first order systems. In a coupled multivariable system, the equivalent control input also serves the purpose of decoupling the control channels such that they behave as independent SISO channels characterised by first order responses, as shown in equation 4.13 in the previous section. Thus, the PDF control structure is ideal for use with the equivalent control input. The RIDE controller methodology combines the properties of equivalent control with the PDF control structure and extends them for use with MIMO systems. The PDF control structure also provides the necessary robustness features which are of key importance to the successful performance of the methods developed in this thesis as will be shown in this section.

Consider an open loop multivariable system transfer function in state space:

$$\dot{x}(t) = Ax(t) + Bu(t) + Fd(t) \tag{4.14}$$

$$w(t) = Mx(t) \tag{4.15}$$

Where *M* is the output matrix designed by the user which determines the feedback measurements (Khalid 2011). Differentiating equation 4.15 and substituting equation 4.14 into it gives:

$$\dot{w}(t) = MAx(t) + MBu(t) + MFd(t) \tag{4.16}$$

If *MB* is not equal to zero and *MA* and *MF* are cancelled, the system is reduced to:

$$w(s) = s^{-1}IMBu(s) \tag{4.17}$$

Figure 4.3 shows the reduced order system under closed loop control in block diagram form:

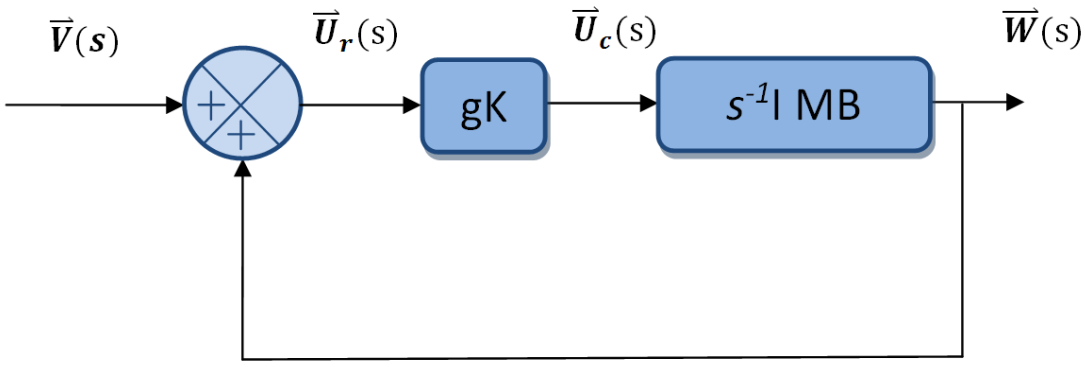

Figure 4.3: Simple feedback control system with the reduced order system

Where *V(s)* is the set-point, *Y(s)* is the system output, *g* is the scalar gain and *K* is the controller gain matrix. If the controller matrix *K* is chosen to be MB^{-1}, the closed loop systems transfer function would be reduced to a perfect first order system and each channel of the multivariable system would behave like a perfect integrator for each control variable i.e. an ideal non interacting Multi - Single Input Single Output (M-SISO) system which can be expressed by:

$$\begin{bmatrix} y_1(s) \\ y_2(s) \\ \vdots \\ y_n(s) \end{bmatrix} = \begin{bmatrix} \frac{g}{s_1+g} & 0 & \cdots & 0 \\ 0 & \frac{g}{s_2+g} & 0 & \vdots \\ \vdots & 0 & \ddots & 0 \\ 0 & \cdots & 0 & \frac{g}{s_n+g} \end{bmatrix} \begin{bmatrix} v_1(s) \\ v_2(s) \\ \vdots \\ v_n(s) \end{bmatrix} \qquad (4.18)$$

Where the closed loop system time constant is *1/g* and the bandwidth is *g*. By selecting the correct feedback for the control system, it is relatively easy to ensure that $MB \neq 0$. The difficulty generally arises when attempting cancel *MA* and *MF*. This particular case is addressed in the RIDE methodology by adding the equivalent control input $u_{eq}(t)$ to the control law as shown in Figure 4.4.

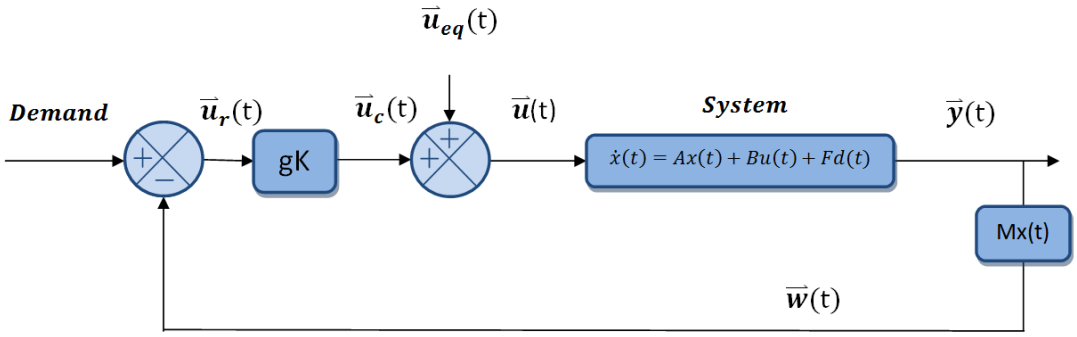

Figure 4.4: Closed loop control system with u_{eq}

By setting the gain matrix *K* to $(MB)^{-1}$ the control law becomes:

$$u_c(t) = g(MB)^{-1}\big(r(t) - w(t)\big) + u_{eq}(t) \qquad (4.19)$$

Where *r(t)* is the demand signal. If equation 4.19 is substituted into equation 4.16, this gives:

$$\dot{w}(t) = MAx(t) + gI\big(r(t) - w(t)\big) + MBu_{eq}(t) + MFd(t) \qquad (4.20)$$

Substituting the equivalent control input equation 4.8 into equation 4.20 results in the *MA* and *MF* terms being cancelled thus reducing the system to:

$$\dot{w}(t) = gI\big(r(t) - w(t)\big) \qquad (4.21)$$

This is equivalent to being a system where *CA=0*. In the Laplace domain, equation 4.21 becomes:

$$w(s) = gI(sI + gI)^{-1}r(s) \qquad (4.22)$$

This control law is valid for all values of the matrix *MA* as the u_{eq} input cancels the *MA* and *MF* terms. Furthermore, substituting this control law into the state equation 4.14 results in $\dot{x}(t) = 0$, meaning u_{eq} has driven the system to steady state. The only requirement for u_{eq} to cancel the *MA* and *MF* terms is $|MB| \neq 0$.

As mentioned earlier in this section, the PDF algorithm provides the perfect control law for controlling a first order system. Since the equivalent control input is able to decouple the multivariable system and reduce each control channel to a perfect integrator, the PDF controller can be used to perfectly control its response, which is a function of its gains. Hence the combination of the PDF algorithm with the equivalent control input theoretically provides a 'perfect control algorithm'. The RIDE control law, which incorporates the PDF structure, is given by:

$$u_c(t) = K_I z(t) - K_P w(t) + u_{eq}(t) \tag{4.23}$$

$$\dot{z}(t) = e(t) = r(t) - w(t) \tag{4.24}$$

The controller is shown in diagrammatic form in Figure 4.5.

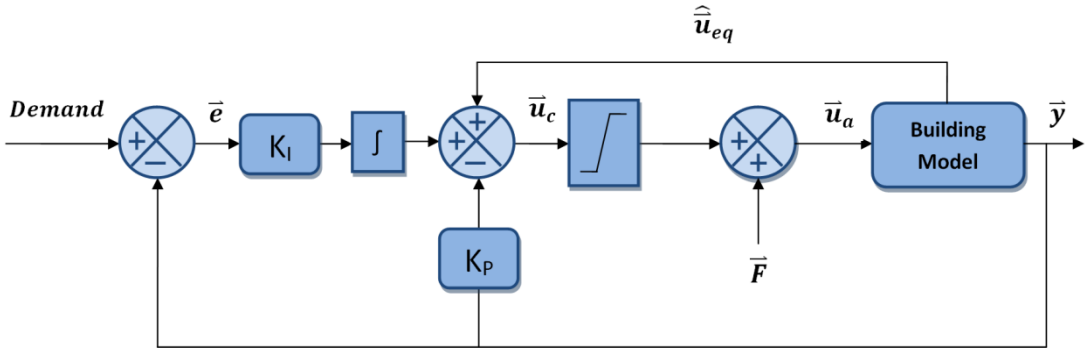

Figure 4.5: RIDE structure

Where $\vec{F}$ is disturbance. If the control law equation 4.23 is substituted into equation 4.16, this gives:

$$\dot{w}(t) = MB\left(K_I z(t) - K_p w(t)\right) \tag{4.25}$$

The closed loop transfer function of the plant and control system illustrated in Figure 4.5 is given by:

$$[G(s)] = [s^2 I_m + s(K_P MB) + K_I MB]^{-1} K_I MB \tag{4.26}$$

Where I_m is an identity matrix. The proportional and integral gains can be selected such that they are expressed as follows:

$$K_P = [MB]^{-1} g \tag{4.27}$$

$$K_I = [MB]^{-1} \rho \tag{4.28}$$

Where $g = 2Z_d\Omega_n$ and $\rho = \Omega_n{}^2$. Z_d and Ω_n are the designed system damping ratio and natural frequency respectively. By setting K_P and K_I as in equations 4.27 and 4.28, the system transfer function can be expressed as a diagonal matrix of ideal second order transfer functions in generalised form as shown below:

$$[G(s)] = \begin{bmatrix} \frac{\Omega_n{}^2}{s^2 + 2Z_d\Omega_n s + \Omega_n{}^2} & 0 & \cdots & 0 \\ 0 & \frac{\Omega_n{}^2}{s^2 + 2Z_d\Omega_n s + \Omega_n{}^2} & 0 & \vdots \\ \vdots & 0 & \ddots & 0 \\ 0 & \cdots & 0 & \frac{\Omega_n{}^2}{s^2 + 2Z_d\Omega_n s + \Omega_n{}^2} \end{bmatrix} \tag{4.29}$$

The diagonal matrix [G(s)] has the dimensions m x m, where m is the number of system inputs. The system response can be shaped by tuning K_P and K_I through Z_d and Ω_n. Thus it is shown that applying the RIDE control law results in the controlled system behaving like an ideal second order system and its response is completely controllable as a function of the controller gains matrices. This allows the control system designer to specify the closed loop bandwidth and damping ratio of the system being controlled thus enabling an improved level of control over the response characteristics of the buildings systems.

So far it has been considered that the equivalent control term is implemented using equation 4.8. In practice, u_{eq} is derived from the model of the system which is

an approximation of the real dynamics of the system. Therefore, the u_{eq} implemented in practice would in fact be an estimate of the real u_{eq} and an error of some magnitude would exist. The RIDE control law would therefore become:

$$u_c(t) = K_I z(t) - K_P w(t) + \hat{u}_{eq}(t) \tag{4.30}$$

Where $\hat{u}_{eq}(t)$ denotes the estimated equivalent control. An error in the estimated equivalent control would result in the system not behaving as a completely decoupled first order system. It can be seen from equation 4.8 that implementing equivalent control in this way is somewhat impractical as full knowledge of the systems dynamics, including any disturbances, as well as measurement of all state variables and disturbances is required. Thus, the implementation of equivalent control in practice is often disregarded. In order to alleviate the difficulty in implementing equivalent control, the RIDE controller algorithm utilises an estimate of the equivalent control (Muir and Bradshaw 1996) which requires less information and knowledge of the system. Consider dividing equation 4.16 by *MB*:

$$\begin{aligned}(MB)^{-1}\dot{w}(t) &= (MB)^{-1}(MAx(t) + MFd(t)) + u(t) \\ &= -u_{eq}(t) + u(t)\end{aligned} \tag{4.31}$$

Rearranging this equation yields another expression for the equivalent control:

$$u_{eq}(t) = u(t) - (MB)^{-1}\dot{w}(t) \tag{4.32}$$

It can be seen from equation 4.32 that the equivalent control can be estimated with knowledge of the matrix *MB*, rate of change of the measured variable *w(t)* and the actuator output *u(t)*. This greatly simplifies the implementation of equivalent control in practice since modelling the system with fully detailed system (*A*) and disturbance (*F*) matrices is no longer required. It is necessary however to assess the sensitivity of MB as it has a direct bearing on the feasibility of perfect control.

4.3.1 Controller Robustness

As the equivalent control used in the RIDE control law is an estimate of the exact equivalent control based on a system model, un-modelled disturbances as well as modelling errors in the *CB* matrix will cause the estimated equivalent control to deviate from the real equivalent control. This will result in the system not behaving as a fully decoupled system and the disturbances will not be fully cancelled. This issue however, is dealt with in the RIDE structure which provides a degree of insensitivity to errors in the u_{eq} estimation (Khalid 2011).

If the control law equation 4.23 is substituted into equation 4.32, this gives:

$$(MB)^{-1}\dot{w}(t) = \hat{u}_{eq}(t) - u_{eq}(t) + K_I\vec{y}(t) - K_P\vec{y}(t) \qquad (4.33)$$

Differentiating equation 4.33 twice and substituting equation 4.24 in and then taking the Laplace transform of the resulting equation gives:

$$[(MB)^{-1}s^2 + K_P s + K_I]w(s) = s\left[\hat{u}_{eq}(s) - u_{eq}(s)\right] + K_I r(s) \qquad (4.34)$$

It can be seen that if the equivalent control estimate approaches the real equivalent control such that $\hat{u}_{eq}(s) = u_{eq}(s)$, then a perfect second order closed loop response which can be shaped through the controller gains is achieved as shown below:

$$\frac{w(s)}{r(s)} = {\Omega_n}^2\left[s^2 + 2Z_d\Omega_n s + {\Omega_n}^2\right]^{-1} \qquad (4.35)$$

In practice however, $\hat{u}_{eq}(t)$ may be somewhat inaccurate due to modelling inaccuracies and un-modelled disturbances as mentioned previously. In that case, in terms of high gain singular perturbation method (Khalid 2011), dividing both sides of equation 4.34 by g and rearranging gives:

$$\left[\frac{s^2}{g} + s + \frac{\rho}{g}\right]w(s) = \frac{sMB\left[\hat{u}_{eq}(s) - u_{eq}(s)\right]}{g} + \frac{\rho}{g}r(s) \qquad (4.36)$$

As g tends to infinity s tends to zero resulting in $w(s)=r(s)$. Of course, in practice, it is not possible to achieve infinite gain. Furthermore, in systems with slow actuation systems, a lower gain value is typically required. Hence, the more accurate the equivalent control calculation, the smaller the $\Delta u_{eq}(s)$ term meaning a lower gain value can be used to make the effects negligible. In this sense, an accurate estimate of $u_{eq}(s)$ makes this a low gain method. Reducing the sensitivity of the controller to $\Delta u_{eq}(s)$ further is the structure of the PDF algorithm itself. This is shown by dividing both sides of equation 4.34 by the integral gain ρ as sown below:

$$\left[\frac{s^2}{\rho}+\frac{gs}{\rho}+1\right]w(s)=\frac{sMB\left[\hat{u}_{eq}(s)-u_{eq}(s)\right]}{\rho}+r(s) \qquad (4.37)$$

It can be seen that, if the integral gain is made to be very high, the system is driven to steady state i.e. $w(s)=r(s)$. Furthermore, as the system tends to steady state i.e. s tends to zero, the effect of $\Delta u_{eq}(s)$ also becomes zero. Therefore the integral gain should be increased as much as possible. There is however, a limit as to how much the integral gain can be increased before increasing the system's sensitivity to unknown dynamics, such as delays from actuator and sensor dynamics which with too high a gain, will eventually drive the system to closed loop instability. The auto-tuning algorithm presented in Chapter 5 alleviates the difficulty in determining this optimum value of gain.

Overall it has been shown that the RIDE control algorithm is robust against errors in the estimated inverse dynamics i.e. u_{eq}. This robustness property makes it an excellent algorithm for dealing with uncertain systems like buildings. It also provides a good foundation for the identification method described in Chapter 6.

4.3.2 Dealing with Actuation System Limits

Actuator limitations are extremely important in controller design as they govern the maximum achievable controller performance, irrespective of the controller design. It is the controller design that determines how close actual performance is to the maximum achievable. Therefore, it is important that the control law is able to operate the system within its limits and does not drive the system to perform an

operation that is out with its capability e.g., in this application, asking the actuator (heater) to deliver more heat than it is physically able to provide. If this situation arises and the controller output continues to build up, demand more output from the actuator, then the actuator will be forced to stay on its limit for longer than is necessary to achieve the desired performance. This is an issue which causes many problems with systems in practice (Khalid 2011). It is therefore necessary that the control algorithm has a means with which to deal with actuator limitations in order to achieve optimum and safe control. The safety criteria for u_{eq} (Counsell 1992) was developed in order to ensure the safe operation of the control system under disturbances and actuator nonlinearities since power limitations on the plants actuation systems cause limitations on maintaining stable tracking. The algorithm works on the principle that when the actuator output, has reached its upper (L_U) or lower (L_L) limits, the control signal to the actuator, $u_c(s)$, must either remain constant or decrease in order to avoid overdriving the actuator and to maintain safe control. This is achieved by using a dynamic method for limiting the control signal produced by the controller. The following commutation law is used with the RIDE control algorithm to provide a Variable Structure Control (VSC) design which prevents the controller output from exceeding the actuator limits:

$$\dot{z}_i(t) = \begin{cases} 0, & if\ \alpha u_i < 0\ \ \boldsymbol{OR}\ \ \alpha l_i > 0 \\ e_i(t), & if\ \alpha u_i > 0\ \ \boldsymbol{OR}\ \ \alpha l_i < 0 \end{cases} \tag{4.38}$$

$$e_i(t) = r_i(t) - y_i(t) \tag{4.39}$$

$$\alpha u_i = (L_U - u_c)_i \tag{4.40}$$

$$\alpha l_i = (L_L - u_c)_i \tag{4.41}$$

Where *i* is the control channel. The tracking criterion, derived in (Counsell, Brindley et al. 2009), which the system must satisfy in order to be able to safely reach its set point is shown below:

$$L_L - \frac{s\hat{\vec{u}}_{eq}(s)}{g} \leq \vec{u}_{eq}(s) \leq L_U - \frac{s\hat{\vec{u}}_{eq}(s)}{g} \tag{4.41}$$

It can be seen from equation 4.38 that providing the closed loop response is fast i.e. g is relatively large compared with rates of change of $u_{eq}(s)$, the tracking criteria reduces to:

$$L_L \leq \vec{u}_{eq}(s) \leq L_U \tag{4.42}$$

This criterion demonstrates that by setting the error signal in the RIDE topology to zero when actuator limits are reached, safety can be ensured on the condition that steady state is reachable i.e. $u_{eq}(s)$ satisfies the criteria in equation 4.38 (Counsell, Brindley et al. 2009).

4.3.3 System Stability

In order to ensure that the system is controllable in a safe and stable manner, a stability analysis for the system must be performed. This involves determining the transmission zeros for the system. The stability of the closed loop system is determined by the locations of the closed loop poles. The closed loop poles of the system are the values of '*s*' at which the system characteristic equation is equal to zero. The locations of the closed loop poles in a PI design vary with differing gain values, however in the RIDE design the final position of the pole(s) are restricted to those given by the characteristic equation in equation 4.35 and by the position of the fixed open loop zeros. Since the open loop zeros (known as transmission zeros for MIMO systems) correspond to the closed loop poles, it is imperative that the transmission zeros are determined so as to establish whether the system can be stabilised when using either high gain feedback control or inverse dynamics (Counsell, Khalid et al. 2011). This is due to the fact that, if the transmission zeros are unstable then the closed loop poles migrate towards these unstable transmission zeros with increasing gain, ultimately making the system unstable. For a system represented by state space equations 4.4 and 4.5, the transmission zeros can be calculated by evaluating the following determinant (Khalid 2011):

$$\begin{vmatrix} A - sI & B \\ C & D \end{vmatrix} = 0 \tag{4.46}$$

4.4 Chapter Conclusions

It was shown that the perfect control input coupled with the PDF algorithm can be used to control highly nonlinear multivariable systems. Furthermore, the algorithm was shown to be robust against modelling inaccuracies and disturbances. This is an important feature and an advantage over PID controllers or PID based controllers whose structure does not offer the same level of robustness. From a building control system design perspective, the RIDE algorithm provides an interesting and unconventional approach for designing robust and high performance control systems. The features of this algorithm described in this chapter make it a good foundation on which the advanced methods described in the subsequent chapters can be developed.

4.5 Chapter References

Bradshaw, A. and J. Counsell (1992). "Design of autopilots for high performance missiles." IMechE Journal of Systems & Control: 75-84.

Counsell, J. (1992). Optimum and Safe Control Algorithm for Modern Missile Autopilot Design. PhD, Lancaster University.

Counsell, J. M., J. Brindley, et al. (2009). Non-linear autopilot design using the philosophy of variable transient response. AIAA Guidance, Navigation and Control Conference.

Counsell, J. M., Y. A. Khalid, et al. (2011). "Controllability of buildings: A multi-input multi-output stability assessment method for buildings with slow acting heating systems." Simulation Modelling Practice and Theory **19**(4): 1185-1200.

Khalid, Y. A. (2011). Controllability of Building Systems. PhD, University of Strathclyde.

Lane, S. H. and R. F. Stengel (1988). Flight Control Design Using Non-Linear Inverse Dynamics, Automatica.

Muir, E. and A. Bradshaw (1996). "Control law design for a thrust vectoring fighter aircraft using robust inverse dynamics estimation (RIDE)." Proceedings of

the Institution of Mechanical Engineers Part G-Journal of Aerospace Engineering **210**(G4): 333-343.

Phelan, R. M. (1977). Automatic control systems. Ithaca, N.Y., Cornell University Press.

Slotine, J. and W. Li (1991). Applied nonlinear control, Prentice Hall - ISBN 0130408905.

Utkin, V. I. (1971). "Equations of the slipping regime in discontinuous systems II." Automation and Remote Control.

Zaher, O. S., J. Counsell, et al. (2011). "Robust control of room temperature and relative humidity using advanced nonlinear inverse dynamics and evolutionary optimisation."

5. Robust Nonlinear HVAC Systems Control with Evolutionary Optimisation

All control systems have parameters which require tuning. Tuning a control system has a direct bearing on its performance such that a control system can be tuned well in order to produce its optimal deliverable performance. On the other hand, a poorly tuned control system will produce sub optimal performance and, in some cases, can lead to system instability. This concept is analogous to the performance tuning of car engines. A highly refined and well-tuned car engine can produce better performance than a poorly tuned engine of the same size. Therefore, tuning is a vital part of the controller design process.

It was shown in the preceding chapter that the controller gains for the RIDE algorithm can be represented as follows:

$$K_P = [MB]^{-1} g \tag{5.1}$$

$$K_I = [MB]^{-1} \rho \tag{5.2}$$

Where $g = 2Z_d\Omega_n$ and $\rho = \Omega_n^2$. Z_d and Ω_n are the designed system damping ratio and natural frequency respectively. This is the case providing the u_{eq} estimation is correct. It was also shown that in order to reduce the effects of inaccuracies in the u_{eq} estimation, the integral gain should be made as high as possible. Increasing the gain too high however can result in closed loop instability due to sensitivity to unknown dynamics, particularly in systems with slow actuators. Therefore it is necessary to tune the gains carefully in order to attain the optimum system performance whilst ensuring stability of the system.

In buildings it is recognised that it is difficult to know exactly the properties or parameters of the building such as air change rates, heat transfer coefficients etc. Therefore, when modelling the building, a degree of uncertainty will exist in the model. This, as mentioned before, can affect the accuracy of the u_{eq} calculation as well as the control law itself. Equations 5.1 and 5.2 show that the gains are reliant on a part of the system model: the MB matrix. Therefore, if the real buildings

performance deviates from that of the model, then the performance of the controller may deteriorate. This deterioration in performance, of course, can be more apparent in some buildings or applications than others. This uncertainty can further complicate the controller tuning process. It is possible, however, to specify a range of uncertainty which the building parameters are known to lie within. Using this method, some of the parameters which are known to cause the biggest performance variation can be accounted for in the model. By tuning the control system gains over the range of uncertainty, the controller can be made to be more robust to these parameter variations.

This chapter sets forth the development of a robust and high performance controller for room temperature and relative humidity control which combines a Genetic Algorithm (GA) based auto-tuning method with the RIDE controller algorithm described in Chapter 4. The auto-tuning method alleviates the difficulty in tuning the closed loop system by automatically tuning the control system such that it is robust to parameter variations which have the most significant effect on the performance of the system.

5.1 Genetic Algorithm Optimisation

Genetic Algorithms (GA) are an evolutionary computation method premised on the principles of natural selection. The basic concept of the GA is to simulate the processes that occur during evolution in nature according to Darwin's theory. Hence they represent an intelligent exploitation of a random search within a defined search space to solve a problem. The GA was first pioneered by John Holland in the 60s, who later published the book Adaption in Natural and Artificial Systems in 1975 (Holland 1975). Since then, GAs have been experimented and applied in many fields of engineering. GA's have become known for their efficacy in global optimisation problems and consistently outperform traditional methods in many applications.

Traditionally, the GA process is performed using binary encoding. This means that the individuals are represented with binary strings; individual being the term used to refer to one solution to the optimization problem. Using the binary representation however can be unnatural and unwieldy for many problems. Real-

coded GAs offer a more natural representation when tackling optimization problems with variables in continuous or discontinuous domains. In real-coded GAs, an individual is coded as a finite-length string of real numbers corresponding to the design variables. The real-coded GA is rigorous, precise, and efficient as the floating point representation is conceptually close to the real design space (Zamanan, Sykulski et al. 2006). Furthermore, the length of the string is reduced to the number of design variables. It has been shown that real-coded GAs outperform binary-coded GAs in many optimisation problems through a comparative study conducted by (Janikow and Michalewicz 1991).

The GA process is illustrated in the flowchart shown in Figure 5.1. From the flowchart it can be seen that the process can be broken down into a series of steps; Initial population, Fitness Evaluation, Stop Criteria Check, Genetic operations.

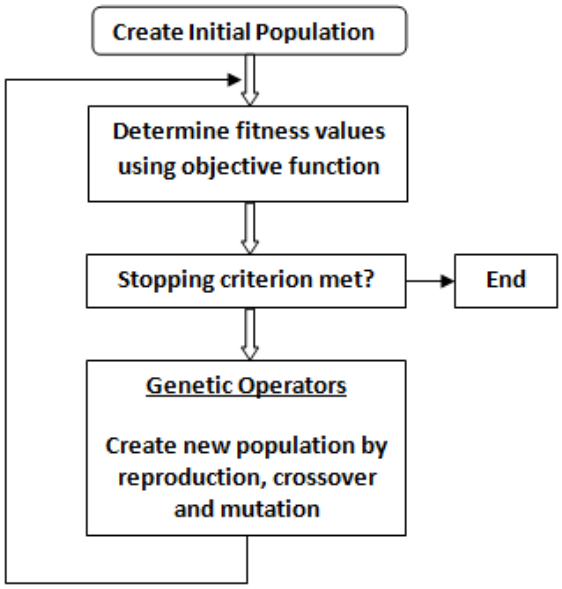

Figure 5.1: GA Process (Zaher, Counsell et al. 2011)

5.1.1 Initial population

In this step, a random initial population of individuals is created by the algorithm. Each individual in the population consists of a number of values, dependent on the problem, which represent a possible solution. For example,

consider a problem in which four parameters are being optimised. The individual in that case would consist of four values which present a possible solution to the problem. The number of individuals in the population is dependent on the user defined population size. The selection of the population size and the method by which the individuals are chosen are two important questions which should be addressed initially when using GAs. There have been several theoretical approaches for selecting the size of the population however the fundamental concept is a trade-off between efficiency and effectiveness. Intuitively, an 'optimal' population size should exist for a given individual size. Selecting a population size which is too small would not allow sufficient room for exploring the search space effectively. Conversely, selecting too large a population size could impair the efficiency of the method such that a solution might not be obtained within a reasonable amount of time. Determining the 'optimal' population size often requires a degree of trial and error. Once the population size as been decided, the initial population must be generated. The values in the initial population are typically generated randomly using a random number generator. These values are all generated within user specified boundaries (constraints) which define the search space. It is sometimes useful to 'seed' the initial population with known good solutions as it can help the GA to find a better solution more quickly than is possible from a random start. A drawback of this method however is that there is a possibility of inducing premature convergence. For the work presented in this thesis, the initial population was generated using the random number generator available in the Visual Studio C++ library. Each population constitutes what is referred to as a generation e.g. the initial population is generation 1 and so on.

5.1.2 Fitness Evaluation

As the GA is based on the principle of 'survival of the fittest', the fitness of each individual must be evaluated. To this end, an objective function, which provides a performance measure for the solution represented by an individual, must be designed. This is typically a function which captures the error between the desired system performance and the actual performance of the system. Based on the user defined objective function, the fitness of each individual in the population is

evaluated. The better the result from the objective function for the individual, the more 'fit' the individual is hence the more likely that individual is to ‘survive’. It is clear that this is an important part of the optimization procedure as it has a direct bearing on the evolution towards the optimal solution.

5.1.3 Stop Criteria Check

GA’s are a stochastic search method that could in principle run forever. Thus, some sort of termination criteria must be put in place in order to stop the evolution process. This can be done by simply terminating the procedure after a specified length of time or number of fitness evaluations. Another option is to track the performance statistics of the GA and terminate the process upon the satisfaction of a performance based criteria e.g. the variance in fitness levels in the population. Measuring the variance of mean fitness of one generation to the next is also a commonly used method. If the variance of the mean fitness falls below a threshold value, the generation is counted as a ‘stall’ generation. A limit can then be put on the number of stall generations allowed before the process is terminated. Alternatively, a number of termination criteria can be specified which terminate the process based on whichever criterion is met first.

5.1.4 Genetic Operations

These operations drive the evolution process by simulating natural evolution processes in order to determine which individuals constitute the subsequent population i.e. the new generation. There are four operators used in the GA in this thesis; elite children, selection, crossover and mutation.

5.1.4.1 Selection

This operator selects a number of individuals from the current population, called parents, who contribute their properties to the next generation through the mutation and crossover genetic operations described in the following sections. The selection process is related to the fitness of the individuals in that the fitter the individual, the more likely it will be chosen as a parent. There are a number of algorithms that have been developed for the selection process such as roulette wheel selection, tournament

selection and ranking. The roulette wheel selection algorithm was found to be sufficient for the purposes of the work in this thesis. Roulette wheel selection uses a probability distribution for selection in which the selection probability of a given string is proportional to its fitness. Figure 5.2 illustrates the concept of roulette wheel selection.

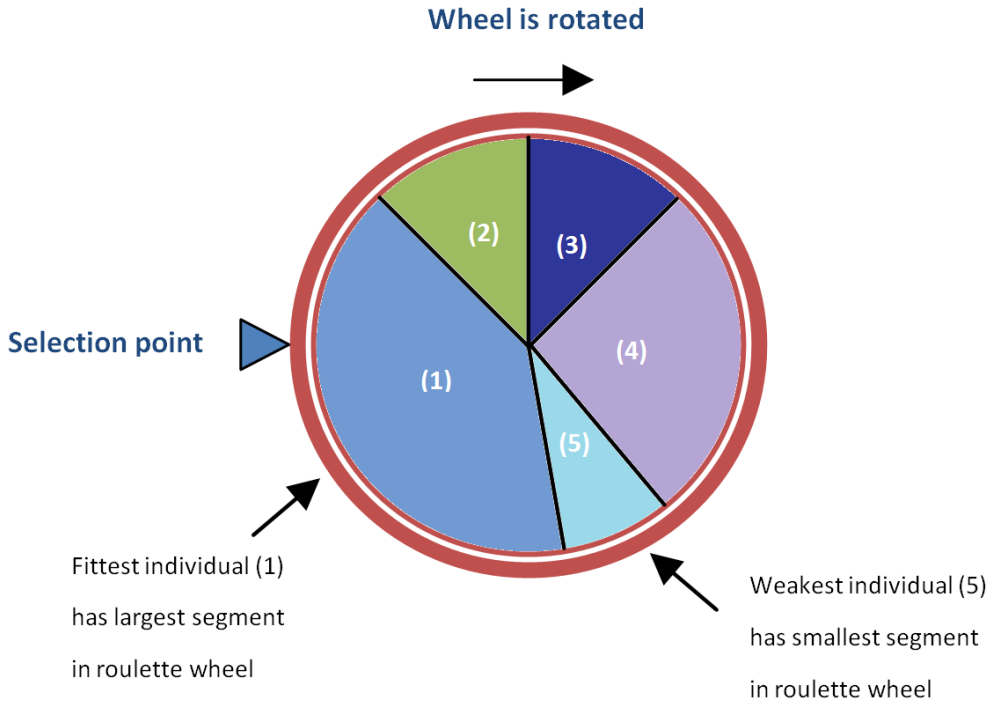

Figure 5.2: Roulette Wheel Selection

Each individual is assigned a probability of selection which is proportional to their fitness. For function minimisation, the lower the fitness value, the more fit the individual is. Therefore, the probability of selection in this case is inversely proportional to the actual fitness value. The total of all the fitness values for the population is calculated then a probability is assigned to each individual using the following equation:

$$Probability = \frac{Inverse\ of\ fitness\ value}{Total\ fitness} \tag{5.3}$$

This returns a probability value between 0 and 1. Pseudo random numbers are then generated between 0 and 1 for each individual and the individual is selected as a

parent if the random number is smaller than the probability value. Fitter individuals will have a larger number and therefore there is a higher probability that the random number will be smaller than it. This follows the principle of 'survival of the fittest' as the fitter individuals are selected as parents and thus survive to contribute their properties to the subsequent generation.

5.1.4.2 Elite Children

This operator insures that a specified number of the fittest individuals survive to go to the next generation without alteration. This is effectively the same as seeding the initial population with known good solutions. It ensures that important good performing solutions are not lost throughout the evolution process and speeds up the convergence process. The number of elite children must be selected carefully however since, as with seeding the initial population, the possibility of inducing premature convergence remains. Many researchers have found that using the elite children operator significantly improves the performance of the GA (Man, Tang et al. 1999).

5.1.4.3 Crossover

The crossover operator takes two of the individuals in the current population that have been selected as parents and creates two new individuals which retain some of the characteristics of each of the parents. There are various crossover methods which have been developed which differ for real coded and binary coded GAs. These methods have different mechanisms for the crossover procedure. The number of parents required and offspring created through the operator varies from one method to another. The crossover method used in this thesis is arithmetic crossover. This involves swapping chromosome parts between individuals but is not performed on every pair of individuals. The crossover frequency is controlled by a crossover probability parameter (Arumugam, Rao et al. 2005). In this method, two parents produce two offspring. Consider two individuals, represented by equations 5.4 and 5.5, who have been selected as parents.

$$x^1 = [x_1^1, \dots, x_n^1] \tag{5.4}$$

$$x^2 = [x_1^2, \dots, x_n^2] \tag{5.5}$$

Where x^i is the *i*th parent n is the number of variables, often referred to as genes, being optimized. The offspring that are generated are then created arithmetically as follows:

$$y^1 = \alpha x^1 + (1 - \alpha)x^2 \tag{5.6}$$

$$y^2 = \alpha x^2 + (1 - \alpha)x^1 \tag{5.7}$$

Where y^i is the *i*th offspring and α is a random number which varies for each generation. This is known as non-uniform arithmetical crossover.

5.1.4.4 Mutation

The mutation procedure creates new genetic material in the population by altering one individual to produce a single new individual for use in the new population. This ensures that a degree of diversity remains in the population. The individuals which undergo mutation are governed by the mutation probability. In this thesis, the non-uniform mutation method, which is commonly used in real coded GAs, is used. This method works by altering one gene (parameter) in the individual to create a new individual. If the individual to be altered is denoted by *x*, the mutated gene is given by:

$$x_i = \begin{cases} x_i + \Delta(k, u_i - x_i), & if\ \tau = 0 \\ x_i + \Delta(k, x_i - l_i), & if\ \tau = 1 \end{cases} \tag{5.8}$$

Where i is then gene position in the individual, u_i and l_i are the upper and lower bounds of x_i respectively, τ is a random digit which takes the value of 0 or 1 and Δ is a function given by:

$$\Delta(k, y) = y\left(1 - \alpha^{\left(1-\frac{k}{T}\right)^b}\right) \tag{5.9}$$

$$y = \begin{cases} u_i - x_i & if\ \tau = 0 \\ x_i - l_i & if\ \tau = 1 \end{cases} \tag{5.10}$$

Where α is a uniformly distributed random number with a value between 0 and 1, k is the current generation number, T is the maximum number of generations and b is the shape parameter which determines the degree of non-uniformity. This form of mutation is designed such that the amount of mutation decreases as k increases.

5.2 Case Study: Robust HVAC Control with GA Based Auto-tuning

This section presents the development of a robust HVAC control system for temperature and relative humidity regulation through application of the RIDE controller with the GA based auto-tuning methodology. The control system is designed based on the RIDE controller principles described in Chapter 4. The controller is then tuned using the GA based auto-tuning method which makes it robust against uncertainty in the heat transfer coefficient of the internal mass. Furthermore, the auto-tuner alleviates the otherwise tedious manual controller tuning process. The proposed controller's performance is compared to an improved PI controller strategy which provides a reasonable representation of control systems commonly used in industry.

5.2.1 Zone Model and HVAC System Description

The building model described in Chapter 3 is used for the controller development and analysis in this case study. The zone model consists of four state variables for temperature and one state variable for humidity. These are: zone air temperature (T_a), internal wall structure temperature (T_{si}), external wall structure temperature (T_{se}), furniture and internal mass temperature (T_{ft}) and zone humidity

(W_a). The zone air is assumed to be fully mixed meaning the temperature distribution across the zone is uniform. The air density is also assumed to be constant and unaffected by changes in temperature and humidity of the zone. The nonlinear differential equations that govern the zone temperature and humidity are as follows:

$$M_a C_a \frac{dT_a(t)}{dt} = \dot{Q}_h(t) + \dot{Q}_{free}(t) - \dot{Q}_{si}(t) - \dot{Q}_F(t) - \dot{Q}_R(t) - \dot{Q}_W(t) - \dot{m}_c(t)C_a\big(T_a(t) - T_o(t)\big) - \dot{m}_{nv}C_a\big(T_a(t) - T_o(t)\big) - \dot{Q}_{ft}(t) \tag{5.11}$$

$$M_{si}C_s \frac{dT_{si}(t)}{dt} = \dot{Q}_{si} - \frac{K_{si}}{Th_{wall}} A_s(T_{si}(t) - T_{se}(t)) \tag{5.12}$$

$$M_{se}C_s \frac{dT_{se}(t)}{dt} = \frac{K_{si}}{Th_{wall}} A_s(T_{si}(t) - T_{se}(t)) - \dot{Q}_{se}(t) \tag{5.13}$$

$$M_{ft}C_{ft} \frac{dT_{ft}(t)}{dt} = U_{ft}A_{ft}(T_a(t) - T_{ft}(t)) \tag{5.14}$$

$$\frac{M_a}{\rho_a}\frac{dW_a}{dt} = \frac{\dot{m}_c(t)}{\rho_a}(W_s(t) - W_a(t)) + \frac{(n_{occ}P_{occ})}{\rho_a} - \frac{\dot{m}_{nv}}{\rho_a}(W_a(t) - W_o(t)) \tag{5.15}$$

When the control system is applied, the zone air temperature (T_a) and relative humidity (W_{rel}) are tracked. The expression defining the relative humidity in the zone is given below in equation (5.16):

$$W_{rel}(t) = 5000.0W_a(t) - 0.771T_a(\mathrm{t}) + 131.68 \tag{5.16}$$

For the control system design the differential equations were rewritten in state space format as shown in equations (5.17) and (5.18).

$$\begin{bmatrix} \dot{T}_a(t) \\ \dot{T}_{si}(t) \\ \dot{T}_{se}(t) \\ \dot{T}_{ft}(t) \\ \dot{W}_a(t) \end{bmatrix} = \begin{bmatrix} a_{11} & a_{12} & 0 & a_{14} & 0 \\ a_{21} & a_{22} & a_{23} & 0 & 0 \\ 0 & a_{32} & a_{33} & 0 & 0 \\ a_{41} & 0 & 0 & a_{44} & 0 \\ 0 & 0 & 0 & 0 & a_{55} \end{bmatrix} \begin{bmatrix} T_a(t) \\ T_{si}(t) \\ T_{se}(t) \\ T_{ft}(t) \\ W_a(t) \end{bmatrix} + \begin{bmatrix} b_{11} & b_{12} \\ 0 & 0 \\ 0 & 0 \\ 0 & 0 \\ 0 & b_{52} \end{bmatrix} \begin{bmatrix} \dot{Q}_H(t) \\ \dot{m}_c(t) \end{bmatrix} + \begin{bmatrix} f_{11} & f_{12} & 0 & f_{14} \\ 0 & 0 & 0 & 0 \\ 0 & f_{32} & 0 & 0 \\ 0 & 0 & 0 & 0 \\ 0 & 0 & f_{53} & f_{54} \end{bmatrix} \begin{bmatrix} \dot{Q}_{free}(t) \\ T_o(t) \\ W_o(t) \\ n_{occ}(t) \end{bmatrix} \tag{5.17}$$

$$\begin{bmatrix} W_{rel}(t) \\ T_a(t) \end{bmatrix} = \begin{bmatrix} -0.771 & 0 & 0 & 0 & 5000 \\ 1.0 & 0 & 0 & 0 & 0 \end{bmatrix} \begin{bmatrix} T_a(t) \\ T_{si}(t) \\ T_{se}(t) \\ T_{ft}(t) \\ W_a(t) \end{bmatrix} + \begin{bmatrix} 131.68 \\ 0 \end{bmatrix} \tag{5.18}$$

The expansion of the coefficients of the state space matrices can be found in Appendix A.

5.2.1.1 Actuation Systems

The actuation systems models used to control the temperature and humidity of the zone in this research are a direct acting heater and mechanical ventilation with first order dynamics as described in Case 1 in chapter 3. The dynamics of the heating system are described in equations (5.19) and 5.20 and the ventilation system is described in equations 5.21 and 5.22.

$$\ddot{Q}_h = \frac{1}{\tau_h}\left(uc_{Qh}(t) - \dot{Q}_h(t)\right) \tag{5.19}$$

$$LL_{Qh} \leq \dot{Q}_h(t) \leq UL_{Qh} \tag{5.20}$$

$$\ddot{m}_c = \frac{1}{\tau_v}\left(uc_v(t) - \dot{m}_c(t)\right) \tag{5.21}$$

$$LL_{mv} \leq \dot{m}_c(t) \leq UL_{mv} \tag{5.22}$$

The values used for the parameters of the actuation system are given in Table 5-1.

Parameter	Value (Units)
$\boldsymbol{LL_{Qh}}$	0 (W)
$\boldsymbol{UL_{Qh}}$	10000 (W)
$\boldsymbol{LL_{mv}}$	0 (kg/s)
$\boldsymbol{UL_{mv}}$	0.35 (kg/s)
$\boldsymbol{\tau_h}$	600 (s)
$\boldsymbol{\tau_v}$	100 (s)

Table 5-1: Actuation system parameters

5.2.1.2 Stability

As explained in Chapter 4, the system's transmission zeros, from which the stability of the system can be assessed, are determined by evaluating the following determinant:

$$\begin{vmatrix} A - sI & B \\ M & D \end{vmatrix} = 0 \tag{5.23}$$

Which can be expanded to:

$$\begin{bmatrix} a11 - s & a12 & 0 & a14 & 0 & b11 & b12 \\ a21 & a22 - s & a23 & 0 & 0 & 0 & 0 \\ 0 & a32 & a33 - s & 0 & 0 & 0 & 0 \\ a41 & 0 & 0 & a44 - s & 0 & 0 & 0 \\ 0 & 0 & 0 & 0 & a55 - s & 0 & b52 \\ -0.771 & 0 & 0 & 0 & 5000 & 0 & 0 \\ 1 & 0 & 0 & 0 & 0 & 0 & 0 \end{bmatrix} = 0 \tag{5.24}$$

For this analysis, the nonlinear state space equations were linearised around the operating point $\dot{m}(t) = 0$, Wa = 0.109kg/m3 and Ta = 21°C. The result of the analysis shows that the system is stable with the transmission zero locations at:
s = -7.79951x10^{-5}, s = -7.93704x10^{-6} and s = -2.96314x10^{-6}

5.2.2 Controller Design

5.2.2.1 Proportional and Integral Control

PI control is very commonly used in building control systems as well as many other industrial applications due to its simplistic design. For this reason, a PI controller tuned with a GA is used in this paper as a representation of common practice in industry. Since the PI controller is tuned with the same robust GA tuning method used with the RIDE controller, this controller represents an improved PI controller which is more robust than a standard PI controller which might be used in industry. This serves as a reasonable benchmark against which the advanced control method presented in this research can be compared.

The PI control law is as follows:

$$uc(t) = K_P e(t) + K_I \int e(t) \tag{5.25}$$

$$e(t) = SP_n - y_n(t) \tag{5.26}$$

Where SP is setpoint. The proportional and integral gains, K_P and K_I respectively, must be tuned in order to attain the best performance according to the design specifications of the system. Since the PI controller is a SISO design, two separate controllers must be designed for each channel. This means that the tuning process is performed twice, once for each channel. The objective function calculation for optimisation of the gains is shown in Section 5.2.2.3.

5.2.2.2 RIDE Controller Design

The RIDE controller design has proven to be highly effective when applied to nonlinear systems (Fielding, Varga et al. 2002) due to its superiority over PI in response to uncertain disturbances. A more detailed explanation of this algorithm is given in Chapter 4. The RIDE control law is given by:

$$\overrightarrow{uc}(t) = \vec{r} - K_P \vec{y}(t) + \vec{u}_{eq}(t) \tag{5.27}$$

$$\dot{\vec{r}} = K_I \vec{e}(t) \tag{5.28}$$

$$\vec{u}_{eq}(t) = -[MB]^{-1} \dot{\vec{y}}(t) + \vec{u}(t) \tag{5.29}$$

Where K_P and K_I are the proportional and integrals gains (which require tuning) respectively. The $\hat{\hat{u}}_{eq}(t)$ term (equation 5.29) is an estimate of the equivalent control which is required to drive the rate of change of the output to zero. The equivalent control estimate uses the dynamic inverse to diminish disturbances, cross-coupling and nonlinear plant dynamics (Counsell 1992). It was shown in Chapter 4 that the proportional and integral gains are expressed as in equations 5.1 and 5.2 respectively and that the system response can be shaped by tuning K_P and K_I through Z_d and Ω_n.

It can be seen then that the information required for the implementation of this algorithm is the MB matrix and measurements of the outputs, i.e. the temperature and relative humidity of the zone, and the actuator input. The MB matrix based on the building model is expressed as follows:

$$[MB] = \begin{bmatrix} -\frac{0.771}{M_a C_a} & \frac{0.771 T_a}{M_a} + 5000\left(\frac{W_s - W_a}{M_a}\right) \\ \frac{1}{M_a C_a} & -\frac{T_a}{M_a} \end{bmatrix} \qquad (5.30)$$

5.2.2.3 Optimisation Objective Function Design

Due to the inherent parameter uncertainty associated with buildings, implementing building control systems in practice which have been designed using a building model can prove difficult. This is caused by the difficulty in accurately capturing the dynamic behaviour of the building since the values of many parameters might not be known exactly. Hence the performance of the building in reality will differ from the model and the controller may not perform as expected. The proposed method in this research attempts to alleviate the problems associated with parameter uncertainty by tuning the controller parameters over a range of uncertainty. This makes the controller more robust against discrepancies between the building model and the real building. This is achieved through the design of the objective function for optimisation.

When designing the optimisation objective function, it is necessary to specify some uncertainty ranges for the building parameters. The building model can be used to identify which parameters have the most significant impact on the control system performance. This is done by altering parameters in the building model and observing which parameters affect the response of the system the most. Through this

method it was identified that the heat transfer coefficient for the internal mass (U_{ft}) had the biggest effect on the control system performance. It is impossible to model the thermal properties of the internal mass due to the wide range of use of a building in its lifetime. Therefore the control system was optimised over the uncertainty range for this parameter.

It is considered that U_{ft} can vary by ±60%. In order to optimise the controller parameters over this range, the objective function was designed such that it calculates the root mean square of the error between the set point and the system response over three simulations: one at the normal operating condition (U_{ft} = 2.0W/m^{2}K) and two others at the extremes of the uncertainty range (U_{ft} = 0.8W/m^{2}K and U_{ft} = 3.2W/m^{2}K). As mentioned in Section 5.2.2.1, the tuning process is performed on each channel separately for the PI controller. The error for the PI case is simply taken as the value of the error on the channel being tuned. However, since the RIDE controller is MIMO and both channels are tuned with the same natural frequency and damping ratio, the error is taken as the absolute value of the sum of the error on both channels. The resulting objective function calculations are shown below:

$$obj = \sqrt{\frac{T_{err}}{3n}} \tag{28}$$

$$T_{err} = (E_1 + E_2 \ldots . + E_n)_{OP-1} + (E_1 + E_2 \ldots . + E_n)_{OP-2} + (E_1 + E_2 \ldots . + E_n)_{OP-3} \tag{29}$$

$$n = \frac{Simulation\ run\ time}{sampling\ time\ interval} \tag{30}$$

Where n is length of the error vector, T_{err} is the total error over all three simulations, OP stand for operating point and E is the value of the error squared and is determined by equations (31) and (32) for the RIDE and PI controllers respectively:

$$E_n{}^{RIDE} = (abs(SP_n - y_n(t))_{TEMP} + abs(SP_n - y_n(t))_{HUMIDITY})^2 \tag{31}$$

$$E_n{}^{PI} = (SP_n - y_n(t))^2 \tag{32}$$

Where y is actual system response and SP stands for setpoint. A detailed explanation of the tailored GA tuning process used in this work is given below in Algorithm 1.

Algorithm 1

1. Set GA parameter values; *max_stall,tol_fun, gen_max, popsize, elite_count, nvars, crossover_fract, mut_prob , UB, LB*
2. Initialise $pop_{i,k}$ with random values between the upper (UB_k) and lower (LB_k) bounds for all i ϵ {1,...,popsize} and k ϵ {1,...,nvars}
3. Initialise generation counter: gen = 1
4. **Do**
5. **For All** i ϵ [1,...,popsize] **do**
6. Set operating point 1 (U_{ft} = 0.8W/m^2K)
7. Evaluate the cumulative error over the simulation $(E_1 + E_2...+ E_n)_{OP\text{-}1}$
8. Set operating point 2 (U_{ft} = 2.0W/m^2K)
9. Evaluate the cumulative error over the simulation $(E_1 + E_2...+ E_n)_{OP\text{-}2}$
10. Set operating point 3 (U_{ft} = 3.2W/m^2K)
11. Evaluate the cumulative error over the simulation $(E_1 + E_2...+ E_n)_{OP\text{-}3}$
12. Evaluate RMSE = $\sqrt{\frac{T_{err}}{3n}}$
13. Assign RMSE to $fitness_i$
14. **End For**
15. Calculate mean fitness for current population ($mean\_fit_{gen}$)
16. **If** $mean\_fit_{gen}$ - $mean\_fit_{gen-1} \leq$ tol_fun
17. stall_num = stall_num + 1
18. **End if**

19. Select elite individuals from current population
20. Perform Roulette wheel selection
21. Determine crossover individuals from current population other than elite: ensure within boundaries
22. Determine mutation individuals from current population other than elite: ensure within boundaries
23. Bring elite, mutation and crossover individuals together to form new population
24. **WHILE** (stall_num < max_stall) AND (gen < gen_max)

The GA used for tuning in this research was coded in C++ and compiled into an executable file. The settings for the GA used in the auto-tuning process are given in Table 5-2.

Parameter	**Value**
Population size	15
Elite count	3
Crossover fraction	0.7
Mutation	0.25
Selection method	Roulette

Table 5-2: GA Parameters

5.2.3 Results

The control systems discussed above where applied to the building model and simulated over a three month winter/spring period with weather data from January to March. Their performance was evaluated over three different operating conditions across the range of uncertainty in the heat transfer coefficient of the furniture. This was done in order to demonstrate each controller's ability to cope with parameter uncertainty which is very common in buildings. The different operating conditions

were: U_{ft} = 0.8W/m^{2}K, U_{ft} = 2.0W/m^{2}K and U_{ft} = 3.2W/m^{2}K, where U_{ft} = 2.0W/m^{2}K is the 'normal' operating condition.

The PI controller was tuned using the same GA optimisation scheme that was used for the RIDE controller so as to provide a representation of a very well-tuned PI controller and to demonstrate the efficacy of using the GA tuning method with the RIDE controller. In reality many PI controllers in use in the buildings industry are not optimally tuned, hence tuning the PI controller with the GA can be considered to provide an example which is better than many controllers in industry. The tuning results for both controller setups are detailed below in Table 5-3 and Table 5-4.

	Channel 1 (Temperature)	**Channel 2 (Humidity)**
No. Generations	10	8
K_P	252.6	298.2
K_I	0.129	0.118

Table 5-3: PI Auto-Tuning Results

No. Generations	8
Z	0.86
Ω	0.00195

Table 5-4: RIDE Auto-Tuning Results

It is clear that the tuning process for the PI-GA controller took longer than the RIDE-GA controller since the PI-GA controller required tuning for each channel separately whereas the RIDE-GA controller is MIMO and so both channels were tuned simultaneously. Another important point to note is that since the RIDE theory allows the controller gains to be tuned using the natural frequency and damping ratio of the closed loop system, the tuning process is simplified as a direct correlation between the system response and the gain values can be observed. Figure 5.3 shows a plot of the zone air temperature and external temperature over three days at all three operating points. It can be seen that the PI-GA controller does not track the temperature set point (21°C) accurately, with significant overshoots occurring for large portions of each day such that the zone air temperature is either too hot or too cold for the majority of each day resulting in a very uncomfortable environment for the building occupants. This is true for all three operating points, as the system

response over the three operating points is similar albeit the overshoots increase slightly as the furniture heat transfer coefficient decreases. This can be expected as the lower the heat transfer coefficient, the lower the thermal inertia. The corresponding heating power used corroborates this result as more heating power is used as the thermal inertia increases. Figure 5.4 shows that the RIDE-GA controller achieves a significantly faster response when compared to the PI-GA controller as well as much improved set-point tracking. A small overshoot can be observed at the beginning of the day however almost perfect tracking is achieved over the rest of each day for all three operating points. This indicates that the RIDE-GA controller is more robust to the uncertainty in the furniture heat transfer coefficient as the response is nearly identical regardless of the operating point.

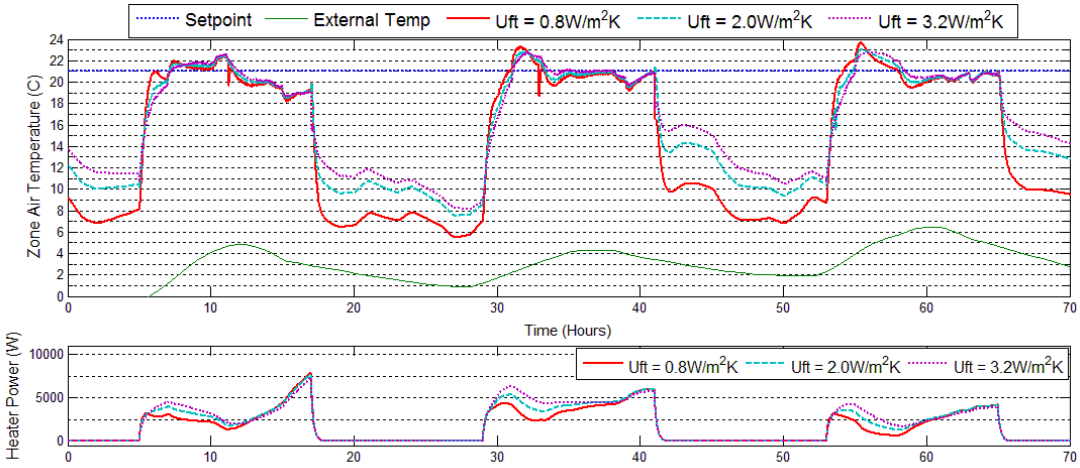

Figure 5.3: Zone air temperature and heat input (PI-GA)

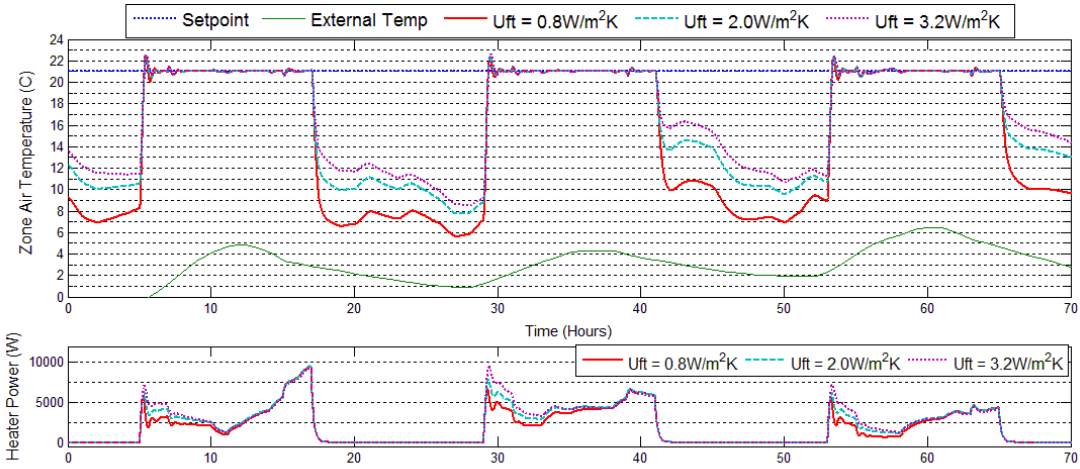

Figure 5.4: Zone air temperature and heat input (RIDE-GA)

The PI-GA controller tracks the relative humidity setpoint (50%) accurately for the majority of each day as can be seen in Figure 5.5. The zone relative humidity can be seen to oscillate rapidly around the setpoint however as the controller is locked in a limit cycle as can be observed from the mechanical ventilation rate. This type of oscillatory behaviour is highly undesirable as it can damage the actuation system in practice. There are also a few spikes which can be observed in the relative humidity which are caused by casual gains which the controller fails to deal with. The relative humidity can be seen to increase above the setpoint for a few hours on the third day however this is due to the setpoint being unreachable i.e. the lower limit of the mechanical ventilation actuation system renders tracking of the setpoint during this period impossible. The RIDE-GA controller again achieves quick and accurate tracking of the setpoint as shown in Figure 5.6. This is achieved without any damaging oscillations in the actuation system resulting in financial savings. The same increase in the zone relative humidity on the third day observed with the PI-GA controller occurs with RIDE-GA controller. However, as explained, this is due to the setpoint becoming unreachable as a result of actuator limitations. Overall, the RIDE-GA controller exhibits a significantly improved performance when compared to the PI-GA controller which, in practice, could result in significantly improved comfort conditions and potential financial savings.

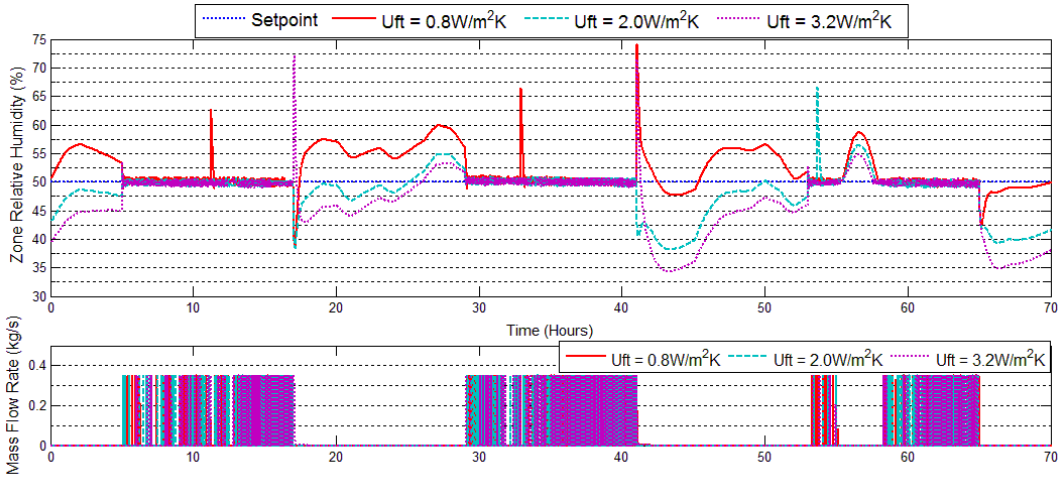

Figure 5.5: Zone relative humidity and mechanical ventilation rate (PI-GA)

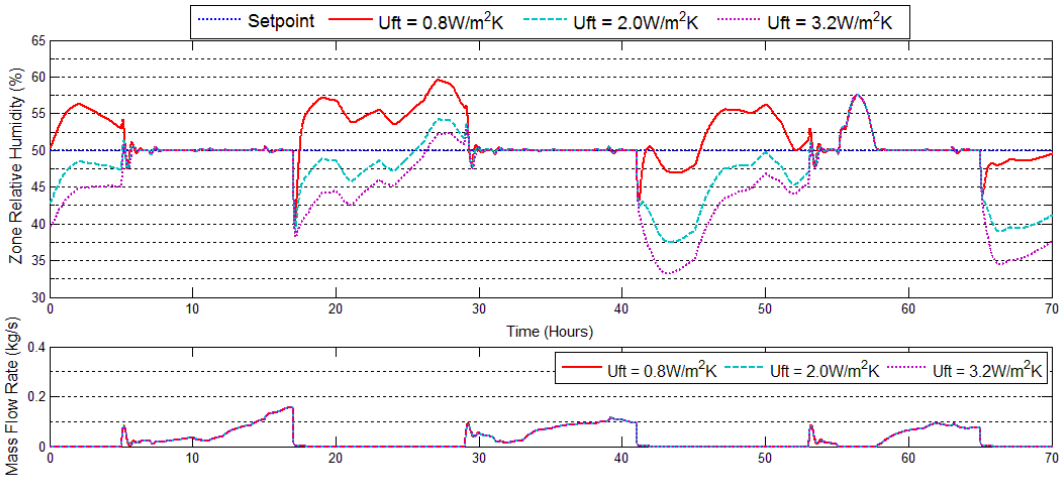

Figure 5.6: Zone relative humidity and mechanical ventilation rate (RIDE-GA)

5.2.3.1 Disturbance Rejection Results

In reality, a building is subject to many disturbances such as people entering and leaving rooms, opening windows and doors etc. Therefore it is necessary that the control system is able to deal with these disturbances i.e. reject the disturbances without an adverse effect on its performance. In order to assess the ability of both controller designs to deal with disturbances, two types of disturbances were simulated; heat loss and heat gain. The first disturbance simulates a heat loss disturbance with a window being opened with an area of $0.1m^2$ for a period of 2 hours. This was done to assess how each controller recovered after a sharp disturbance. Results for this are shown over a three day period with the disturbance being simulated on the third day from 56-58 hours.

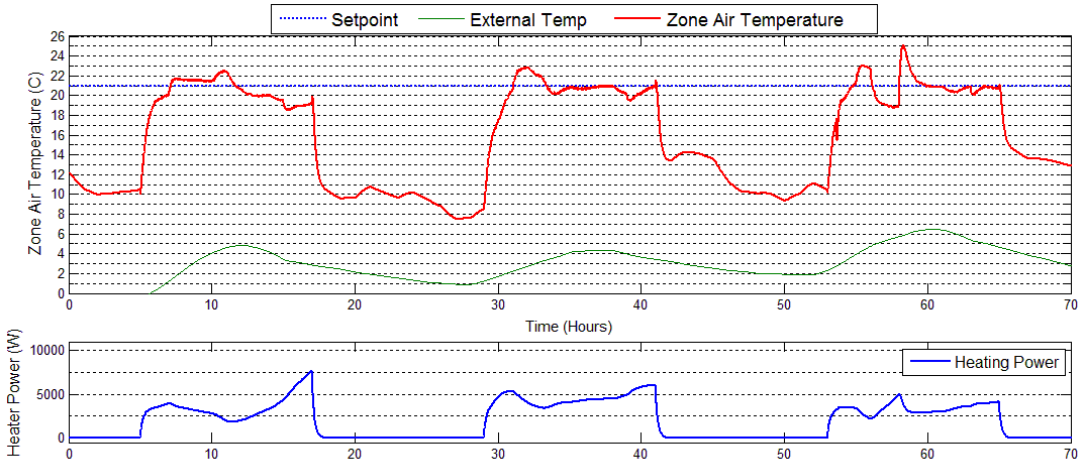

Figure 5.7: Zone air temperature and heat input with heat loss disturbance (PI-GA)

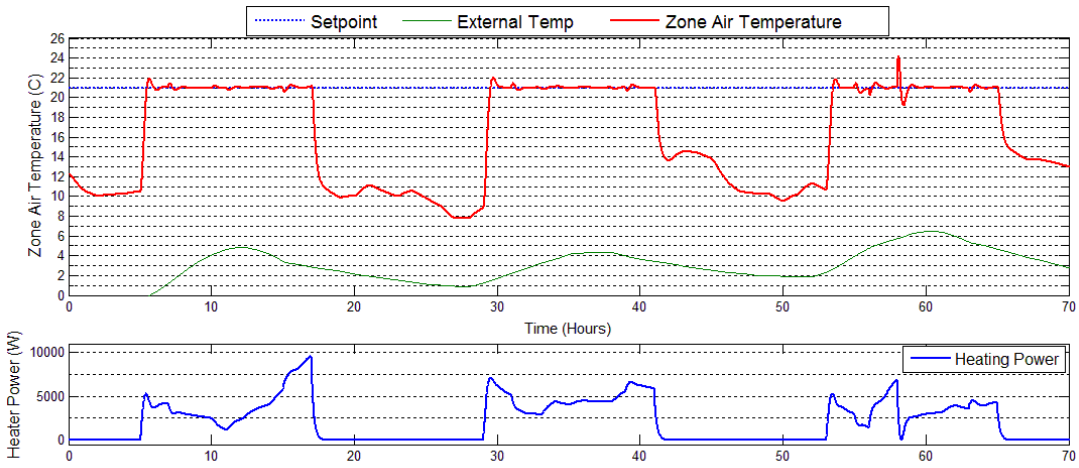

Figure 5.8: Zone air temperature and heat input with heat loss disturbance (RIDE-GA)

Figure 5.7 shows that when the window is opened the temperature drops significantly and the PI-GA controller increases the heating power in an attempt to compensate for the heat being lost through the open window. The response is too slow however and the controller is unable to reject the disturbance on time instead causing a large overshoot in temperature (approx. 4°C) when the window is closed. The result is the zone air temperature dropping below the setpoint for a period of two hours and then rising above the setpoint for approximately two hours also. The RIDE-GA controller on the other hand demonstrates greatly improved disturbance rejection as shown in Figure 5.8. The zone air temperature can be seen to oscillate around the setpoint briefly when the window is opened and then the controller resumes accurate tracking of the setpoint. The PI-GA controller shows effective disturbance rejection on the relative humidity channel as can be seen from the second spike on the third day in Figure 5.9. The relative humidity response for the RIDE-GA controller can be seen to spike in Figure 5.10 however it can be seen that the actuator (mechanical ventilation) is on the lower limit when this happens and so the setpoint is unreachable during this period. The relative humidity then briefly oscillates around the setpoint and then the controller resumes accurate tracking. These results highlight the efficacy of the RIDE/GA controller's robust structure which makes its tracking performance less sensitive to disturbances.

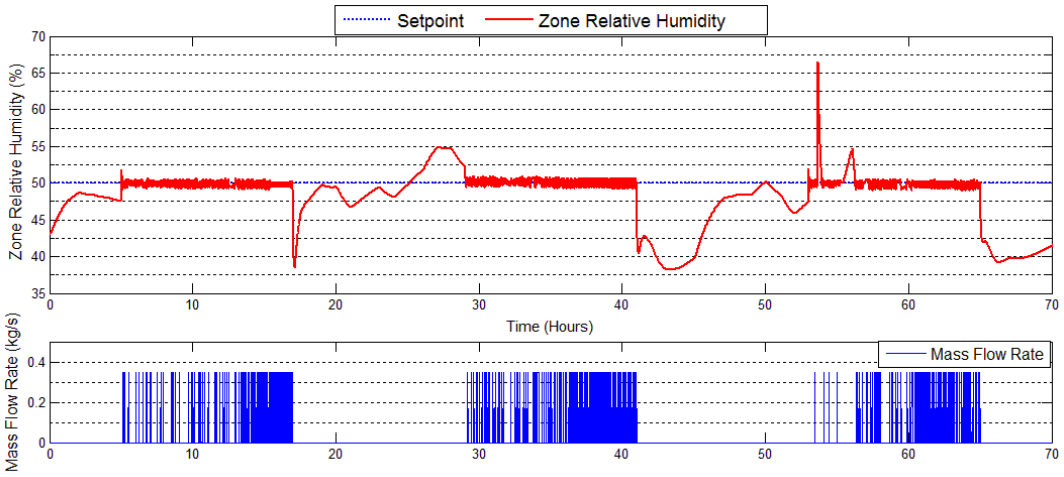

Figure 5.9: Zone relative humidity and ventilation rate with heat loss disturbance (PI-GA)

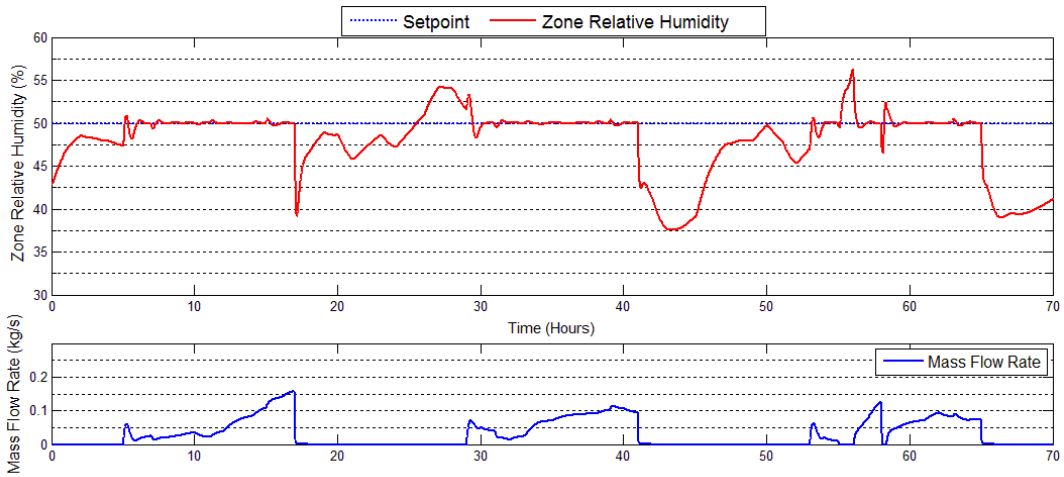

Figure 5.10: Zone relative humidity and ventilation rate with heat loss disturbance (RIDE-GA)

The second disturbance simulates a heat gain by raising the number of room occupants by 10 for a period of 3 hours. This represents situations which could arise such as group meetings where a room will temporarily have extra occupants. Figure 5.11 and Figure 5.12 show the zone air temperature, under PI-GA control and RIDE-GA control respectively, over a three day simulation period with the disturbance simulated on the second day between 35-38 hours. The PI-GA controller demonstrates poor disturbance rejection as can be seen from Figure 5.11. The temperature increases to 23°C when the extra of occupants enter the room and remains above the setpoint for the majority of the time before the occupancy level drops again. This shows that the controller does not react quickly enough to reject the disturbance and would result in uncomfortable thermal conditions. The RIDE-GA

controller again deals with the disturbance effectively with minor oscillations occurring. The controller can be seen to reduce the heating power when the disturbance occurs in order to accommodate for the heat gain. Therefore, it manages to maintain accurate tracking of the set point. From Figure 5.13 and Figure 5.14, the zone relative humidity response of both controllers can be seen to be unaffected by the heat gain disturbance. The RIDE-GA controller rejects the disturbance by reducing the ventilations rate over the disturbance period. The PI-GA controller response is oscillating rapidly around the setpoint and so appears to be unaffected by the disturbance.

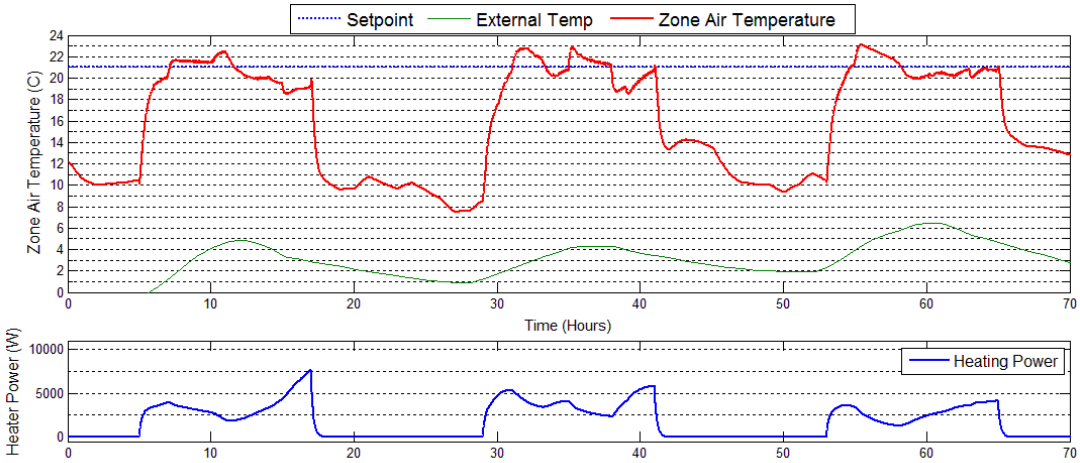

Figure 5.11: Zone air temperature and heat input with heat gain disturbance (PI-GA)

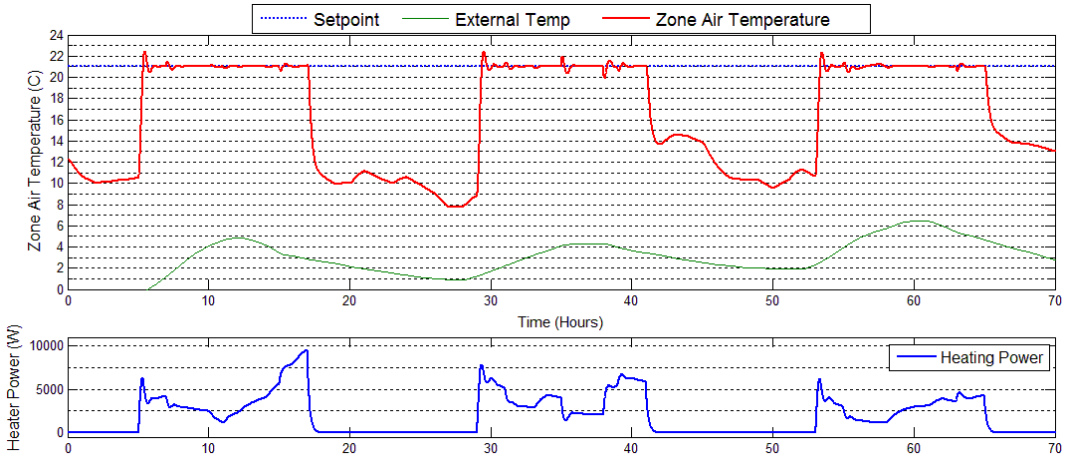

Figure 5.12: Zone air temperature and heat input with heat gain disturbance (RIDE-GA)

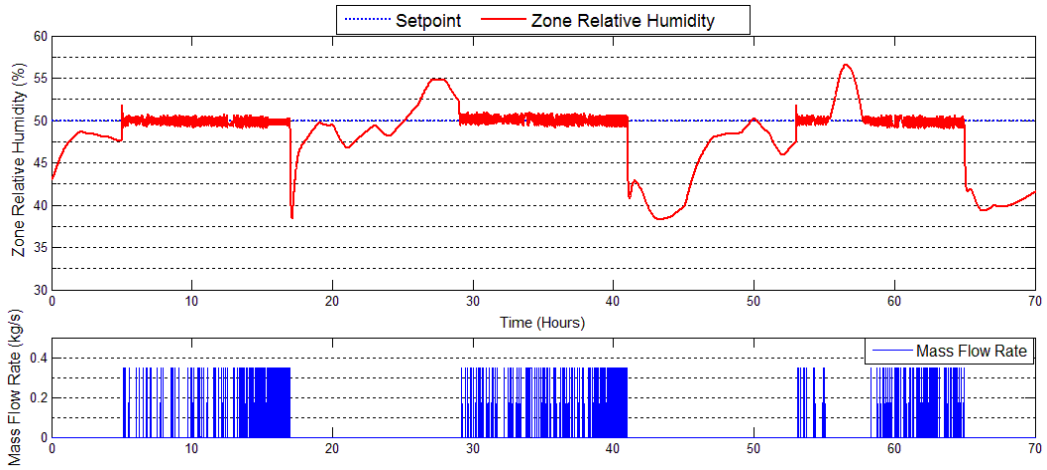

Figure 5.13: Zone relative humidity and ventilation rate with heat gain disturbance (PI-GA)

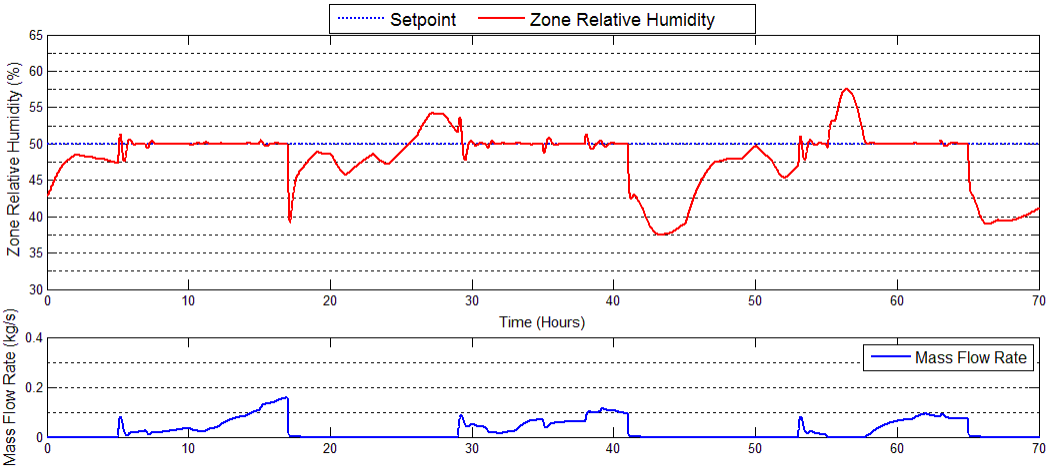

Figure 5.14: Zone relative humidity and ventilation rate with heat gain disturbance (RIDE-GA)

The results presented in this section showcase the proposed RIDE-GA controller's superiority over the PI-GA controller with respect to disturbance rejection, as in all cases presented it is able to reject the disturbances effectively.

5.3 Chapter Conclusions

It was shown in the simulation results that the RIDE control method combined with the GA optimisation is a highly effective control strategy. This was clearly demonstrated through the case study using the simplified building physics model. The results show that the developed control strategy offers the following advantages over the PI controller tuned with the GA:

- Faster response
- Increased accuracy and stable tracking
- Improved disturbance rejection
- Decreased sensitivity to parameter variation
- No oscillatory behaviour translating to less damage to actuators

These benefits of the control system mean that an improved level of thermal comfort for the occupants is achieved as well as potential financial savings due to prolonged life of actuation systems.

5.3.1 Limitations and Improvements Made in other Work

The auto-tuning process described in this chapter was shown to be effective in applications in which there are a small number of parameters with uncertainty which must be accounted for. A limitation of this method however, is that it may become inefficient if it is used to account for uncertainty in a large number of parameters. The auto-tuning method was also designed for use in systems for which models have been developed and the control system designer wishes to tune the control system based on the model. This way, using the system model, the control system can be tuned to produce close to optimal performance when implemented in practice. In some applications however, a system model is unavailable or is difficult to develop due to certain unknown parameters such as transport lag. Therefore, an alternative method which can be used to implement high performance control systems without a detailed model of the system which has been previously developed is required. In Chapter 6, control methods which are capable of dealing with these difficulties are presented.

5.4 Chapter References

Arumugam, M. S., M. Rao, et al. (2005). "New hybrid genetic operators for real coded genetic algorithm to compute optimal control of a class of hybrid systems." Applied Soft Computing **6**(1): 38-52.

Counsell, J. (1992). Optimum and Safe Control Algorithm for Modern Missile Autopilot Design. PhD, Lancaster University.

Fielding, C., A. Varga, et al. (2002). Advanced techniques for clearance of flight control laws, Springer.

Holland, J. H. (1975). Adaptation in natural and artificial systems: an introductory analysis with applications to biology, control, and artificial intelligence, University of Michigan Press.

Janikow, C. Z. and Z. Michalewicz (1991). An experimental comparison of binary and floating point representations in genetic algorithms. Proceedings of the fourth international conference on genetic algorithms, San Diego, CA.

Man, K. K. F., K.-S. Tang, et al. (1999). GENETIC ALGORITHMS.: Concepts and Designs, Avec disquette, Springer Verlag.

Zaher, O. S., J. Counsell, et al. (2011). "Robust control of room temperature and relative humidity using advanced nonlinear inverse dynamics and evolutionary optimisation."

Zamanan, N., J. K. Sykulski, et al. (2006). Real Coded Genetic Algorithm Compared to the Classical Method of Fast Fourier Transform in Harmonics Analysis. Universities Power Engineering Conference, 2006. UPEC'06. Proceedings of the 41st International, IEEE.

6. Robust System Identification Based Nonlinear Inverse Dynamics Control

The aim of the work presented in this chapter is to create a high performance MIMO control strategy for control of thermal comfort conditions in buildings which is easy to implement and overcomes the difficulties mentioned in the previous chapters. Chapter 5 presented an auto-tuning method which can be used to apply the advanced RIDE control methodology for building HVAC systems control. This method required the development of a building physics model for use in the controller design. The derivation of a model which accurately represents the dynamics of a building is not a trivial task, particularly for an operator with limited knowledge of the building physics. Furthermore, obtaining knowledge of certain parameters in a building model can be difficult due to the wide range of use of a building in its lifetime, or in some cases the parameters cannot be known prior to the use of the building e.g. transport lag. The buildings industry is generally reluctant to adopt many of the advanced methods which have been developed by the research community, due to the difficulty in their implementation or extra parameters which require specification resulting in a more lengthy commissioning process. Consequently, traditional PID controller designs are predominantly used in the industry on account of their simplicity and ease of commissioning. Much advancement has been made towards improving PID controller designs in the areas of self-tuning and adaptation however these methods suffer from the drawbacks discussed in Chapter 2. Therefore it is desirable to develop a method which borrows from the advantageous features of these methods whilst achieving an improved performance through advanced design. This chapter presents a methodology which combines the self-tuning principles of the aforementioned methods with the robust NID controller principles presented in Chapter 4. This methodology aims to enable a building control systems designer to apply fundamentally complex and high performance controller design methods with minimal input and extra knowledge required.

6.1 System Identification based Rate Compensated Inverse Dynamics (SI-RCID) Methodology

It has been established that PID control remains the most common control method used in the buildings industry due to its simplicity and familiarity. It is known that one of the main difficulties with designing PID HVAC control systems is tuning (Bi, Cai et al. 2000). In order to tune a PID controller, an accurate model of the process being controlled is required as well as an effective controller design rule. The tuning procedure is often time-consuming, expensive and complicated. In practice, some HVAC control engineers can take over three days to tune a single control loop. Furthermore, in large HVAC system's, re-tuning of the controller is often required, which adds further cost and time onto a project. Consequently, many of the advancements made in PID controller designs for HVAC systems are based on auto-tuning and self-tuning/adaptive control. These methods offer advanced methods for tuning the gains of the control systems based on identification of the system being controlled using input-output data. Since most of the processes in HVAC systems can be approximated by first order models, the identification methods employed in these controllers typically aim to identify a first order plus dead time (FOPDT) model using step response data. This has proven to be an effective method in many cases however one of the drawbacks of these controller methods is robustness to changes in operating conditions and inaccuracies in the identified models.

Since identification of FOPDT models of HVAC systems from step response data is an established methodology which the buildings industry is familiar with, it is logical to utilise this method whilst improving on the drawbacks of these control strategies. Hence, the methodology presented in this chapter utilises the step response system identification method in a robust NID controller structure which overcomes the robustness drawbacks commonly found in PID controllers whilst offering significant performance improvements.

Consider a system represented by the state equations below:

$$\dot{x}(t) = Ax(t) + Bu(t) + Fd(t) \tag{6.1}$$

$$y(t) = Cx(t) \tag{6.2}$$

$$w(t) = Mx(t) \tag{6.3}$$

From Chapter 4, it was shown that the RIDE control law is given by equation 6.4-6.6.

$$u_c(t) = K_I z(t) - K_P w(t) + u_{eq}(t) \tag{6.4}$$

$$\dot{z}(t) = e(t) = r(t) - w(t) \tag{6.5}$$

$$u_{eq}(t) = u(t) - (MB)^{-1}\dot{w}(t) \tag{6.6}$$

Where:

$$K_P = [MB]^{-1} g \tag{6.7}$$

$$K_I = [MB]^{-1} \rho \tag{6.8}$$

It can be seen that in order to implement the RIDE control algorithm in practice, the only part of the system model required is the MB matrix. Therefore, in order to apply this control algorithm to an unknown system only the MB matrix would have to be identified. The requirement to identify the MB matrix only, simplifies the identification process as one of the difficulties encountered in identification is often identifying the structure of the model that is to be identified. The structure of the MB matrix however is fixed for any system as it is a square matrix with a number of rows and columns equal to the number of inputs to the system.

When identifying the model of the building it is desirable to do it at a time when disturbances are small or have a small effect. In an office building it would be reasonable to assume that disturbances would be smallest at night time. Hence, within an adequately small time frame, the disturbances can be assumed to be negligible. Based on this assumption, for a building whose dynamics are represented by the state space equations 6.1-6.3, the state equation 6.1 would become:

$$\dot{x}(t) = Ax(t) + Bu(t) \tag{6.9}$$

It is possible to separate a system represented in state space into its fast and slow parts. The fast part of the system is influenced directly by the input and the slow state is subsequently influenced by the fast state (Khalid 2011). The system expressed in equations 6.9 can be decomposed into fast and slow modes in the form shown below:

$$\dot{x}_1(t) = A_{11}x_1(t) + A_{12}x_2(t) \tag{6.10}$$

$$\dot{x}_2(t) = A_{21}x_1(t) + A_{22}x_2(t) + B_2u(t) \tag{6.11}$$

A set of states can be transformed into another set using a transformation matrix J as follows:

$$x(t) = [x_1(t) \quad x_2(t)]^T = Jx(t) \tag{6.12}$$

Where the transformation matrix J is given by:

$$J = \begin{bmatrix} J_1 \\ J_2 \end{bmatrix} \tag{6.13}$$

Thus:

$$JAJ^{-1} = \begin{bmatrix} A_{11} & A_{12} \\ A_{21} & A_{22} \end{bmatrix} \tag{6.14}$$

The transformation is based on the condition that:

$$J_1B = 0 \tag{6.15}$$

Therefore, based on the assumption that B_2 and C_2 are non-singular and that the CB matrix is full rank:

$$JB = \begin{bmatrix} 0 \\ B_2 \end{bmatrix} \tag{6.16}$$

$$CJ^{-1} = [C_1 \quad C_2] \tag{6.17}$$

The state space representation then becomes:

$$\begin{bmatrix} \dot{x}_1(t) \\ \dot{x}_2(t) \end{bmatrix} = \begin{bmatrix} A_{11} & A_{12} \\ A_{21} & A_{22} \end{bmatrix} \begin{bmatrix} x_1(t) \\ x_2(t) \end{bmatrix} + \begin{bmatrix} 0 \\ B_2 \end{bmatrix} [u(t)] \tag{6.18}$$

$$[y(t)] = [C_1 \quad C_2] \begin{bmatrix} x_1(t) \\ x_2(t) \end{bmatrix} \tag{6.19}$$

In the case of thermal comfort control, the controlled states are typically the internal air temperature, humidity and CO_2 concentration which are the fast states. Therefore, the feedback, w(t), can be expressed as:

$$[w(t)] = [0 \quad M_2]\begin{bmatrix} x_1(t) \\ x_2(t) \end{bmatrix} \tag{6.20}$$

If equation 6.20 is differentiated and equation 6.11 is substituted into it then this gives:

$$\dot{w}(t) = M_2A_{21}x_1(t) + M_2A_{22}x_2(t) + M_2B_2u(t) = M_2\dot{x}_2(t) \tag{6.21}$$

In many cases w(t)=x_2 such that M_2=1 for a SISO system, or M_2=I for a MIMO system. For now, let us consider a SISO system. In buildings, it is reasonable to assume that the slow modes of the system are much slower than the fast modes of the system i.e. the states that are directly controlled using the actuators, such as temperature and humidity, have a much faster response than the wall temperature for example (Khalid 2011). When this is true, it can be assumed that, within a given time frame, the slow modes of the system are approximately constant. This time frame should be long enough for the fast modes to respond and reach steady state whilst being short enough such that the slow modes remain constant. Therefore, if the input to the system is initially zero and then a step input is applied to the system, then equation 6.21 at the initial conditions and after the step input will be represented by equations 6.22 and 6.23 respectively:

$$M_2\dot{x}_2(0) = M_2A_{21}x_1(0) + M_2A_{22}x_2(0) \tag{6.22}$$

$$M_2\dot{x}_2(T) = M_2A_{21}x_1(T) + M_2A_{22}x_2(T) + M_2B_2u(T) \tag{6.23}$$

Where T is the time taken for the system to reach steady state after the step input has been applied. Considering equation 6.21 in terms of the difference caused by the step input will give:

$$M_2\Delta\dot{x}_2(t) = M_2A_{22}\Delta x_2(t) + M_2B_2\Delta u(t) \tag{6.24}$$

Dividing through by M_2:

$$\Delta\dot{x}_2(t) = A_{22}\Delta x_2(t) + B_2\Delta u(t) \tag{6.25}$$

The standard format of a first order differential equation is given by:

$$\tau \dot{x}(t) = x(t) + Gu(t) \tag{6.26}$$

Where τ is the time constant and G is the process gain. It can be seen that equation 6.25 can be rearranged in this format as follows:

$$\frac{1}{A_{22}} \Delta \dot{x}_2(t) = \Delta x_2(t) + \frac{B_2}{A_{22}} \Delta u(t) \tag{6.27}$$

This shows that there is a first order relation between the system input and output where:

$$\tau = \frac{1}{A_{22}} \tag{6.28}$$

$$G = \frac{B_2}{A_{22}} \tag{6.29}$$

Therefore, if a step input is applied to the system, the process gain and time constant of the system can be determined. Since M_2 is known, as it is specified by the user, M_2B_2 can subsequently be determined by rearranging equation 6.29 and multiplying by M_2 to give:

$$M_2 B_2 = M_2 G A_{22} \tag{6.30}$$

This can be determined since the gain and time constant ($1/A_{22}$) have been identified.

6.1.1 MIMO System Identification

The method described above can also be used to identify the MB matrix in MIMO systems. Consider equation 6.25 for a two input two output MIMO system. The expanded matrices would be as follows:

$$\begin{bmatrix} (\Delta \dot{x}_2)_1(t) \\ (\Delta \dot{x}_2)_2(t) \end{bmatrix} = \begin{bmatrix} (A_{22})_{11} & (A_{22})_{12} \\ (A_{22})_{21} & (A_{22})_{22} \end{bmatrix} \begin{bmatrix} (\Delta x_2)_1(t) \\ (\Delta x_2)_2(t) \end{bmatrix} + \begin{bmatrix} (B_2)_{11} & (B_2)_{12} \\ (B_2)_{21} & (B_2)_{22} \end{bmatrix} \begin{bmatrix} \Delta u_1(t) \\ \Delta u_2(t) \end{bmatrix} \tag{6.31}$$

In a system where the fast states are not dependent on one another, as is the case in many systems, the A_{22} matrix will be diagonal. The three main thermal comfort parameters that are controlled in a building are temperature, humidity and CO_2 concentration. These three parameters are not dependant on one another e.g. a change

in air temperature does not affect the absolute humidity of the zone and the same is true for CO_2 concentration. The exception is relative humidity, which is a function of air temperature and absolute humidity. This however can be dealt with by considering the effect of the states on one another in the B matrix, as will be demonstrated in the case study section 6.2, thus keeping the A matrix diagonal. In light of this, equation 6.31 can be rewritten as:

$$\begin{bmatrix}(\Delta\dot{x}_2)_1(t)\\(\Delta\dot{x}_2)_2(t)\end{bmatrix} = \begin{bmatrix}(A_{22})_{11} & 0\\0 & (A_{22})_{22}\end{bmatrix}\begin{bmatrix}(\Delta x_2)_1(t)\\(\Delta x_2)_2(t)\end{bmatrix} + \begin{bmatrix}(B_2)_{11} & (B_2)_{12}\\(B_2)_{21} & (B_2)_{22}\end{bmatrix}\begin{bmatrix}\Delta u_1(t)\\\Delta u_2(t)\end{bmatrix} \quad (6.32)$$

If a step input is applied to one channel at a time and the input for the other channel is kept as zero, the MB matrix can be identified as follows. Applying a step input to the first channel i.e. $(x_2)_1$ will result in both equations being expressed as:

$$(\Delta\dot{x}_2)_1(t) = (A_{22})_{11}(\Delta x_2)_1(t) + (B_2)_{11}\Delta u_1(t) \quad (6.33)$$

$$(\Delta\dot{x}_2)_2(t) = (A_{22})_{22}(\Delta x_2)_2(t) + (B_2)_{21}\Delta u_1(t) \quad (6.34)$$

Both of these equations can be rearranged in the format of standard first order equations as shown below:

$$\frac{1}{(A_{22})_{11}}(\Delta\dot{x}_2)_1(t) = (\Delta x_2)_1(t) + \frac{(B_2)_{11}}{(A_{22})_{11}}\Delta u_1(t) \quad (6.35)$$

$$\frac{1}{(A_{22})_{22}}(\Delta\dot{x}_2)_2(t) = (\Delta x_2)_2(t) + \frac{(B_2)_{21}}{(A_{22})_{22}}\Delta u_1(t) \quad (6.36)$$

Where the process gain G_i and time constant τ_i for each channel (i) are given by:

$$\tau_1 = \frac{1}{(A_{22})_{11}} \quad (6.37)$$

$$G_1 = \frac{(B_2)_{11}}{(A_{22})_{11}} \quad (6.38)$$

$$\tau_2 = \frac{1}{(A_{22})_{22}} \quad (6.39)$$

$$G_2 = \frac{(B_2)_{21}}{(A_{22})_{22}} \quad (6.40)$$

Hence, with knowledge of the process gain and time constants, the parameters of the B_2 matrix relating the first input to both channels can be determined by rearranging equations 6.38 and 6.40 as follows:

$$(B_2)_{11} = G_1(A_{22})_{11} \quad (6.41)$$

$$(B_2)_{21} = G_2(A_{22})_{22} \quad (6.42)$$

Thus the cross coupling of inputs across channels is known. The above process can then be repeated for the second channel and the remaining parameters of the B_2 matrix can be determined. The M_2B_2 matrix can then be determined by multiplying the M_2 and B_2 matrices together. This process can be extended to MIMO systems with any number of inputs and outputs, providing the number of inputs and outputs are the same.

6.1.2 System Identification from Step Response

In the previous section it was shown that the M_2B_2 matrix can be determined through the identification of the first order response characteristics of the input-output relation of the building zone and HVAC system within a given time frame. Hence, a first order system identification technique must be adopted in order to do this. Since most thermal processes in buildings and HVAC systems can be approximated by first order plus dead time (FOPDT) models (Bi, Cai et al. 2000), there are numerous methods which can be found in the literature for the identification of FOPDT models from input-output data. The FOPDT model transfer function is shown below:

$$TF = \frac{K}{T_C s + 1} e^{-Ls} \quad (6.43)$$

Where K is the system gain, T_C is the time constant and L is the dead time. Dead time represents the time taken for the system to respond, or for a response to be observed, after the moment the input is applied to the system. Dead time in buildings is an issue which has adverse effects on the performance of control systems and is often the cause of poor performance of building control systems in practice. Section

6.1.6 details an advanced method designed to deal with time delay in the RIDE controller structure.

Two basic and common identification methods which are used to identify first order process models from open loop step response data are the two point method and the area method (Kealy and O'Dwyer 2002). The area method is based on integrals of the step response. Integrals of specific areas of the open loop step response data are taken and based on the resulting values the dead time and time constant are determined.

In the two point algorithm approach, the system gain is determined by dividing the steady state output value by the steady state input value as shown below:

$$K = \frac{\Delta y_{ss}}{\Delta u_{ss}} \tag{6.44}$$

The time constant and dead time of the process are then determined from the time taken for the process to reach 28% and 63% of the final steady state output value. These two points in the output response are then used in equations 6.45 and 6.46 as follows:

$$T_{63} = T_D + T_c \tag{6.45}$$

$$T_{28} = T_D + \frac{T_c}{3} \tag{6.46}$$

Where T_D and T_C are the dead time and time constant respectively. There have been several new developments in advanced identification methods from step response data however for the purposes of the work presented in this thesis, the two point algorithm was found to be sufficiently effective.

Buildings are slowly varying systems, as mentioned by Geng and Geary (1993), therefore continuous adaptation is generally not necessary. Therefore, the system can be adapted slowly e.g. every night or every weekend.

6.1.3 Robustness

Once the MB matrix has been obtained using the procedure explained above, it can be used in the control system design. As shown in equation 6.6, the equivalent

control equation is calculated based on the MB matrix. Therefore the equivalent control can be implemented using the identified MB matrix. As the RIDE controller structure is inherently robust to errors in the u_{eq} calculation, the control system will consequently be robust to errors in the identified MB matrix which might cause inaccuracy in the u_{eq} estimation. Going back to section 4.3.1 explaining the robustness of the RIDE control structure, it can be seen from equations 6.47 and 6.48 below that the integral gain (g) and proportional gain (p) can be increased to decrease the effect of the error in MB and u_{eq}.

$$\left[\frac{s^2}{g} + s + \frac{\rho}{g}\right] w(s) = \frac{sMB\left[\hat{u}_{eq}(s) - u_{eq}(s)\right]}{g} + \frac{\rho}{g} r(s) \qquad (6.47)$$

$$\left[\frac{s^2}{\rho} + \frac{gs}{\rho} + 1\right] w(s) = \frac{sMB\left[\hat{u}_{eq}(s) - u_{eq}(s)\right]}{\rho} + r(s) \qquad (6.48)$$

The MB matrix used in the gain equations might differ from real MB in which case the MB matrix will be cancelled out however the natural frequency and damping ratio of the closed loop system might not correspond exactly with what the user has specified in the proportional and integral gains according to equations 6.7 and 6.8. This can be dealt with using the method presented in the section 6.1.5.

The robust structure of the controller design provides a good framework which reduces sensitivity to identification errors and can reject plant changes, which cause the MB matrix to differ from the identified one, as disturbances providing they are not excessively large such that the error in u_{eq} is greater than u_{eq} itself. In the case that the MB matrix does vary significantly, the system identification process can be performed at different operating points such that different MB matrices can be scheduled and used at different points in the operating range.

6.1.4 Novel Improved Commutation Law for Dealing with Actuation System Limits

While the original commutation law for the RIDE controller given in equation 4.38 works well in most cases, there are certain conditions in which it has an adverse

effect on the controller performance. Let us consider the effect of equation 4.38 on the control signal produced by equation 6.4 using the example of a zone temperature control system. If we assume that the controller is switched on at the beginning of the day and that initially the zone air temperature is lower than the set point such that the error is positive, then a positive control signal is required i.e. heat input is required. Looking at equation 6.6 it can be seen that in order for the u_{eq} term in equation 6.4 to be positive, the rate of change of the output must be negative since the actuator input u(t) is initially zero. If at the beginning of the day however, the rate of change of output (temperature) is positive due to casual heat gains or rising external temperature, which is common, the control action produced by u_{eq} will be negative. The proportional action in equation 6.4 will always be negative in a zone air temperature control system unless the zone air temperature is below zero which we can assume to be unlikely in most cases. Thus, in this scenario, in order for the control action produced by equation 6.4 to be positive the following must be true:

$$|K_I z(t)| > \left|K_P w(t) + \hat{u}_{eq}(t)\right| \tag{6.49}$$

Thus, for the condition in equation 6.49 to be true, the error must be large enough to make the magnitude of the integral action larger than the magnitude of the proportional and u_{eq} action. This is unlikely to be true at the point when the controller is switched on since the integral of error has not yet been given time to build up. Therefore the overall control action produced will be negative i.e. it is attempting to drive the system in the wrong direction. In reality however, the heater will not produce negative heat. Thus, the lower limit of the actuator is zero. According to the original commutation law in equation 4.38, the error term is set to zero when the controller demands action which is out with the limits of the actuation system in order to avoid integrator wind up which forces the system to remain on the actuation limit for longer than necessary. In this scenario however, by setting the error to zero, the control action produced will be negative and will continue to be negative since the integral term will not build up. Thus, this commutation law forces the system to become locked on the lower limit despite the system requiring positive control action. In order to overcome this problem, a new commutation law with an extra criterion shown in equations 6.50 and 6.51 is proposed:

$$\dot{z}_i(t) = \begin{cases} 0, & if\ (\alpha u_i < 0\ AND\ \beta_i > 0\ )\ \boldsymbol{OR}\ \ (\alpha l_i > 0\ AND\ \beta_i < 0) \\ e_i(t), & if\ \alpha u_i > 0\ \ \boldsymbol{OR}\ \ \alpha l_i < 0 \end{cases} \quad (6.50)$$

$$\beta_i = abs\big(r_i(t)\big) - abs\left(y_i(t)\right) \quad (6.51)$$

Based on the above commutation law, the error in the integral term is only set to zero when the control system is on the limit **and** the system output is on the correct side of the set point. Therefore, in the scenario described above, the error would not be set to zero and consequently the integral term would build up. This would lead to the condition in equation 6.49 becoming true and a positive control signal would be produced. Therefore this new improved commutation law overcomes the issues which occur with the original commutation law and is effective in all conditions.

6.1.5 Stability and Tuning

In order to apply high gain or inverse dynamics control, the transmission zeros of the open loop system must be stable as they dictate the final location of the closed loop poles. Therefore, it is necessary to check if the systems transmission zeros (TZ's) are stable. If the system has not been modelled, then the existence of RHP TZ's can be determined simply by observing the response of the system to a step test as this type of system shows an initial movement in the opposite direction i.e. a non-minimum phase system. If the TZ's are found to be stable, then the RIDE controller can be applied, providing the MB matrix is full rank. In the case that the TZ's are found to be unstable, then the feedback must be changed until the system no longer exhibits the non-minimum phase characteristics.

Most cases of degenerate MB matrices in practice arise due to one of the matrices M or B not having maximal rank. It is possible to assess this without modelling the system by looking at the inputs and outputs of the system (Khalid 2011). An example could be if one input is applied to control more than one state, the columns of the B matrix corresponding to these controls would be collinear causing the matrix to be degenerate (Khalid 2011). It is also possible to identify whether the MB matrix will be full rank or not by analysing the step response of the system. If a step input is

applied and no response is observed in the corresponding output being controlled then the MB matrix will not be full rank.

It was shown in Chapter 4 that when the equivalent control input is used, the closed loop system transfer function becomes:

$$[G(s)] = [s^2 I_m + s(K_P MB) + K_I MB]^{-1} K_I MB \tag{6.52}$$

By setting the gains to equations 6.7 and 6.8, the MIMO system is then represented by SISO channels characterised by ideal second order transfer functions with the designed damping ratio and natural frequency as shown below:

$$[G(s)] = \begin{bmatrix} \frac{{\Omega_n}^2}{s^2 + 2Z_d\Omega_n s + {\Omega_n}^2} & 0 & \cdots & 0 \\ 0 & \frac{{\Omega_n}^2}{s^2 + 2Z_d\Omega_n s + {\Omega_n}^2} & 0 & \vdots \\ \vdots & 0 & \ddots & 0 \\ 0 & \cdots & 0 & \frac{{\Omega_n}^2}{s^2 + 2Z_d\Omega_n s + {\Omega_n}^2} \end{bmatrix} \tag{6.53}$$

In reality however, errors in the MB matrix can result in the natural frequency and damping ratio being different from those specified by some factor k_i (where i is the control channel) meaning equation 6.52 now becomes:

$$[G(s)] = \begin{bmatrix} \frac{k_1{\Omega_n}^2}{s^2 + 2kZ_d\Omega_n s + k{\Omega_n}^2} & 0 & \cdots & 0 \\ 0 & \frac{k_2{\Omega_n}^2}{s^2 + 2kZ_d\Omega_n s + k{\Omega_n}^2} & 0 & \vdots \\ \vdots & 0 & \ddots & 0 \\ 0 & \cdots & 0 & \frac{k_m{\Omega_n}^2}{s^2 + 2k\Omega_n s + k{\Omega_n}^2} \end{bmatrix} \tag{6.54}$$

This factor can be compensated for by applying a step input on the closed loop system and observing the response. It is known that the rise time (T_r) of a second order system can be approximated by equation 6.55:

$$T_r \approx \frac{1.8}{\omega_n} \tag{6.55}$$

The rise time is defined as the time taken for the system response to go from 10% to 90% of the final steady state value. Therefore, the natural frequency of the closed loop system can be calculated approximately from the step response of the closed loop system (Ding, Bradshaw et al. 2006). If it is found that ω_n is not the same as what was specified by the user, then the natural frequency specified in the gains can be adjusted to compensate for this error. It is very important however that the closed loop bandwidth (ω_n) of the system is at least three times slower than the actuator bandwidth (ω_a) in order to ensure tracking is possible (Khalid 2011). Hence, the closed loop step response test should be performed with the bandwidth specified at a value lower than $\omega_a/3$.

6.1.6 Time Delay Compensation

In buildings, thermal systems with large dead time are common. Dead time, as mentioned in Section 6.1.2, is the time taken for a response to be observed by the output of the system after an input has been applied to the system. Dead time is commonly associated with large times taken for energy to be transferred and is therefore often referred to as transport lag. This can occur in AHUs in buildings due to long ducting which can cause a significant delay in the time taken for the heat transferred from the heating system to the supply air reaching the outlet or zone. Another example which is common in building zone thermal comfort control is large transport lag due to poor sensor placement. If the temperature sensor is located at some distance from the heat source e.g. on the opposite side of a large room, a lag will exist due to the time taken for the heat transferred from the source to reach the temperature sensor on the other side of the room. This becomes more problematic with increasing room size. During this lag time, a situation is created in which the control system essentially becomes open loop as there is no feedback from the sensor measuring the effect the heater is having on the room air temperature i.e. it is feeding back outdated information. This causes significant problems for control systems as dead time reduces gain and phase margins and is often a cause for poor performance of building control systems in practice (Vodencarevic 2010). Therefore, dead time is an important issue which must be considered in the control system design.

The most established method for dealing with time delays in control systems is the Smith's Predictor (SP) (Smith 1957). The SP concept is based on the principle of using a model of the system to predict the system response during the time that there is no up to date feedback data. This way the time delay can be eliminated from the characteristic equation of the closed loop system (Moreno, Guzmán et al. 2013). The Smith Predictor method can be better explained using Figure 6.1 showing a SP feedback control system applied to a system with dead time. G is the lag free part of the system, L is the dead time, C is the controller, $\hat{G}$ is a model of the delay free system and $\hat{L}$ is the model delay.

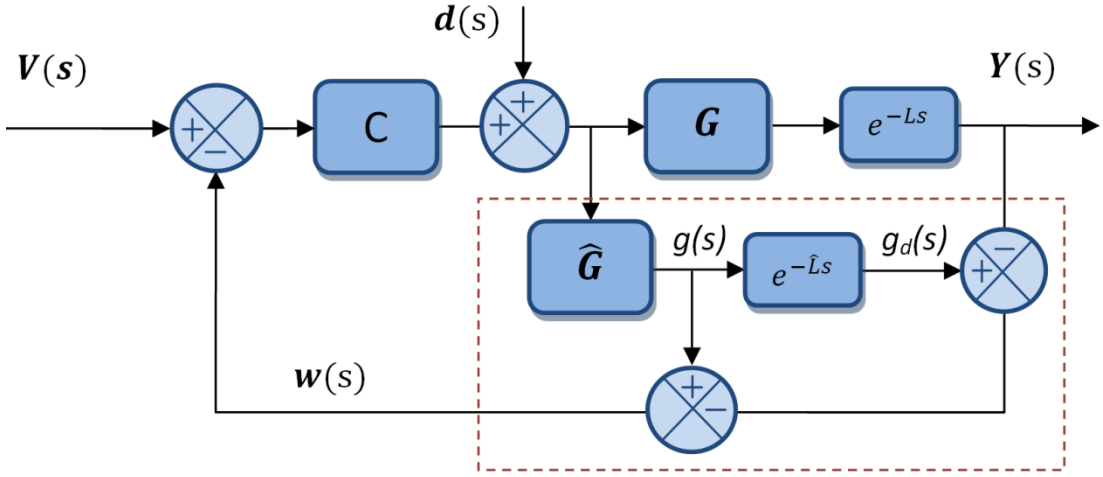

Figure 6.1: Smiths Predictor (SP) control

It can be seen from Figure 6.1 that there are two feedback loops in the control system. One loop feeds the measured data from the process back to the controller as normal. Due to the dead time however, the performance of the controller with this single loop alone will be impaired. The second inner loop is designed to alleviate this problem by using the model of the plant as a predictor to control the system during the time which no up to date data is available i.e. the plant output is unobservable. Therefore the feedback signal w(s) is given by:

$$w(s) = g(s) - \left(g_d(\mathrm{s}) - \mathrm{Y(s)}\right) \qquad (6.56)$$

It can be seen from equation 6.56 that if the model of the plant corresponds exactly to the plant itself, then the feedback from outer and middle loops, g_d(s) and Y(s) respectively, cancel each other and the effect of the time delay will be negated. In

reality, the output from the model g(s) may not match the output of the real system however some corrective action is produced by the error between $g_d(s)$ and Y(s).

While the SP control method is effective in many cases, it is known that the main drawback of this method is that modelling errors, particularly in the dead time, typically result in severe degradation in the control performance and can drive the system to instability. Many modifications of the SP have been proposed in the literature, which offer improvements over the original SP [(Liu, Zhang et al. 2005), (Astrom, Hang et al. 1994), (Torrico and Normey-Rico 2005), (Normey-Rico, Bordons et al. 1997)]. The majority of these methods are more complex than the original SP (Normey-Rico and Camacho 2009). A solution proposed by Normey-Rico (2007) which improves the robustness of the SP to modelling mismatches is the Filtered Smith Predictor (FSP). The FSP structure was originally introduced in (Normey-Rico, Bordons et al. 1997) for FOPDT stable processes. Then the authors presented a unified approach for designing the FSP in such a way that it can be used to compute a controller taking into account the robustness, coping with unstable plants, improving the disturbance rejection properties and decoupling the set-point and disturbance responses (Normey-Rico and Camacho 2009). The FSP controller design is the same as the conventional SP with two additional filters as shown in Figure 6.2.

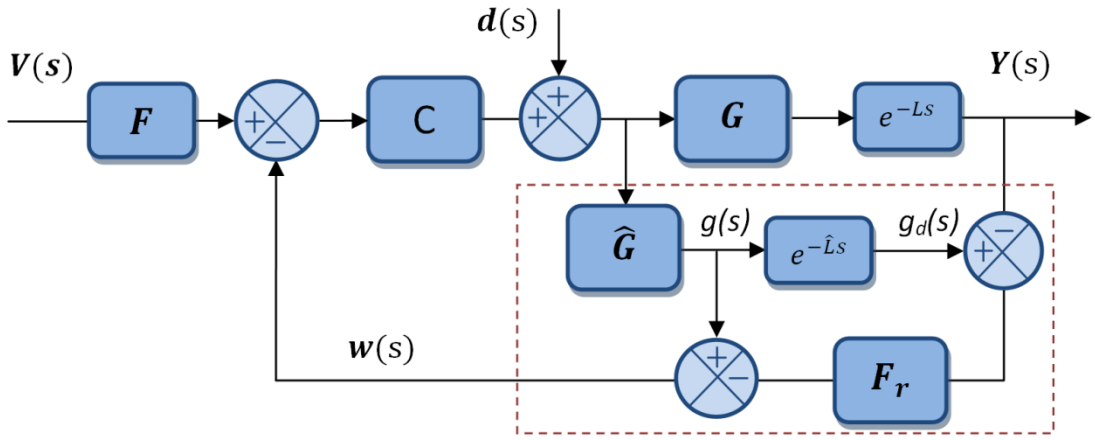

Figure 6.2: Filtered Smiths Predictor (FSP) control

F(s) is a traditional reference filter used to improve the set-point response and Fr(s) is a predictor filter used to improve the properties of the predictor. In the structure in Figure 6.2, $P_n = \hat{G}e^{-\hat{L}s}$ is a model of the process where $\hat{G}$ is the delay free part of

the plant model, $\hat{L}$ is the model delay and C is the primary controller. The actual plant is $P = Ge^{-Ls}$. In this structure, the nominal closed loop transfer functions when the model of the plant is perfect i.e. $P(s) = P_n(s)$, are as follows (Normey-Rico and Camacho 2009):

$$H_v(s) = \frac{Y(s)}{V(s)} = \frac{F(s)C(s)P_n(s)}{1 + C(s)\hat{G}(s)} \tag{6.57}$$

$$H_d(s) = \frac{Y(s)}{D(s)} = P_n(s)\left[1 - \frac{C(s)P_n(s)F_r(s)}{1 + C(s)\hat{G}(s)}\right] \tag{6.58}$$

In order to analyse the robustness, consider a family of plants P(s) such that $P(s) = P_n(s)[1 + dP(s)]$ and:

$$|\delta P(j\omega)| \leq \overline{\delta P}(\omega) \quad \forall \omega > 0 \tag{6.59}$$

Thus, the robust stability condition for the FSP is [(Normey-Rico 2007; Normey-Rico and Camacho 2009)]:

$$\overline{\delta P}(\omega) < dP(\omega) = \frac{\left|1 + C(j\omega)\hat{G}(j\omega)\right|}{\left|C(j\omega)\hat{G}(j\omega)F_r(j\omega)\right|} \quad \forall \omega > 0 \tag{6.60}$$

It can be seen that only $\frac{Y(s)}{D(s)}$ and $dP(\omega)$ are modified by the inclusion of the filter. Therefore, the filter $F_r(s)$ can be utilised for improving the robustness or the disturbance rejection capabilities of the system without affecting the nominal set-point response. Furthermore, when controlling unstable plants, $F_r(s)$ can be tuned to obtain an internal stable system (Normey-Rico and Camacho 2009). A detailed explanation of the tuning procedures for various types of systems as well an in depth stability analysis of this FSP can be found in [(Normey-Rico 2007; Normey-Rico and Camacho 2009)].

6.1.6.1 Time delay and RIDE

It is known that the existence of a time delay in a control loop reduces the gain and phase margins of the system and thus there are limits on the gain which can be used i.e. it is no longer possible to use a high gain controller. By increasing the gain

in a closed loop system, the closed loop poles are driven towards the locations of the open loop zeros. Since the u_{eq} term in the RIDE controller essentially places the closed loop poles of the system over the zeros of the open loop system, the u_{eq} term achieves the equivalent effect as a high gain controller and thus the existence of a time delay in the control loop has severe adverse effects on the performance of the RIDE controller. When a significant time delay exists in the system, **the u_{eq} term in the RIDE controller actually results in the system becoming unstable and it cannot be stabilised by reducing the gain** as is possible with other controller designs. This is a very important observation which allows us to understand the effects of having a time delay in the system when using equivalent control. If we assess the equation for the u_{eq} term in the RIDE controller, we can see that it acts on the derivative of the output signal. This exacerbates the problem due to the derivative signal having increased sensitivity to incorrect data caused by the time delay. If the rate of the delayed output signal is negative when in reality the rate of output is positive, then according to u_{eq} equation 6.6, the equivalent control will produce a positive control signal forcing the output in the wrong direction. Therefore, when a large enough transport lag exists in the system, the RIDE controller often exhibits highly oscillatory behaviour whereas a PI or PDF controller may be less oscillatory as will be shown in section 6.2.2.2. It was found however, that for systems with a relatively small time delay, typically in the order of $\frac{T_d}{\tau} \leq 0.1$, the oscillation in the RIDE controller's response could be diminished by eliminating the lag effect in the derivative signal used in u_{eq} only, i.e. only compensating for the time delay in the derivative signal. This is due to the u_{eq} term producing corrective control action for the incorrect control signal caused by the time delay produced by the PDF part of the controller. Therefore, a novel rate compensated equivalent control strategy using the SP concept explained above is presented in this section. Figure 6.3 shows a block diagram of the conventional u_{eq} method used in the RIDE controller.

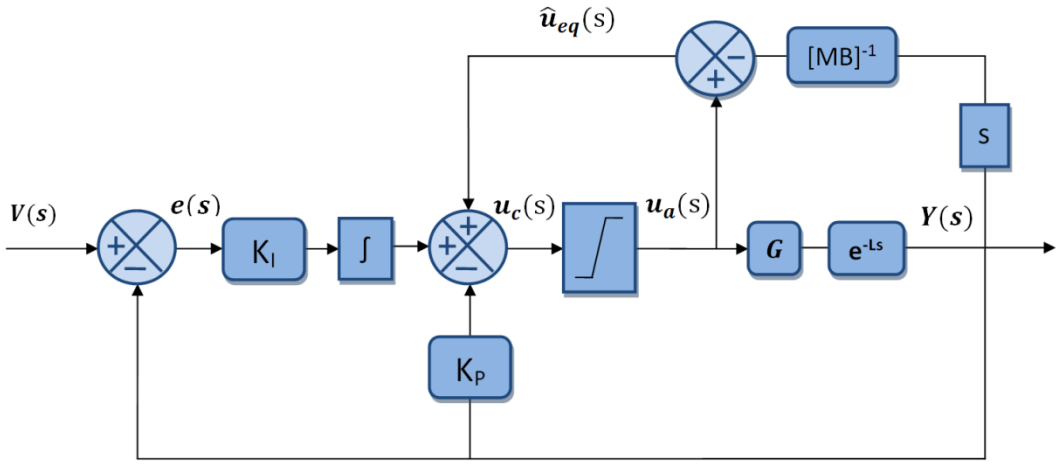

Figure 6.3: RIDE controller with time delay plant

As explained above, the u_{eq} term is acting on the derivative of the delayed feedback signal which causes the oscillatory behaviour. In order to compensate for the delay effect in the rate feedback signal, the new rate compensated u_{eq} method shown in Figure 6.4 based on the SP method is proposed.

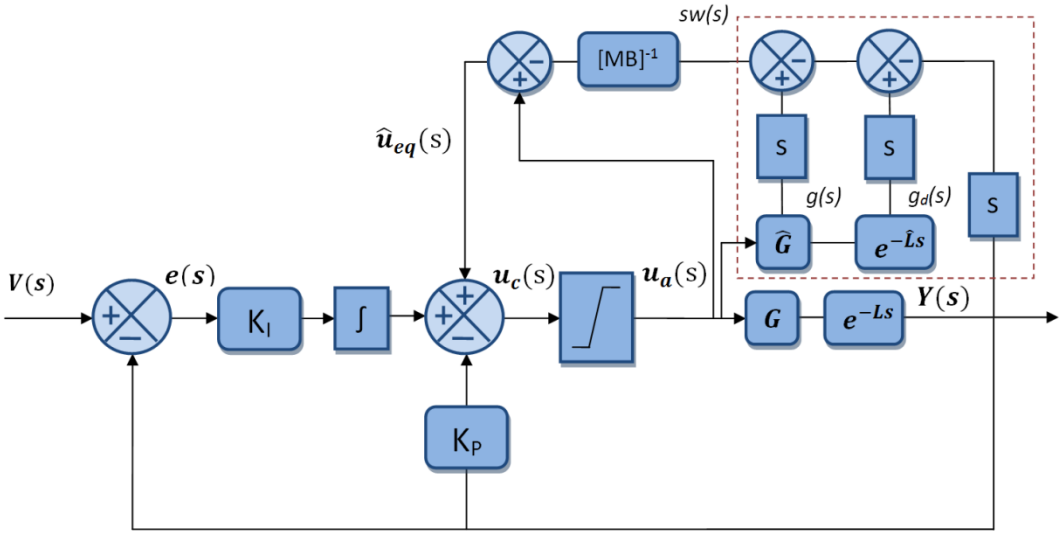

Figure 6.4: Rate compensated inverse dynamics for time delay system control

Using the principles of the conventional SP, a model of the system can be used to compensate for the outdated rate output signal used in the u_{eq} calculation. The new rate feedback signal sw(s) used in u_{eq} becomes:

$$sw(s) = sg(s) - \left(sg_d(s) - \mathrm{sy(s)}\right) \qquad (6.61)$$

Thus, if the rate output from the model matches the rate output of the actual system, then the delayed model and plant outputs will cancel out and the effect of the time delay on the measured rate output signal will be negated and in turn u_{eq} will correct the control signal produced by the PDF part of the controller. In some cases, there might remain some effect of the time delay on the PDF part of the controller however the controller gains can be reduced slightly to overcome this if necessary. If the rate output of the model does not match the actual system then the error between the delayed rate signals from the model and system ($sg_d(s)$-$sy(s)$) will provide some corrective action to the rate feedback signal from the model. Another benefit of using the rate compensation method above is that the PDF controller structure provides robustness to inaccuracies in the u_{eq} estimation, as shown in section 6.1.3.

Time Delay Compensation for Long Time Delay Systems *($T_d/\tau > 0.1$)*

As mentioned earlier, the method presented above is able to remove the oscillatory behaviour from the RIDE controller for systems with a relatively small time delay. It was found however that this method was not sufficient for systems with long time delays. Therefore a new method which is capable of handling longer time delays is required. First let us consider the original SP concept applied in the RIDE controller framework as shown in Figure 6.5.

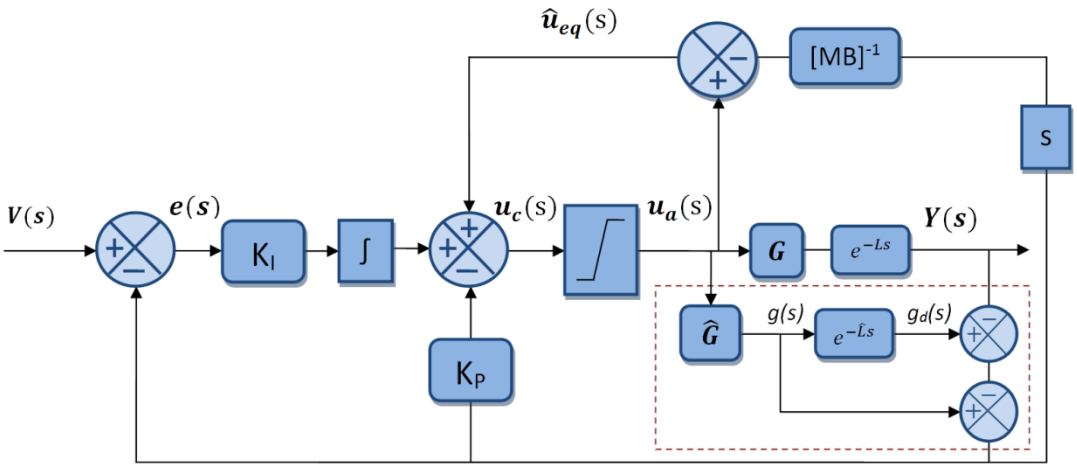

Figure 6.5: RIDE controller with time delay compensation based on original SP

When the above setup was tested, it was found that in the presence of small modelling inaccuracies, large overshoots or even unstable behaviour was produced.

This is demonstrated through application of the controller to a simple first order model with the following transfer function:

$$TF = \frac{0.12}{6s + 1} e^{-1s} \tag{6.62}$$

Initially, the standard RIDE controller is applied to the plant model. A unit step input is applied to the closed loop system firstly without any time delay and then with a 1 second time delay. It can be seen from Figure 6.6 that the controller becomes unstable when there is a time delay in the plant.

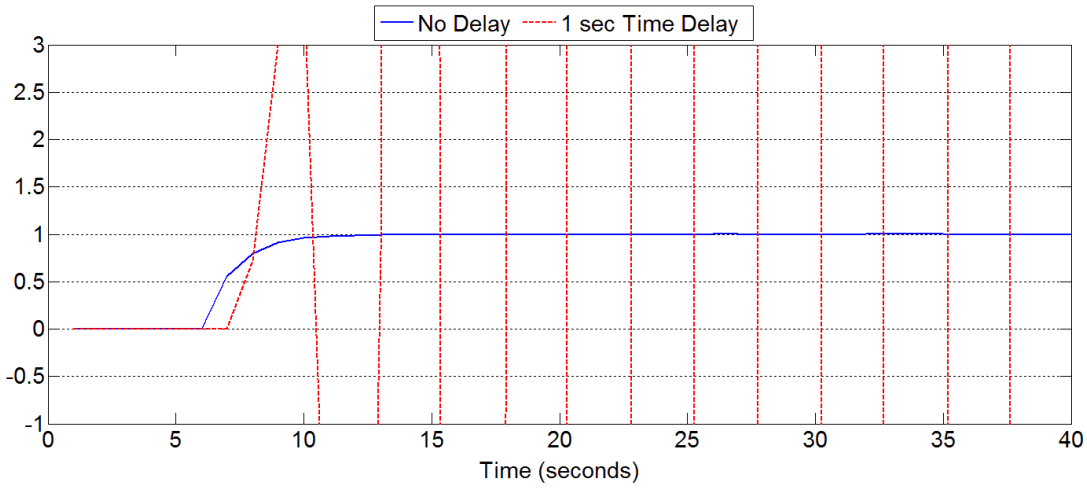

Figure 6.6: RIDE controller response with first order delayed and non-delayed system

Applying the RIDE controller with the SP as shown in Figure 6.4 to the same first order system, the effect of the time delay can be negated and the response stabilised as demonstrated in Figure 6.7. If an error is put in the model used in the SP compensator however, from Figure 6.7 it can be seen that the closed loop system response becomes unstable.

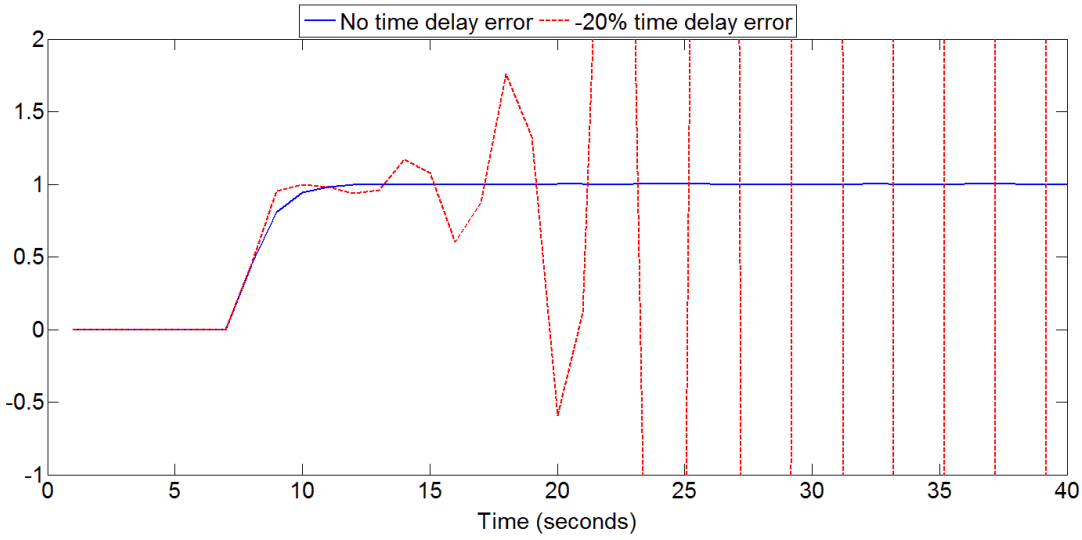

Figure 6.7: RIDE-SP controller response with no time delay error and -20% time delay error

Therefore, a novel time delay compensation method for equivalent control using a modified version of the SP, shown in Figure 6.5, was developed using the concept of correcting the rate of the model used for prediction as opposed to the actual value, as well as the inclusion of a filter for improving robustness to modelling inaccuracies. This novel controller structure will be referred to as SI-RCID.

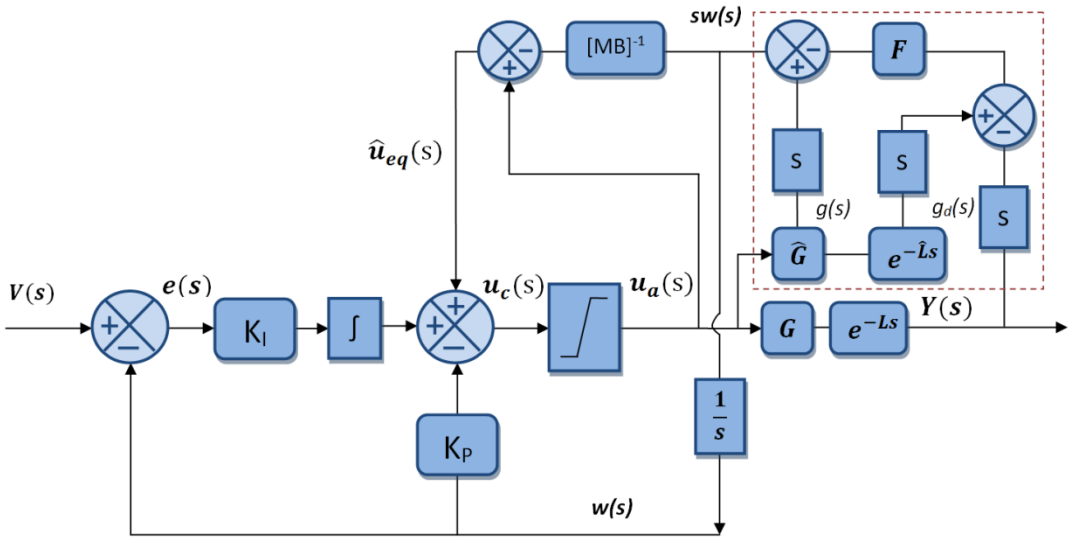

Figure 6.8: Novel SI-RCID controller structure

The corrected rate signal produced by the rate predictor is integrated in order to produce the correct value of output for feedback. The integration initial condition is set as the value of the measured signal at the point when the control action is started.

Figure 6.9 shows the SI-RCID controller applied to the system given in equation 6.62 with a -20% error in the model time delay. It can be seen that the closed loop response is stable and tracks the set point accurately with a very slight overshoot.

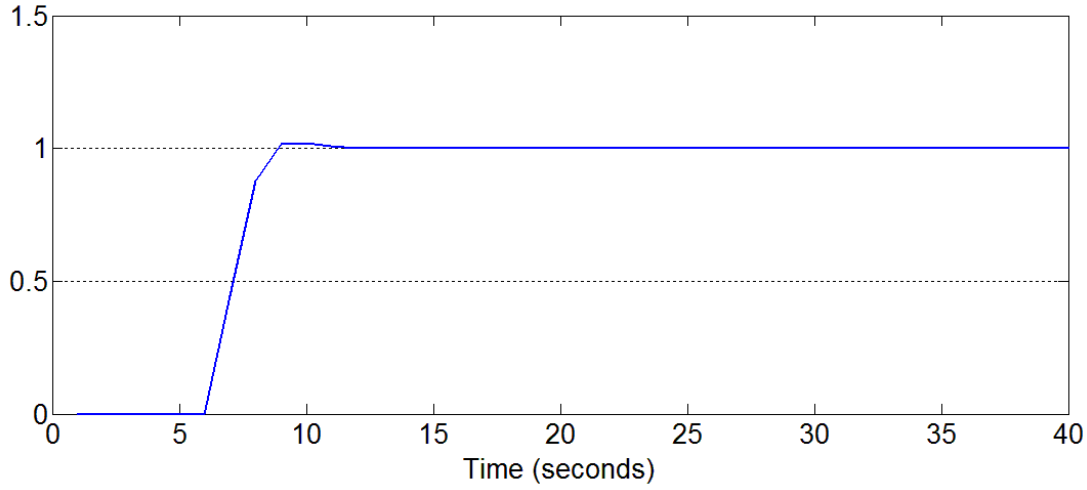

Figure 6.9: SI-RCID unit step response with -20% time delay error

Unfortunately due to a lack of available time in this PhD project, an in depth analysis and design procedure for the filter was not possible and therefore this is an area for future work as explained in chapter 7. In the work presented in this thesis, a first order filter was used and was found to produce good results and an improved robustness to modelling errors including time delay estimation errors as is shown in the case study in Section 6.2.

6.1.6.2 Robustness to Signal Noise

It is important to assess the robustness of the controller design to signal noise as this is an issue which can cause problems in control systems in practice. In order to do this, the SI-RCID controller was applied to the system given in equation 6.62 however with the addition of signal noise. A time delay modelling error of -20% is also included in the model. The signal noise was generated using the Gaussian noise generator in Matlab with a variance of 0.08 and sample time of 0.01. The closed loop response of the system as well as the measured feedback signal is shown in Figure 6.10. It can be seen that control system is unaffected by the signal noise and maintains accurate tracking. This is due to the filter in the feedback loop as well as the fact that the feedback is dominated by the model response as opposed the noisy

system feedback signal. This makes the SI-RCID controller effective in practical situations.

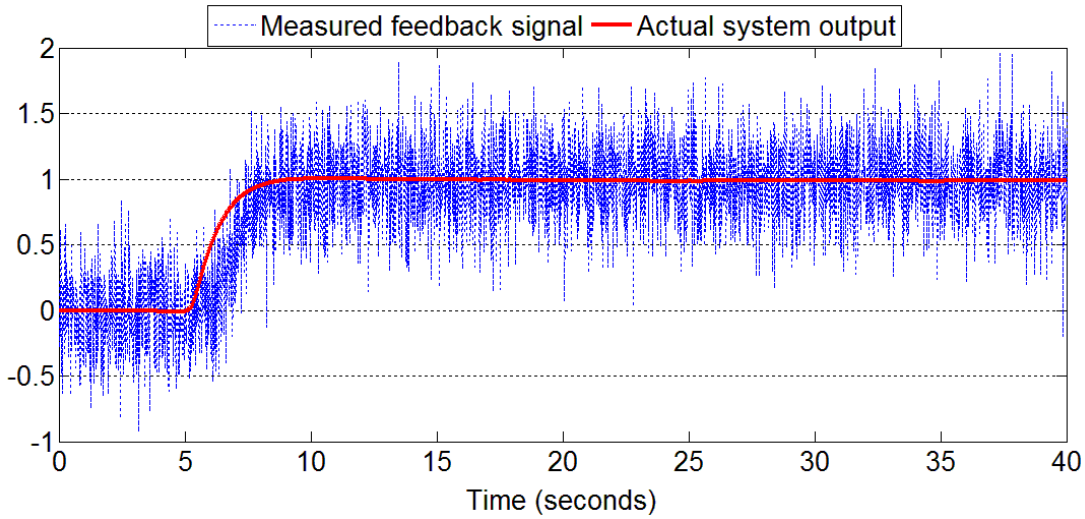

Figure 6.10: SI-RCID robustness to feedback signal noise

6.2 Case Study: Robust SI Based NID Control

This section presents the application of the robust SI based NID control methodology described above to the zone model and AHU described in Chapter 3. Firstly, the procedure of designing the RIDE controller for the HVAC system is demonstrated in order to showcase the difficulties that would be encountered using the conventional design procedure. The proposed SI-RCID controller method is then applied in order to demonstrate the benefits of this method and how it alleviates many of the difficulties encountered whilst also solving problems that cannot be solved using the conventional RIDE controller method. Details of a self-tuning proportional plus integral (ST-PI) control method and a filtered smith predictor (FSP) method which the proposed method is compared with are given. Finally, simulation results demonstrating the performance of all three control methods are presented.

6.2.1 HVAC Controller Design

The building zone model with the full AHU actuation system (Case 2) described in Chapter 3 is used for all controllers in this case study. Full details of the differential equations representing the zone and AHU as well as the building parameter values are given in Chapter 3. There are a number of ways that the differential equations can be represented when developing the control system. These are dependent on the choices of the control system designer on the control strategy e.g. the inputs and outputs of the system and whether a separate control loop (cascade) should be used to control the AHU or should it be single loop structure etc. This will be shown in detail in Section 6.2.1.1 on designing the RIDE control system using the conventional modelling methodology.

In this section, four different controller design processes will be shown; RIDE designed with the conventional method based on the model of the system; the proposed SI-RCID controller method; the ST-PI controller; and the FSP controller. The conventional RIDE design procedure is performed in order to demonstrate the lengthy procedure and difficulties encountered when designing the RIDE controller in this way. The comparison with the ST-PI and FSP controller methods is to demonstrate the performance benefits of the proposed controller over a typical controller currently used in industry and a more advanced method recently developed in the literature.

Before beginning the controller design process, it is important to understand what the control objective is and what the different inputs and outputs to the system are in order to identify the suitable control setups. The control objective in this case study is to regulate the air temperature (T_a) and relative humidity (W_{rel}) of the zone. As explained in chapter three, the AHU provides the inputs to the zone which can be used to control the comfort conditions within it. The AHU supplies air at a certain temperature (T_{sup}) and humidity (W_{sup}) into the zone which consequently affects the temperature and humidity of the air within the zone. The inputs to the AHU which control the conditions of the air that it supplies are the humidification rate of the humidifier (h) and the heat supplied from the heating coil (Q_{coil}). The air supplied to the zone from the AHU is drawn from outside at external conditions and is flowing at

a mass flow rate ($\dot{m}_c$) which can be controlled by the fan in the AHU. Based on the control objective, the overall outputs of the control system are clear i.e. they are T_a and W_{rel}. In order to control these however, T_{sup} and W_{sup} must be regulated. The mass flow rate of the air being supplied to the zone will affect the rate at which the zone comfort conditions are affected by the supply air. Hence a decision must be made as to how the zone air temperature will be heated – the data used for this case study is for a building in the UK during the winter, hence the AHU is used in heating mode. The different options are: T_{sup} can be kept constant and $\dot{m}_c$ varied in order to control the rate of heating – constant temperature-variable volume (CTVV); $\dot{m}_c$ can be kept constant and T_{sup} varied – variable temperature-constant volume (VTCV); or varying both T_{sup} and $\dot{m}_c$ (VTVV). The difficulty of varying T_{sup} is that it can only be varied within a certain temperature range since too hot or cold a temperature will result in uncomfortable conditions for the zone occupants. The same decision must be made regarding regulation of W_{rel}. Regardless of whichever setup is chosen, there are three inputs to the zone, $\dot{m}_c$, T_{sup} and W_{sup}, and there are only two outputs T_a and W_{rel}. In order for the system to be controllable i.e. the MB matrix not degenerate, only one control input can be used to control each output. Therefore, the controller design should be selected carefully in order to deal with this as the difficulty of the control problem varies from one setup to another. The final control setup which was used for all of the results is a two-loop controller design detailed in section 6.2.2.1.

6.2.1.1 AHU Control Setup

There are some aspects of the AHU controller strategy which were designed based on practical considerations and are common to all of the control algorithms tested. These aspects have been designed to improve the performance of the AHU and reduce energy consumption. Firstly, the AHU is used in a variable temperature - variable volume (VT-VV) setup. This means that the mass flow rate and temperature of the supply air are variable. The air temperature however, only varies between three set values, 35˚C, 40˚C and 45˚C, which is a reasonable temperature range for the supply air in heating mode during the winter. This is based on the consideration that having too high or too low a supply temperature will cause discomfort for occupants. The heating power required to heat the zone air dictates the variation of

the supply air temperature i.e. T_{sup} increases with increasing heat demand Q_h as shown in Table 6-1.

Heat Demand (kW)	Supply Air Temperature Set Point (˚C)
0 - 2	35
2 - 5.5	40
5.5+	45

Table 6-1: Variation of AHU supply air temperature set-point

The mass flow rate of the supply air is determined accordingly using the following equation:

$$\dot{m}_c(t) = \frac{Q_h(t)}{C_a\left(T_{sup}(t) - T_a(t)\right)} \tag{6.63}$$

The damper ratio which controls the ratio of outside air to return air in the mixing chamber is also varied based on the heating power required. It is logical that using a larger amount of warm return air will result in warmer air flowing through the AHU which in turn means less heating power is required from the heating coil to increase the supply air temperature. Of course in reality using 100% return air would be hazardous for occupants and would result in unacceptable CO2 levels. Since CO2 is not controlled in this controller setup, the damper ratio is set to use 90% return air for heat demands above 7.5kW and 60% return air for all other heat demands.

6.2.2 RIDE Controller Design

The design procedure that would be used if the control system for the zone and AHU system were to be designed using the conventional design method for RIDE will be considered in this section. Given a set of differential equations which represent the system, like those in chapter three, this process involves rearranging the equations into state space format such that they can be used for the controller design. The state space equations must be arranged based on decisions on what the inputs and outputs of the system should be which will affect the stability and controllability

of the system. Once a suitable setup has been chosen based on these decisions and the equations arranged accordingly, the MB matrix can be determined and the actuator dynamics considered and hence the control system developed.

There are a number of different control arrangements that are possible for this system, however only two setups will be shown in this section: a single loop setup and a two-loop cascade setup. The two-loop cascade control setup is the final design which was used in all of the results however the single loop setup is shown here in order to demonstrate the process for designing the RIDE controller using the conventional approach. As explained in chapter three, there are essentially two systems or processes to be controlled in this case study: the AHU and the zone. It is possible to control these systems with two separate loops i.e. an outer loop controlling the zone and a cascade loop controlling the AHU. It is also possible however to consider both systems as one, and design the control system as one single loop. Let us consider the single control loop setup with the control inputs being $\dot{m}_c$, Q_{coil} and h and the outputs being T_a , T_{sup} and W_a i.e. a three input - three output MIMO controller. This setup can be expected to create a difficult control scenario due to the heavy dependence of both the zone air and the AHU supply air on the mass flow rate through the AHU. This can be corroborated through the design process. The single loop setup would result in all of the AHU equations being included in the main system model and the state space matrices would be expressed as follows:

$$A = \begin{bmatrix} a_{11} & a_{12} & a_{13} & a_{14} & a_{15} & 0 & 0 & 0 & 0 & 0 \\ a_{21} & a_{22} & a_{23} & 0 & 0 & 0 & 0 & 0 & 0 & 0 \\ 0 & a_{32} & a_{33} & 0 & 0 & 0 & 0 & 0 & 0 & 0 \\ a_{41} & 0 & 0 & a_{44} & 0 & 0 & 0 & 0 & 0 & 0 \\ 0 & 0 & 0 & 0 & a_{55} & 0 & 0 & 0 & 0 & 0 \\ 0 & 0 & 0 & 0 & 0 & 0 & 0 & 0 & 0 & 0 \\ 0 & 0 & 0 & 0 & 0 & 0 & a_{77} & 0 & 0 & 0 \\ a_{81} & 0 & 0 & 0 & 0 & 0 & 0 & 0 & 0 & 0 \\ 0 & 0 & 0 & 0 & 0 & 0 & 0 & 0 & 0 & 0 \\ 0 & 0 & 0 & 0 & 0 & 0 & 0 & 0 & 0 & 0 \end{bmatrix} \quad (6.64)$$

$$x(t) = \begin{bmatrix} T_a(t) \\ T_{si}(t) \\ T_{se}(t) \\ T_{ft}(t) \\ T_{sup}(t) \\ T_{duct}(t) \\ T_{co}(t) \\ W_a(t) \\ W_{sup}(t) \\ W_{co}(t) \end{bmatrix} \tag{6.65}$$

$$M = \begin{bmatrix} 1 & 0 & 0 & 0 & 0 & 0 & 0 & 0 & 0 & 0 \\ 0 & 0 & 0 & 0 & 1 & 0 & 0 & 0 & 0 & 0 \\ -0.771 & 0 & 0 & 0 & 0 & 0 & 0 & 5000 & 0 & 0 \end{bmatrix} \tag{6.66}$$

$$B = \begin{bmatrix} b_{11} & 0 & 0 \\ 0 & 0 & 0 \\ 0 & 0 & 0 \\ 0 & 0 & 0 \\ b_{51} & 0 & 0 \\ b_{61} & 0 & 0 \\ b_{71} & 0 & b_{73} \\ b_{81} & 0 & 0 \\ b_{91} & b_{92} & 0 \\ b_{10,1} & 0 & 0 \end{bmatrix} \tag{6.67}$$

$$u(t) = \begin{bmatrix} \dot{m}_c(t) \\ \dot{Q}_{coil}(t) \\ h(t) \end{bmatrix} \tag{6.68}$$

$$w(t) = \begin{bmatrix} T_a(t) \\ T_{sup}(t) \\ W_a(t) \end{bmatrix} \tag{6.69}$$

The coefficients of the A, B and F matrices as well as the disturbance vector d(t) are given in Appendix B. From equations 6.66 and 6.67, the MB matrix would be:

$$MB = \begin{bmatrix} b_{11} & 0 & 0 \\ b_{51} & 0 & 0 \\ -0.771b_{11} + 5000b_{81} & 0 & 0 \end{bmatrix} \tag{6.70}$$

With this single loop setup, it can be seen that the MB matrix is rank defective and hence the controller cannot be designed. In order to solve this problem, model order reduction must be performed by considering $T_{duct}(t)$, $T_{co}(t)$, $W_{sup}(t)$ and $W_{co}(t)$ to be steady state i.e.:

$$\dot{T}_{duct}(t) = \dot{T}_{co}(t) = \dot{W}_{sup}(t) = \dot{W}_{co}(t) = 0 \tag{6.71}$$

The steady state equations can then be substituted into the remaining equations. This process results in the model becoming sixth order and $\dot{T}_{sup}(t)$ and $\dot{W}_a(t)$ being expressed as:

$$\frac{dT_{sup}(t)}{dt} = \frac{\dot{m}_c(t)C_a}{C_h\rho_a}\left[\frac{\dot{Q}_{coil}(t) + (UA_{ah} + \dot{m}_o(t)C_a)T_o(t) + \dot{m}_r(t)C_aT_a(t)}{\dot{m}_c(t)C_a + UA_{ah}}\right] - \frac{\dot{m}_c(t)C_a}{C_h\rho_a}T_{sup}(t) + \alpha_h\left(T_o(t) - T_{sup}(t)\right) \tag{6.72}$$

$$\frac{dW_a(t)}{dt} = \frac{\dot{m}_c(t)}{M_a}\left[\left(\dot{m}_r(t)W_a(t) + \dot{m}_o(t)W_o(t) + h(t)\right) - W_a(t)\right] + \frac{P(t)}{M_a} - \frac{\dot{m}_{nv}(t)}{M_a}\left(W_a(t) - W_o(t)\right) \tag{6.73}$$

The MB matrix then becomes:

$$MB = \begin{bmatrix} b_{11} & 0 & 0 \\ {b_{51}}^* & {b_{52}}^* & 0 \\ -0.771b_{11} + 5000{b_{61}}^* & 0 & 5000{b_{63}}^* \end{bmatrix} \tag{6.74}$$

Where b_{11} is the same as before, however the coefficients with the star (*) superscript are altered due to the model order reduction. Some of the coefficients of the A matrix are also altered by the model order reduction. The altered matrix coefficients are given in Appendix B. It can be seen from the coefficients of the MB matrix that the control problem is complex as there is cross-coupling between the channels and it is nonlinear. The dependence of the supply air on $\dot{m}_c$ means that when $\dot{m}_c$ decreases, the heating power required (Q_{coil}) will have to increase

substantially in order to heat the zone and supply air. Therefore, this control setup is unnecessarily overcomplicated.

6.2.2.1 Two Loop Controller Design

As mentioned earlier, the systems in this case study can be considered as two systems and a two loop (cascade) controller design can be used to control them. Using a cascade controller design would make for a simpler control problem as will be shown. This section presents a novel controller setup with a RIDE controller on the outer loop controlling the zone air temperature and humidity and a RIDE controller on the inner loop controlling the supply air temperature from the AHU. Let us first consider the outer loop controller. The outputs for this loop are T_a and W_{rel}. The inputs are selected as h(t) for controlling W_a and Q_h for controlling T_a. Using Q_h to control T_a instead of $\dot{m}_c$ simplifies the equations since using $\dot{m}_c$ means that many terms are included in the B matrix which make it highly nonlinear. Therefore the state space matrices, excluding the disturbance matrix, for the outer loop after the necessary model order reductions are represented as follows:

$$\begin{bmatrix} \dot{T_a}(t) \\ \dot{T_{si}}(t) \\ \dot{T_{se}}(t) \\ \dot{T_{ft}}(t) \\ \dot{W_a}(t) \end{bmatrix} = \begin{bmatrix} a_{11} & a_{12} & 0 & a_{14} & 0 \\ a_{21} & a_{22} & a_{23} & 0 & 0 \\ 0 & a_{32} & a_{33} & 0 & 0 \\ a_{41} & 0 & 0 & a_{44} & 0 \\ 0 & 0 & 0 & 0 & a_{55} \end{bmatrix} \begin{bmatrix} T_a(t) \\ T_{si}(t) \\ T_{se}(t) \\ T_{ft}(t) \\ W_a(t) \end{bmatrix} + \begin{bmatrix} b_{11} & 0 \\ 0 & 0 \\ 0 & 0 \\ 0 & 0 \\ 0 & b_{52} \end{bmatrix} \begin{bmatrix} \dot{Q}_H(t) \\ h(t) \end{bmatrix} \tag{6.75}$$

$$\begin{bmatrix} T_a(t) \\ W_{rel}(t) \end{bmatrix} = \begin{bmatrix} 1 & 0 & 0 & 0 & 0 \\ -0.771 & 0 & 0 & 0 & 5000 \end{bmatrix} \begin{bmatrix} T_a(t) \\ T_{si}(t) \\ T_{se}(t) \\ T_{ft}(t) \\ W_a(t) \end{bmatrix} \tag{6.76}$$

The MB matrix for the outer loop controller is shown below:

$$MB^o = \begin{bmatrix} b_{11} & 0 \\ -0.771 b_{11} & 5000 b_{52} \end{bmatrix} \tag{6.77}$$

The coefficients for all of the matrices above are given in Appendix C. While the MB matrix is still nonlinear, by using Q_h to control T_a, the MB matrix is less

complex than when using a single loop design. This MB matrix can then be used in the u_{eq} calculation and the gains. The proportional and integral gains are given below:

$$K_I{}^o = \begin{bmatrix} b_{11} & 0 \\ -0.771b_{11} & 5000b_{52} \end{bmatrix}^{-1} \begin{bmatrix} \omega^2 & 0 \\ 0 & \omega^2 \end{bmatrix} \tag{6.78}$$

$$K_P{}^o = \begin{bmatrix} b_{11} & 0 \\ -0.771b_{11} & 5000b_{52} \end{bmatrix}^{-1} \begin{bmatrix} 2\upsilon\omega & 0 \\ 0 & 2\upsilon\omega \end{bmatrix} \tag{6.79}$$

The natural frequency of all channels should be set as three times slower than the actuator bandwidth as explained in section 6.1.5. The natural frequency of the T_a channel of the outer loop controller must be at least three times slower than the natural frequency of the inner loop controller thus the inner loop controller must be designed first.

The inner loop controller is a SISO system represented by equation 6.72 where Q_{coil} is used to control T_{sup}. MB for the inner loop is:

$$MB^i = \frac{\dot{m}_c(t)C_a}{C_h\rho_a(\dot{m}_c(t)C_a + UA_{ah})} \tag{6.80}$$

Thus, the inner loop control problem is also nonlinear. The RIDE controller can be designed for this loop with the gains specified as follows:

$$K_P = [MB^i]^{-1}2\upsilon\omega \tag{6.81}$$

$$K_I = [MB^i]^{-1}\omega^2 \tag{6.82}$$

The bandwidths of all of the actuation systems in the AHU used in this case study are given in chapter 3. The values of natural frequency and damping ratio defining the gains for both the inner and outer loops are given below in Table 6-2.

Control Channel	υ	ω (rad/s)
T_a	1.5	0.0073
W_{rel}	1.5	0.03
T_{sup}	1.5	0.022

Table 6-2: Natural frequency and damping ratio for SI-RCID controller

6.2.2.2 RIDE Controller Tests

Simulation results showing the performance of the cascade RIDE controller design described above are shown in this section. The performance of the controller is shown over a two day period with control starting at 7am and ending at 7pm on both days. The zone air temperature and relative humidity set points are 21˚C and 50% respectively. It was necessary to use the new commutation law detailed in section 6.1.4 with the RIDE controller since using the original commutation law resulted in the inner loop controller being stuck on the lower limit and not producing any heat throughout the day. Initially, the RIDE controller is tested without any time delay in the outer loop. The supply air temperature from the AHU however has an inherent time delay in its dynamics due to the long ducting between the heating source and the outlet. Therefore the inner loop controller was not tested without time delay. Figure 6.11 shows the outer loop controller tracking the zone air temperature set point of 21°C.

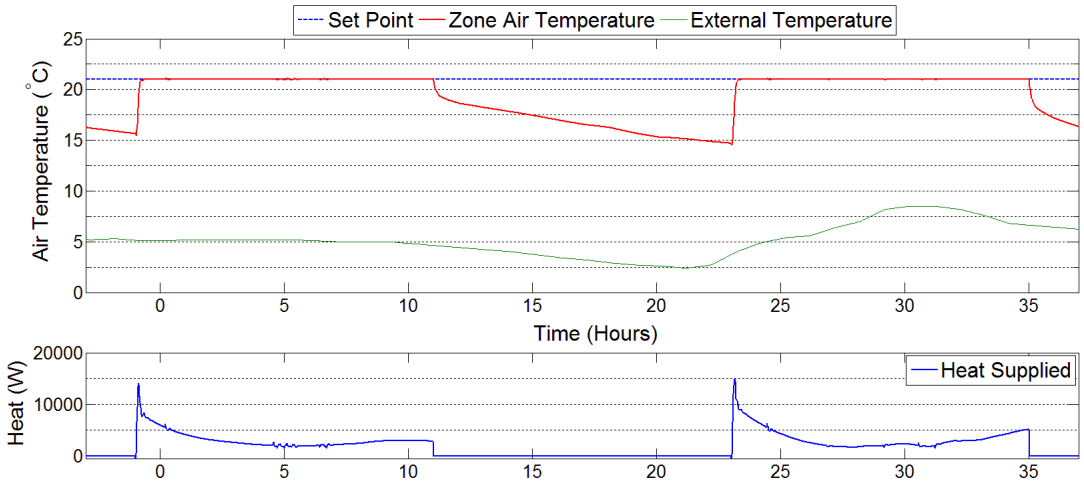

Figure 6.11: Zone air temperature with heat supplied to zone from AHU (RIDE control)

Excellent tracking of the zone temperature set point was achieved and the rise time for the system is approximately 5 minutes as defined by the controller gains in Table 6-2. Figure 6.12 shows the corresponding supply air temperature from the AHU controlled by the inner loop controller. The supply temperature set point is at the highest level of 45˚C at the initial part of both days as expected. The set point then varies throughout the day according to the heat demand from the outer loop controller. The inner loop controller is able to maintain accurate tracking of the set point, however there is an initial large overshoot of approximately 4˚C followed by oscillations. These oscillations are caused by the time delay as explained earlier. The controller responds well to set point changes albeit a slight overshoot can be observed as well as some oscillations on the first day at approximately 5hrs on Figure 6.12. The heat supplied by the AHU as shown on Figure 6.11 is smooth due to the mass flow rate, shown in Figure 6.14, varying according to the supply temperature set point in order to match the heat demanded by the outer loop controller. Hence, the tracking of air temperature by the outer loop controller is not affected by the oscillations observed in the supply air temperature. The variation of mass flow rate does however affect the heat transfer rate from the heating coil to the supply air. Therefore, the mass flow rate acts as a disturbance to the inner loop controller. The inner loop controller however rejects this disturbance effectively and maintains accurate tracking of the set point.

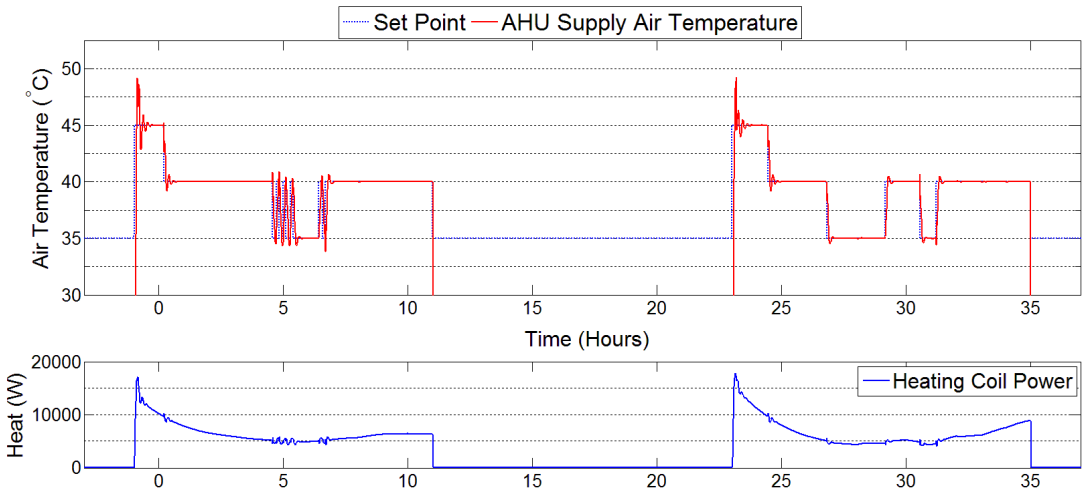

Figure 6.12: AHU supply air temperature with heating coil power (RIDE Control)

Figure 6.13 shows that the outer loop controller is also able to track the zone relative humidity set point accurately. The humidifier initially reaches its maximum humidification rate for a short period in order to bring the zone relative humidity to the set point. It then comes off the limit and maintains the zone relative humidity at the desired set point throughout the day on both days. Again, the mass flow rate acts as a disturbance to the humidification loop since the rate of mass transfer, i.e. humidification, between the supply air and the zone air is dependent on the mass flow rate of the supply air. The outer loop controller rejects this disturbance again showcasing the efficacy of the RIDE control algorithm with regards to disturbance rejection.

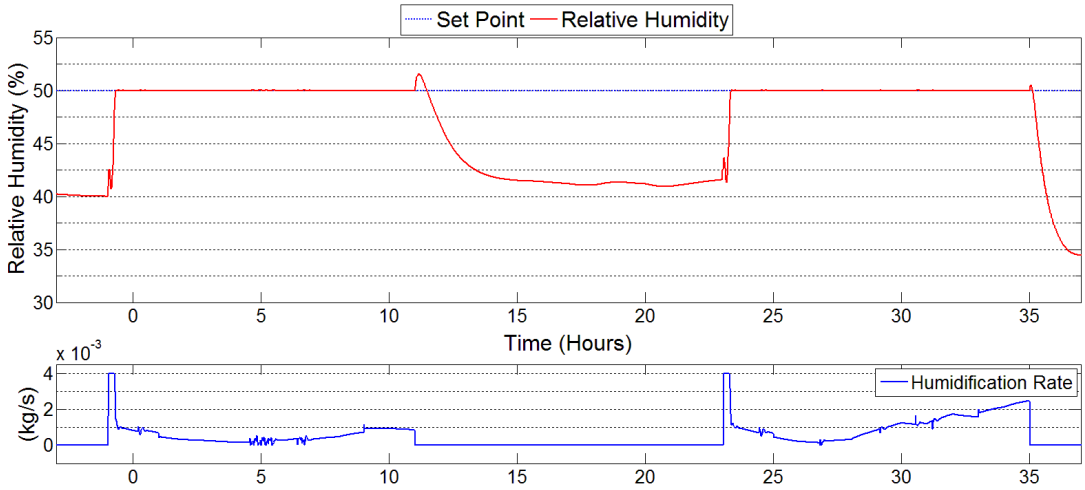

Figure 6.13: Zone relative humidity with humidification rate (RIDE control)

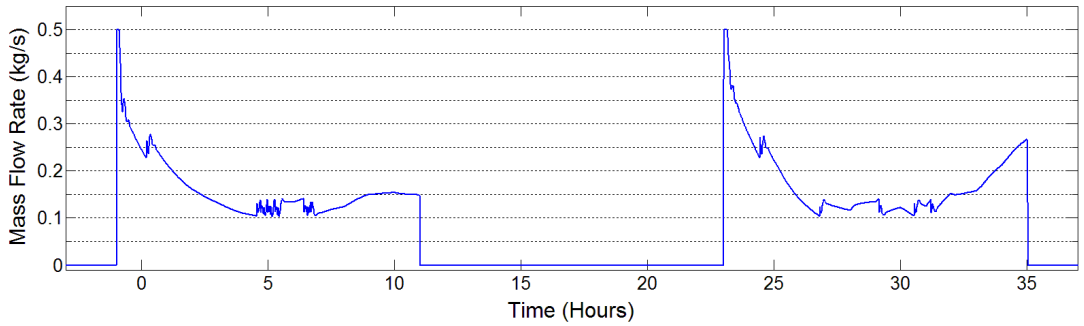

Figure 6.14: AHU supply air mass flow rate (RIDE control)

In reality, a delay normally exists in the zone dynamics between the moment when an input is applied to the zone and the moment the sensor recognises this input. This period is dependent on sensor placement and the size of the zone. In order to

simulate the effect that a time delay can have on the RIDE controller, a 5 minute time delay signifying transport lag for both the temperature and humidity sensors is introduced in both channels of the outer loop. Figure 6.15-Figure 6.18 show that the large time delay has a severe adverse effect on the controller performance. Large oscillations in both the zone air temperature and relative humidity can be observed. These oscillations in turn cause large oscillations in the inner loop controller also.

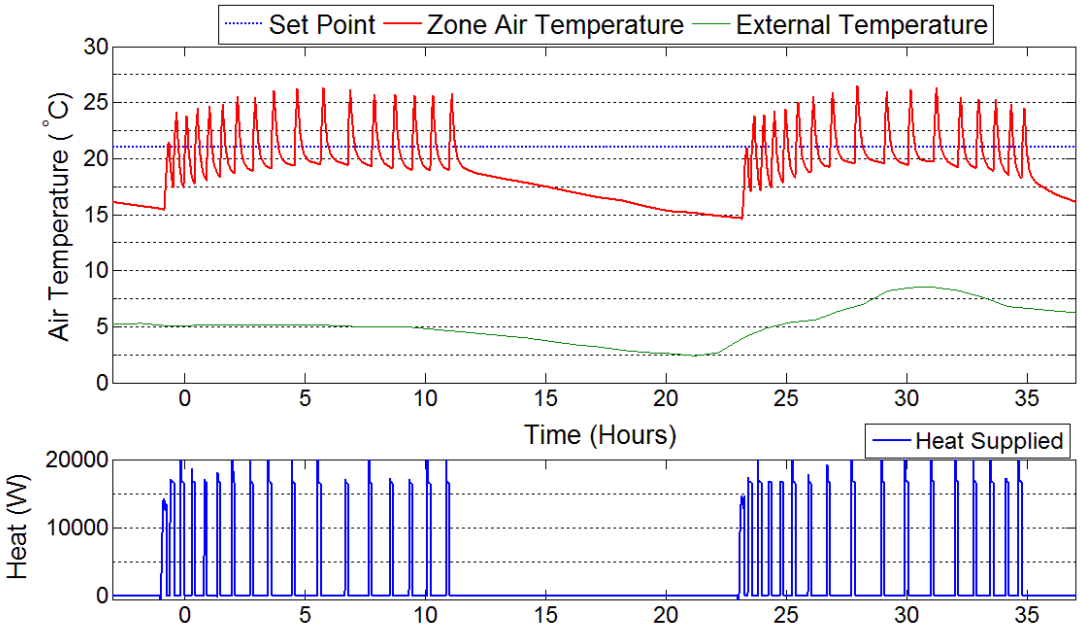

Figure 6.15: Zone air temperature with heat supplied to zone from AHU (RIDE control with time delay)

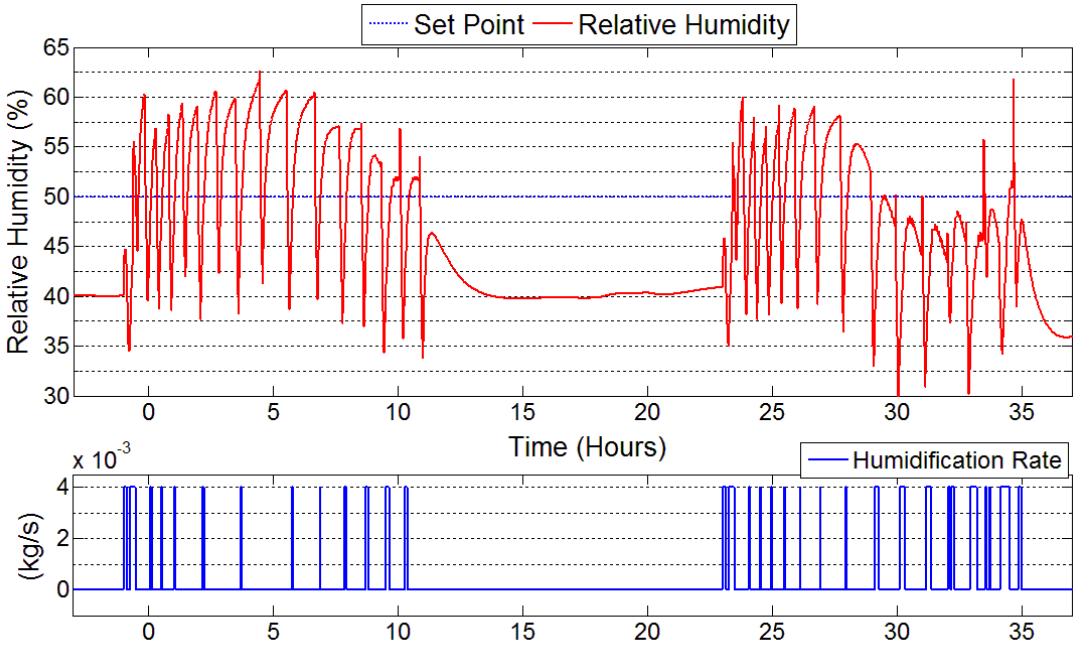

Figure 6.16: Zone relative humidity with humidification rate (RIDE control with time delay)

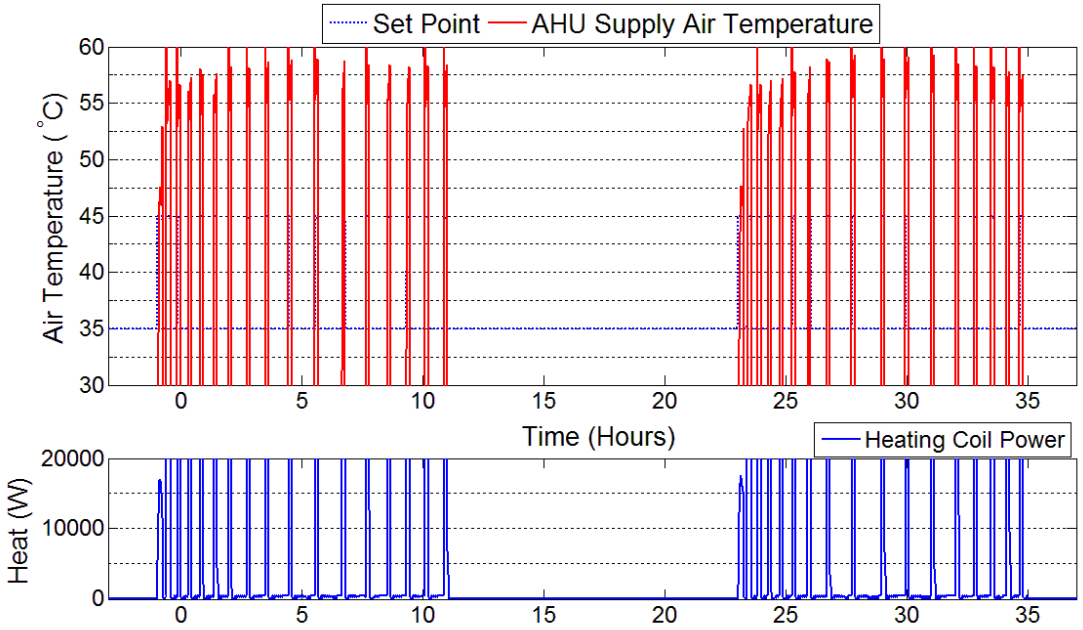

Figure 6.17: AHU supply air temperature with heating coil power (RIDE Control with time delay)

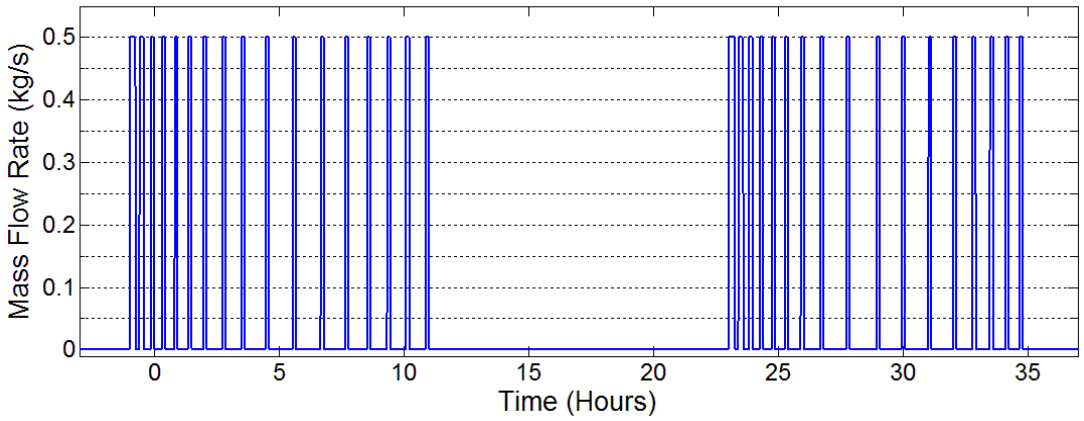

Figure 6.18: AHU supply air mass flow rate (RIDE control with time delay)

The cascade RIDE controller is shown to be an effective and high performance control strategy which is able to deal with the nonlinearity in both the zone and AHU. It also displays good disturbance rejection ability. Thus it is able to attain fast and accurate set point tracking for both the zone comfort conditions and AHU supply air. It is shown however, that a large time delay has a severe adverse effect on the performance of the controller which is unacceptable.

With regards to the design procedure, the conventional controller design process is clearly a lengthy and complicated procedure which would most likely lead to it not being adopted in the buildings industry. Therefore, despite its high performance, this strategy is flawed in the same way that a large number of advanced HVAC control strategies found in the literature are.

6.2.3 SI-RCID Controller Design

This section presents the application of the SI-RCID controller method described above. Using this controller design methodology described, the controller design process is greatly simplified. The controller design process is as follows:

1. Select controller setup
2. Assess stability from step response
3. Identify MB and dead time using robust SI method
4. Calculate controller parameters accordingly
5. Assess closed loop step response to check gains etc. and adjust if necessary

Firstly, the inputs and outputs (controller setup) must be selected as before, which is a necessary step in any controller design. The same two loop controller setup described in section 6.2.2.1 is used in all controller designs tested in this case study. With the SI-RCID controller methodology described in section 6.1, there is no need to rearrange any equations or perform model order reduction as was necessary in the conventional RIDE methodology. The stability of the system can be checked by observing the step responses of both the inner and outer loops. The response of the inner loop to a step input of 1.5kW from the heating coil and a constant supply air mass flow rate of 0.35kg/s is shown in Figure 6.19.

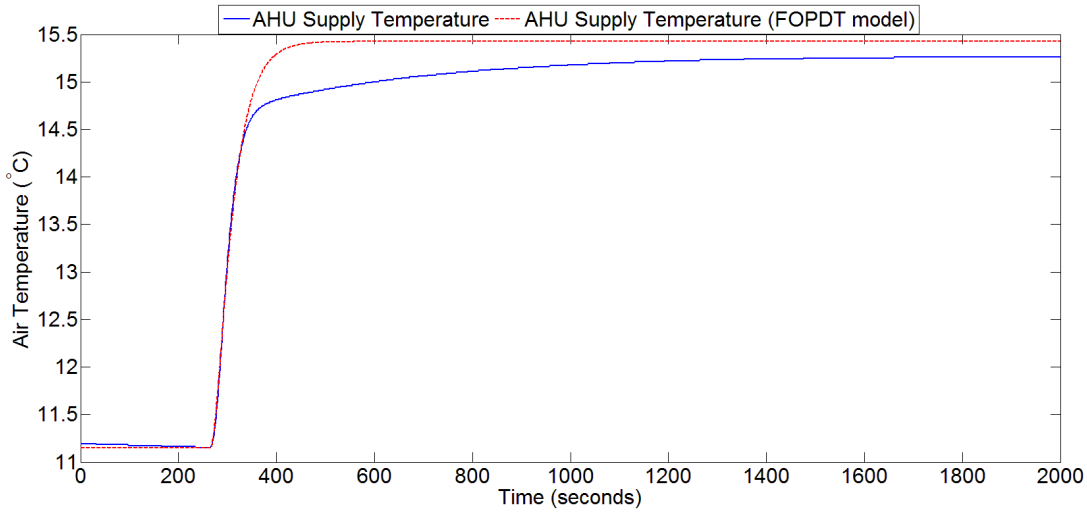

Figure 6.19: AHU supply air temperature step response

The system can be seen to show no non-minimum phase characteristics so the open loop transmission zeros can be considered stable for both the inner and outer loops. Based on this step response data, the system can be identified using the simple method given in equations 6.45-6.47. The identified FOPDT model describing the behaviour of the inner loop is:

$$TF_{Tsup/Qcoil} = \frac{0.00285}{33s+1}e^{-3s} \qquad (6.83)$$

The response of the FOPDT model, shown in Figure 6.19, can be seen to be similar to the actual system however a steady state error of approximately 0.2˚C exists. It follows then from equations 6.28 and 6.29 that MB is calculated as follows:

$$MB = \frac{0.00285}{33} = 0.0000864 \qquad (6.84)$$

6.2.3.1 Outer loop

The same process must be performed using the MIMO system identification method described in section 6.1.1 to design the outer loop controller. The same 5 minute time delay introduced in section 6.2.2.2 is included the outer loop dynamics. Firstly, the dynamics associated with the heat input Q_h from the AHU are identified. This entails applying a step input of heat whilst keeping the humidification input at zero. Figure 6.20 and Figure 6.21 show the response of the zone air temperature and relative humidity to a step heat input of 4kW respectively.

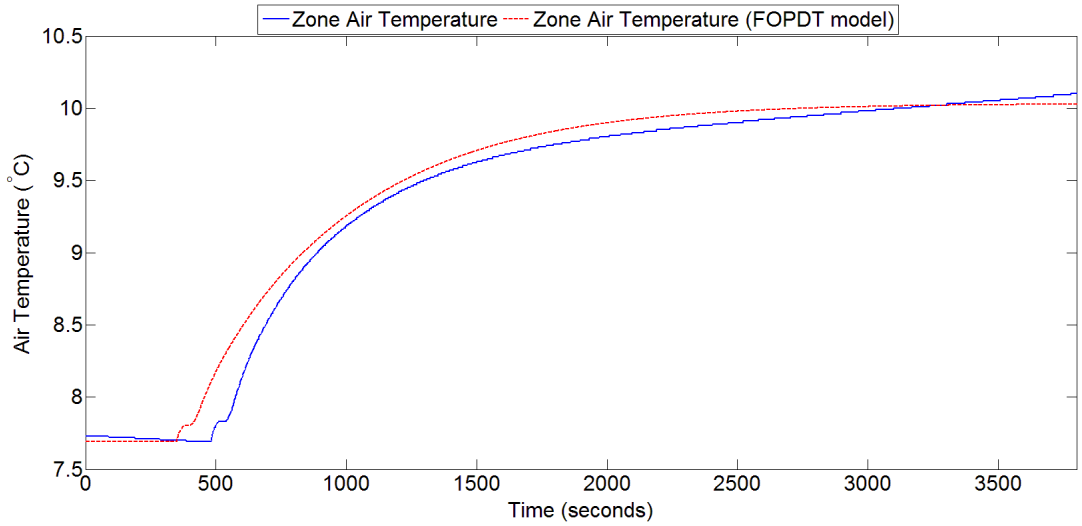

Figure 6.20: Zone air temperature response to step heat input (Q_h)

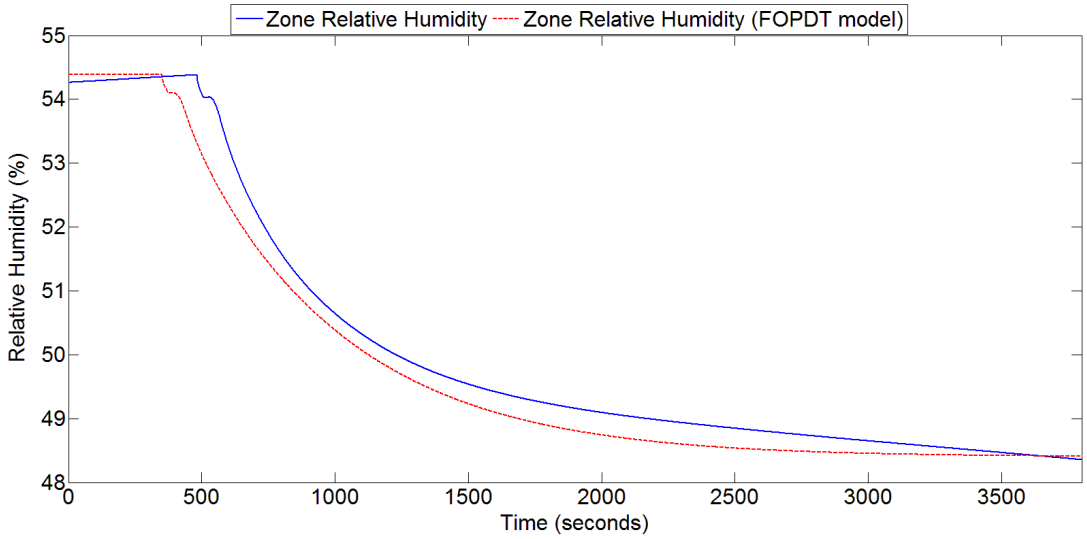

Figure 6.21: Zone relative humidity response to step heat input (Q_h)

It can be seen that in both cases there is no sign of non-minimum phase behaviour and so the open loop transmission zeros can be considered to be stable. The FOPDT models derived from this data describing the response of T_a and W_{rel} to the heat input Q_h are given below:

$$TF_{Ta/Qh} = \frac{0.000587}{543s + 1} e^{-287s} \tag{6.85}$$

$$TF_{Wrel/Qh} = \frac{-0.0015}{543s + 1} e^{-287s} \tag{6.86}$$

The simple identification method used results in an underestimation of the dead time of 13 seconds. Section 6.2.6.1 will show tests on the robustness of the controller to delay estimation errors. From Figure 6.20 and Figure 6.21, it can be seen that the FOPDT models have similar differences to the actual system behaviour. The identified models show a slightly faster response and steady state errors exists initially, however the actual system continues to increase (or decrease in the case of relative humidity) never quite reaching steady state. This however is most likely cause by disturbances such as the external temperature. The modelling errors that exist will serve as a test to the robustness of the controller to modelling errors. This is a necessary test since modelling errors always exist in reality. From equations 6.37-6.40 the first column of the MB matrix can be determined as follows:

$$MB_{11} = \frac{0.000587}{543} = 1.082\text{x}10^{-6} \quad (6.87)$$

$$MB_{21} = \frac{-0.0015}{543} = -2.762\text{x}10^{-6} \quad (6.88)$$

The remaining parameters of the MB matrix must then be determined by applying a step humidification input whilst keeping the heat input at zero. Figure 6.22 shows the response of W_{rel} to a step humidification input of 0.002kg/s with a constant supply air mass flow rate of 0.35kg/s.

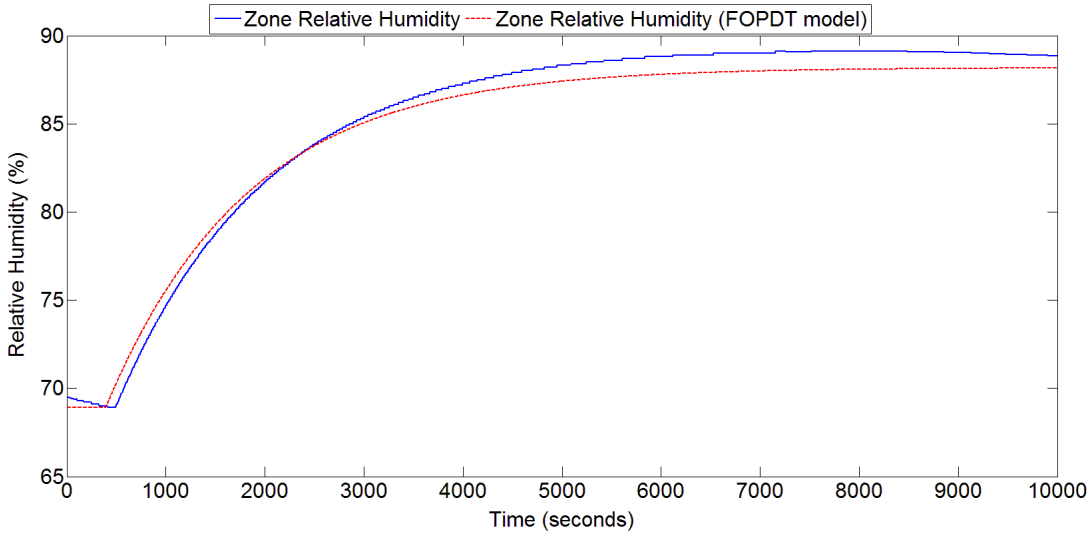

Figure 6.22: Zone relative humidity response to step humidification input

The humidifier does not have any effect on T_a and therefore the associated parameter in the MB matrix (MB_{12}) is equal to zero. From the data in Figure 6.22, the FOPDT model describing the relation of W_{rel} to the humidification rate (h) is derived as:

$$TF_{Wrel/h} = \frac{9641.5}{1435s + 1} e^{-321s} \quad (6.89)$$

Again, an error exists in the dead time estimation however this time it is an overestimation of 21 seconds. The logical choice of dead time for the relative humidity channel would be the shorter dead time. The response of the identified FOPDT model is shown in Figure 6.22. In section 6.2.6.1 however, the robustness of the controller to under and overestimation of the dead time will be tested. The

parameter of the MB matrix associated with the humidifier input (h) is determined as follows:

$$MB_{22} = \frac{9641.5}{1435} = 6.72 \tag{6.90}$$

The overall MB matrix for the outer loop is:

$$MB^o = \begin{bmatrix} 1.082\text{x}10^{-6} & 0 \\ -2.762\text{x}10^{-6} & 6.72 \end{bmatrix} \tag{6.91}$$

The closed loop bandwidth and natural frequency for the inner and outer loop controllers can then be selected in the same way as described in section 6.2.1.2 for the conventional RIDE controller i.e. the bandwidth can be set as 3 times slower than the actuator bandwidth and the damping ratio can be selected to give an over-damped response. Therefore, the natural frequency and damping ratio used in the inner loop controller for this case study are the same as in Table 6-2.

6.2.3.2 FRP filter design

For time delay compensation, the SI-RCID controller structure shown in Figure 6.6 is used. This requires the use of a model for prediction of the rate of change of the system output. The FOPDT models given in equations 6.85, 6.86 and 6.89 are used in this case. However, since the relative humidity channel is affected by both inputs, the overall model describing its behaviour is:

$$TF_{Wrel} = \frac{9641.5}{1435s + 1} e^{-287s} - \frac{0.0015}{543s + 1} e^{-287s} \tag{6.92}$$

Note, for simplicity, the same dead time is used for both parts of the model. As mentioned earlier, the robustness of the controller to different dead time errors will be tested in section 6.2.6.1. The prediction filters for both channels must also be designed. Based on testing for this case study, the use of first order prediction filters was found to be sufficient and produces good results. A crude rule the author has found for selecting the time constants of the filters which was found to produce tenable results for this case study is given below:

$$\tau_F = \frac{L}{2} \tag{6.93}$$

Where τ_F is the time constant of the prediction filter. This design however has not been verified with a robustness or stability analysis and therefore it is by no means a final or ideal design and requires further work as highlighted in section 7.4.2. Based on the design rule in equation 6.93, the prediction filters for the zone air temperature and relative humidity channels are given below:

$$F_{Ta} = F_{Wrel} = \frac{1}{143s + 1} \tag{6.94}$$

It can be seen from the controller design process that it is a straightforward and easy process for designing a high performance control system. The design process is greatly simplified in comparison to the conventional RIDE controller design procedure. All of the parameters of the controller are designed based on rules which could be calculated automatically and so it involves a similar level of user input as the commonly used self-tuning PI controllers. Thus, this is a strategy which could be used in the buildings industry due to its ease of implementation as well as the fact that it is not computationally expensive.

6.2.4 Self-Tuning PI Controller Design

It is well-known that the ST-PI controller design is very commonly used in industrial control systems. Therefore, this section details the design of a ST-PI controller for this case study. The same two loop controller structure is used however two separate SISO controllers are designed for controlling the two channels in the outer loop. The PI controller structure is given in equation 6.95:

$$u_c(s) = K_P \left(1 + \frac{1}{T_I s}\right) e(s) \tag{6.95}$$

The tuning rules from (Skogestad 2003) are used to design the PI controllers. These are shown below:

$$K_P = \frac{1}{k'}\frac{1}{\tau_{cl} + L} \tag{6.96}$$

Where:

$$k' = \frac{K}{T_c} \tag{6.97}$$

$$T_I = min\{T_c, 4(\tau_{cl} + L)\} \tag{6.98}$$

Where τ_{cl} is the closed loop time constant. Based on the FOPDT models of the inner and outer loop dynamics in equations 6.83, 6.85 and 6.89, the controller gains were calculated using the tuning rules above. The close loop time constants were selected to be the same as those specified in the SI-RCID controller gains. The resulting gains for the PI controller are given in Table 6-3.

Control Channel	K_p	T_I (seconds)	τ_{cl} (seconds)
T_a	1722	543	250
W_{rel}	0.000429	1388	60
T_{sup}	137.8	33	81

Table 6-3: ST-PI controller gains

This ST-PI controller serves as a good representation of a typical controller used in the buildings industry as many industrial PI controllers are tuned using the methodology described in this section i.e. using an identified FOPDT with known tuning rules.

6.2.5 FSP Controller Design

This section shows the application of the FSP controller design described in section 6.1.6. The FSP controller has different design procedures based on the type of system being controlled (Normey-Rico and Camacho 2009). Since the behaviour of the systems considered in this case study are simplified for controller design purposes using stable FOPDT models, the FSP tuning procedure provided for this type of system is used here (Normey-Rico and Camacho 2009).

The first step of the tuning procedure is to design the base controller (C in Figure 6.2) as a PI controller using the following rules:

$$K_P = \frac{T_c}{T_r K} \tag{6.99}$$

$$T_I = T_c \tag{6.100}$$

Where T_r defines the closed loop pole (Normey-Rico and Camacho 2009). The filter F_r is then designed based on the following equations:

$$F_r = \frac{(1 + sT_r)(1 + s\beta)}{(1 + sT_o)^2} \tag{6.101}$$

$$\beta = T_c \left[1 - \left(1 - \frac{T_o}{T_c}\right)^2 e^{-\frac{L}{T_c}}\right] \tag{6.102}$$

There are two tuning parameters, T_r and T_o, which must be selected to obtain the best trade-off between robustness and performance. T_r defines the speed of response of the closed loop system and T_o affects the robustness. Normey-Rico and Camacho (2009) state that T_o can be increased arbitrarily in order to increase the system robustness if the system is open loop stable, which is true for the systems in this case study. Based on the FOPDT models in equations 6.83, 6.85 and 6.89, the calculated base PI controller gains as well as the closed loop and disturbance rejection time constants for the inner and outer loops are given in Table 6-4. The disturbance rejection time constant for the W_{rel} channel had to be increased significantly in order to prevent a highly oscillatory response.

Control Channel	K_p	T_I **(seconds)**	T_r **(seconds)**	T_o **(seconds)**
T_a	3700	543	250	200
W_{rel}	0.00248	1435	60	600
T_{sup}	142.95	33	81	100

Table 6-4: Base PI controller gains and time constants for FSP controller

The filters for the T_a, W_{rel} and T_{sup} control channels are given below:

$$F_r^{Ta} = \frac{(1+250s)(1+415.3s)}{(1+200s)^2} \tag{6.103}$$

$$F_r^{Wrel} = \frac{(1+60s)(1+1037s)}{(1+600s)^2} \tag{6.104}$$

$$F_r^{Tsup} = \frac{(1+81s)(1-91.2s)}{(1+100s)^2} \tag{6.105}$$

The FSP controller design provides an example of a more advanced method recently presented in the literature which is specifically designed to control time delay systems. Despite this method requiring more time and effort to tune than the ST-PI and proposed SI-RCID methods, it is still relatively simple to tune and is therefore a representation of an advanced method recently developed in the literature which could be used in industry as an alternative to simple PI controllers.

6.2.6 Simulation Results

In this section, simulation results showing the performance of the proposed two-loop SI-RCID controller design compared with the ST-PI and FSP controller designs are presented. All three controller designs are applied to the zone and AHU model described in chapter 3-case 2 with the inclusion of a 5 min time delay in the measurement of both the zone air temperature and relative humidity signifying transport lag in the system. All controllers were applied with their respective controller parameters stated in sections 6.2.3-6.2.5. In each case, the controllers were designed based on the identified dead time in the outer loop of 287 seconds i.e. an underestimation error of 13 seconds. The performance of the controllers is shown over a two day period with control starting at 7am and ending at 7pm on both days. The zone air temperature and relative humidity set points are 21˚C and 50% respectively.

The original gains for the supply and zone air temperature loops of the FSP and ST-PI controllers given in Table 6-3 and Table 6-4, which were obtained using the design procedures described by their respective authors, were too low resulting in the

air temperatures being significantly lower than the desired set point. Therefore, for both controller designs, the proportional and integral gains for the supply and zone air temperature loops were increased by a factor of 5 in order for them to achieve a reasonable response. This was the maximum amount the gains could be increased by before the controllers became highly oscillatory. This process took time and of course, in practice, is undesirable. Figure 6.23-Figure 6.25 show the performance of the three controller designs in tracking the zone air temperature set point of 21°C.

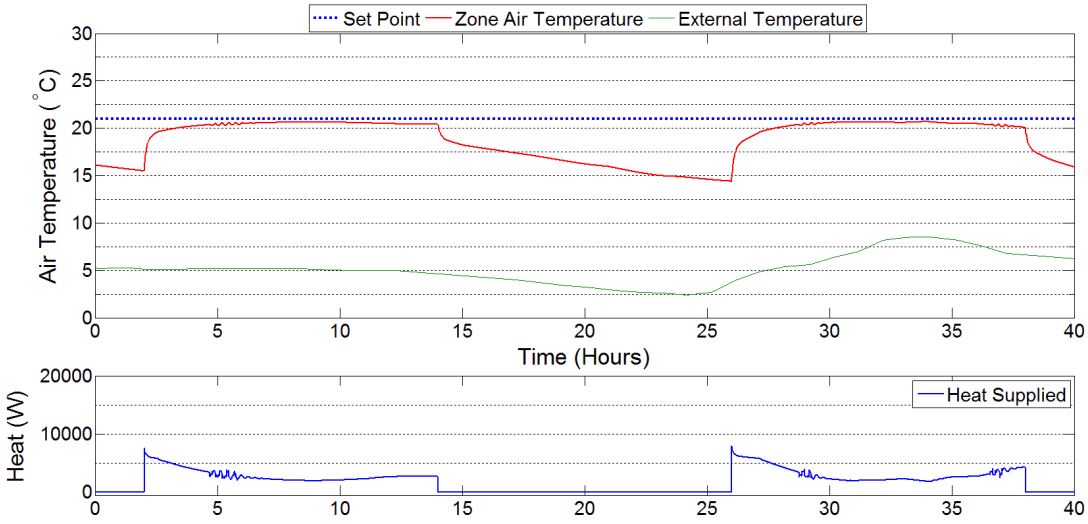

Figure 6.23: Zone air temperature response with ST-PI controller

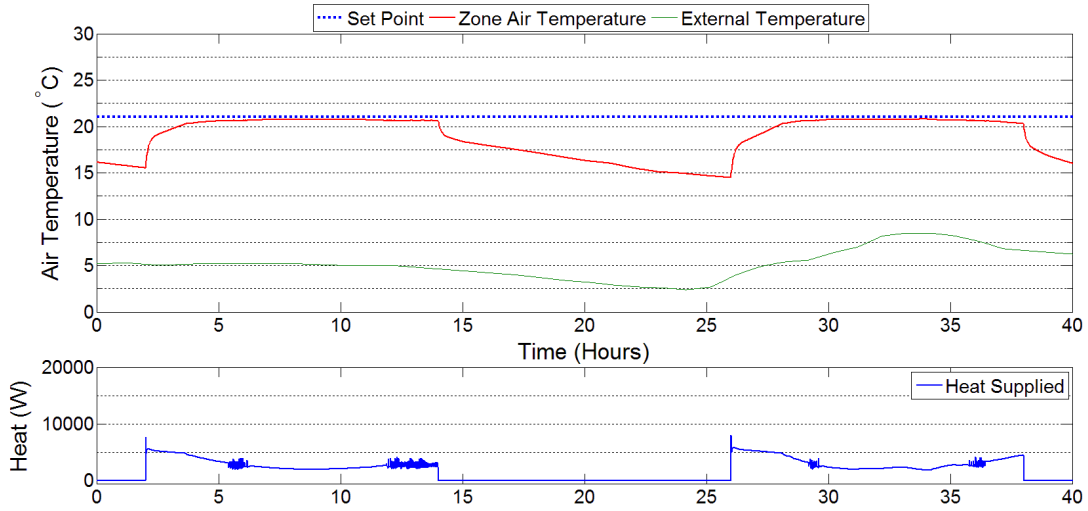

Figure 6.24: Zone air temperature response with FSP controller

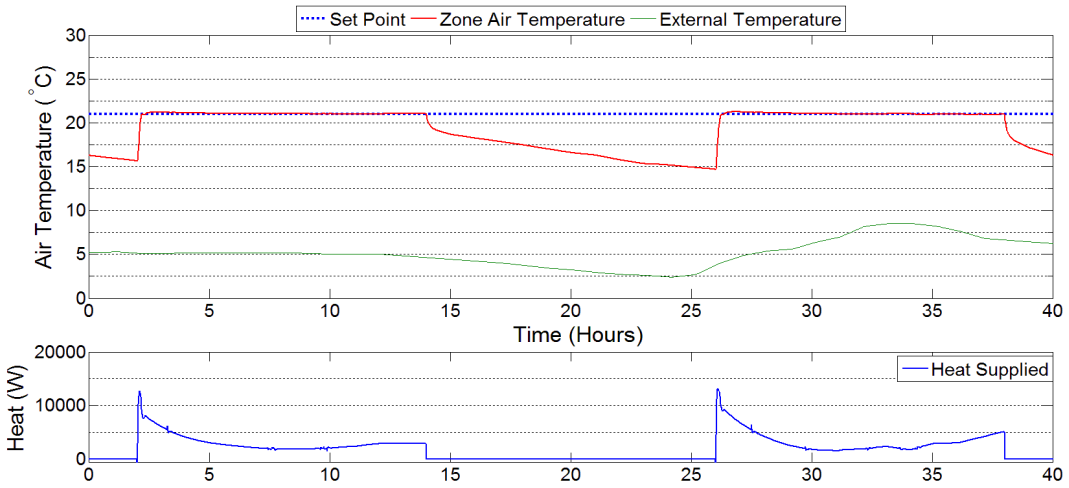

Figure 6.25: Zone air temperature response with SI-RCID controller

The ST-PI and FSP controllers show similar poor response behaviour. T_a rises very slowly, reaching the set point in approximately 2.5 hours. Furthermore, T_a can be seen to deviate from the set point near the end of both days. It is clear that the FSP and ST-PI controllers are unresponsive however as mentioned earlier, increasing the gain values further caused the system to become oscillatory. The SI-RCID controller on the other hand can be seen to reach the set point quickly (approx 10 mins) and then tracks the set point perfectly for the duration of both days, unaffected by the external temperature or other casual gain disturbances. The performance of the outer loop control of T_a is of course affected by the AHU supply air temperature, T_{sup}, and it is therefore important to look at the performance of the controllers in tracking T_{sup}. The performance of the controllers in tracking T_{sup} is shown in Figure 6.26-Figure 6.28. Here, the performance of the SI-RCID controller is clearly superior to the other controllers. The SI-RCID controller tracks the changing set point very accurately with very little or no overshoots. On the first day, between 5 and 10 hours in Figure 6.28, some slight oscillation can be seen however this is caused by the set point changing rapidly based on the demand from the outer loop controller which the inner loop controller handles very well and maintains accurate tracking. Both the FSP and ST-PI controllers show very poor responses. The responses are very sluggish and T_{sup} never reaches the set point in both cases. Again, increasing the gain for the inner loop was not possible as it caused the system to become highly oscillatory. The oscillations seen in both controllers' responses in Figure 6.26 and Figure 6.27 are caused by the rapidly changing set point due to the demand of the outer loop

controller for T_a. It is important to note that, although both of the outer loops are nonlinear as their behaviour varies with the AHU air mass flow rate, the effect of the nonlinearity is greatest on the inner loop as it can be seen to have a significant impact on T_{sup} from equation 6.72. The SI-RCID controller however is able to deal with the nonlinearity and disturbances and maintain stable and accurate tracking.

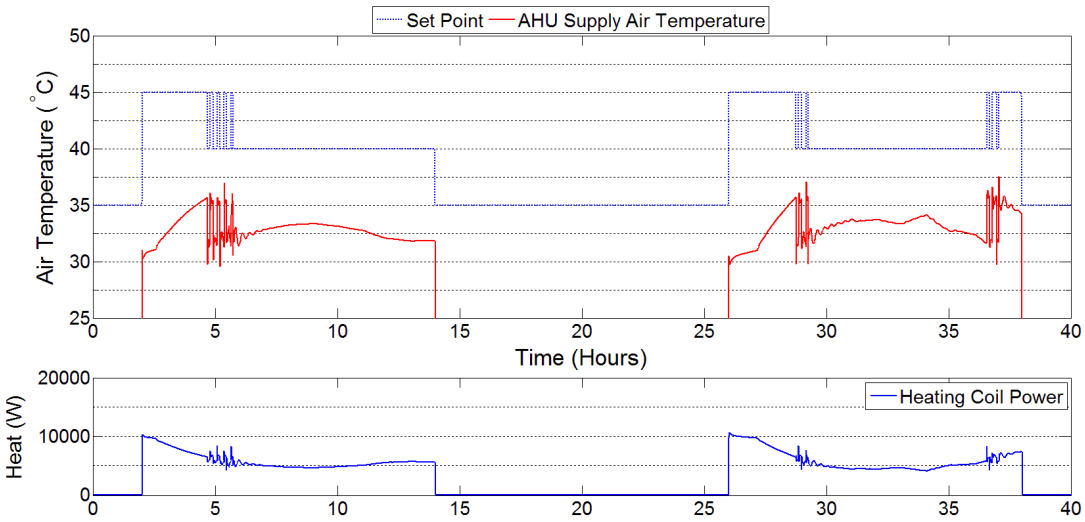

Figure 6.26: AHU supply air temperature with ST-PI controller

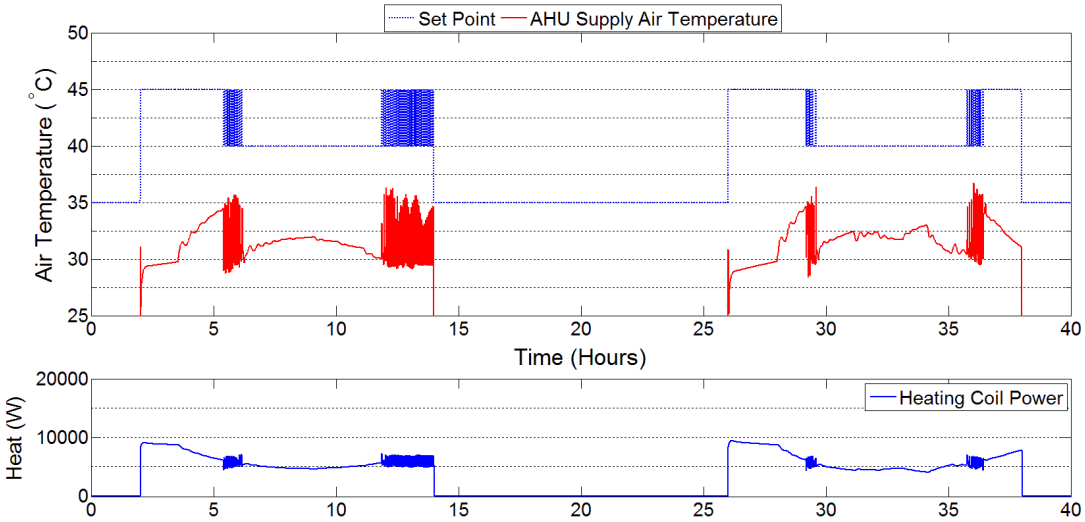

Figure 6.27: AHU supply air temperature with FSP controller

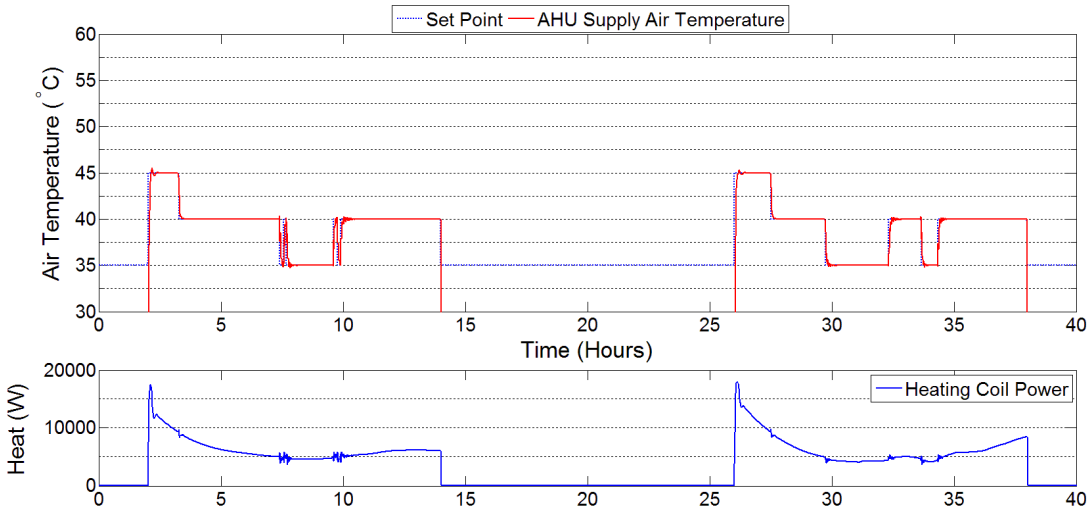

Figure 6.28: AHU supply air temperature with SI-RCID controller

Figure 6.29-Figure 6.31 show the zone relative humidity (W_{rel}) tracking response of the controllers. The ST-PI controller exhibits a slow response and a steady state error can be seen to exist. The tracking is poor on both days as W_{rel} deviates significantly from the set point, particularly on the second day where it drops to approximately 45% near the end of the day. Some small oscillations, caused by oscillations in the inner loop, can be seen on both days. This performance is unsatisfactory and would result in poor comfort conditions for occupants. The FSP controller produces an improved response relative to the ST-PI controller with better set point tracking over both days. A large overshoot of approximately 7-9% is produced on both days however and oscillations around the set point can be seen. The controller takes around 2.5 hours to settle on the first day however it tracks the set point accurately for the rest of the day. The settling time on the second day is longer with the system taking approximately 4 hours to settle. The FSP controllers tracking performance on the second day is also slightly worse as it can be seen to deviate from the set point slightly at times. The SI-RCID controller produces a significantly improved performance relative to the other controllers. A quick response with little overshoot is achieved. There is some slight oscillation at the beginning of both days however overall stable and accurate control is maintained. The corresponding AHU air mass flow rate for each controller is shown in Appendix D.

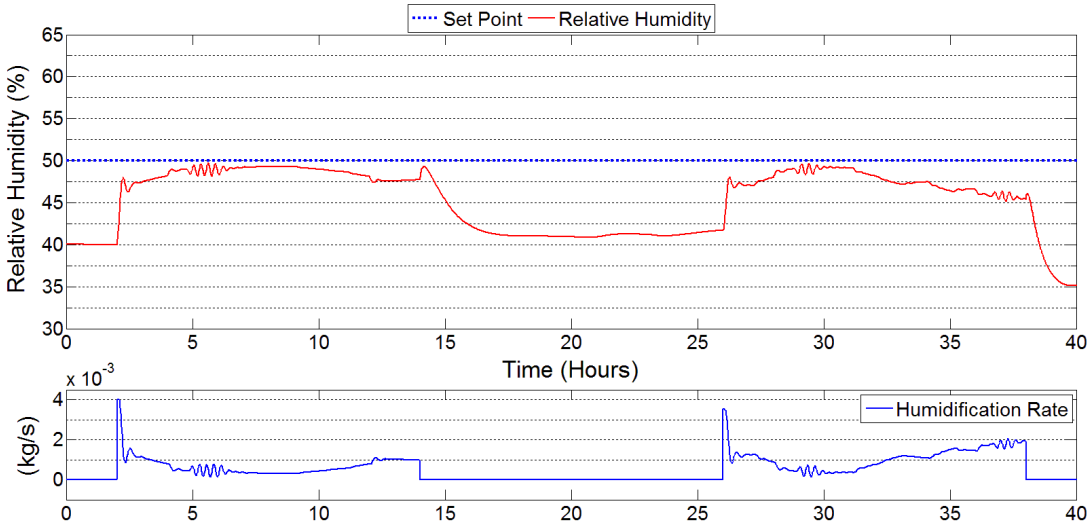

Figure 6.29: Zone relative humidity with ST-PI controller

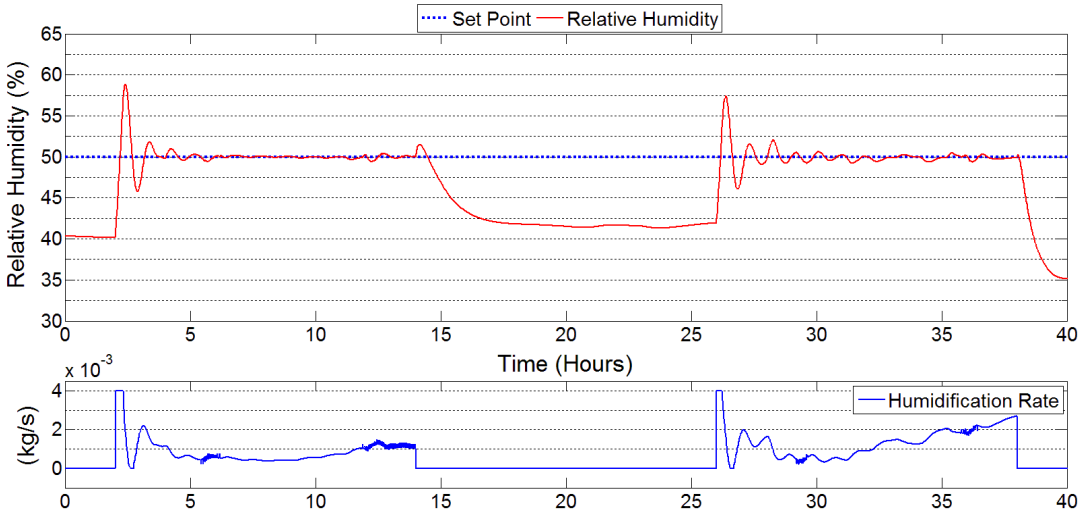

Figure 6.30: Zone relative humidity with FSP controller

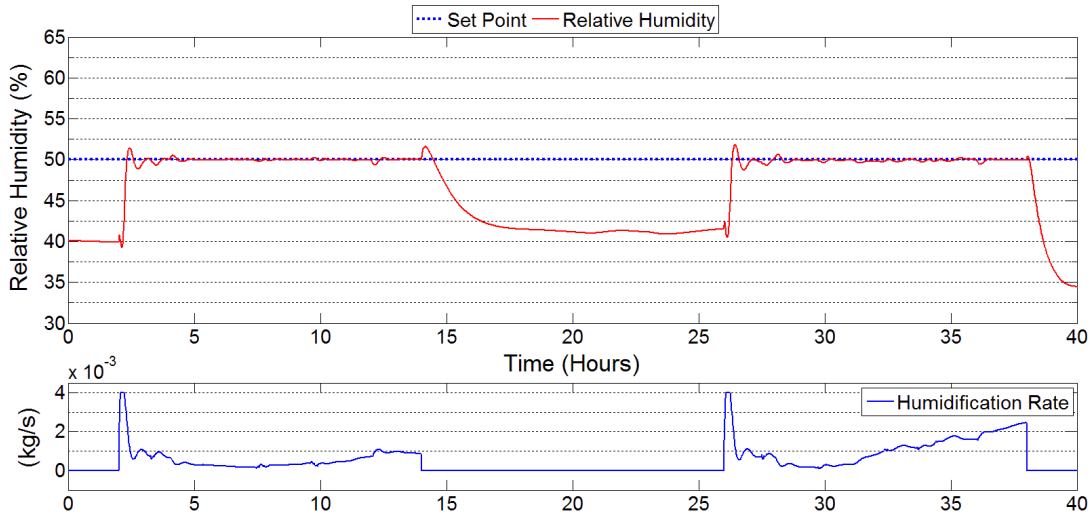

Figure 6.31: Zone relative humidity with SI-RCID controller

6.2.6.1 Controller Robustness to Time Delay Estimation Errors

It is important to test the robustness of the controller to errors in the estimation of the time delay in order to assess how the controller would be affected by large errors that might arise in practice. In the previous section, the controllers were designed with an underestimation error in the time delay of 13s. In this section the performance of the FSP and SI-RCID controllers will be assessed with time delay estimation errors of ±30%. Thus for a 5 min time delay, the controllers will be designed based on time delays of 210 seconds and 390 seconds. The parameters of the base PI controller in the FSP controller design are unaffected by changes in the time delay estimation however the filter parameters are. Similarly, the gain values in the SI-RCID controller are also unaffected however the filter parameters were required to be changed. The new filters for the FSP and SI-RCID controllers calculated based on their respective design procedures are given in Table 6-5 and Table 6-6 respectively.

Control Channel	F_r (-30% error)	F_r (+30% error)
$\mathbf{T_a}$	$\frac{(1+250s)(1+395.8s)}{(1+200s)^2}$	$\frac{(1+250s)(1+437.3s)}{(1+200s)^2}$
$\mathbf{W_{rel}}$	$\frac{(1+60s)(1+1015s)}{(1+600s)^2}$	$\frac{(1+60s)(1+1037s)}{(1+600s)^2}$

Table 6-5: Filters for FSP controller designed with time delay estimation errors

Control Channel	F (-30% error)	F (+30% error)
$\mathbf{T_a}$	$\frac{1}{105s+1}$	$\frac{1}{195s+1}$
$\mathbf{W_{rel}}$	$\frac{1}{105s+1}$	$\frac{1}{195s+1}$

Table 6-6: Filters for SI-RCID controller designed with time delay estimation errors

The performance of the SI-RCID controller in tracking T_a and W_{rel} with time delay estimation errors of ±30% are shown in Figure 6.32 and Figure 6.33. The AHU supply air temperature and air mass flow rate behaviour for all controllers is shown in Appendix E.

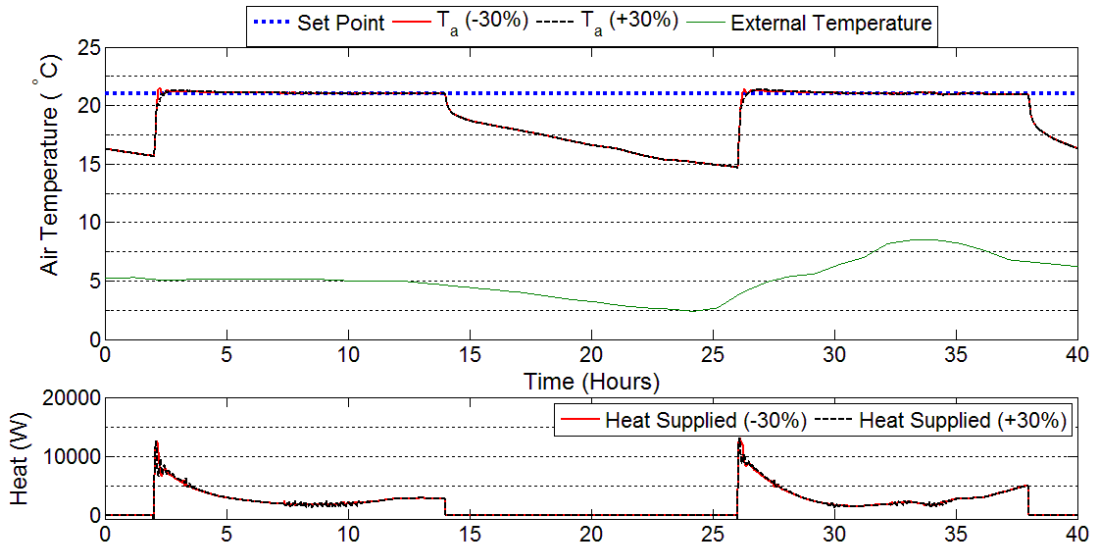

Figure 6.32: Zone air temperature with SI-RCID controller (with time delay estimation errors)

Figure 6.32 shows that the SI-RCID controller performs almost identically when designed with both of the erroneous time delay estimations. In the case with the +30% time delay error, the response curve approaching the set point appears to be slightly smoother than with the -30% time delay error. In both cases the controller is able to attain very accurate and stable tracking of the set point. It can be seen from Figure 6.33 that there is a slight difference in the zone relative humidity tracking performance between the two cases. With the overestimated time delay, a slightly higher overshoot (approximately 1%) is produced in the initial transient period on both days. Both cases however, have the same settling time and maintain accurate tracking over both days.

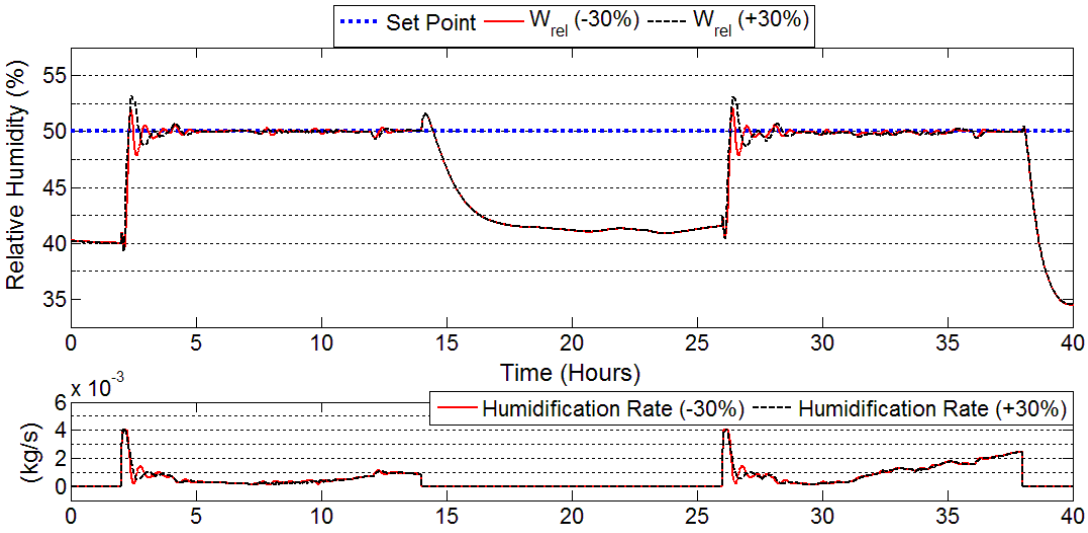

Figure 6.33: Zone relative humidity with SI-RCID controller (with time delay estimation errors)

The performance of the FSP controller with ±30% time delay estimation errors is shown in Figure 6.34 and Figure 6.35. As with the SI-RCID controller, there is no difference in the FSP controllers tracking of Ta with the different time delay errors. In both cases the FSP controller produces a slow response and deviates from the set point slightly towards the end of the second day. In Figure 6.35 it can be seen that a large over shoot and oscillations are produced in W_{rel} at the beginning of both days with both time delay errors. However, when the time delay is underestimated, a larger overshoot (approximately 2.5%) and more oscillations are produced.

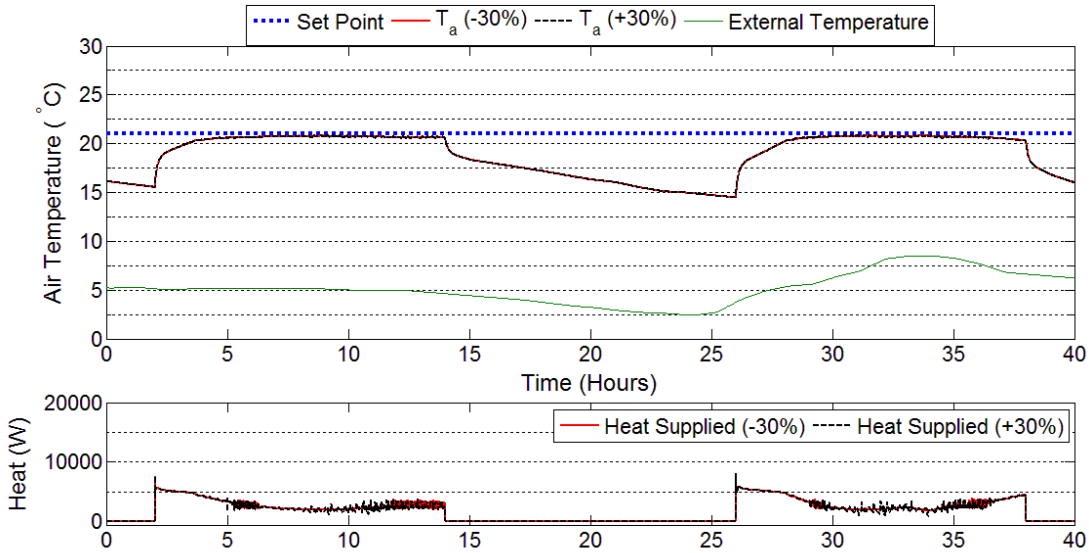

Figure 6.34: Zone air temperature with FSP controller (with time delay estimation errors)

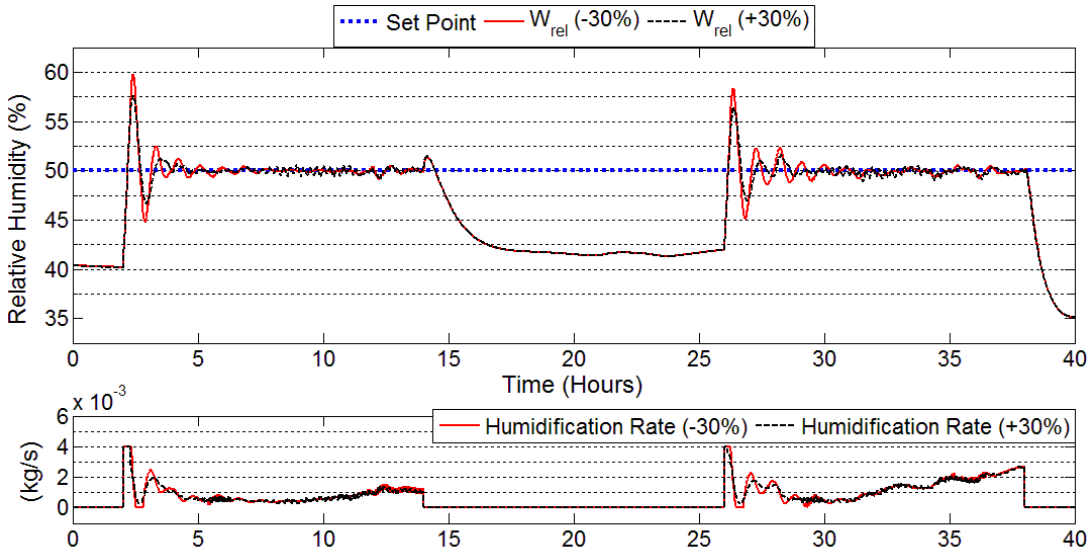

Figure 6.35: Zone relative humidity with FSP controller (with time delay estimation errors)

6.3 Chapter Conclusion

The overall performance of the SI-RCID controller algorithm in tracking all three variables is superior to the other controllers tested. Furthermore, the SI-RCID controller also demonstrates good robustness to modelling errors as it is able to maintain accurate set point tracking in the presence of inaccuracies in the identified FOPDT models as well as large errors in the model time delay. In reality this improved performance would result in improved thermal comfort conditions for occupants being maintained even in the presence of disturbances such as the casual gains and external temperature variation explained in chapter 3. In addition to the improved performance, the design procedure for the SI-RCID controller was demonstrated to be simple and straightforward and did not require any further user input. The FSP and ST-PI controllers on the other hand required further tuning after the initial setting of the parameters based on the design rules specified by their respective authors. As mentioned earlier, this is undesirable in practice as one of the main issues in industrial control systems is controller tuning. Therefore, it is a significant benefit to be able to design a control system based on set rules which produce good performance without further user input. The SI-RCID controller is able to achieve a significantly improved performance over the compared controllers and

does so using the initial parameters designed using the specified rules. Thus, the SI-RCID controller design method presented above provides a practical yet effective controller design process for applying a fundamentally advanced controller design to HVAC processes in industry.

6.4 Chapter References

Astrom, K. J., C. C. Hang, et al. (1994). "A new Smith predictor for controlling a process with an integrator and long dead-time." Automatic Control, IEEE Transactions on **39**(2): 343-345.

Bi, Q., W. J. Cai, et al. (2000). "Advanced controller auto-tuning and its application in HVAC systems." Control Engineering Practice **8**(6): 633-644.

Ding, L., A. Bradshaw, et al. (2006). Design of discrete-time RIDE control system. UKACC International Conference (Control-06), August, Glasgow, UK.

Geng, G. and G. M. Geary (1993). "On Performance and Tuning of Pid Controllers in Hvac Systems." Second Ieee Conference on Control Applications, Vols 1 and 2: 819-824.

Kealy, T. and A. O'Dwyer (2002). Comparison of open and closed loop process identification techniques in the time domain. Conference papers.

Khalid, Y. A. (2011). Controllability of Building Systems. PhD, University of Strathclyde.

Liu, T., W. Zhang, et al. (2005). "Analytical design of two-degree-of-freedom control scheme for open-loop unstable processes with time delay." Journal of Process Control **15**(5): 559-572.

Moreno, J., J. Guzmán, et al. (2013). "A combined FSP and reset control approach to improve the set-point tracking task of dead-time processes." Control Engineering Practice **21**(4): 351-359.

Normey-Rico, J., C. Bordons, et al. (1997). "Improving the robustness of dead-time compensating PI controllers." Control Engineering Practice **5**(6): 801-810.

Normey-Rico, J. E. (2007). Control of dead-time processes, springer.

Normey-Rico, J. E. and E. F. Camacho (2009). "Unified approach for robust dead-time compensator design." Journal of Process Control **19**(1): 38-47.

Skogestad, S. (2003). "Simple analytic rules for model reduction and PID controller tuning." Journal of Process Control **13**(4): 291-309.

Smith, O. (1957). "Closer control of loops with time delays." Chem. Eng. Prog **53**: 216-219.

Torrico, B. C. and J. E. Normey-Rico (2005). "2DOF discrete dead-time compensators for stable and integrative processes with dead-time." Journal of Process Control **15**(3): 341-352.

Vodencarevic, A. (2010). Design of PLC-based Smith Predictor for Controlling Processes with Long Dead Time. Proceedings of the International MultiConference of Engineers and Computer Scientists.

7. Discussion, Conclusions and Further Work

It has been established that designing effective building control systems to achieve accurate and efficient control of the indoor comfort conditions of a building is a complex task, particularly with the increasingly sophisticated designs, materials as well as advanced HVAC systems found in modern climate adaptive buildings. The simple control systems which are still widely used in the buildings industry are often unable to cope with the aforementioned complex dynamics of buildings. Hence, a substantial amount of energy is wasted as a result of these poor control systems which cause unnecessary heating, fabric and ventilation losses**.** Therefore, the buildings industry is in need of upgraded control systems which are able to achieve desired comfort levels whilst making efficient use of energy. In response to this requirement, many advanced controller designs have been developed in the literature. Chapter 2 in this thesis provided a review of a wide range of control systems which have been proposed. From this review, it was deduced that, despite the significant advancements that have been made in building control systems design in the academic world, the buildings industry has often been reluctant to adopt these designs. This is down to a number of reasons from lengthy commissioning times due to overcomplicated design procedures, to a reluctance to adopt methods that may have to be treated as 'black box' due to robustness issues. Thus, the ultimate goal for building HVAC control systems design and the research objectives for this body of work, as defined in chapter 1, were to design a robust high performance HVAC control strategy that is capable of dealing with the complexities associated with modern building control whilst being a low cost solution which is easy to design and implement. Furthermore, the control algorithm should not be computationally intensive so as to allow for implementation on the low cost hardware that is currently being used in industry.

The first area of development in this thesis was the development of the building zone and HVAC system models detailed in chapter 3. Developing a model is a necessary part of the controller design process in order to design the algorithms and evaluate controller performance. The thermal dynamics of the building zone and HVAC systems were modelled using classical differential equations for heat transfer

and thermodynamics and implemented in the ESL modelling environment. This modelling approach was necessary for capturing the important dynamics of the building whilst remaining simple enough to be represented in state space format and used for controller design.

Once the model was developed, the performance of different controller algorithm designs was then investigated. The fundamentals of the advanced nonlinear inverse dynamics (NID) based control algorithms developed in this thesis were described in chapter 4. It was seen from the literature review in chapter 2 that inverse dynamics based controller designs have not been developed for HVAC systems in the literature and so this in itself was a novel research area. It was demonstrated through the fundamentals of the advanced controller design, how it is possible to overcome the aforementioned complexities which can be encountered by a control system. In this thesis, there are two main controller designs developed based on the research objectives specified. These controller designs, detailed in chapters 5 and 6, provide solutions which tackle the building HVAC control problem from different perspectives. The following sections provide summaries of the research presented in these chapters and the conclusions and outcomes drawn from the research will be discussed. Suggestions for future work are also given.

7.1 Conclusions - Robust Nonlinear HVAC Systems Control with Evolutionary Optimisation

Chapter 5 detailed the development of an auto-tuning algorithm which relieves the difficulty in the manual tuning process of the NID based RIDE control algorithm. The auto-tuning algorithm was developed using a genetic algorithm (GA) optimisation scheme which optimises the control system tuning parameters based on a set of user specified criteria. The optimisation scheme takes into account uncertainty in the building model by optimising the controller parameters over a range of uncertainty in selected building parameters. The auto-tuner was implemented in Visual C++ and combined with the ESL model representing the zone and HVAC system. In this chapter, the zone model was used with the direct heater and mechanical ventilation system described in case 1 in chapter 3. The first step in

the controller design process was to convert the model into state space representation such that it could be used to design the RIDE controller algorithm. The RIDE control system parameters were then tuned using the GA auto-tuner.

The proposed RIDE-GA controller was tested on the building zone model and its performance compared to a PI control system which was also optimised using the same GA based auto-tuning algorithm. The robustness of both controllers to parameter uncertainty was tested by varying the value of the thermal mass heat transfer coefficient by ±60% of the value used for the controller design and testing their performance at all three operating points. The results showed that the GA auto-tuner worked very well with the RIDE controller and was able to achieve significantly improved performance over the auto-tuned PI controller. The RIDE-GA controller produced a significantly faster response as well as more stable and accurate set-point tracking when tested over the range of uncertainty in the building model. It was also shown that the RIDE-GA controller was unaffected by the variation in the thermal mass heat transfer coefficient as its performance was nearly identical regardless of the operating point. The PI-GA controller on the other hand, showed different response characteristics over the three operating points. The RIDE-GA controller also showed superior disturbance rejection performance compared to the PI-GA controller.

7.1.1 Limitations of this method

The GA auto-tuning process described in chapter 5 was shown to be effective in applications in which there are a small number of parameters with uncertainty which must be accounted for. As discussed in section 5.3.1 however, there are a few limitations with this method which could lead to it being perceived as impractical for building HVAC control systems in industry as is the case with many advanced control algorithms developed in the literature. One limitation of this method is that it may become inefficient if it is used to account for uncertainty in a large number of parameters. The auto-tuning method was also designed for use in systems for which models have been developed and the control system designer wishes to tune the control system based on the model. This way, using the system model, the control system can be tuned to produce close to optimal performance when implemented in

practice. In some cases however, a system model is unavailable or is difficult to develop due to certain unknown parameters such as transport lag. The control methods developed in chapter 6 address the limitations of the method presented in chapter 5 and come together to provide a practical solution which is suitable for use in industry.

7.2 Conclusions - Robust System Identification based Nonlinear Inverse Dynamics Control

In chapter 6, a full control solution, named System Identification based Rate Compensated Inverse Dynamics (SI-RCID), was developed in order to overcome all of the issues and satisfy all of the criteria specified in the research objective i.e. a high performance control algorithm which is suitably straightforward for use in industry. A number of contributions were made in this chapter, in order to develop a methodology for applying a fundamentally complex control algorithm in a simple manner. It was mentioned in the previous section that in some cases it is difficult to develop a model of a building due to certain unknown parameters and the variability of a building during its lifetime. Furthermore, a controller design which requires a dynamic model of the building zone to be created for use in the control law is unlikely to be adopted in industry due to its complexity and lengthy design procedure. Thus, in order to overcome this issue, the novel system identification strategy for identifying the necessary part of the model (MB matrix) for use in the NID based control law was developed. Using a well-known simple system identification technique for obtaining FOPDT models from step input data, this strategy allows the control systems designer to apply the NID controller without any more input than would be required for the popular self-tuning PID control methods commonly used in industry. A design strategy for SISO and MIMO systems was developed in chapter 6.

A novel commutation law for governing the behaviour of the control system around actuator saturation limits was also developed. It was identified that the original commutation law used in the RIDE controller would cause the controller to become stuck on the actuator limits in certain circumstances due to complications

with the equivalent control law. Therefore, a new law which included extra criteria was developed which overcomes these complications.

Through testing on the equivalent control law with transport lag systems, an important observation was made which provides valuable insight into the effects of large time delays on a controller which uses equivalent control. It was found that using equivalent control on systems with large time delay caused the system to become unstable and the system cannot be stabilised by reducing the system gain. The reason for this is that using equivalent control achieves the same effect as a high gain controller. That is, the closed loop poles of the system are moved to the locations of the open loop zeros. It is known that high gain control cannot be used with systems with large time delay. Therefore, it is not possible to use equivalent control in these cases as it is the same as permanently using high gain control.

In order to overcome this issue i.e. to enable the use of equivalent control on systems with large time delay, a novel time delay compensation method for equivalent control based on the long established Smith Predictor method was developed. This method uses an identified model of the system in order to predict the rate of change of the non-delayed system and correct the rate of change of the actual measured output signal. A first order filter is used on the corrective error signal in the predictor to improve robustness of the controller to modelling errors. The final SI-RCID control algorithm combines all of the aforementioned features into one control solution which is straightforward in its design and implementation.

7.2.1 Outcomes from controller design and results

When applying the various control algorithms to the building model, the first step was to design the setup of the AHU to be used with all of the controllers tested. The AHU was used in a variable temperature variable volume setup (VTVV) i.e. the temperature and mass flow rate of the AHU supply air was allowed to vary based on the demand for conditioning the zone thermal comfort. A two loop control setup was used for all controllers tested, with the outer loop controlling the zone comfort conditions and the inner loop controlling the AHU supply air based on the demand from the outer loop.

The conventional design procedure for the RIDE controller was shown in chapter 6 in order to showcase the difficulties that would be encountered while implementing this algorithm in practice. It was shown that the design procedure for the RIDE controller was lengthy and too complicated to be adopted in industry. From a performance perspective, the RIDE controller was shown to produce fast and accurate set-point tracking without the presence of time delay in the measurement signals. When time delays were added in the measurements however, the controller was shown to become unstable.

The performance of the SI-RCID algorithm was tested on the building zone model with the full AHU actuation system described in case 2 in chapter 3. A self-tuning PI controller and a Filtered Smith Predictor (FSP) controller were also designed and tested in order to provide a comparison with the proposed method. The design procedure of the SI-RCID controller was relatively straightforward and in fact required less input than the other controllers due to the other controllers producing unsatisfactory performance after the initial design procedure. The results showed that the SI-RCID controller's performance was superior to the other controllers tested. It produced a faster response as well as more accurate set-point tracking and improved disturbance rejection. It also displayed improved robustness to large modelling errors in both the first order model as well as the time delay (±30% error) when compared to the FSP controller. Thus, overall the proposed controller overcame all of the difficulties mentioned and fulfilled all of the research objectives set out in this project. It is a high performance control strategy which has the potential to improve the performance of building HVAC systems in practice and is easy to design and implement thus making it suitable for use in industry.

7.3 Novelties and Contributions of Research

The main contributions and novelties presented in the research in this thesis can be summarized as follows:

1. Development of a mathematical model of a building with a full AHU actuation system using models developed in (Murphy 2012) and (Tashtoush, Molhim et al. 2005).

2. Development of a novel auto-tuning algorithm for the RIDE controller with robustness for parameter uncertainty using Genetic Algorithm optimization.

3. Presentation of a case study demonstrating the application of the proposed GA based auto-tuning algorithm with the RIDE controller applied to a building zone and HVAC system model.

    a. Comparison of the proposed control strategy to a PI controller tuned with the GA based auto-tuning algorithm

4. Novel use of the RIDE algorithm in a two loop control structure for building zone control with AHU inner control loop.

5. Novel system identification based NID controller strategy (SI-RCID) using system identification from step response for inverse dynamics estimation and transport lag compensation.

6. Development of a novel improved commutation law for governing the behaviour of equivalent control based controllers SI-RCID and RIDE.

7. Contribution of knowledge providing valuable insight and explanation of the effects of large time delays on equivalent control based controller designs.

8. Design of a novel transport lag/dead time compensation method for an equivalent control based NID controller using modified smith's predictor principle.

9. Presentation of a full methodology for designing a low cost controller design which is simple to implement and is capable of dealing with time delay, parameter uncertainty, nonlinearity, interacting MIMO systems, unknown system parameters (identification) and tuning/re-tuning.

10. Novel application of inverse dynamics to HVAC systems using a practical approach for designing full HVAC system and zone control.

11. Presentation of a case study demonstrating the application of the proposed SI-RCID controller design to a building zone and AHU system model.

    a. Comparison of the proposed controller strategy to an industry standard self-tuning PI controller and a more advanced Filtered Smith Predictor method recently developed in the literature

7.4 Further Work

The overall control algorithms and design methodologies presented in this thesis are of archival value for both researchers and industrial engineers in this field as they provide a strong platform which can be easily built upon. While the final controller designs presented satisfies the research objectives set out to be achieved in this thesis, there are a number of areas where improvements can be made to the developed controller design in order to further improve its performance and suitability for industry.

7.4.1 Incorporation of an improved identification algorithm

The system identification algorithm used for the identification of the MB matrix and for the model used in the dead time compensation method in thesis is very basic. While it was sufficient for the work presented, there are many step response identification methods that have been developed in the literature which could be used. The simple identification algorithm used in this thesis resulted in significant modelling errors. Although this showcased the robustness of the controller to modelling errors, the performance of the controller could be improved if more accurate models were identified. Furthermore, the incorporation of a more advanced identification method could extend the range of application of the controller since open loop unstable plants could be identified.

7.4.2 Stability analysis and development of a robust design procedure for dead-time compensator filter

It was shown in chapter 6 that the error between the model and the actual system output was passed through a first order filter in order to improve the robustness of the controller to modelling errors. As mentioned in chapter 6, this filter design was selected as it was found to produce good results and was not verified with a stability analysis due to a lack of time available in this project. If a full analysis of the effect of the filter on the controller was to be performed, an amplitude dependant stability criterion could be established whilst also assessing the potential for the filter design to be improved and in turn the controller performance improved. Moreover, a robust design procedure for the filter characteristics could be developed since the current design procedure is based on a very crude rule for selecting the time constant for the first order filter.

7.4.3 Combination of SI-RCID method with detailed simulation packages

Models created using detailed simulation packages such as ESP-r or CFD are normally not suitable for controller design purposes due to their vast complexity and detail. Therefore, controller design is typically performed using low order models which can be represented in state space format. The novel SI-RCID method developed in this thesis however eliminates the necessity of developing a low order model for use in the controller design procedure as it uses system identification to design the control system. Thus, it only requires to be connected to the system that needs to be controlled i.e. the building HVAC system, and it will identify a low order system model for use in the design process which can be easily automated. This opens up the possibility of easily integrating the SI-RCID controller with detailed energy simulation packages by developing a simulation-in-loop environment. The controller can identify a low order model from the detailed simulation and the controller can be designed. This would enable advanced control systems to be developed and tested in a highly detailed and realistic simulation environment. This

would be very useful for use in the conceptual building design stage or simply for testing algorithms prior to their implementation in a real life system.

7.4.4 Implementation in an industrial/experimental environment

The results presented in this thesis were all obtained in a dynamic simulation environment. The models developed in this thesis included many of the difficulties that would be encountered when designing a control system in practice and therefore the results provide a good indication of how the controller would perform in a real life system. The best way to evaluate the performance of the controller however would be to test it in practice in industry or in an experimental setup. This way a practical assessment of the controller methodology could be made and further improvements could be made to the controller if necessary in order to ready the controller for industrial deployment.

7.5 Chapter References

Murphy, G. B. (2012). Inverse Dynamics based Energy Assessment and Simulation. PhD, University of Stratchlyde.

Tashtoush, B., M. Molhim, et al. (2005). "Dynamic model of an HVAC system for control analysis." Energy **30**(10): 1729-1745.

Appendix A. State Space Matrix Coefficients

$$a_{11} = \frac{1}{M_a C_a}\left(-h_i A_s - U_f A_f - U_r A_r - U_w A_w - \dot{m}_{nv} C_a - U_{ft} A_{ft}\right) \quad \text{(A.1)}$$

$$a_{12} = \frac{1}{M_a C_a}\left(-h_i A_s\right) \quad \text{(A.2)}$$

$$a_{14} = \frac{1}{M_a C_a}\left(U_{ft} A_{ft}\right) \quad \text{(A.3)}$$

$$a_{21} = \frac{1}{M_{si} C_s}\left(h_i A_s\right) \quad \text{(A.4)}$$

$$a_{22} = \frac{1}{M_{si} C_s}\left(-h_i A_s - \frac{K_{si} A_s}{Th_{wall}}\right) \quad \text{(A.5)}$$

$$a_{23} = \frac{1}{M_{si} C_s}\left(\frac{K_{si} A_s}{Th_{wall}}\right) \quad \text{(A.6)}$$

$$a_{32} = \frac{1}{M_{se} C_s}\left(\frac{K_{si} A_s}{Th_{wall}}\right) \quad \text{(A.7)}$$

$$a_{33} = \frac{1}{M_{se} C_s}\left(-\frac{K_{si} A_s}{Th_{wall}} - h_e A_s\right) \quad \text{(A.8)}$$

$$a_{41} = \frac{1}{M_{ft} C_{ft}}\left(U_{ft} A_{ft}\right) \quad \text{(A.9)}$$

$$a_{44} = \frac{1}{M_{ft} C_{ft}}\left(-U_{ft} A_{ft}\right) \quad \text{(A.10)}$$

$$a_{55} = -\frac{\dot{m}_{nv}}{M_a} \quad \text{(A.11)}$$

$$b_{11} = \frac{1}{M_a C_a} \quad \text{(A.12)}$$

$$b_{12} = -\frac{T_a}{M_a} \quad \text{(A.13)}$$

$$b_{52} = \frac{W_s - W_a}{M_a} \quad \text{(A.14)}$$

$$f_{11} = \frac{1}{M_a C_a} \tag{A.15}$$

$$f_{12} = \frac{1}{M_a C_a}(U_r A_r + U_w A_w + \dot{m}_{nv} C_a) \tag{A.16}$$

$$f_{32} = \frac{1}{M_{se} C_s}(h_e A_s) \tag{A.17}$$

$$f_{53} = \frac{\dot{m}_{nv}}{M_a} \tag{A.18}$$

$$f_{54} = \frac{P_{occ}}{M_a} \tag{A.19}$$

Appendix B. State Space Matrix Coefficients

$$d(t) = \begin{bmatrix} \dot{Q}_{free}(t) \\ T_o(t) \\ W_o(t) \\ n_{occ}(t) \end{bmatrix} \tag{B.1}$$

$$a_{11} = \frac{1}{M_a C_a}\left(-h_i A_s - U_f A_f - U_r A_r - U_w A_w - \dot{m}_{nv} C_a - U_{ft} A_{ft}\right) \tag{B.2}$$

$$a_{12} = \frac{1}{M_a C_a}(-h_i A_s) \tag{B.3}$$

$$a_{14} = \frac{1}{M_a C_a}\left(U_{ft} A_{ft}\right) \tag{B.4}$$

$$a_{21} = \frac{1}{M_{si} C_s}(h_i A_s) \tag{B.5}$$

$$a_{22} = \frac{1}{M_{si} C_s}\left(-h_i A_s - \frac{K_{si} A_s}{Th_{wall}}\right) \tag{B.6}$$

$$a_{23} = \frac{1}{M_{si} C_s}\left(\frac{K_{si} A_s}{Th_{wall}}\right) \tag{B.7}$$

$$a_{32} = \frac{1}{M_{se} C_s}\left(\frac{K_{si} A_s}{Th_{wall}}\right) \tag{B.8}$$

$$a_{33} = \frac{1}{M_{se} C_s}\left(-\frac{K_{si} A_s}{Th_{wall}} - h_e A_s\right) \tag{B.9}$$

$$a_{41} = \frac{1}{M_{ft} C_{ft}}\left(U_{ft} A_{ft}\right) \tag{B.10}$$

$$a_{44} = \frac{1}{M_{ft} C_{ft}}\left(-U_{ft} A_{ft}\right) \tag{B.11}$$

$$a_{55} = \frac{\alpha_h}{C_h} \tag{B.12}$$

$$a_{77} = \frac{UA_h}{C_{ah}} \tag{B.13}$$

$$a_{81} = -\frac{\dot{m}_{nv}}{M_a} \tag{B.14}$$

$$b_{11} = \frac{\left(T_{sup} - T_a\right)}{M_a} \tag{B.15}$$

$$b_{51} = -\frac{C_a}{C_h \rho_a}(T_{duct} - T_{sup}) \tag{B.16}$$

$$b_{61} = \frac{(h_{in} - h_{out})(T_{co} - T_{duct})C_a}{h_{in} M_{duct} C_{duct}} \tag{B.17}$$

$$b_{71} = \frac{C_a}{C_{ah}}(\gamma T_a + (1-\gamma)T_o - T_{co}) \tag{B.18}$$

$$b_{73} = \frac{1}{C_{ah}} \tag{B.19}$$

$$b_{81} = \frac{1}{M_a}\left(W_{sup} - W_a\right) \tag{B.20}$$

$$b_{91} = \frac{\left(W_{co} - W_{sup}\right)}{v_h \rho_a} \tag{B.21}$$

$$b_{92} = \frac{1}{v_h \rho_a} \tag{B.22}$$

$$b_{10,1} = \frac{(\gamma W_a + (1-\gamma)W_o - W_{co})}{V_{ah} \rho_a} \tag{B.23}$$

$$f_{11} = \frac{1}{M_a C_a} \tag{B.24}$$

$$f_{12} = \frac{1}{M_a C_a}(U_r A_r + U_w A_w + \dot{m}_{nv} C_a) \tag{B.25}$$

$$f_{32} = \frac{1}{M_{se} C_s}(h_e A_s) \tag{B.26}$$

$$f_{52} = \frac{18.3}{C_h} \tag{B.27}$$

$$f_{72} = \frac{UA_{ah}}{C_{ah}} \tag{B.28}$$

$$f_{83} = \frac{\dot{m}_{nv}}{M_a} \tag{B.29}$$

$$f_{84} = \frac{P_{occ}}{M_a} \tag{B.30}$$

$$a_{55}{}^{*} = -\alpha_h \tag{B.31}$$

$$a_{66}{}^{*} = -\frac{\dot{m}_{nv}}{M_a} \tag{B.32}$$

$$b_{51}{}^{*} = \frac{\dot{m}_c C_a}{C_h \rho_a}\left(\frac{(UA_h + (1-\gamma)\dot{m}_c C_a)}{\dot{m}_c C_a + UA_h} T_o + \frac{\gamma \dot{m}_c C_a}{\dot{m}_c C_a + UA_h} T_a - T_{sup}\right) \tag{B.33}$$

$$b_{52}{}^{*} = \frac{\dot{m}_c C_a}{C_h \rho_a (\dot{m}_c C_a + UA_h)} \tag{B.34}$$

$$b_{61}{}^{*} = \frac{\gamma \dot{m}_c W_a + (1-\gamma)\dot{m}_c W_o - W_a}{M_a} \tag{B.35}$$

$$b_{63}{}^{*} = \frac{\dot{m}_c}{M_a} \tag{B.36}$$

Appendix C. Two Loop Controller State Space Matrix Coefficients

$$a_{11} = \frac{1}{M_a C_a}\left(-h_i A_s - U_f A_f - U_r A_r - U_w A_w - \dot{m}_{nv} C_a - U_{ft} A_{ft}\right) \quad \text{(C.1)}$$

$$a_{12} = \frac{1}{M_a C_a}(-h_i A_s) \quad \text{(C.2)}$$

$$a_{14} = \frac{1}{M_a C_a}\left(U_{ft} A_{ft}\right) \quad \text{(C.3)}$$

$$a_{21} = \frac{1}{M_{si} C_s}(h_i A_s) \quad \text{(C.4)}$$

$$a_{22} = \frac{1}{M_{si} C_s}\left(-h_i A_s - \frac{K_{si} A_s}{Th_{wall}}\right) \quad \text{(C.5)}$$

$$a_{23} = \frac{1}{M_{si} C_s}\left(\frac{K_{si} A_s}{Th_{wall}}\right) \quad \text{(C.6)}$$

$$a_{32} = \frac{1}{M_{se} C_s}\left(\frac{K_{si} A_s}{Th_{wall}}\right) \quad \text{(C.7)}$$

$$a_{33} = \frac{1}{M_{se} C_s}\left(-\frac{K_{si} A_s}{Th_{wall}} - h_e A_s\right) \quad \text{(C.8)}$$

$$a_{41} = \frac{1}{M_{ft} C_{ft}}\left(U_{ft} A_{ft}\right) \quad \text{(C.9)}$$

$$a_{44} = \frac{1}{M_{ft} C_{ft}}\left(-U_{ft} A_{ft}\right) \quad \text{(C.10)}$$

$$a_{55} = -\frac{\dot{m}_{nv}}{M_a} \quad \text{(C.11)}$$

$$b_{11} = \frac{1}{M_a C_a} \quad \text{(C.12)}$$

$$b_{52} = \frac{\dot{m}_c}{M_a} \quad \text{(C.13)}$$

$$f_{11} = \frac{1}{M_a C_a} \quad \text{(C.14)}$$

$$f_{12} = \frac{1}{M_a C_a}(U_r A_r + U_w A_w + \dot{m}_{nv} C_a) \quad \text{(C.15)}$$

$$f_{32} = \frac{1}{M_{se} C_s}(h_e A_s) \quad \text{(C.16)}$$

$$f_{53} = \frac{\dot{m}_{nv}}{M_a} \quad \text{(C.17)}$$

$$f_{54} = \frac{P_{occ}}{M_a} \quad \text{(C.18)}$$

Appendix D. AHU Air Mass Flow Rate For Case Study Section 6.2.6

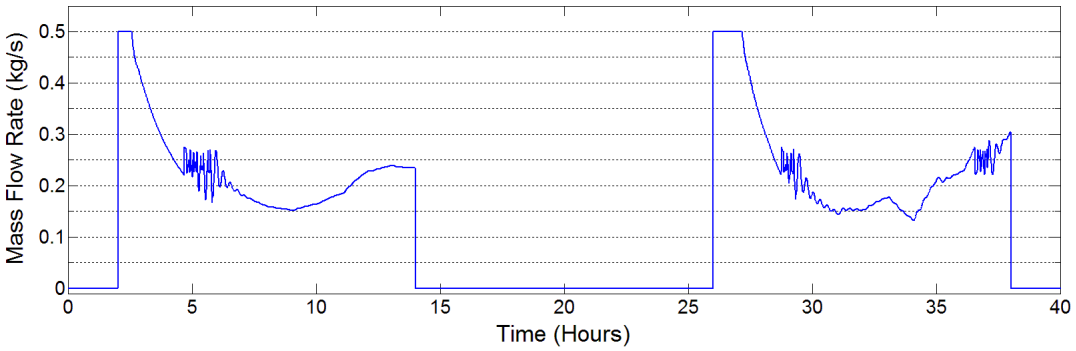

Figure D-1: AHU air mass flow rate with ST-PI controller

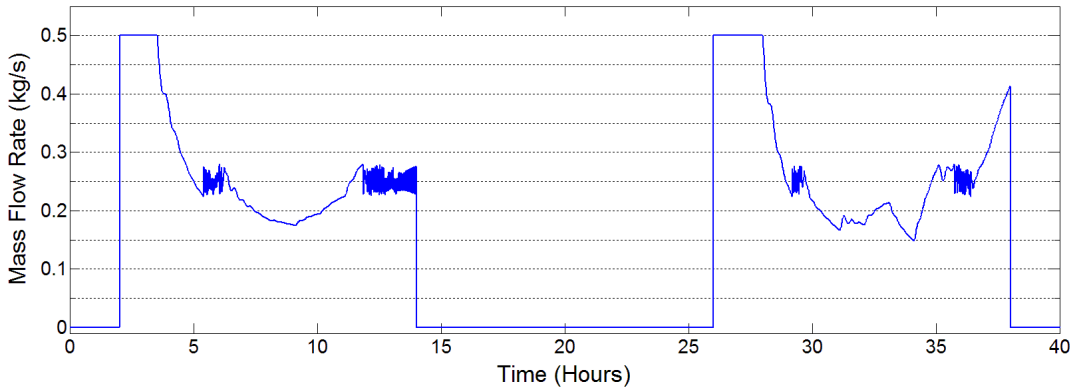

Figure D-2: AHU air mass flow rate with FSP controller

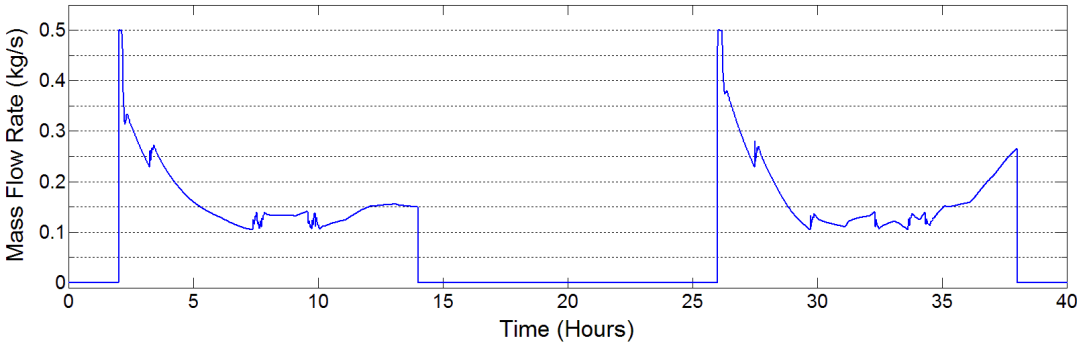

Figure D-3: AHU air mass flow rate with SI-RCID controller

Appendix E. Supply Air Temperature and AHU Air Mass Flow Rate (Case Study Section 6.2.6.1)

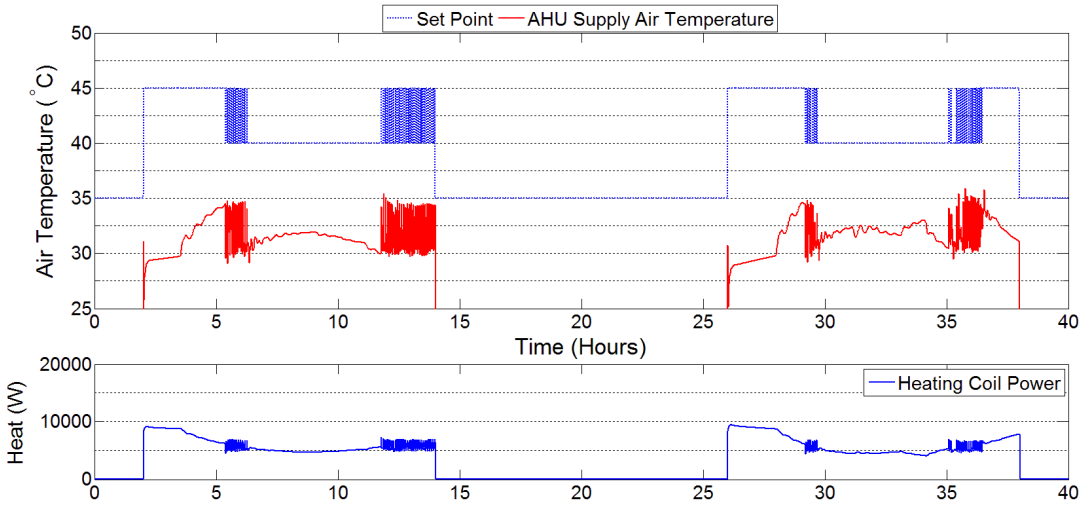

Figure E-1: AHU supply air temperature with FSP controller (-30% delay estimation error)

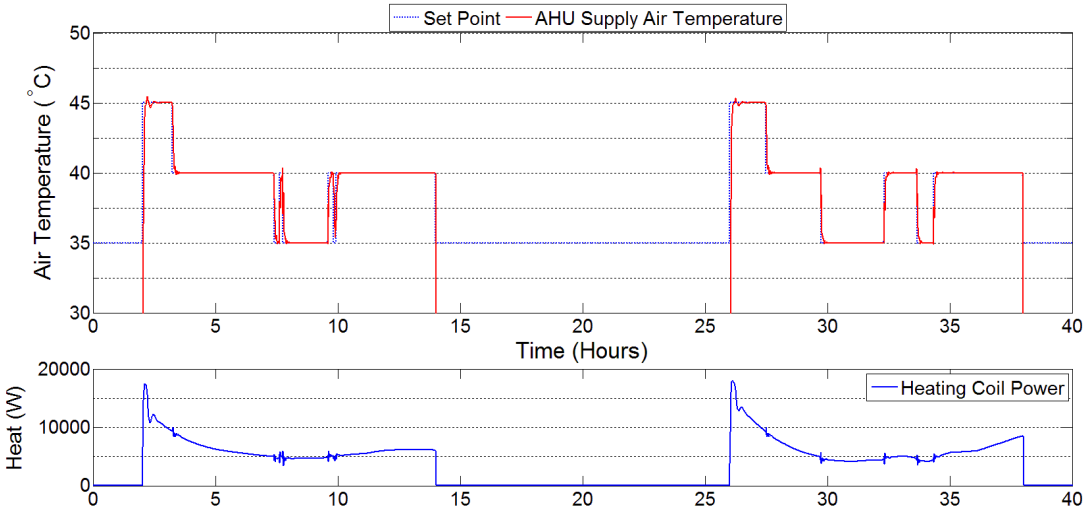

Figure E-2: AHU supply air temperature with SI-RCID controller (-30% delay estimation error)

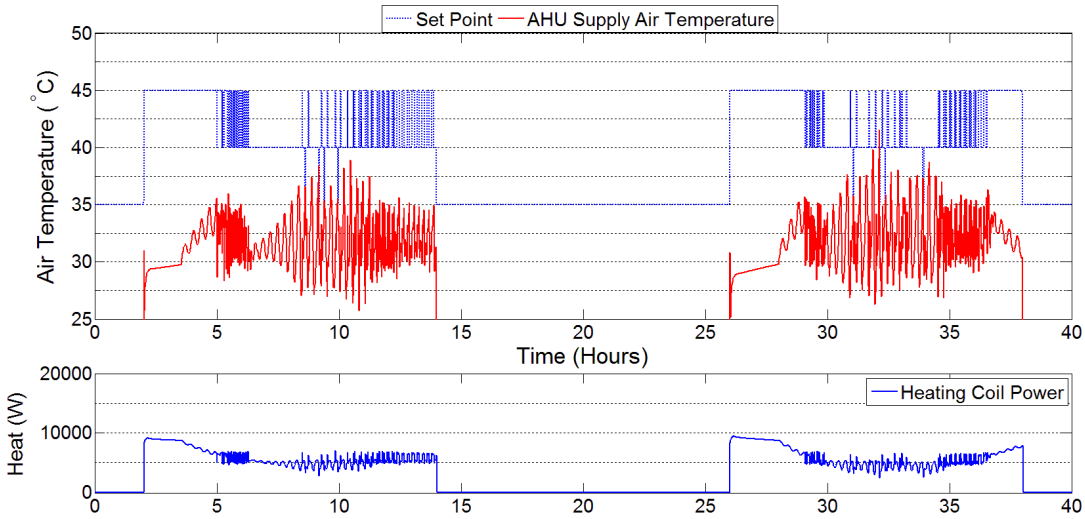

Figure E-3: AHU supply air temperature with FSP controller (+30% delay estimation error)

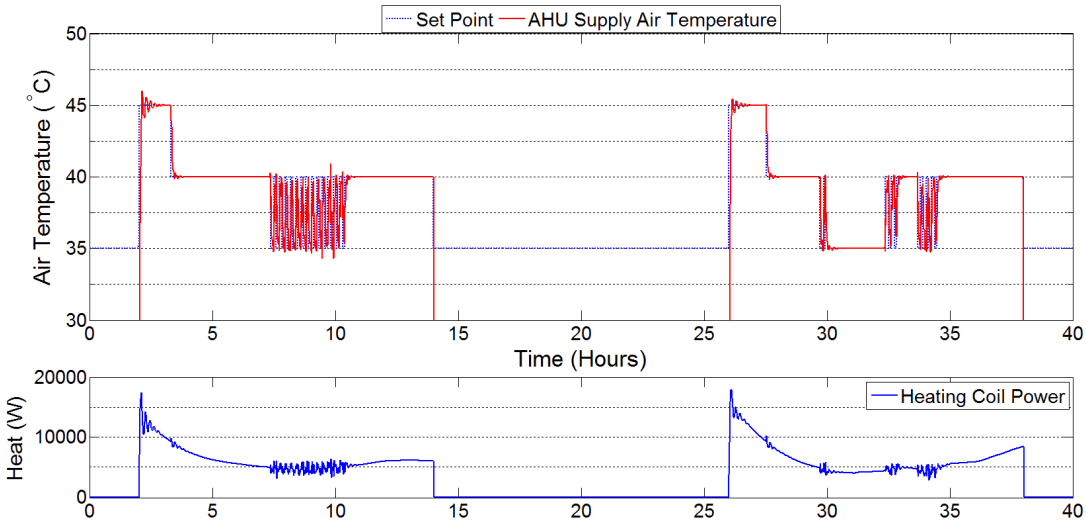

Figure E-4: AHU supply air temperature with SI-RCID controller (+30% delay estimation error)

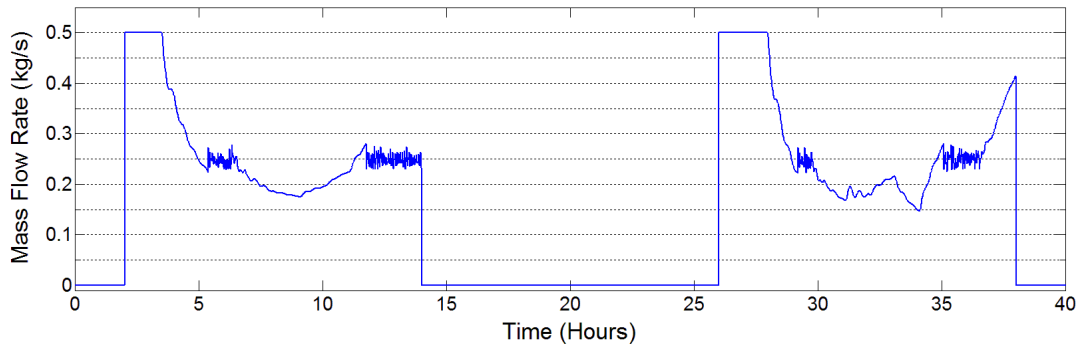

Figure E-5: AHU air mass flow rate with FSP controller (-30% delay estimation error)

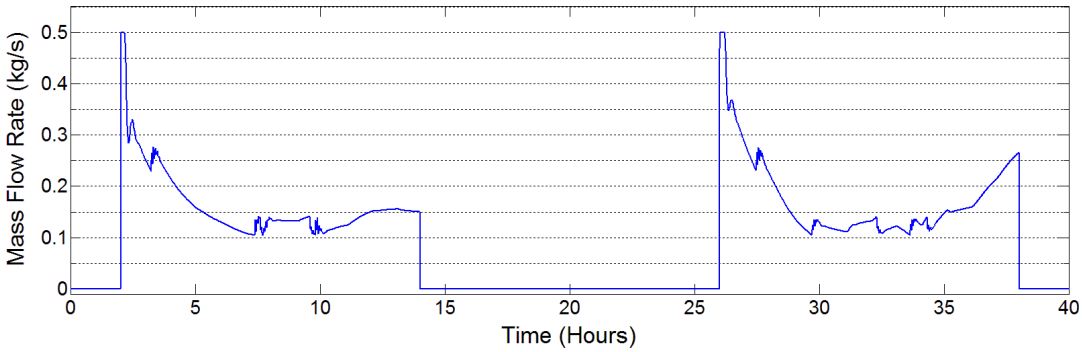

Figure E-6: AHU air mass flow rate with SI-RCID controller (-30% delay estimation error)

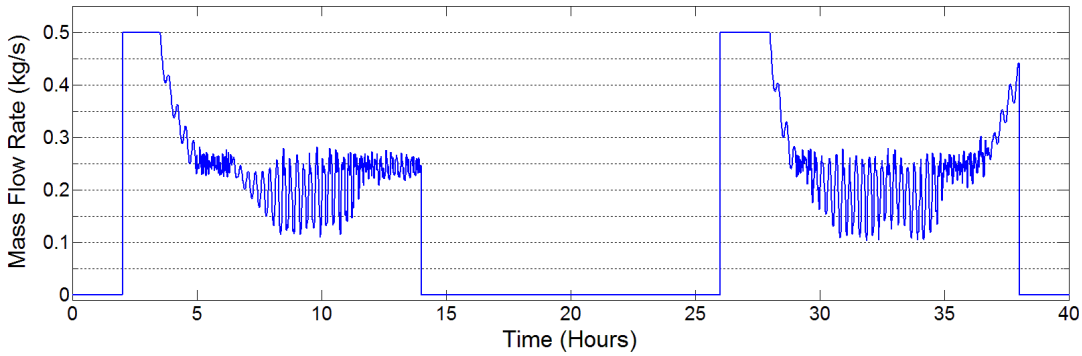

Figure E-7: AHU air mass flow rate with FSP controller (+30% delay estimation error)

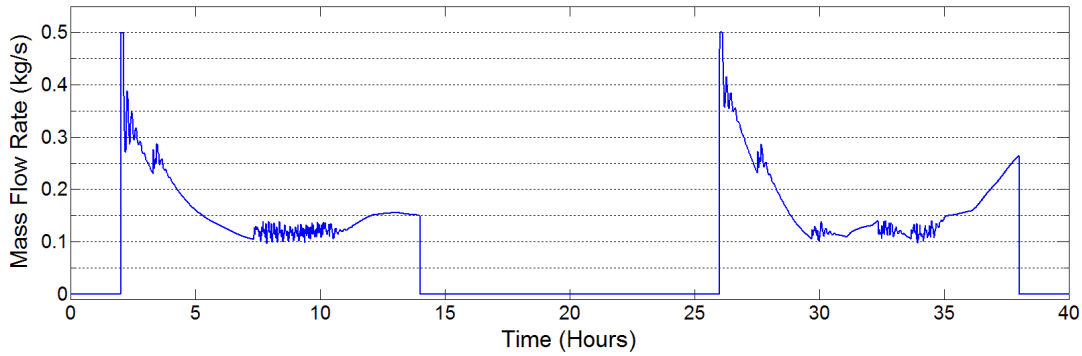

Figure E-8: AHU air mass flow rate with SI-RCID controller (+30% delay estimation error)